

Development of Indole Fused Heteroacene based Sensitizers for Dye Sensitized Solar Cell Applications

By

NITHA P. R.

10CC15A39009

A thesis submitted to the
Academy of Scientific and Innovative Research
for the award of the degree of
DOCTOR OF PHILOSOPHY
in
SCIENCES

Under the supervision of
Dr. JUBI JOHN



**CSIR-National Institute for Interdisciplinary
Science and Technology (CSIR-NIIST),
Thiruvananthapuram - 695 019**



Academy of Scientific and Innovative Research
AcSIR Headquarters, CSIR-HRDC campus
Sector 19, Kamla Nehru Nagar,
Ghaziabad, U.P. - 201 002, India

June 2022

CSIR-National Institute for Interdisciplinary Science and Technology

(Formerly Regional Research Laboratory)



Council of Scientific & Industrial Research (CSIR)

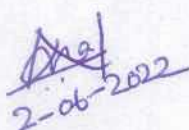
Industrial Estate P.O., Trivandrum - 695 019


Kerala, INDIA




CERTIFICATE

This is to certify that the work incorporated in this Ph.D. thesis entitled, *“Development of Indole Fused Heteroacene based Sensitizers for Dye Sensitized Solar Cell Applications”*, submitted by *Ms. Nitha P. R.*, to the Academy of Scientific and Innovative Research (AcSIR) in fulfilment of the requirements for the award of the Degree of *Doctor of Philosophy in Sciences*, embodies original research work carried out by the student. We further certify that this work has not been submitted to any other University or Institution in part or full for the award of any degree or diploma. Research materials obtained from other sources and used in this research work has been duly acknowledged in the thesis. Images, illustrations, figures, tables etc., used in the thesis from other sources, have also been duly cited and acknowledged.

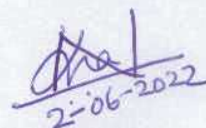

Nitha P. R.


Dr. Jubi John
(Supervisor)


Dr. Suraj Soman
(Co-Supervisor)

STATEMENTS OF ACADEMIC INTEGRITY

I, Nitha P. R., a Ph.D. student of the Academy of Scientific and Innovative Research (AcSIR) with Registration No. 10CC15A39009 hereby undertake that, the thesis entitled "*Development of Indole Fused Heteroacene based Sensitizers for Dye Sensitized Solar Cell Applications*" has been prepared by me and that the document reports original work carried out by me and is free of any plagiarism in compliance with the UGC Regulations on "*Promotion of Academic Integrity and Prevention of Plagiarism in Higher Educational Institutions (2018)*" and the CSIR Guidelines for "*Ethics in Research and in Governance (2020)*".



Nitha P. R.

June 2nd, 2022

Thiruvananthapuram

It is hereby certified that the work done by the student, under our supervision, is plagiarism free in accordance with the UGC Regulations on "*Promotion of Academic Integrity and Prevention of Plagiarism in Higher Educational Institutions (2018)*" and the CSIR Guidelines for "*Ethics in Research and in Governance (2020)*".



Dr. Jubi John

June 2, 2022

Thiruvananthapuram



Dr. Suraj Soman

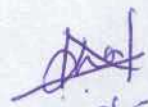
June 2, 2022

Thiruvananthapuram

DECLARATION

I, Nitha P. R., bearing AcSIR Registration No. 10CC15A39009 declare: that my thesis entitled, "*Development of Indole Fused Heteroacene based Sensitizers for Dye Sensitized Solar Cell Applications*" is plagiarism free in accordance with the UGC Regulations on "*Promotion of Academic Integrity and Prevention of Plagiarism in Higher Educational Institutions (2018)*" and the CSIR Guidelines for "*Ethics in Research and in Governance (2020)*".

I would be solely held responsible if any plagiarised content in my thesis is detected, which is violative of the UGC regulations 2018.


2-06-2022

Nitha P. R.
June 2nd, 2022

Thiruvananthapuram

ACKNOWLEDGEMENTS

It is with immense pleasure that I express my deep sense of gratitude to my research supervisors, Dr. Jubi John and Dr. Suraj Soman, for suggesting the research topic and for their guidance, constant support and encouragement that led to the successful completion of this work.

I wish to thank Dr. A. Ajayaghosh, Director, CSIR-NIIST Thiruvananthapuram, for providing the necessary facilities for carrying out the research work.

I would like to acknowledge Dr. Mangalam S. Nair, Dr. R. Luxmi Varma, Dr. C. H. Suresh, and Dr. V. Karunakaran the former and present AcSIR programme coordinators, CSIR-NIIST for the timely help and advice for the academic procedures of AcSIR.

I am very thankful to Dr. Luxmi Varma R., Dr. Jayamurthy P., and Dr. Vijayakumar C. (my Doctoral Advisory Committee members) for their help, support and encouragement throughout my Ph. D. period.

I like to thank all the AcSIR faculty members of CSIR-NIIST for their help and support during the course work period.

My sincere thanks are also due to:

- *Dr. K. V. Radhakrishnan, Dr. P. Sujatha Devi, Dr. R. Luxmi Varma, and Dr. K. R. Gopidas, present and former Heads, Chemical Sciences and Technology Division for their endless support.*
- *Dr. Kaustabh Kumar Maiti, Dr. B. S. Sasidhar, Dr. L. Ravi Shankar, Dr. Sunil Varughese, Dr. Kumaran A. Scientists of Organic Chemistry Section for their encouragement and help.*
- *Dr. C. H. Suresh (CSIR-NIIST), Dr. Rakesh Mishra (NIT Uttarakhand) and Aravind K. (S B College Changanassery) for computational studies and Dr. Rajiv K. Sukumaran for help rendered during 800 work.*
- *Mrs. Saumini Mathew, Mr. Saran P. Raveendran and Mr. Rakesh Gokul are acknowledged for recording NMR spectra. Mrs. S. Viji and Ms. S. Aathira are acknowledged for mass spectral analysis.*
- *Mr. Jayadev V, Mr. Andrew, Ms. Sreelakshmi and Ms. Sruthi M. for helping me with the device fabrication part.*

- *Mr. Anoop and Mr. Vimal Kumar for helping me during 800 work*
- *Ms. Vrinda Raj, Ms. Saranya P. V., Ms. Aswathy S. S, Mr. Taj Tony (MSc project students) for helping me to carry out some of my lab work.*
- *Mr. Vishnu K. Omanakkuttan, Ms. Sheba Ann Babu, Mr. Rahul P., Mr. Akhil Krishnan R, Dr. Dipankar Paul, Ms. Angel Johny, Ms. Reshma K, Dr. Jagadeesh Krishnan, Ms. Uthara K (Present and former members of JJ family) are greatly acknowledged for their love, care and support throughout my research period.*
- *Mr. Jayadev P., Mr. Sourav C., Ms. Anooja, Ms. Sruthi M, Ms. Sreelakshmi, Mr. Andrew, Mr. Sreenandhu, Ms. Jebin P, Ms. Kanishka (SS group) are also greatly acknowledged*
- *My seniors and former colleagues: Dr. Shimi M, Dr. Preethanuj P. Dr. Aparna P. S., Dr. Santhini P.V., Dr. Saranya S., Dr. Dhanya B. P., Dr. Ajesh Vijayan, Dr. Sasikumar P., Dr. Greeshma Gopalan, Dr. Maya R.J., Dr. Athira Krishna, Dr. Sreedevi P, Dr. Sharathna P., Dr. Santhi S, Dr. Neethu S., Dr. Meenu M. T., Ms. Aswathy, M, Mr. Madhu Krishnan, Mrs. Biji M., Ms. Rajimol P. R., Ms. Ummu Jumaila, Ms. Irfana Jesin, Mr. Cijil M., Mr. Vimal Kumar, Ms. Alisha Valsan, Ms. Anuja Joseph, Ms. Priyadarsini T.S are also acknowledged*
- *Mrs. Reshma Mathew, Ms. Ashitha K. T, Mr. Valmiki Praveen, Mrs. Amrutha S, Ms. Sumitha, Mr. Arun Kumar K. T, Mr. Vijayakumar for their friendship and support*
- *All present and former members of CSTD for their friendship and creative inspirations.*
- *All my teachers and friends for their care and support.*
- *My parents and family members for their endless caring love and support.*
- *Council of Scientific and Industrial Research (CSIR), for the financial assistance.*

Nitha P. R.

TABLE OF CONTENTS

Certificate	i
Statement of academic integrity	ii
Declaration	iii
Acknowledgement	iv
Table of contents	vi
List of abbreviations	x
Preface	xiii
CHAPTER 1	
Indole Fused Heterocycles as Sensitizers in Dye-Sensitized Solar Cells: an Overview	
1.1 Introduction	2
1.2 Dye Sensitized Solar Cell	2
1.3 Sensitizer: Characteristics and design principles	2
1.3.1 Characteristics of a good sensitizer	2
1.3.2 Metal based sensitizer versus organic sensitizer	3
1.3.3 Molecular engineering of organic dyes	4
1.4 Fabrication and characterization of solar cells	5
1.4.1 Device structures	5
1.4.2 Device fabrication	6
1.4.3 Solar cell characterization	6
1.5 Utilization of indole fused systems for DSSC	8
1.5.1 Indoloquinoline based sensitizers for DSSCs	8
1.5.2 Indolocarbazole based sensitizers for DSSCs	14

1.5.3	Triazatruxene based sensitizers for DSSCs	22
1.5.4	Indeno[1,2- <i>b</i>]indole based sensitizers for DSSCs	28
1.5.5	Thieno[3,2- <i>b</i>]indole (TI) and thieno[2,3- <i>b</i>]indole based sensitizers for DSSCs	33
1.5.6	Tetraindole based sensitizers for DSSCs	37
1.6	Objective of the work	38
1.7	References	39

CHAPTER 2

Chapter 2A: Investigation of Indolo[3,2-*b*]indole Donor based D- π -A Dyes for DSSC

2.1	Introduction	52
2.2	Synthesis and Characterization of IID-1, IID-2, and IID-3	54
2.3	Photophysical and Electrochemical properties	55
2.4	Computational Studies	56
2.5	Photovoltaic Performance	59
2.6	Synthesis and Characterization of IID-4, IID-5, and IID-6	61
2.7	Photophysical and Electrochemical properties	62
2.8	Computational Studies	63
2.9	Photovoltaic Performance	65
2.10	Conclusion	67

Chapter 2B: Investigation of Indolo[2,3-*b*]indole Donor based D- π -A Dyes for DSSC

2.11	Synthesis and Characterization of IID-7, IID-8, and IID-9	69
2.12	Photophysical and Electrochemical properties	70
2.13	Computational Studies	71
2.14	Photovoltaic Performance	72
2.15	Conclusion	74
2.16	Experimental Section	75

2.17 References:	87
------------------	----

CHAPTER 3

Chapter 3A Investigation of Benzothieno[3,2-*b*]indole Donor based D- π -A Dyes for DSSC

3.1 Introduction	91
3.2 Synthesis and Characterization	92
3.3 Computational Studies	93
3.4 Photophysical Properties	95
3.5 Electrochemical Properties	96
3.6 Photovoltaic Performance	98
3.7 Conclusion	102

Chapter 3B Investigation of Benzothieno[3,2-*b*]indole Donor based D- π -A Dyes for DSSC

3.8 Synthesis and characterization	103
3.9 Computational Studies	104
3.10 Photophysical and Electrochemical Studies	105
3.11 Photovoltaic Studies	107
3.12 Conclusion	109
3.13 Experimental section	110
3.14 References	117

CHAPTER 4

An Investigation into the Photovoltaic Performance of Indolo[3,2-*b*]indole and Indolo[2,3-*b*]indole based D(π -A)₂

4.1 Introduction	119
4.2 Design Strategy	121
4.3 Synthetic Strategy	121
4.4 Photophysical Properties	123

4.5 Electrochemical Properties	123
4.6 Infrared spectroscopic studies	124
4.7 Computational Studies	126
4.8 Photovoltaic Properties	127
4.8.1 J-V and IPCE measurements	127
4.8.2 Electron lifetime studies and charge extraction measurements	129
4.9 Indoor light measurements	130
4.10 Conclusion	131
4.11 Experimental section	132
4.12 References	138
Abstract of the thesis	140
List of Publications	141
Papers Presented at conferences	142
Attachment of the photocopy of publications	143

List of Abbreviations

A	Acceptor
AM	Air mass
Ag	Silver
AgCl	Silver chloride
BMI	1-Butyl-3-methylimidazolium iodide
°C	Degree celsius
CHCl ₃	Chloroform
CFL	Compact fluorescent lamp
cm	centimeter
C _μ	Chemical capacitance
CE	Charge extraction
CDCA	Chenodeoxycholicacid
CDCl ₃	Deuteriated chloroform
CV	Cyclic voltammogram
D	Donor
DCM	Dichloromethane
DFT	Density functional theory
DMAc	N,N-dimethyl acetamide
DSSC	Dye sensitized solar cell
eV	Electron volt
E _{ox}	Oxidation potential
E _{o-o}	Zero point energy
E _{CB}	Conduction band energy
EQE	External quantum efficiency
EIS	Electrochemical impedance spectroscopy
et al.	Et allii/alia
F _c	Ferrocene
F _c ⁺	Ferrocenium
FF	Fill factor
FTIR	Fourier transform infrared

FTO	Fluorine doped tin oxide
H ₂ O	Water
HFIP	Hexafluoroisopropanol
HOMO	Highest occupied molecular orbital
Hz	Hertz
HRMS	High resolution mass spectroscopy
I	Current
I ⁻	Iodide
I ₃ ⁻	Triiodide
I ₂	Iodine
ICT	Intramolecular charge transport
IMVS	Intensity modulated photovoltage spectroscopy
IMVS	Intensity modulated photocurrent spectroscopy
IPCE	Incident photon to current conversion efficiency
J	Current
J _{sc}	Current density
LUMO	Lowest unoccupied molecular orbital
LHE	Light harvesting efficiency
M	Molar
mA	Milliampere
mg	Milligram
mL	Millilitre
MHz	Mega hertz
mM	Millimolar
mmol	Millimole
MCR	Multicomponent reaction
MeOH	Methanol
MO	Molecular orbital
N	Nitrohen
Na	Sodium
nm	Nanometer
NMR	Nuclear magnetic resonance
NHE	Normal hydrogen electrode

NIR	Near infrared
°C	Degree celsius
OFET	Organic light emitting diode
Pd	Palladium
PCE	Power conversion efficiency
PTSA	p-Toluenesulfonic acid
R_t	Transport resistance
R_{ct}	Recombination resistance
THF	Tetrahydrofuran
TDDFT	Time dependent density functional theory
TPV	Transient photovoltage
TPC	Transient photocurrent
t-BuOH	Tertiary butanol
TiO ₂	Titanium dioxide
TiCl ₄	Titanium tetrachloride
UV	Ultra violet
V	Voltage
V_{oc}	Open circuit potential

PREFACE

Among the third generation photovoltaic technologies, dye sensitized solar cells (DSSC) excels with many attractive features. DSSC consists of three major components, photoanode, electrolyte and a counter electrode. Dyes occupy a prominent position among components in DSSC. Recently organic dyes have emerged as the most promising candidate for DSSC due to their performance, ease of synthesis, stability, tunability, low cost and eco-friendly characteristics. Among various organic dyes, heterocycles, mainly N- and S-containing, have found immense applications as sensitizers. The objective of our investigation was directed towards unravelling the potential of fused indole systems to construct new and novel photosensitizers.

The thesis is organized into four chapters. **Chapter 1** initiates with a brief introduction on the evolution of photovoltaic technology and proceeds in detail to the specific aspects of dye sensitized solar cells (DSSC). Final section of the chapter describes back ground literatures where indole fused heterocycles were used as either donor or π -spacer to construct photosensitizers for DSSC applications. The upcoming chapters deals with detailed investigation of dyes which are based on indole fused systems as donor. Chapter 2A deals with dyes **IID1-IID6** and chapter 2B deals with **IID7-IID9**. Chapter 3 involves benzothienoindole based systems. While Chapter 3A deals with **BID1-BID3**, the second part of the chapter deals with **BID4-BID6**. Chapter 4 involves di-anchoring dyes **IID10-11D12**.

Chapter 2 which is divided into two parts deals with the utilization of indoloindole as donor to develop D- π -A dyes for DSSC. Part A of the chapter was initiated with the development of D- π -A dyes which utilizes indolo[3,2-*b*]indole as donor, cyanoacrylic acid as acceptor/anchoring group and varied the π -spacer employed such as benzene, thiophene and furan to construct sensitizers **IID-1**, **IID-2** and **IID-3** respectively. To minimize dye aggregations, the two *N*-atoms of indolo[3,2-*b*]indole core was functionalized with hexyl chains. Though furan substituted dye was exhibiting higher light harvesting efficiency with wider absorption profile, **IID-1** having benzene as π -spacer outperformed the other two with higher photovoltage and current density. Co-adsorbent chenodeoxycholic acid (CDCA) optimization studies further enhanced the performance with maximum efficiency realized using 20 mM CDCA concentration. This indicated significant dye aggregations happening in the system and we concluded that the slightly twisted conformation of **IID-1** may be helping the system to alleviate dye aggregation and also the approach of oxidized species (hole) in the

electrolyte coming closer to semiconductor. Further we did molecular engineering by replacing the hexyl group with dodecyl chain as an approach towards reducing dye aggregation. The dyes thus developed are **IID-4**, **IID-5** and **IID-6** with π -spacer as benzene, thiophene and furan respectively.

By adopting this structural modification, all the dyes could outperform the previous set even in the absence of any co-adsorbent. This indicates the efficacy of dodecyl chains in inhibiting aggregate formation than hexyl chain and thus preventing the back electron transfer reactions. In the absence of aggregate formation, light harvesting efficiencies of dyes improved contributing significantly towards the power conversion efficiency (PCE) and furan substituted dye exhibited maximum PCE of 4.4 % and the minimum was delivered by the benzene substituted dye **IID-4**. In Part B dodecyl chain incorporated indolo[2,3-*b*]indole was used as donor to synthesize **IID-7**, **IID-8**, and **IID-9** with benzene, thiophene and furan respectively as π -spacer. Like in the previous case, light harvesting efficiency dominated the overall PCE and thus furan spacer showcased superior performance followed by thiophene and benzene. The performance of indolo[2,3-*b*] based dyes were lesser than their indolo[3,2-*b*] counterparts in terms of both photocurrent and photo voltage. On moving from **IID-1** to **IID-9** light harvesting efficiency played a crucial role in the current generation which in turn contributed significantly to the overall power conversion efficiency of the corresponding devices.

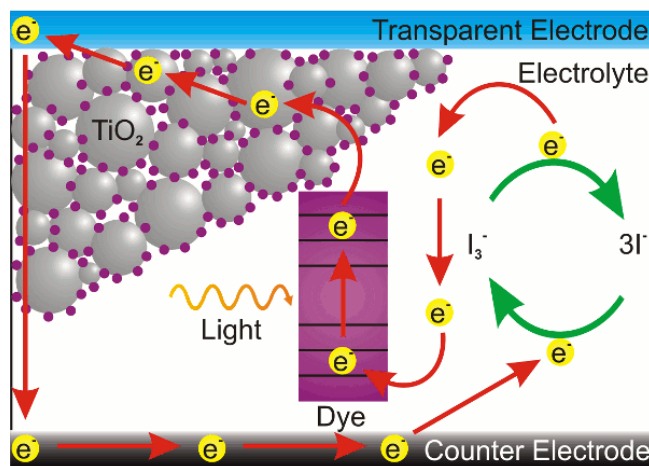
Chapter 3A deals with another class of electron donors, benzothieno[3,2-*b*]indole. We successfully synthesized three new D- π -A organic dyes based on benzothieno[3,2-*b*]indole as donor and by varying the π -spacer unit with benzene (**BID-1**), thiophene (**BID-2**) and furan (**BID-3**). With judicious selection of π -spacer, the optical properties are controlled in a way to realize improved photovoltaic performance. Furan substituted dye, **BID-3** showcased the best performance with a PCE of 4.11%. The efficiency value increased in the order **BID-1** (1.16%) < **BID-2** (3.10%) < **BID-3** (4.11%). Better planarity of the molecular backbone helped **BID-3** in achieving improved donor- acceptor interactions and superior charge separation leading to larger dipole moment thereby realizing improved light harvesting and photovoltaic performance. Similar kind of investigation was also performed on benzothieno[2,3-*b*]indole donor based D- π -A dyes. The dyes thus constructed **BID-4**, **BID-5**, and **BID-6** with benzene, thiophene and furan spacer respectively are included in chapter

3B. Here also furan spacer outperformed the rest with better current density and photovoltage.

The systematic investigations of donors in the previous sections revealed the superiority of indolo[3,2-*b*]indole in device performance. Hence, in **Chapter 4** we adopted the innovative molecularly engineered bifunctional D(π -A)₂ architecture taking indolo[3,2-*b*]indole as donor. We changed the π -spacer as benzene (**IID-10**) and furan (**IID-11**) keeping the acceptor/anchoring group fixed as cyanoacrylic acid. Our objective was to increase the absorption capabilities of the fused heterocyclic dyes in the visible region by exploiting the extended conjugation of the newly designed molecular design. In addition, multi anchoring approach has also proved to ensure effective coupling and electron injection with the semiconductor. The devices were subjected to both outdoor (full sun) as well as indoor (artificial light) measurements. Under full sun illumination, **IID-10** and **IID-11** differs significantly in current density with **IID-11** achieving the maximum current density leading to an efficiency of 4.81%. Along with higher light harvesting efficiency, better electron collection efficiency and electron injection ability could be attributed to the observed trend in the net photovoltaic performance. The charge extraction measurements revealed a positive shift for the conduction band in the case of devices fabricated with **IID-11**. This might have helped effective electron injection in the case of **IID-11**. Next we synthesized dye **IID-12** with the same molecular architecture utilizing indolo[2,3-*b*]indole as donor, furan as π -spacer and cyanoacrylic acid as the anchoring/acceptor group. **IID-12** showcased poorer performance than the previous di-anchoring dyes with an efficiency of 2.87%. While the measurement of devices using a day light CFL revealed improved performance for **IID-10** and **IID-11**, **IID-12** showed a decrease in PCE. While the indoor performance of **IID-10** almost remained constant on going from 1000 lux to 200 lux, an increment in PCE was observed for **IID-11** based devices delivering a maximum of 13.4% at DL CFL-200 Lux illumination.

CHAPTER 1

Indole Fused Heterocycles as Sensitizers in Dye-Sensitized Solar Cells: An Overview



Abstract

The past three decades have witnessed extensive research in the development of non-metallic organic dyes for dye sensitized solar cells (DSSC). Dyes occupy a prominent position among the components in DSSC, and organic dyes have emerged as one of the most promising candidate for DSSC due to their performance, ease of synthesis, stability, tunability, low cost and eco-friendly characteristics. In addition to this, so far, the best and highest performing DSSCs reported in literature use metal-free organic dyes. Organic dyes also provide flexibility to be used along with alternate new generation cobalt and copper electrolytes. Among various organic dyes, heterocycles, mainly *N*- and *S*-containing, have found immense application as sensitizers. Indole fused heterocycles were used by different research groups in their dye designs, mainly as a donor and π -spacers. The planarity of these electron-rich fused indole systems is advantageous as it helps to initiate more prominent ICT transitions. In addition, the possibility for selective functionalization of *N*-atom with long or branched alkyl chains prevents the aggregation of the sensitizer, increases the solubility and is effective in custom dyes designing which are in turn capable of preventing back electron transfer (recombination). Fused indole moieties utilized in the design of sensitizers are stable and offer ease of synthesis

1.1 Introduction

Fossil fuel-based resources have been primarily satisfying the energy demands of humankind for more than a century. The ever-increasing energy demands that are fuelled by the growing human population contributed to environmental issues with depletion of conventional resources, necessitating the need for research in developing efficient methods to harness alternative energy sources.¹ Solar energy is considered one of the most promising alternatives that could sustainably provide inexhaustible energy.² The stepping stone for photovoltaic technology was laid with the demonstration of the first silicon-based solar cells by Bell laboratories which exhibited an efficiency of ~6%. Since then, the technology has witnessed many advancements in introducing thin films in the late 70's and finally reaching up to the third-generation solar cells.³ The third-generation photovoltaics consist of dye-sensitized solar cells, organic solar cells, quantum dot solar cells and perovskite solar cells.⁴ Though their efficiencies are still lagging behind the conventional silicon-based devices, the lower fabrication cost of these devices along with lesser environmental impact are promising factors that urge the scientific community to carry out research and technological advancements in third-generation photovoltaics.⁵

1.2 Dye Sensitized Solar Cell

Dye sensitized solar cell research received momentum in early 90's with the pioneering work carried out by Brian O'Regan and Michael Gratzel in 1991, where they used Ru metal complex sensitized nanocrystalline TiO₂ film, realizing a power conversion efficiency of 7%.⁶ DSSC has many attractive features, including lower fabrication cost and short payback time with minimum environmental hazards.⁷ In addition, it can be designed for both outdoor as well as indoor light harvesting.⁸ DSSC consists of three major components, photoelectrode, electrolyte and a counter electrode. The dye sensitized mesoporous semiconductor layer coated on a conductive glass/plastic substrate collectively acts as the photoanode. The electrolyte is responsible for both regeneration of dye as well as charge transport to the counter electrode. Liquid electrolytes which consist of redox mediators in organic solvents are typically used in DSSC. To address the leakage and device lifetime issues originating from the use of liquid electrolytes, efforts are being made to explore quasi-solid electrolytes and solid conductors. Counter electrode is composed of transparent conductive oxides (ITO/FTO) coated with catalysts like platinum/PEDOT/Carbon for fast electron transfer reactions. The mechanism of current generation with DSSC starts with the

absorption of light by the sensitizers that are adsorbed on the semiconductor surface. These photoexcited electrons are then injected into the conduction band of the semiconductor which diffuses through the conductive substrate and finally reaches the counter electrode. The oxidized dye molecules are subsequently regenerated by the redox mediators present in the electrolyte which are then reduced at the counter electrode. This cycle continues generating current without net chemical change in the system (Figure 1).⁹

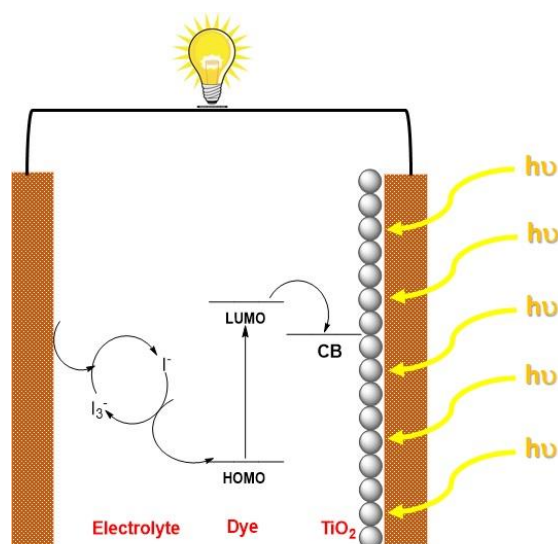


Figure 1. Operating principle of DSSC

Unlike conventional PV devices, DSSC excels with the advantage that different components are carrying out light absorption, charge generation, and charge transport. This opens up broader possibilities of achieving higher photovoltaic performance by selectively optimizing each component used in the device.

1.3 Sensitizer: Characteristics and Design principles

1.3.1 Characteristics of a good sensitizer

Dye sensitizer represents the core unit in DSSC, responsible for light absorption and electron injection into the semiconductor layer. Designing of dye sensitizer with intensified absorption profile from visible to NIR region is a critical factor for light harvesting. It should also possess higher molar extinction coefficient. The optimum redox potential of the dye energy levels (HOMO-LUMO) is necessary to achieve efficient electron injection into the semiconductor conduction band and to realize effective regeneration of dye ground state by the redox electrolyte. The sensitizer should also possess features such as suitable binding

groups (-COOH, -PO₃H₂) to anchor onto the semiconductor surface and also need to be engineered in such a way to minimize aggregation on the semiconductor. The prevention of dye aggregation is highly desirable to reduce recombination losses and increase the open circuit potential of the devices, which can also contribute to the stability of the device as a whole.¹⁰

1.3.2 Metal based sensitizer versus Organic sensitizers

Ruthenium-based sensitizers dominated the first two decades in DSSC research since their inception in the early nineties due to their broad absorption and higher power conversion efficiencies and reached up to a PCE of 11.5% using conventional iodide/triiodide electrolyte.¹¹ Though these sensitizers appear to be feasible for practical applications, with progressing research, a lower molar extinction coefficient of metal complexes along with the scarcity of Ru have slowly paved the way for the advent of metal-free sensitizers. Additionally, the introduction of alternate cobalt and copper electrolyte further encouraged the scientific community to expand the research on organic dyes, which are most suitable with alternate electrolytes. The introduction of metal-free sensitizers has also opened up an arsenal of strategies to develop more efficient devices at a lower cost and in an eco-friendly manner.¹² Metal-free sensitizers generally display high molar extinction coefficients, but the narrow absorption of many sensitizers possess serious concern over light harvesting. The emergence of a co-sensitization strategy helped to alleviate this limitation by realizing panchromatic absorption through the sensitization of a combination of different dyes having complementary absorption.¹³ This also reduced the possibility for dye aggregation. The strongest side of organic sensitizers involves the flexibility in tuning the chemical structure with the help of well-established synthetic strategies.¹⁴ According to the recent reports, the PCE of DSSC based on single metal free organic sensitizers has reached 13.6% using cobalt electrolyte, 11.7 for solid state DSSC and 32% for indoor light harvesting. The co-sensitization strategy could realize 14.3% PCE using cobalt based electrolyte.¹⁵

1.3.3 Molecular engineering of organic dyes

Molecular engineering of dyes deals with designing systems with potential light-harvesting ability over the entire visible region with proper energetics that realizes electron transfer from the excited state of the dye to the metal oxide upon light absorption. The most widely employed molecular architecture is the donor- π -spacer-acceptor (D- π -A) strategy.¹⁶ Anchoring groups are supposed to be bifunctional, serving the purposes of adsorption as well

as electron acceptance. Although many new anchoring groups have emerged, cyanoacrylate group is generally found to outperform others because of its agreement with the two functions mentioned above. The strong electron withdrawing nature of cyanoacrylate moiety facilitate the broadening of absorption spectra of molecules along with strong adsorption capability to the semiconductor surface increases the injection ability and device lifetime. A wide variety of choices are present for both donor and π -spacer moieties. The derivatives of arylamine, carbazole, coumarins and phenothiazine are some of the popular donor groups of continued interest used in DSSC.¹⁷ The π -linkers have also got paramount importance in tuning the communication between donor and acceptor units, thereby increasing the light-harvesting ability of the dyes. Though thiophene, furan, benzene and oligothiophenes have been used extensively as π -spacer in dyes, fused ring planar systems with strategies to prevent π - π aggregation are not explored to its full extent.¹⁸ Apart from modulating each building block of a sensitizer, considerable effort was also laid in engineering new dye design strategies, which resulted in the introduction of architectures like D-A- π -A, D-D- π -A, A- π -D- π -A and D- π -A-A.¹⁹

1.4 Fabrication and characterization of solar cell

1.4.1 Device structures

A sandwiched structure in which both the conducting and working electrode are built on conducting glass substrate is the standard device structure. Transparency and electrical conductivity are two important parameters needed for a transparent conductive substrate. Though ITO film has higher percentage of transparency than FTO, low sheet resistance coupled with chemical and thermal stability make FTO films better in most of the cases. A mesoporous TiO₂ layer (active layer) is coated over the TCO followed by the light scattering layer to improve the light capture in the device. Further engineering is usually done at the photo electrode to reduce the back electron transfer reactions which are called blocking layers. This is achieved by coating thin and compact layer of TiO₂ between FTO plate and active layer called pre-blocking layers. Post-blocking layers are coated over the light scattering layer. Working electrode completes after the sensitization of semiconductor with dye. The counter electrode is composed of TCO with catalyst such as Pt nanoparticles, carbon etc. These two electrodes are then sealed using thermoplastic with a thin layer of electrolyte between them.

1.4.2 Device fabrication

All the devices reported in the thesis were fabricated in the sandwiched configuration. Working electrodes (FTO, TEC15, GreatCell Solar) were cleaned using ultrasonic bath in soap solution, deionized water and isopropyl alcohol followed by heating to 500 °C. The pre-blocking layer was coated on the UV-Ozone treated substrates by immersing in 40 mM TiCl_4 solution at 70 °C for 30 min. 16 μm titanium dioxide semiconductor layer (12 μm transparent layer and 4 μm scattering layer) was coated on the substrates and were heated to 500 °C through ramped heating. The TiO_2 coated electrodes were soaked in 0.2 mM of respective dye solutions 15 hours in acetonitrile at room temperature. Pre-drilled, platinum coated FTO was used as the counter electrodes and the cells were assembled using a 25 μm surlyn spacer. The space between working and counter electrodes were filled with electrolyte composed of 0.5 M BMII, 0.1 M LiI, 0.03 M I₂ and 0.5 M tbp in acetonitrile.

1.4.3 Solar cell characterization

An equivalent circuit diagram can be used to draw useful information about the solar cell parameters (Figure 2). An ideal solar cell can be modelled by a current source in parallel with a diode. To meet with the real time scenario or the non-ideal behaviour of solar cell, a shunt resistance and series resistance can be added to the model.²⁰

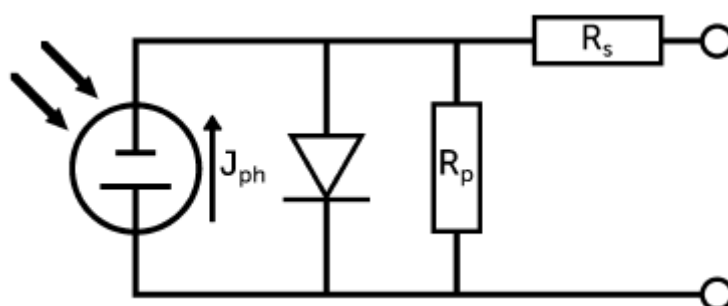


Figure 2. Representation of a solar cell as a schematic circuit

The power conversion efficiency, which is the most significant parameter in defining the efficiency of a solar cell can be deduced from the J - V curve which is obtained by irradiating the solar cell by a solar simulator under the conditions of illumination with 100 mW cm^{-2} light with AM1.5G spectral distribution, while the cell is kept at 25 °C. The cell parameters which are associated with this measurement are:

1. Short circuit current (I_{SC})

It is the highest current that can be drawn from a solar cell. The voltage at this point is zero. Hence the generated power is also zero. When short circuit current is divided by the active area of the cell, we obtain short circuit current density (J_{SC})

2. Open circuit potential (V_{OC})

It is the highest voltage of a solar cell at a given light intensity. It is also the potential where current flows through a solar cell is zero.

3. Fill factor (FF)

It describes the quality and idealness of a solar cell. It is the ratio of maximum power generated to the theoretical power maximum. At both I_{sc} and V_{oc} while one of the parameter is at its maximum the other will be zero so that the product will be zero and hence power will be zero (Figure 3). The maximum power obtained from the cell will be at some intermediate resistance in the cell.

$$FF = \frac{V_{max}I_{max}}{V_{oc}I_{sc}}$$

High series resistance and low shunt resistance causes the FF to go down.

4. Power conversion efficiency (PCE, η)

It is the ratio of electrical power output to the solar power input. The input solar power is the product of solar irradiance incident on the cell and the active surface area.

$$PCE = \frac{P_{out}}{P_{in}}$$

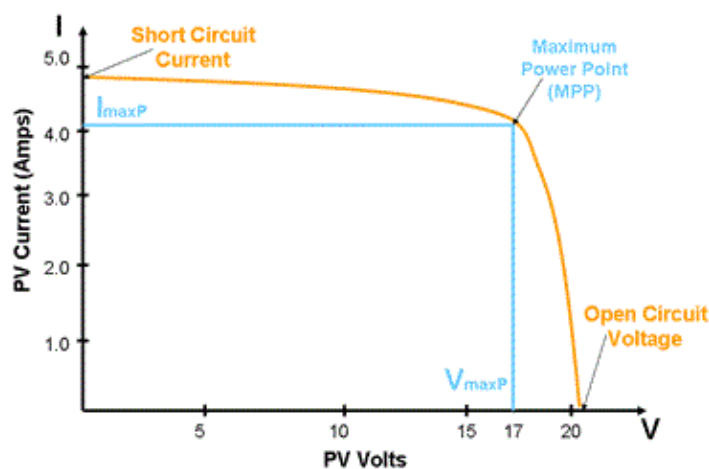


Figure 3. I - V curve under light conditions

5. Incident photon to current efficiency

The ratio of the current density obtained in the output circuit to the photon flux incident on the cell active area is termed as the incident photon to current conversion efficiency. It is also called the external quantum efficiency (EQE) and is also expressed in percentage. The current produced in the external circuit when monochromatic light falls on the cell is monitored over the desired wavelength range. The area under the obtained curve would thus give the total number of charge carriers or the integration of the IPCE curve would give the photocurrent density. IPCE measures the device's ability to generate charge carriers at each irradiated wavelength. IPCE is the product of light harvesting efficiency, injection efficiency, regeneration efficiency and charge collection efficiency associated with the semiconductor.

1.5 Utilization of Indole fused systems for DSSC

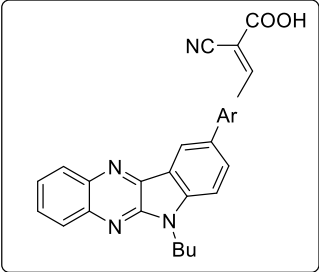
This section deals with literature reports on the application of some of the indole fused systems like indoloquinoxaline, indolocarbazole, indenoindole, triazatruxene, thienoindole and tetraindole as donor/ π -spacer for the development of sensitizers.

1.5.1 Indoloquinoxaline based sensitizers for DSSCs

Indolo[2,3-*b*]quinoxaline (IQ), a built-in donor-acceptor chromophore, consists of an electron-rich indole moiety fused with an electron-deficient quinoxaline unit. The condensation of isatin with *o*-phenylenediamine affords these planar heteroarenes.²¹ By appropriately functionalizing the indole and quinoxaline motifs with electron-donating or electron-withdrawing groups, the electronic properties of this chromophore can be custom-tuned in line with the application. It has been documented that the donating ability of the indole motif and the donor-acceptor interaction with the quinoxaline unit is enhanced by functionalizing the indole core with electron-donating groups.²²

The first utilization of this scaffold as a building block in DSSC was done by Venkateswararao *et al.*²³ They constructed dyes **2-6**, which are having IQ as electron donor and cyanoacrylic acid as anchoring unit (Figure 4). Sensitizers differed in the π -spacer employed, which were either phenyl or thiophene fragments. Dye **1**, which lacks any π -spacer, delivered least efficiency of 0.86%. Among the remaining sensitizers, **6** showed a red shifted and distinct ICT band implying more effective conjugation. Two dye baths were used to fabricate devices, one with DCM and the other with a combination of CH₃CN/*tert*-butanol/DMSO (3.5/3.5/3, v/v). All the sensitizers exhibited better efficiencies in the latter case. The change in PCE was mainly caused by significant changes in the photocurrent

generated. Though ICT was more prominent in the case of **6**, a relatively higher degree of planarity might have caused aggregation of dyes leading to decreased light harvesting. Dye **2** with simple thiophene as the π -spacer outperformed other dyes with PCE of 3.45% with J_{sc} of 9.29 mA/cm² and V_{oc} of 579 mV. Other dyes showcased PCE in the order **6**>**5**>**3**>**4**. The introduction of acetylene was not found to be beneficial for transmitting charges in the current design.



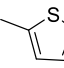
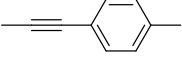
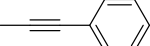
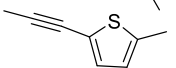
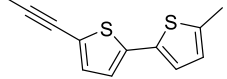
SI No.	Ar	PCE (%)
1	NIL	0.86
2		3.45
3		1.65
4		1.08
5		2.72
6		2.68

Figure 4. Photosensitizers **1-6** based on indolo[2,3-*b*]quinoxaline core

Later, Qian *et al.* developed three D- π -A dyes having indolo[2,3-*b*]quinoxaline and cyanoacrylic acid as donor and acceptor groups, respectively.²⁴ The sensitizers **7**, **8**, and **9** differ in the selection of conjugated spacers, which were oligothiophene, thienylcarbazole, and furylcarbazole, respectively (Figure 5). The dyes exhibited efficiencies in the order **7**>**9**>**8**. The maximum efficiency of 7.62% was delivered by **7**, mainly contributed by the significantly larger short circuit current density ($J_{sc} = 16$ mA/cm²) of this dye. The electron-rich, oligothiophene π -bridge makes the absorption spectra of **7** more red-shifted with an absorption maximum at 480 nm for the ICT band followed by **8** and **9**. The IPCE performance of the devices is following the absorption behaviour of dyes. While **7** shows broad absorption from 400-770 nm, in the case of **8** and **9**, the absorption furnishes onset at 700 and 690 nm, respectively illustrating the trend in the dyes' J_{sc} and light-harvesting ability. Though lower current density was delivered by **9**, the higher open circuit potential ($V_{oc} = 742$ mV) helped **9** to outperform **8**.

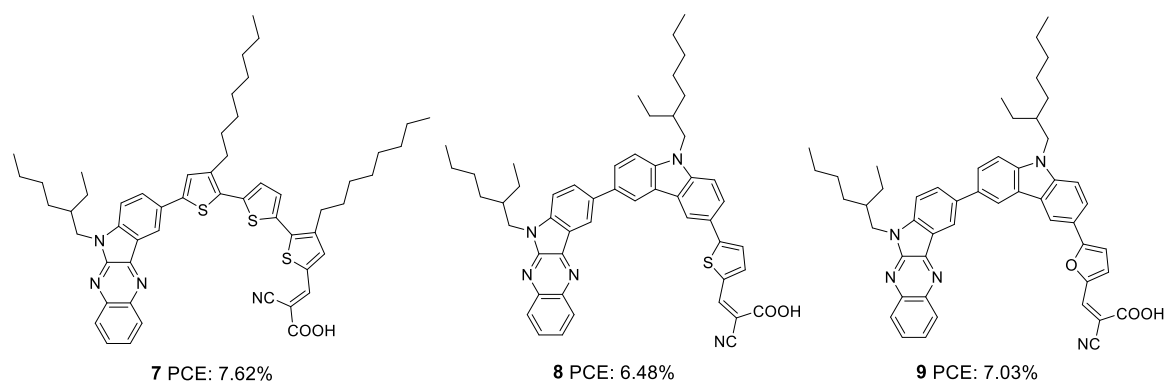


Figure 5. Photosensitizers **7-9** based on indolo[2,3-*b*]quinoxaline core

Soon after, the authors used the same scaffold to realize D-D- π -A and D- π -A systems.²⁵ In D-D- π -A design, indoloquinoxaline was used as the primary donor and phenothiazine was used as an auxiliary donor, cyanoacrylic acid as acceptor and thiophene/furan as π -bridge to afford **12** and **13** respectively (Figure 6). These dyes were then compared with **10** and **11**, which were D- π -A dyes based on indoloquinoxaline and phenothiazine, respectively, as donors. Among the dyes, **12** having D-D- π -A design was found to outperform the rest. Sensitizer **12** excelled with an efficiency of 8.28% followed by **13** with 7.56%. Compared to furan, the electron richness of thiophene was aiding good ICT transitions reducing the HOMO-LUMO gap for **12**, which resulted in more red-shifted and enhanced absorption spectra for **12** compared to that of **13** with furan as π -spacer. The IPCE spectra of dyes show a similar trend, with **12** giving over 60% IPCE value from 359 to 600 nm with maximum absorption of 86% at 490 nm. This illustrates the reason for the highest light-harvesting ability and J_{sc} (15.3 mA/cm²) for **12**. The V_{oc} values obtained are in order **12**>**13**>**11**>**10**.

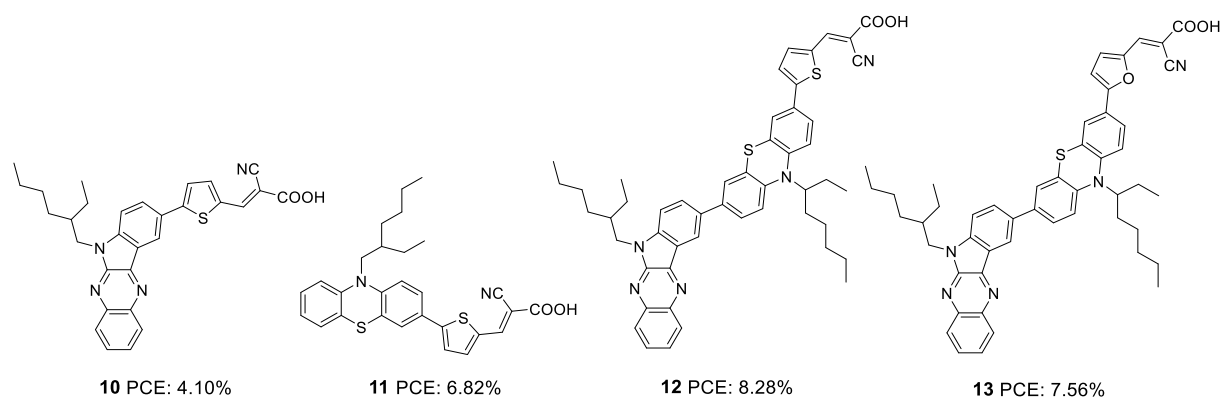


Figure 6. Photosensitizers **10-13** based on indolo[2,3-*b*]quinoxaline and phenothiazine cores

Later in 2017, the authors utilized indoloquininoxaline as an acceptor in a (D)₂-A- π -A dye design in which two triphenylamine groups were used as two branches of the primary donor unit. The dyes **14-17** differed in the π -bridges (furan and thiophene) and acceptor groups (cyanoacrylic acid and 2-(1,1-dicyanomethylene)rhodanine or DCRD) (Figure 7).²⁶ These dyes exhibited efficiencies in the range of 4.55% to 7.09%. Dyes **14** and **15**, which were having cyanoacrylic acid as the acceptor group outperformed the corresponding dyes having DCRD as the acceptor unit. Though the absorption spectra of **16** and **17** were much red-shifted compared to **14** and **15**, higher dye loading of the latter resulted in larger J_{sc} values. This is also apparent from the IPCE spectra. Though the spectra of **14** and **15** are blue-shifted with 30 and 20 nm differences respectively with respect to **17**, the increase in J_{sc} value contributed to a better PV performance. Dye **15** could deliver over 60% IPCE value from 400 to 600 nm with a maximum of 83% at 450 nm, resulting in a J_{sc} value of 12.9 mA/cm². While comparing the π -spacers, furan substituted sensitizers **15** and **17** were found to deliver better efficiencies than their thiophene substituted counterparts. While **15** delivered a PCE of 7.09% with the highest J_{sc} and V_{oc} values, **14** slightly lagged with a power conversion efficiency of 6.05%. DCRD substituted dyes **16** and **17** showcased relatively poor performances with PCE of 4.55% and 4.81%, respectively.

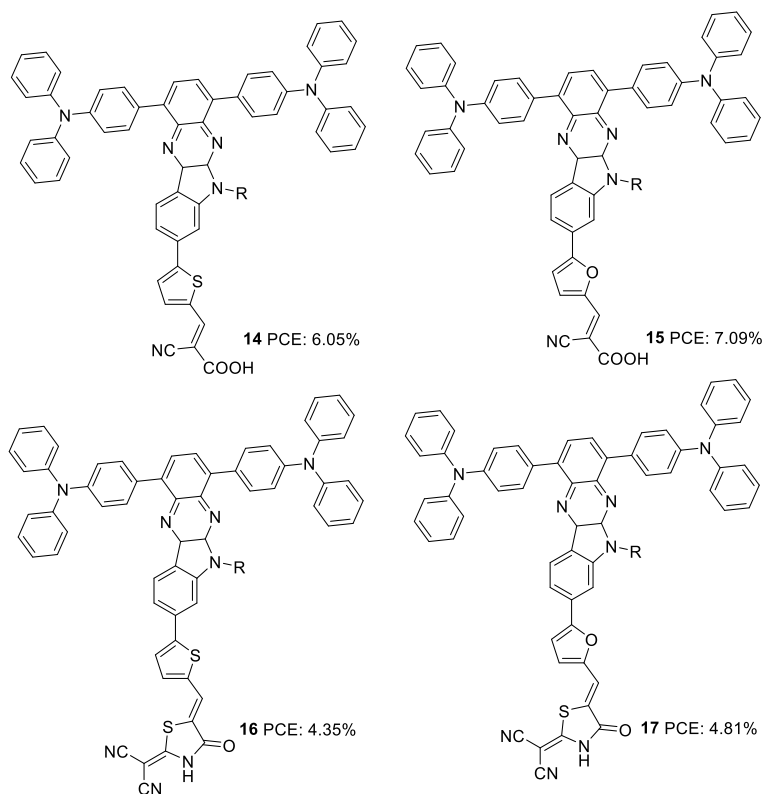


Figure 7. Photosensitizers **14-17** with indolo[2,3-*b*]quininoxaline core

Later, Su and co-workers introduced sensitizers **18-20** based on new molecular architecture, D-D|A- π -A (Figure 8).²⁷ Here, D|A represents the fused donor-acceptor unit, indolo[2,3-*b*]quinoxaline. The effect of additional donors was investigated systematically by introducing triphenylamine, carbazole and phenothiazine donors to the indole unit. More significant dye loading in devices based on **18** resulted in effective monolayer formation on TiO₂ surface, thereby preventing recombination effectively. This contributed to the highest open-circuit potential for devices fabricated using **18**. When it comes to photocurrent, the hexyl chains incorporated on the end donors of **19** and **20** helped decrease aggregations, contributing to improved J_{sc} . Maximum efficiency was delivered by **19** (2.72%), followed by **18** (2.65%) and **20** (2.61%). Later, these new generation D-D|A- π -A organic dyes were used successfully as co-sensitizers to improve the PCE of conventional Ru dye (**21**). The device fabricated with **21** alone showed an efficiency of 7.46%. Co-sensitization of **18-20** improved the efficiency in all three cases with a maximum of 7.94%, when **19** was employed as a co-sensitizer with **21**. An increment in open-circuit potential was observed with the co-sensitization approach, which could be attributed to the improved surface coverage of TiO₂, resulting in retardation of aggregation and recombination. When it comes to photocurrent, only the device with **19** as co-sensitizer showed an increment in current density from 19.00 mA/cm² to 19.37 mA/cm². More significant dye loading in the remaining cases might have resulted in competitive absorption at the overlapping regions between the Ru dye and organic co-sensitizer.

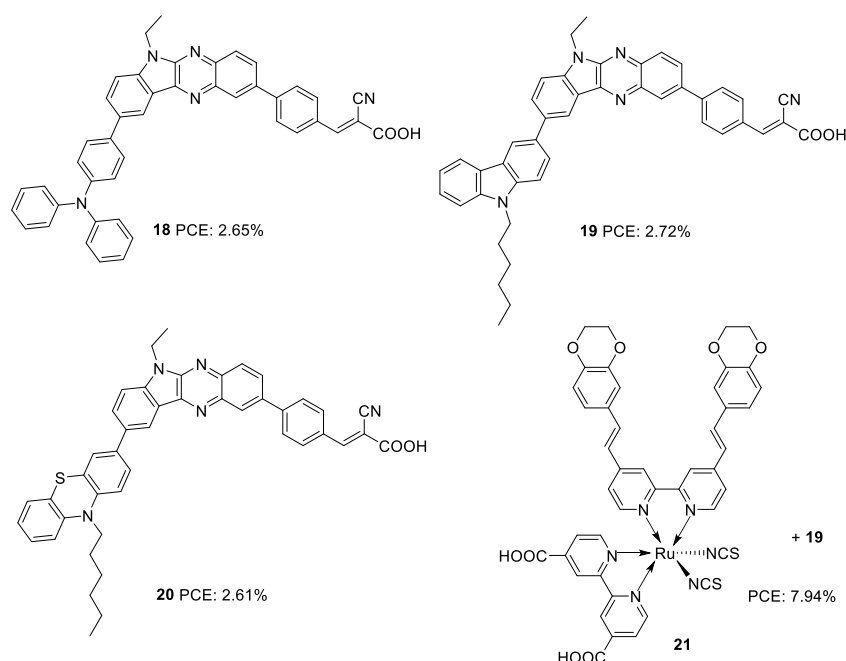


Figure 8. Photosensitizers with indolo[2,3-*b*]quinoxaline moiety and Ru-complex

Later, Su *et. al.* introduced a di-branched di-anchoring approach to the previous molecular architecture to develop D-D|A-(π -A)₂ dyes **22** and **23**, which differed in additional donors between triphenylamine and carbazole, respectively (Figure 9).²⁸ The performances were also compared with devices based on **19**. The dianchoring approach was found to help form adequate surface coverage, which is also evident from the higher dye loading present in these dyes. This could cause an increment in V_{oc} of dianchored dyes compared to **19** due to minimal recombination. Among the dianchored dyes, **23** with hexyl chain incorporated carbazole as the secondary donor exhibited highest V_{oc} . Dye **19** excelled when photocurrent is taken into account, which even contributed to higher PCE compared to the rest. The downfall in light-harvesting efficiency of **22-23** was brought about by the increased dihedral angle and strain induced by the di-anchoring branches. A more prominent donating ability of carbazole caused a slightly higher increment in J_{sc} of **23** compared to **22**. Co-sensitization of these dyes with **21** could enhance the efficiency with the highest PCE of 8.67% for **23**, followed by **13** (8.16%) and **19** (7.50%). While the considerably improved V_{oc} contributed the increment in device performance of co-sensitized **22-23**, a slight increment in current density for **19** caused a corresponding increment in PCE.

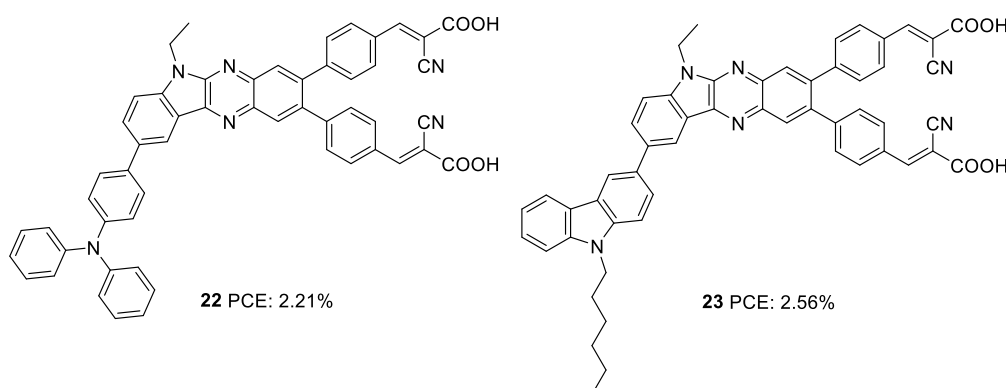


Figure 9. Photosensitizers **22-23** with indolo[2,3-*b*]quinoxaline moiety

In the subsequent work, the π -spacer in **18-20** was changed to thiophene from benzene, and the performance of the sensitizers (**24-26**) was evaluated under full sun illumination (Figure 10).²⁹ The dyes exhibited efficiencies in the range 4.92-5.27%, which was higher than previously reported sensitizers having phenyl as a spacer. Dye **24**, having triphenylamine as donor, displayed the maximum PCE of 5.27% with a V_{oc} of 0.67 V and FF of 70.1 with improved J_{sc} of 11.10 mA/cm². Higher dye loading seems to be responsible for improving FF and open-circuit potential for the triphenylamine donor dye **24**. Though the highest photocurrent was observed for **26** due to its increased light-harvesting ability, comparatively

lower values obtained for the rest of the parameters contributed towards inferior PCE of 4.92% for **26**. Co-sensitization of **21** with these dyes also resulted in improved V_{oc} and FF. In addition, the competition for light absorption resulted in a considerable reduction of photocurrent, leading to net poor performance for the co-sensitized device compared to the individual dyes.

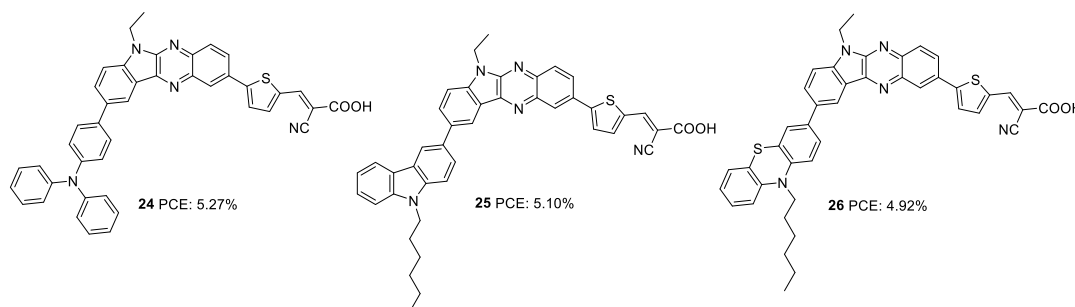


Figure 10. Photosensitizers **24-26** with indolo[2,3-*b*]quinoxaline moiety

It is clear that indoloquinoxaline is a potential scaffold for dye sensitizers in DSSC. The highest efficiency achieved so far using IQ based sensitizer is 8.2%, where the IQ unit and π -spacer (thiophene) is attached to either end of the auxiliary donor (phenothiazine) with cyanoacrylic acid as the acceptor unit. In the same architecture itself, optimum tuning of auxiliary donors and π -spacers along with the alkyl groups could render sensitizers capable of delivering more than 10% PCE. From the reported sensitizers using IQ, it is impossible to generalize suitable π -spacers for the system that could change depending on the donor attached to it and the IQ position (indole/quinoxaline end) to which it is attached. Many studies were not carried out in this direction of anchoring units, opening up further possibilities towards efficient IQ-based devices.

1.5.2 Indolocarbazole based sensitizers for DSSCs

Indolocarbazole, especially indolo[3,2-*b*]carbazole isomer, is a linear pentacene with two N-atoms with the possibility of introducing alkyl chains of any length requirement either to improve solubility or to prevent back electron transfer. When compared to carbazole, indolocarbazole possesses better energetics, improved electron-donating capabilities and superior absorption profiles. These characteristics find indolocarbazoles a unique position among various applications involving organic thin-film transistors, organic light-emitting diodes and photovoltaics.³⁰ Indolocarbazoles can be prepared either by Fischer indole synthesis of 1,4-bis(2-phenylhydrazono)cyclohexane or by Cadogen reaction of appropriate nitroarenes.³¹

Indolocarbazole was first used as a donor in DSSC by Zang *et al.* (Figure 11).³² They synthesized dyes **27** and **28**, which differ in the number of thiophene groups incorporated as the π -linker. While a red shift in the absorption profile was observed for **28** when adsorbed on TiO₂, higher electron injection efficiency was obtained for **27** sensitized devices. The trade-off between the two factors renders **28** with slightly higher J_{sc} compared to that of **27**. The difference in efficiencies of the two dyes was also brought about by the fill factor. While **27** possess FF of 0.67, the larger molecular size of **28** resulted in a FF of 0.62. This resulted in a higher PCE of 7.3% for **27** and 6.7% for **28**.

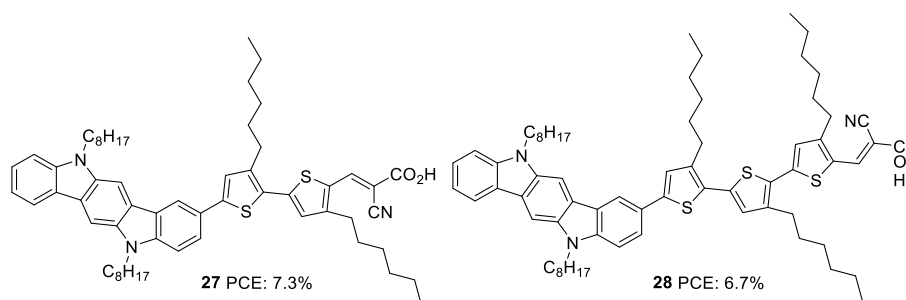


Figure 11. Photosensitizers **27-28** with indolocarbazole moiety

Cai *et al.* designed four dyes based on 5,7-dihexyl-6,12-diphenyl-5,7-dihydroindolo[2,3-*b*]carbazole (DDC) with benzothiadiazole (or thiophene) and thieno[3,2-*b*]thiophene (TT) (or thiophene) as π -spacer and 2-cyanoacrylic acid as acceptor (Figure 12).³³ Along with the high electron-donating ability, the fused carbazole systems also contribute towards improved π -conjugation, which will be advantageous in promoting the ICT and the photostability of the system. The two phenyl rings integrated on the donor DDC unit, and the alkyl groups on the nitrogen atom effectively reduced the aggregation and improved lifetime for devices fabricated with these dyes. The devices were also subjected to comparison with carbazole based D- π -A sensitizer **33**. The molar extinction coefficients of both ICT and π - π transition bands display significant enhancement in **29-32** compared to **33** indicating the improved light-harvesting ability of the new fused conjugated donor. Except for **31**, the J_{sc} value for all other dyes was higher than **33**. This is apparent from the IPCE spectra, where the performance follows the order **32**>**29**>**30**>**33**>**31**, which is consistent with the dye loading present in the fabricated devices. Though the V_{oc} value of **32** (674 mV) was not very high compared to **31** (768 mV), **32** exhibited the highest efficiency of 6.4% among these sensitizers with a J_{sc} of 13.96 mA/cm² and FF of 0.68. The photo-stability evaluation of the dyes by adopting the methods of Katoh and co-workers revealed that the new donor is

effective in stabilizing the cation formed after irradiation of light compared to the carbazole based dye. The benzothiadiazole containing dyes possess more stability which is consistent with the previous reports.³⁴ The results also paved the way to the observation that TT was also beneficial in contributing towards photo-stability. Compound **32**, having both BTD and TT as π -spacer, exhibited maximum photo-stability, while **29** was least stable among the indolocarbazole based dyes. All the dyes were also found to be thermally stable.

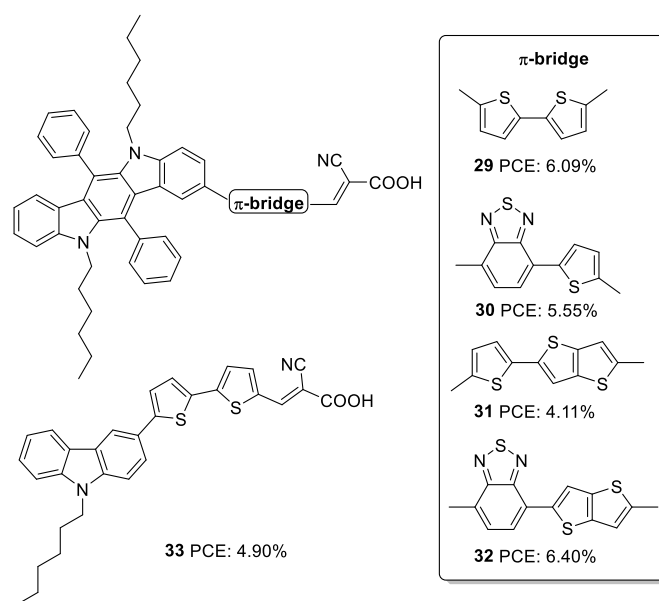


Figure 12. Photosensitizers with indolo[2,3-*b*]carbazole (**29-32**) and carbazole (**33**) units

The same group further attempted to introduce a bridge with extended conjugation to widen the absorption spectra of the indolocarbazole dyes (Figure 13).³⁵ Among the dyes, **36**, which contains benzothiadiazole as auxiliary acceptor along with alkylated thiophenes flanked on both sides, showed maximum red-shifted spectra followed by **35** having alkyl-substituted benzothiadiazole as auxiliary acceptor and **34** with simple D- π -A architecture having terthiophene as a spacer with a difference of 78 and 50 nm respectively compared to **36**. The device efficiency was tested under two conditions. In one case, the TiO₂ films were made of 3 μ m thickness with 13 nm sized nanoparticles (TSP) and scattering layer of 4 μ m thickness, and in the second case, the TiO₂ films were made of 3 μ m thickness with 13 nm sized nanoparticles (TSP) and scattering layer of 8 μ m thickness. Though higher dye loading is possible in the second case, a thick scattering layer can cause chances of recombination. This resulted in a trend of increase in current density and decrease in V_{oc} for all the dyes fabricated with 8 μ m scattering layer when compared to those of 3 μ m thickness. A trade-off between these two factors leads to higher PCE with a thicker scattering layer for all the dyes. In the

first condition, the highest IPCE value was obtained for **36** with an absorption maximum of 81.2% at 460 nm followed by **35** (77.2% at 500 nm) and **34** (69.9% at 520 nm). A more comprehensive absorption profile for **36** contributed towards the highest J_{sc} value of 14.91 mA/cm². The least J_{sc} value of 10.40 mA/cm² was obtained for **34** due to the narrow IPCE spectra resulting from a lower absorption profile. When devices were fabricated using 8 μ m scattering layer, dye **35** showed improved IPCE profile and J_{sc} value, while dye **36** resulted in lower molar extinction coefficients, low dye loading amount, and low electron injection yield. The trend in V_{oc} was the same in both the conditions with the least value delivered by **36**. While **35** excelled with the highest PCE of 7.49%, **34** delivered a lower photovoltaic performance of 6.01%. The stability studies reinforced the observation that BTD units are capable of increasing the photo-stability of dyes.

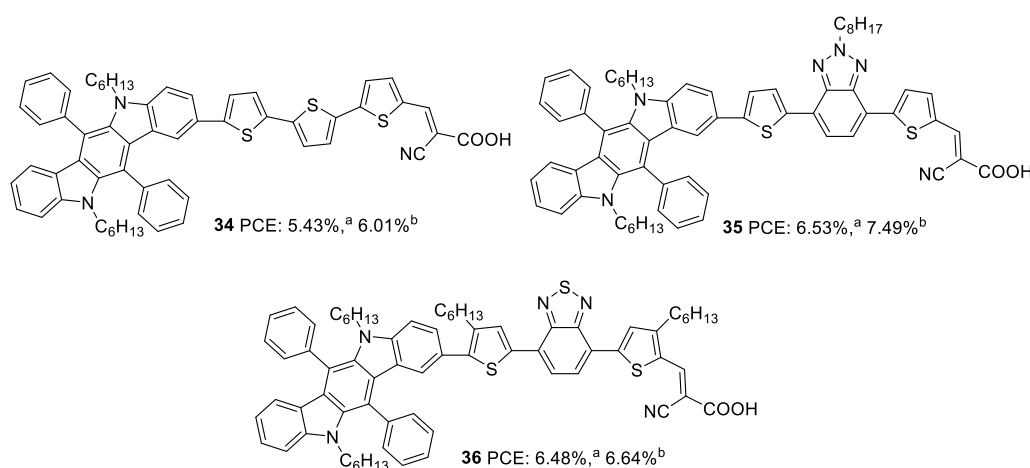


Figure 13. Photosensitizers **34-36** with indolo[2,3-*b*]carbazole moiety. ^aTiO₂ films were made of with 4 μ m thick scattering layer. ^bTiO₂ films were made with 8 μ m thick scattering layer. In both cases, the active layer was made of 3 μ m thick 13 nm particles

Later in 2016, Qian *et al.* investigated the same donor groups in a new photosensitizer design. They synthesized four dyes utilizing modified donor units (Figure 14) consisting of indolo[3,2-*b*]carbazole as the primary donor and groups such as ethylbenzene, *N,N*-diethylaniline, ethyloxybenzene, and octyloxybenzene graphed to indolo[3,2-*b*]carbazole as secondary donor groups, thiophene as the π -conjugated linker, and 2-cyanoacrylic acid unit as the electron acceptor/anchoring group.³⁶ The secondary donor groups assist in improving the donating strength of the system, but it was also highly beneficial in reducing the aggregation and recombination. Thus the nonplanar secondary groups could enhance the photovoltage of the device. The IPCE performance of the dyes parallels with the electron-donating ability of the secondary donor. The most robust donor, *N,N*-diethylaniline attached dye **38** displayed a

broad IPCE response and highest J_{sc} of 15.2 mA/cm² followed by **40**, **39** and **37**. The efficiency of the devices also follows the same trend, with **30** having the highest PCE of 8.09%, and the most deficient performance was showcased by **37** with 6.25%.

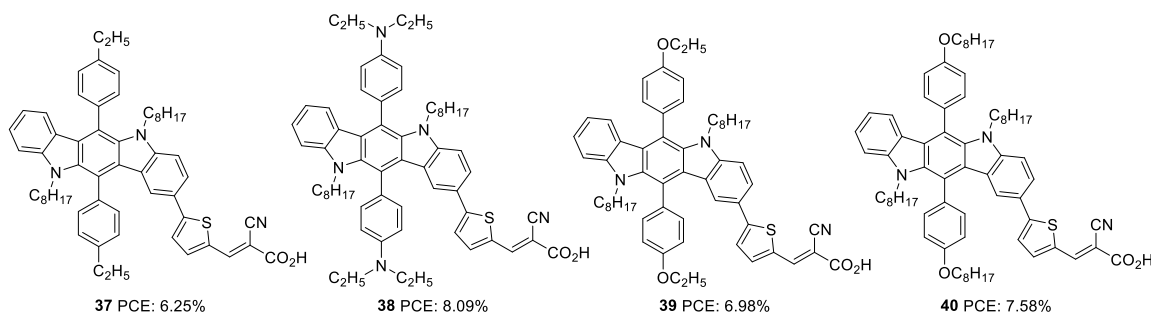


Figure 14. Photosensitizers **37-40** with indolo[2,3-*b*]carbazole moiety

Later, Xiao *et al.* also employed 6,12-diphenylindolo[3,2-*b*]carbazole as auxiliary donors in D-D- π -A dyes.³⁷ The sensitizers **41**, **42** and **43** differ in the donor groups: triphenylamine, trimethoxyphenyl and trimethoxybromine, respectively (Figure 15). Unlike the previous work, the additional donor and π -spacers were appended to the end of phenylene groups attached to the indolo[3,2-*b*]carbazole moiety. The ICT absorption bands of these compounds were not showing much difference compared to the π - π^* transition, which can be attributed to the interrupted charge transfer in the molecules resulting from the non-planar conformation of the attached phenyl groups. The absorption behaviour of the compounds was consistent with the electron-donating ability of the secondary donor. The triphenylamine donor in **41**, which has a higher electron-donating ability, contributed to the broader absorption and higher molar extinction coefficient for **41**, followed by **42** and **43**. Though these dyes could deliver reasonably good V_{oc} (0.61-0.75 V) and FF (0.69-0.74) using Γ/I_3^- electrolyte, a relatively low value of J_{sc} resulted in moderate PCE (1.65-3.11%). Dye **41** yielded the highest efficiency of 3.11% followed by **42** and **43**.

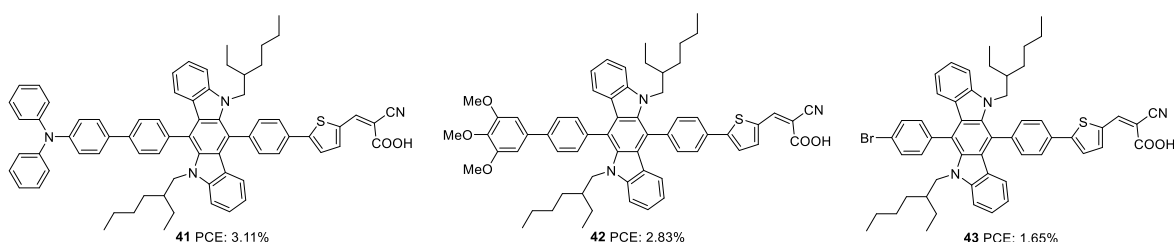


Figure 15. Photosensitizers **41-43** with indolo[2,3-*b*]carbazole moiety

Further investigations by the same group to increase the photoconversion efficiency of **41** resulted in the synthesis of **44** and **45** where triphenylamine donor was attached to indolo[3,2-*b*]carbazole via ninth and eighth positions, respectively (Figure 16).³⁸ Co-planarity and π -electron delocalization were found to improve, which is apparent from the absorption profile of the new dyes **44** and **45**. Dye **45**, where the phenylene/thiophene rings were connected onto the para positions of *N*-atom, showed more red-shifted absorption with an absorption maximum at 500 nm whereas, absorption of **44** was blue-shifted by 38 nm. While **44** showed improvement in PCE when it was used in conjunction with CDCA (10 mM), **45** responded in a reverse manner. This can be accounted for by the molecular orientation of the dyes when adsorbed on TiO₂. Dye **44** adopted a perpendicular orientation to the substrate plane. Somewhat hindered conformation of **45** resulted in more inclination of the dye towards the TiO₂ surface. This resulted in fewer aggregations and recombinations, making **45** capable of delivering more photocurrent even with a lower dye loading of 3.64×10^{-7} molcm⁻² compared to 4.54×10^{-7} molcm⁻² for **44** and without co-adsorbent CDCA. Photosensitizer **45** outperformed **44** with a J_{sc} of 12.85 mA/cm², V_{oc} of 0.72 V, FF of 0.69 and PCE of 6.34%. The co-sensitization of **44/45** further improved the performance to 7.03%.

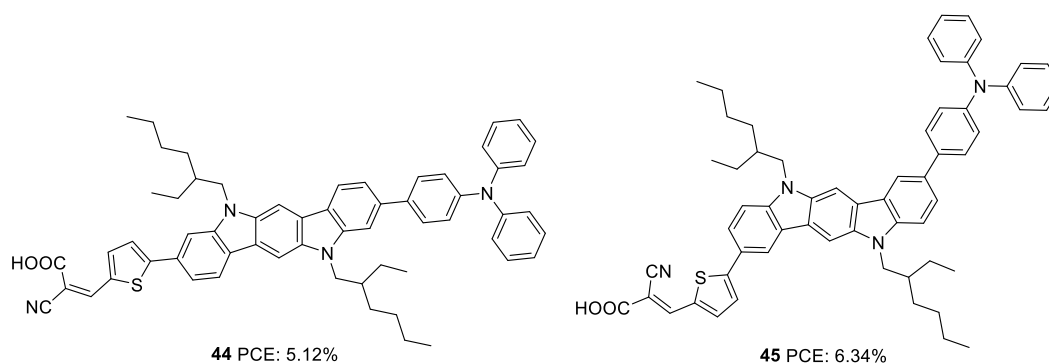


Figure 16. Photosensitizers **44-45** with indolo[2,3-*b*]carbazole moiety

Indolo[2,3-*b*]carbazoles were rarely explored for optoelectronic applications due to a lack of efficient synthetic strategies. Su *et al.* could establish new strategies for synthesising indolo[2,3-*b*]carbazoles and their utilization to construct DSSC sensitizers with a PCE of up to 6.02%.³⁹ The curved molecular conformation of indolo[2,3-*b*]carbazole dye synthesized by Su *et al.* (**46**), along with its rigid and planar nature, offer the possibility to be explored as a di-anchor dye. The sensitizer **46** adopt A- π -D- π -A architecture in which bithiophene is introduced as the π -bridge between the electron-rich indolo[2,3-*b*]carbazole core and cyanoacrylic acid acceptor unit (Figure 17). FTIR analysis of the pristine **46** and the compound loaded TiO₂ film reveals the involvement of both the carboxylic group in

anchoring the dye on the TiO₂ surface. This is further confirmed by the Deacon Philips rule, where a frequency difference of 224 cm⁻¹ suggests a bidentate binding mode for **46**. An efficient electron transfer from HOMO of **46**/(TiO₂)₇₀ (Indolo[2,3-*b*]carbazole) to the LUMO of **46**/(TiO₂)₇₀ (TiO₂ nano cluster) was illustrated using computational analysis.

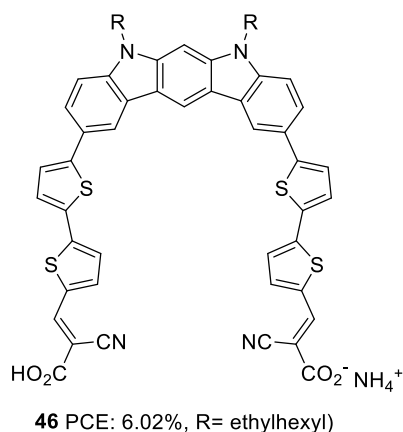


Figure 17. Molecular structure of photosensitizer **46**

Indolo[2,3-*a*]carbazole was first introduced in DSSC by Zhang *et. al.*⁴⁰ Taking this new system as a donor and cyanoacrylic acid as an acceptor, they studied the effect of conjugate mode of π -spacers such as thienyl-thieno[2,3-*b*]thiophene and terthiophene in photovoltaic performance (Figure 18). To control dye aggregation and prevent recombination, alkyl-substituted terthiophene was employed as π -spacers to construct **49**. Sensitizers **47** and **49** outperformed **48** in J_{sc} and V_{oc} . **48** gave an efficiency of 5.28%. The spatial effect of hexyl groups on the π -backbone of **49** resulted in the highest efficiency of 5.98% and the highest photocurrent and photovoltage, followed by **47** with 5.78% PCE.

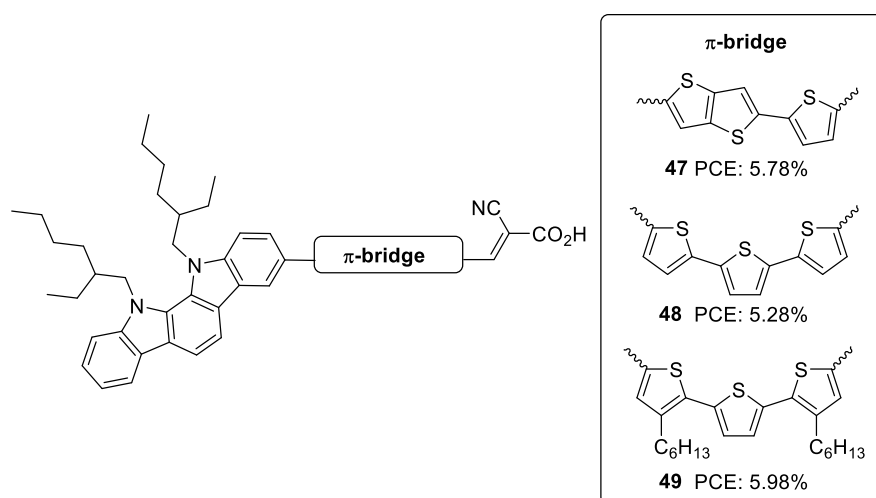


Figure 18. Photosensitizers **47-49** with indolo[2,3-*a*]carbazole moiety

Indolo[3,2,1-*jk*]carbazole is another positional isomer of indolocarbazole where indole is fused with the carbazole moiety in a slightly strained manner. The system was found to be thermostable and showcase strong electron-donating ability, which resulted in its application as charge transport materials and conducting film materials. Luo *et. al.* utilized this core for developing a sensitizer for DSSC by integrating it as a donor in a D- π -A architecture (Figure 19).⁴¹ They developed four devices based on the dyes **50-53**, which exhibited PCE in the range 1.59-3.68%. Among the dyes, **51** outperformed others with a PCE of 3.68%. With its lower stabilization energy, Thiophene enabled the system to have more delocalization and efficient light-harvesting ability. This can be accounted for by the enhanced photocurrent in dyes **51** and **53** using thiophene as the π -linker. Low spectral coverage leads to decreased performance in **50** and **52**. Even an attempt to increase the π -bridge conjugation by introducing the phenyl group in **52** was not found to be an effective strategy to increase the PCE.

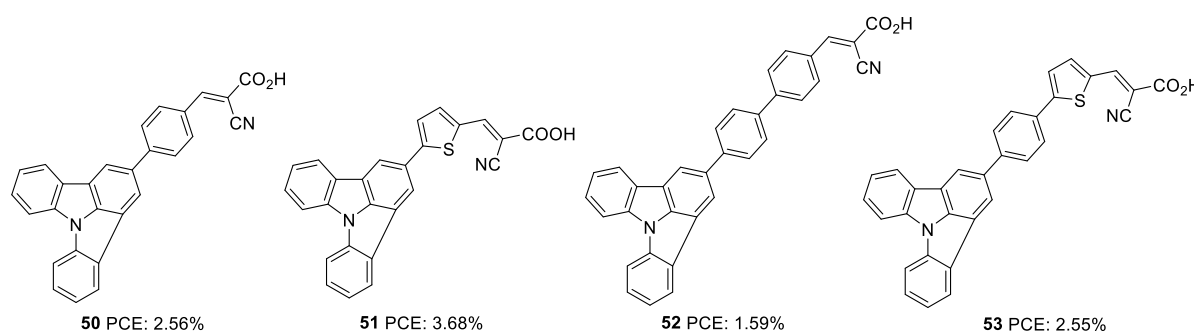


Figure 19. Photosensitizers **50-53** with indolo[3,2,1-*jk*]carbazole moiety

Further attempts were carried out to investigate the effect of π -linkers on the performance of indolo[3,2,1-*jk*]carbazole based dyes by Cao *et al.* (Figure 20).⁴² Dyes **54** and **55** incorporate bithiophene and unsubstituted bithiophene, respectively as π -linkers. The slightly twisted conformation of **55** resulted in lower dye loading on TiO_2 than **54**, resulting in a slight increment in J_{sc} value for **54**, the reverse trend of what was observed for V_{oc} . The significant improvement in J_{sc} of **54** based device, when adsorbed with CDCA, illustrates the aggregation tendency of these sensitizers on TiO_2 . While **54** based devices delivered PCE of 4.68% in the presence of 10 mM CDCA, dye **55** could yield 4.66% with 1 mM CDCA.

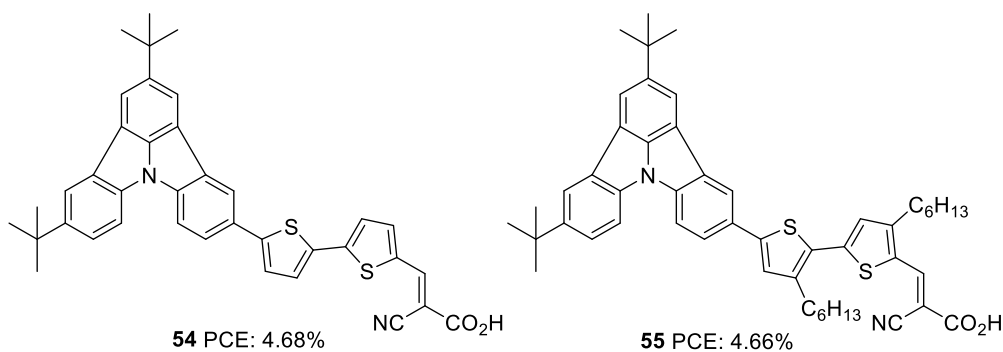


Figure 20. Photosensitizers **54-55** with indolo[3,2,1-*jk*]carbazole moiety

Among different isomers of indolocarbazole, indolo[3,2-*b*]carbazole is the most explored isomer for DSSC applications. The comparison of efficiency versus structure reveals that to improve the device's performance, systematic investigation of the position of attachment of π -spacer and the additional donor on indolo[3,2-*b*]carbazole is also needed, along with the integration of suitable donor and spacer groups. From the reported data so far, the substitution of donor and spacer unit at the second and eighth position of indolo[3,2-*b*]carbazole is more effective than substitution ninth and third. When the donor group was changed to DDC, the additional phenyl groups integrated at sixth and twelfth were found to prevent recombination while preserving the donating ability and the backbone's planarity. However, attempts to increase the light-harvesting by allowing modifications at these phenyl groups could not lead to as expected due to the non-planar confirmation of the phenyl groups as seen in the case of dyes **41** and **42**.

1.5.3 Triazatruxene based sensitizers for DSSCs

Triazatruxene (TAT) is an expanded π -conjugated system with good electron-donating capacity, consisting of three indole units combined using one benzene ring. Due to its favourable features such as electron richness and rigid π -extended structure, it has found application in various optoelectronic fields like organic field-effect transistors (OFETs), organic light-emitting diodes (OLEDs), two-photon absorption (TPA) materials, non-linear optics and liquid crystal displays⁴³ The most widely used method for the synthesis of TAT is by the reaction between indole and indolone in the presence of bromine and POCl_3 .⁴⁴

The first attempt to use TAT as a donor in DSSC was reported by Qian *et al.*⁴⁵ They succeeded in developing three D- π -A dyes (**56**, **57**, **58**) with variable π -spacers achieving more than 5% efficiency. These dyes were made using TAT as the donor and cyanoacrylic acid as the acceptor/anchoring group (Figure 21). The system's efficiency was studied by

changing the π -spacers (thiophene **56**, furan **57** and benzene **58**). Though high open-circuit voltage was found in dye **58**, with a reduced current density, devices fabricated with **58** only realized a low PCE of 5.11%. The highest efficiency of 6.1% was contributed by the device fabricated using dye **56**. The higher PCE resulted from higher current density showcased by **56**, which was also evident from the IPCE response. Better electron delocalization and superior electron-donating capabilities render the TAT system improved light-harvesting behaviour to be used as an efficient sensitizer in DSSC.

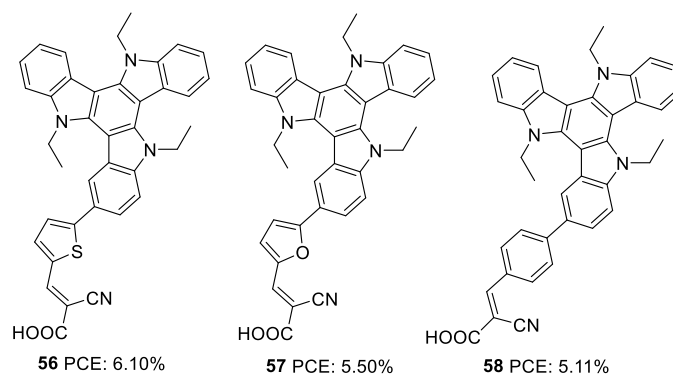


Figure 21. Photosensitizers **56-58** with triazatruxene moiety as a donor

As an extension of the previous experiments, the effect of rhodanine-3-acetic acid as an electron-withdrawing/acceptor group was studied by the same group (Figure 22).⁴⁶ Though much broader absorption was obtained for dyes with rhodanine-3-acetic acid, the performance of these dyes was inferior to the dyes being synthesized using cyanoacrylic acid as the electron-withdrawing group. This is attributed to the interruption of electron transfer from the dyes to the semiconductor by the broken (NCH₂COOH) conjugation in rhodanine-3-acetic acid. Instead of displaying broader absorption spectra with higher ϵ , devices fabricated using **59** showed lower current density. The trend can be rationalized from the LUMO energy level of the dyes, which are in the order of **60** (-1.16 V) > **59** (-1.02 V), indicating more effective electron injection from **60** to the semiconductor. Thus **60** could yield a higher PCE of 3.60% with a short-circuit photocurrent density of 8.33 mA/cm², an open-circuit photovoltage of 617 mV, and a fill factor of 0.70.

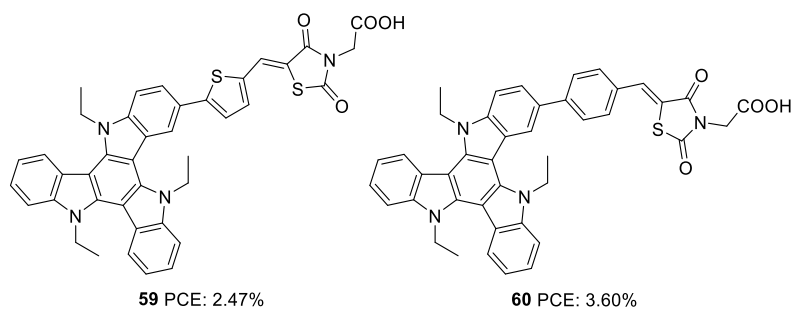


Figure 22. Photosensitizers **59-60** with triazatruxene moiety as a donor

Triazatruxene was incorporated as a donor in D-A- π -A based sensitizers by Pan and co-workers in 2018 (Figure 23).⁴⁷ These sensitizers employed benzothiadiazole as auxiliary acceptor, and they introduced variation in acceptors (carboxylic acid and cyanoacrylic acid), and the connectivity between the donor and auxiliary acceptor was modified using single bond and ethynyl linkages. The introduction of ethynyl linker and cyanoacrylic acid were found to increase the conjugation of the dye molecules. Dyes **62** and **64** having cyanoacrylic acid as the acceptor group showed better light-harvesting capability with broader absorption and higher IPCE value. These observations also reflected in the J_{sc} value of the corresponding sensitizers. Another critical parameter that determines the efficiency of the system is the V_{oc} . Dyes **61** and **63** with single carboxylic acid acceptor exhibited higher photovoltage compared to the rest. Among the two sets of D-A- π -A sensitizers having triazatruxene donor (single bonded and ethynyl bridged), dyes **61** and **64** showed maximum efficiencies of 7.51% and 7.26%, respectively, which indicates that a delicate balance between J_{sc} and V_{oc} are essential to obtain higher power conversion efficiencies.

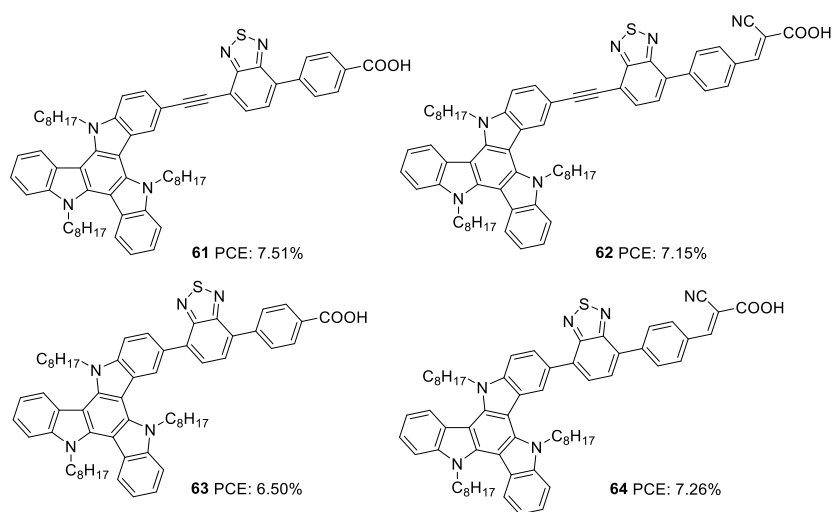


Figure 23. Photosensitizers **61-64** with triazatruxene moiety as a donor

Qian and co-workers used triazatruxene as a secondary donor to construct porphyrin-based sensitizers (Figure 24).⁴⁸ Triazatruxene was attached directly to the meso-position of the porphyrin ring, and two variants were synthesized by changing the acceptor groups (carboxylic acid and cyanoacrylic acid). When cyanoacrylic acid was employed as an acceptor group, improvement was found in the dye's light-harvesting ability, which is evident from the broader and enhanced IPCE spectra resulting in a higher J_{sc} value dye. The V_{oc} value also follows the same trend, which resulted in a maximum PCE of 6.05% for **66**. The efficiencies of both dyes were found to improve when co-adsorbent chenodeoxycholic acid (CDCA) was used, which implies the possibility of intermolecular aggregation of the dyes on the TiO_2 surface.

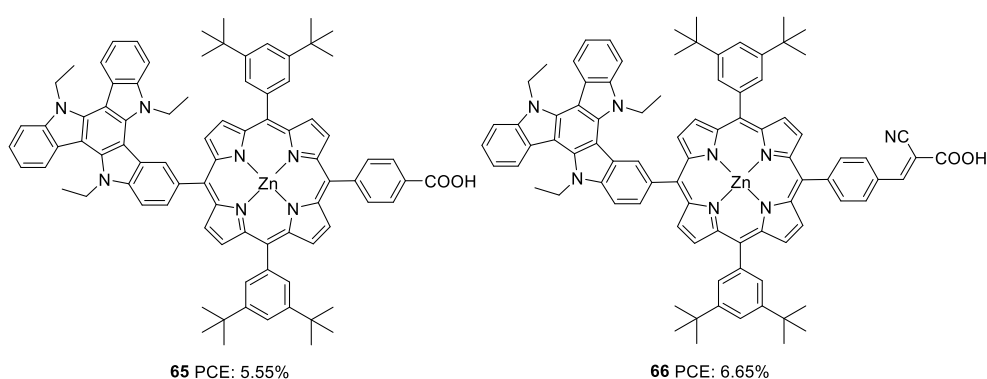


Figure 24. Photosensitizers **65-66** with triazatruxene moiety as secondary donor and porphyrin ring as primary chromophore

Qin *et. al* also incorporated TAT to the meso-position of the porphyrin chromophore to obtain **67** (Figure 25).⁴⁹ Dye **67**, which was used in ssDSSC, spiro-MeOTAD being the HTM showcased an efficiency of 5.2 % in the presence of co-adsorbent CDCA.

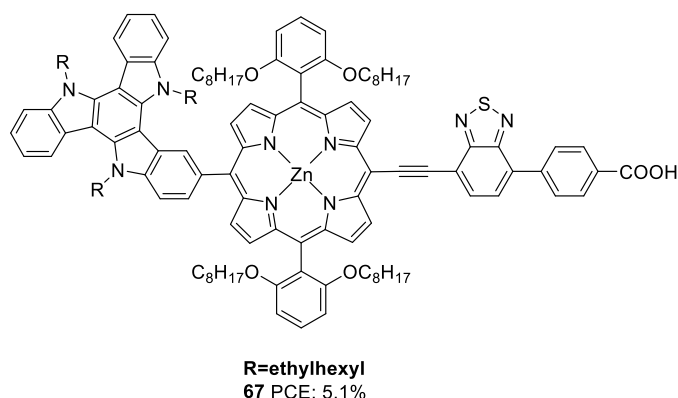


Figure 25. Photosensitizer **67** with triazatruxene moiety as a secondary donor and porphyrin ring as primary chromophore

The most efficient DSSC's based on TAT molecules were reported by Zhang and co-workers.⁵⁰ They systematically modified the D- π -A backbone and developed two dyes employing TAT as donor, 4,7-Bis(4-hexylthiophen-2-yl)benzo[c][1,2,5]thiadiazole (BTBT) as π -bridge and 4-ethynyl benzoic acid (EBA) as acceptor, which differs in the linkage between the donor and π -bridge (Figure 26). The study aimed to evaluate the effect of the rigid single bond and flexible z-type double bond on various parameters that determine the efficiency of the device. The optimized devices based on **68** and **69** achieved PCEs of 13.6% and 12.8%, respectively, using cobalt-based redox electrolyte ($[\text{Co}(\text{bpy})_3]^{+2/+3}$). Though the double bond was found to widen and enhance the absorption of the molecules, the J_{sc} value for **68** was found to be higher than **69**, which resulted from the more significant dye loading observed for the former. Devices fabricated using **68** also showcased better open-circuit potential (956 mV) than **69** (887 mV). The efficient electron injection in **68**, evident from the femtosecond transient absorption and up-conversion fluorescence studies, reinforces the observation mentioned earlier. Dye **68** and **69** were also applied to ssDSSC using spiro-OmeTAD as the hole transporting material (HTM).⁵¹ Longer electron lifetime and high regeneration efficiency caused **68** to outperform **69** with a PCE of 6.6%. Dye **69** exhibited a PCE of 5.4% .

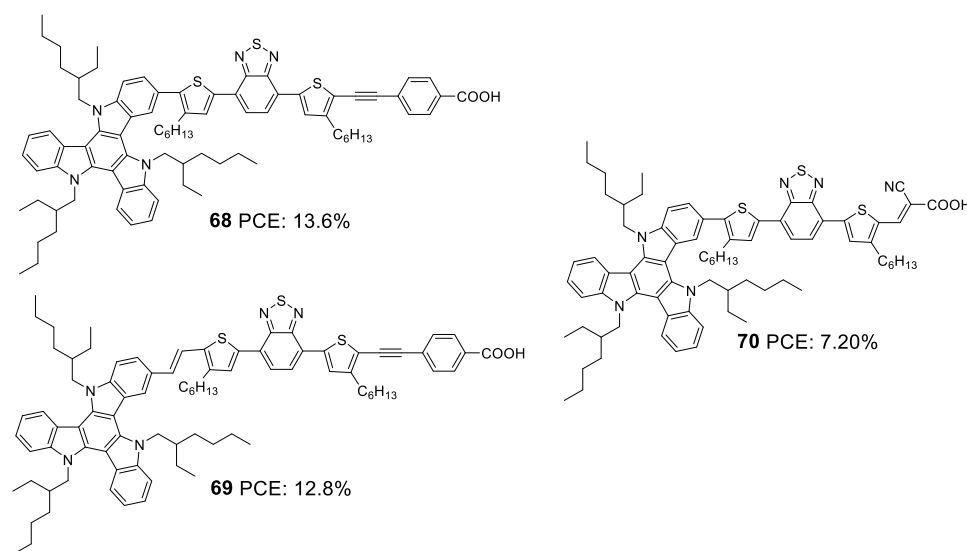


Figure 26. Photosensitizers **68-70** with triazatruxene moiety as a donor

In order to probe the effect of rigid 4-ethynylbenzoic acid acceptor group in **68**, dye **70** was synthesized by the same group (Figure 26) with Z-type cyanoacrylic acid and fabricated devices using cobalt-based redox electrolyte ($[\text{Co}(\text{bpy})_3]^{+2/+3}$).⁵² Higher dye loading, better light-harvesting ability and improved electron injection efficiency made **68** deliver the

highest efficiency of 13.4%, while there was a drastic drop in PCE for **70**, which could only afford a PCE of 7.2%. This again clearly illustrates that rigid structures are pertinent when it comes to designing sensitizers that will be beneficial to reduce energy loss during electron injection, leading to improved current density and photovoltage. Fine-tuning of the molecular backbone without compromising the energetics is highly required to realize higher PCE.

Later, Li *et al.* tried to improve the efficiency of **68** by developing two modified dyes **71** and **72** using TAT donor (Figure 27).⁵³ While benzothiadiazole (BT) functions as the auxiliary acceptor in **71**, and BT was replaced with difluorobenzo[*c*][1,2,5]thiadiazole (DFBT) in **72**. The attempt to introduce fluorine on BT was justified by lowering the LUMO level of the molecule by the electron-withdrawing (inductive) effect of fluorine. The electron-donating mesomeric effect was found to dominate the former. This renders **72** with a large band gap and blue-shifted absorption spectrum compared to that of **71**. The higher dye loading in **71** (1.4 times) and wider absorption band compensated the reduction in molar extinction coefficient, resulting in a higher J_{sc} of 15.1 mA/cm². This ended up in maximum efficiency of 10.2% for **71** and a lower efficiency of 8.6% for **72** using cobalt-based redox electrolyte ([Co(bpy)₃]^{+2/+3}).

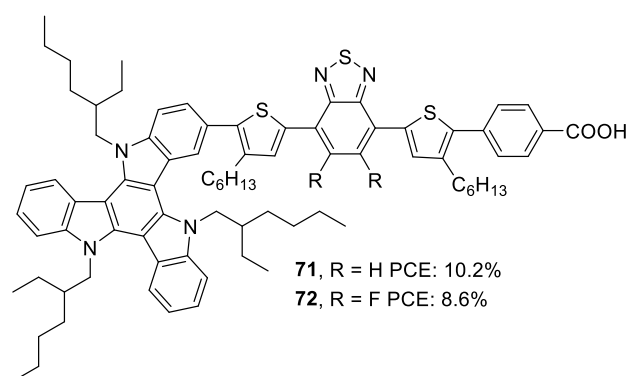


Figure 27. Photosensitizers **71-72** with triazatruxene moiety as a donor

Yao *et al.* found that introducing bulky groups on TAT successfully hindered dye aggregation and recombination (Figure 28).⁵⁴ They synthesized two modified TAT sensitizers (**73** and **74**) having a more conjugated TAT donor unit. Their attempt resulted in a larger V_{oc} for **73** (926 mV) and **74** (911 mV). Higher dye loading in **73** compared to **74** allowed adequate coverage of semiconductor surface, abating the chances of dark current formation (recombination), leading to higher V_{oc} . DFT studies also revealed more planar conformation for **74** than **73**, which confirms the slightly red-shifted absorption profile of **74**. It was also observed that there was an upshift in HOMO level for **74**, which affected the regeneration

rate of dye adversely. Poor regeneration and lower dye loading resulted in lower current density and V_{oc} for **74** compared to **73**. Thus, PCE of 11.7% and 10.6% were obtained for **73** and **74**, respectively.

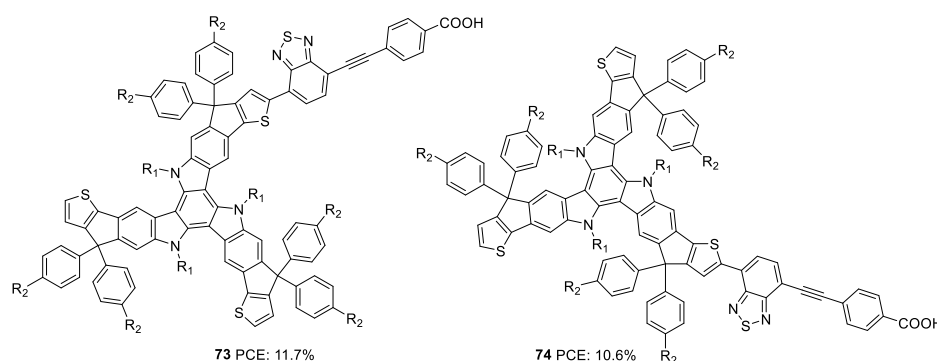


Figure 28. Photosensitizers **73-74** with triazatruxene moiety as a donor

Triazatruxene was incorporated as a donor in D- π -A dyes and studies were done to evaluate the effect of different π -spacers and anchoring groups. When it comes to the anchoring group, cyanoacrylic acid has proved to outperform other acceptor units (Rhodanine-3-acetic acid, carboxylic acid) in terms of light-harvesting and electron injection capability, which is consistent with the many reports available. Though devices based on thiophene bridged dye **56** could showcase higher PCE than those of phenyl substituted dye **58**, this trend reverses when the anchoring group was changed to rhodanine-3-acetic acid. Devices fabricated with phenyl bridged dye **60** delivered higher PCE with higher J_{sc} and V_{oc} compared to those of **59** with thiophene spacer. This implies that selecting a suitable π -spacer depends on the other components of the molecular architecture. Introduction of auxiliary acceptor improved the photovoltaic parameters, and the highest efficiency achieved so far using metal-free dyes is from devices based on **68** (13.6%) where BTBT was used as the π -bridge. The takeaway from the consecutive studies performed by Zang and co-workers is that molecular engineering has to be done in such a way as to reduce energy loss during electronic transitions, which could, in turn, lead to efficient PCE.

1.5.4 Indeno[1,2-*b*]indole based sensitizers for DSSCs

Indeno[1,2-*b*]indole consists of an indole unit fused with an indene moiety, making it planar and electron-rich with efficient electron delocalization. In addition to the alkylation of the *N*-atom in the tetracene, the indene unit also offers the flexibility to be alkylated. This possibility has a positive effect on the photovoltaic performance as the presence of multiple alkyl groups increases the solubility of indeno[1,2-*b*]indole based dyes and prevents its

aggregation. At the same time, the presence of alkyl groups is also effective in blocking the approach of the oxidized species coming close to the semiconductor and thereby improving lifetime. The well-established synthetic route towards preparing this tetracene is by the Fisher indole synthesis involving indanone and phenyl hydrazine.⁵⁵

The first report on the use of indeno[1,2-*b*]indole as a donor in DSSC came in 2016 by Qian *et al.*⁵⁶ They designed four dyes (Figure 29) based on D- π -A design, and the basic skeleton employs indeno[1,2-*b*]indole as a donor and cyanoacrylic acid as the acceptor. Tuning of device performance was carried out by changing the π bridges (furan and thiophene) and introducing alkyl groups (ethyl and hexyl) on the indene ring. The attached alkyl groups were at a particular angle with the molecular plane, which was beneficial in reducing aggregation of dyes and thereby increasing the PCE. All four dyes exhibited good power conversion efficiency in the range 6.52-7.64%. Among these dyes, the sensitizer **76**, featuring furan as the π -spacer and ethyl groups as the alkyl chain, contributed the highest PCE of 7.64% with a J_{sc} of 15.8 mA/cm² and a V_{oc} of 763 mV.

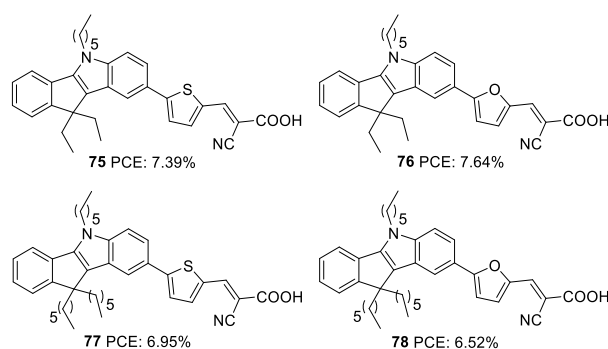


Figure 29. Photosensitizers **75-78** with indeno[1,2-*b*]indole moiety as a donor.

Qian and co-workers later designed three more dyes with indeno[1,2-*b*]indole as the donor to investigate the role of different acceptor groups on the photovoltaic performance of devices.⁵⁷ The synthesized D- π -A dyes had indeno[1,2-*b*]indole as donor and benzene as the π -bridge. The dyes differed in the acceptor groups incorporated, which were cyanoacrylic acid, rhodanine-3-acetic acid and 2-(1,1-dicyanomethylene)rhodanine (DCRD) respectively (**79**, **80** and **81**) (Figure 30). The results revealed better PCE for devices fabricated using dye having cyanoacrylic acid as the acceptor over the other two groups. Though dye **79** showed blue-shifted absorption, it contributed towards the highest efficiency of 6.29% with better J_{sc} and V_{oc} compared to other dyes. To assess the effect of different π -spacer on the DCRD acceptor, dye **82** was synthesized with thiophene as the π -bridge. The introduction of thiophene increased the efficiency of **81** from 3.60% to 5.41%, illustrating the importance of

tuning the π -spacer of the sensitizer while changing the acceptor functionality in a way to achieve higher PCE.

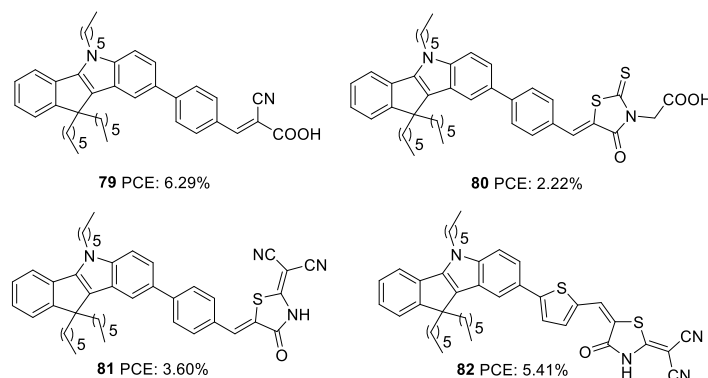


Figure 30. Photosensitizers **79-82** with indeno[1,2-*b*]indole moiety as a donor and variable acceptor groups

Yan *et al.* later designed and synthesized indeno[1,2-*b*]indole based D- π -A dyes with extended conjugation of π -spacer by introducing ethynyl group and variation of π -spacer and auxiliary acceptor. To this end, they constructed D- π -A dyes, which employ indeno[1,2-*b*]indole as the donor and cyanoacrylic acid as the acceptor group (Figure 31).⁵⁸ The dyes **83** and **84** vary in the π -bridge between benzene and thiophene, respectively. They also incorporated the ethynyl group as the linker between the donor and π -spacer to decrease the repulsion and increase the conjugation of the dye molecules. A third dye, **85** with benzothiadiazole as the auxiliary acceptor, was developed to compare with the previous set realizing D- π -A architecture. The dye with an auxiliary acceptor (**85**) was found to deliver the highest efficiency with the highest J_{sc} and V_{oc} . Among the D- π -A dyes, thiophene substituted dye **84** showed the highest efficiency with significantly improved current density, though V_{oc} was highest for the benzene substituted dye **83**. Co-sensitization of **84** and **85** outperformed all other dyes delivering an efficiency of 8.37%. This is attributed to the increment in the J_{sc} value of the device.

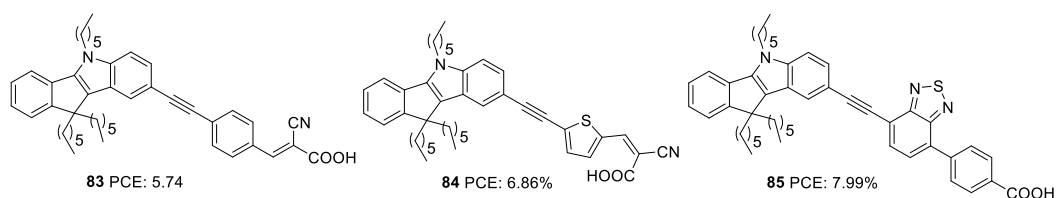


Figure 31 Photosensitizers **83-85** with indeno[1,2-*b*]indole moiety as a donor

Dai and co-workers first synthesized indeno[1,2-*b*]indole-spirofluorene (IISF) and used it as a donor unit in DSSC dyes. This molecular engineering was carried out to combine the electron-donating ability of the indenoindole with the steric effect of the spirofluorene.⁵⁹ They were successful in developing two dyes, **86** and **87**, with IISF as the donor, dithieno[3',2'-b:2',3'-d]pyrrole (DTP) as π -bridge and cyanoacrylic acid as acceptor (Figure 32). The dye **87** also employs 2,1,3-benzothiadiazole (BTD) as an auxiliary acceptor. Both **86** and **87** delivered efficiencies above 8%, which was further enhanced with the combined effect of co-adsorption with CDCA and co-sensitization with **88**. The highest efficiency of 9.56% was obtained from the co-sensitization of **86** with **88** in the presence of co-adsorbent, CDCA.

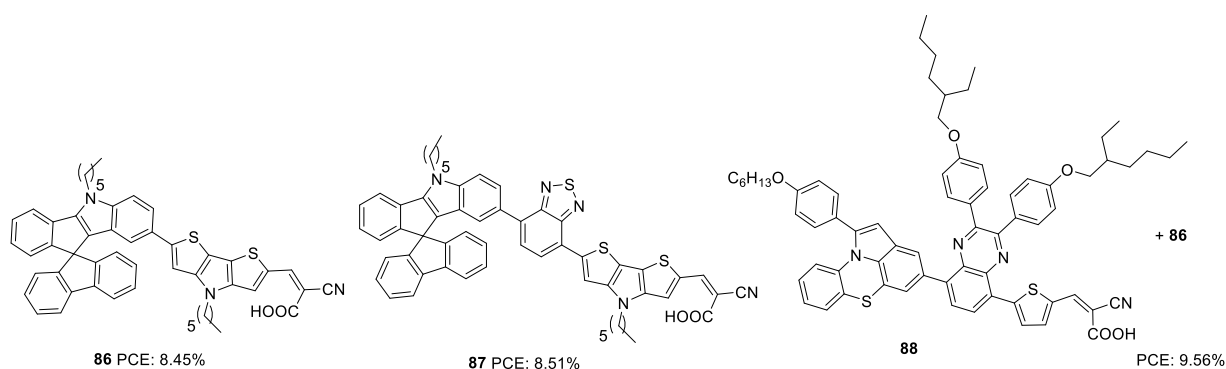


Figure 32. Photosensitizers **86-87** with indeno[1,2-*b*]indole-spirofluorene moiety as a donor

Later the same group synthesized two sets of dyes based on IISF to study the effect of position of attachment of π -spacer to IISF (indole/indene end) and the effect of the additional donors (Figure 33).⁶⁰ The D- π -A dyes **89** and **91** consists of IISF as the donor, thiophene as π -spacer and cyanoacrylic acid as acceptor. While thiophene is attached to the indene ring in **89**, dye **91** is having π -spacer attached to the indole end. Additional donor group (hexyloxydiphenylamine) was attached to **89** to obtain **90**, and dye **92** as the latter's regioisomer. Dyes with additional donors exhibited bathochromic as well as intensified spectra compared to D- π -A dyes. Among the two regioisomers, the one with π -spacer attached to the indole end of IISF is seen to facilitate more ICT transition. The IPCE spectra of **90** and **92** showed wider but downshifted absorption behaviour than **89** and **91**. A higher adsorption angle of **89** (41.83°) and **91** (42.33°) helped them to achieve higher dye loading of 115.83 and 118.14 nmol/cm², respectively. The bulkier donor group in **90** and **92** caused decreased dye loading compared to their D- π -A counterpart, but **92** managed to obtain 77%

dye loading of **91** due to its larger adsorption angle (49.5°). Though dye loading was lower for **92** (90.97 nmol/cm^2) than **89** and **91**, the broader absorption could compensate it for having the highest J_{sc} (13.52 mA/cm^2). While **89** and **91** exhibited comparable J_{sc} of 11.59 and 12.43 mA/cm^2 , respectively, **90** delivered the least J_{sc} value of 6.84 mA/cm^2 . Apart from the lower dye loading, the weak driving force for degeneration also caused the downfall in current density for **90**. This was again illustrated by changing alternate electrolytes for device fabrication which are having lower oxidation potential than $[\text{Co}(\text{phen})_3]^{2+/3+}$ (0.56 V for $[\text{Co}(\text{bpy})_3]^{2+/3+}$, and 0.43 V for $[\text{Co}(\text{dmbpy})_3]^{2+/3+}$). The current density of **90** increased in the order $[\text{Co}(\text{dmbpy})_3]^{2+/3+} > [\text{Co}(\text{bpy})_3]^{2+/3+} > [\text{Co}(\text{phen})_3]^{2+/3+}$. While the bulky hexyloxy diphenyl helped **92** alleviate recombination and achieve higher V_{oc} , the same group adversely affected the V_{oc} in **90** by breaking the compact layer formed by dye **89**. A trade-off between J_{sc} and V_{oc} in **89** and **91** lead to comparable efficiencies for them. While **92** showcased the highest PCE of 7.40% , dye **90** delivered the lowest PCE of 6.84% . Co-sensitization of **92** was carried out with **89/91**. In both cases, increment in current density was observed, **91/92** being the combination with the highest PCE (8.32%)

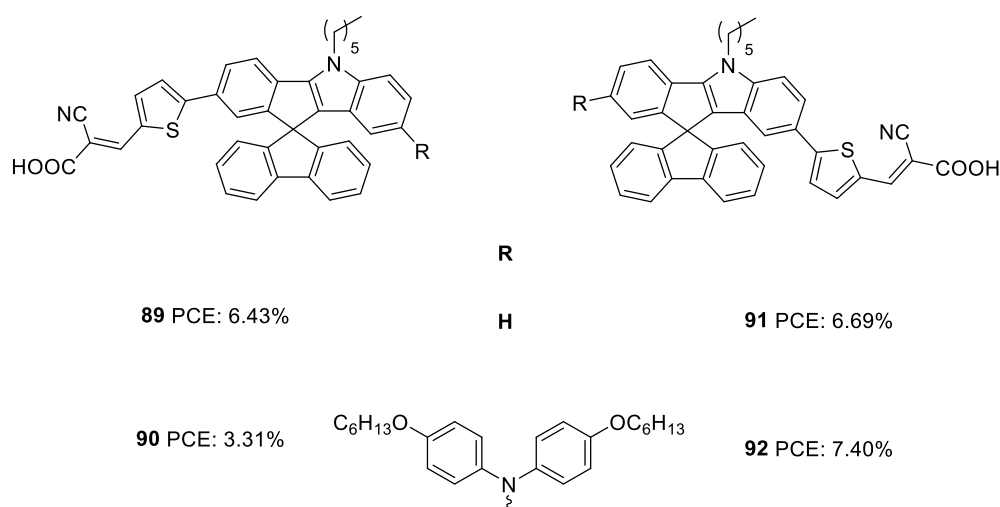


Figure 33. Photosensitizers **89-92** with indeno[1,2-*b*]indole-spirofluorene moiety as a donor.

On comparing the sensitizers **77**, **78** and **79** having the same dye skeleton and differing only in their π -spacer, sensitizer **77** having thiophene as the π -spacer outperformed the rest of the dyes with higher current density. Though sensitizer **79** was having higher V_{oc} , the least PCE was delivered due to lower current density. A triple bond was introduced between the indenoindole unit and π -spacer in **77** and **79** to furnish **84** and **83**. Though the motive was to increase the conjugation and PCE of the devices, it was found to showcase low PCE

compared to its predecessor. Though the new structure could bring about an increment in V_{oc} , current density followed the reverse trend.

1.5.5 Thieno[3,2-*b*]indole (TI) and thieno[2,3-*b*]indole based sensitizers for DSSCs

In thieno[3,2-*b*]indole (TI), an electron-rich system like thiophene is fused to the five-membered ring of the indole moiety at the 2-3 positions. It has been proved that thieno[3,2-*b*]indole is a better donor than both indole and carbazole units. The introduction of thieno[3,2-*b*]indole as a component in the dye design would certainly improve photovoltaic performance due to the co-planarity and strong electron-donating ability of these heteroacenes. Thieno[3,2-*b*]indole moiety can be easily synthesized using Cadogen reaction of suitable functionalized 2-(2-nitrophenyl)thiophene.⁶¹

The first report of thieno[3,2-*b*]indole based DSSC was reported by Zang *et al.* in 2010.⁶² They synthesized three dyes (**93**, **94** and **95**) employing 4-ethyl-4*H*-thieno[3,2-*b*]indole moiety as an electron donor, *n*-hexyl substituted oligothiophene units as a π -spacer and cyanoacrylic acid as an electron acceptor/anchoring group (Figure 34). A comparison was also made with dyes having *N*-ethyl carbazole, which consists of the same dye skeleton.⁶³ The electron lifetime measurement values obtained for TI based devices are lower than their parent D- π -A carbazole dyes, leading to lower V_{oc} for these devices, having the least value of 660 mV for **95** based device. According to the DFT calculations, the dihedral angle between the thienyl group and the donor part is found to be less for TI based sensitizers in comparison to that of carbazole dyes. This increase in planarity and better electron-donating capabilities reflected on the broader absorption spectra and higher ϵ values displayed by dyes employing thieno[3,2-*b*]indole as the donor unit. This resulted in an increment in current density, which was in line with the increment in the number of thiophene groups in the π -backbone. Among the TI dyes, **94** exhibited a higher PCE of 7.8%, and the minor performance was delivered by **95** (7.3%). An increase in the number of thiophene moieties resulted in higher HOMO levels for **95**. Though this tendency could produce low bandgap sensitizers with better light-harvesting, a decrease in driving force for dye regeneration and the chances of recombination of injected electrons with the oxidized dyes may be responsible for decelerating the performance of **95**.

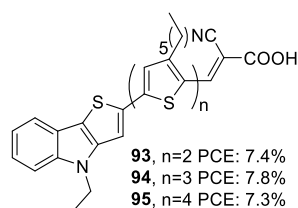


Figure 34. Photosensitizers **93-95** with thieno[3,2-*b*]indole moiety as a donor

The role of thieno[3,2-*b*]indole (TI) as a π -spacer was demonstrated successfully by Kim and co-workers.⁶⁴ In their initial work, they designed and synthesized D-A- π -A sensitizers using TI (**97**, **98**) as π -spacer and a comparative investigation were made between dyes with thieno[3,2-*b*]benzothiophene (TAB) as π -spacer (**96**) (Figure 35). The more electron-donating nature of TI could induce effective charge transfer in **97** and **98** with resultant wider absorption behaviour and ϵ -values compared to those of **96**. These molecules also exhibited effective electron injection efficiency, with **98** being the best performer with improved light-harvesting ability. The IPCE performance of the dyes parallels these observation leading to the highest J_{sc} for **98** (19.39 mA/cm²) followed by **97** (18.35 mA/cm²) and **96** (16.84 mA/cm²). The hexyl chain was found to minimize the dye aggregations effectively in **98** with lesser recombination, which resulted in a higher V_{oc} (825 mV) for the same. The trends described above in device parameters ended in highest PCE for **98** (11.84%) followed by **97** (11.04%) and **96** (9.83%) using CDCA co-adsorbent and cobalt electrolyte ([Co(bpy)₃]^{+2/+3}).

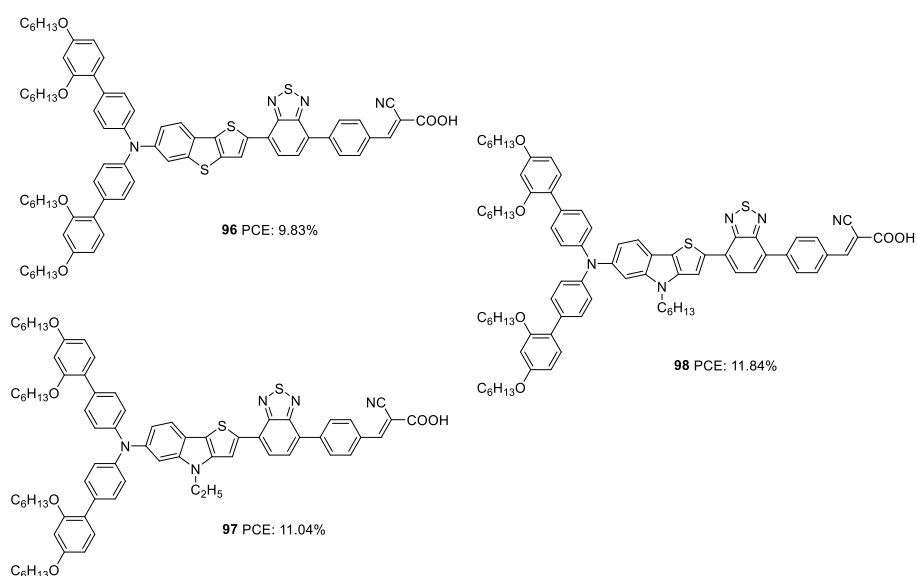


Figure 35. Photosensitizers with thieno[3,2-*b*]indole moiety (**97**, **98**) and thieno[3,2-*b*]benzothiophene (**96**) as π -spacer

Later the same group synthesized **99-102**. The objective was to reduce the aggregation-induced recombination occurring in devices fabricated with **98**. The donor group in **98** was substituted with fluorenyl derivatives with the other building blocks remains unchanged using D-A- π -A architecture with BTB as auxiliary acceptor and cyanoacrylic acid as acceptor/anchoring group (Figure 36).⁶⁵ The synthesized dyes **99-102** employs bis(9,9-dimethyl-9H-fluoren-2-yl)amino (FA), [20] bis(6,7-bis(hexyloxy)-9,9-dimethyl-9H-fluoren-2-yl)amino (HFA), bis(6,7-bis(decyloxy)-9,9-dimethyl-9H-fluoren-2-yl)amino (DFA), and bis(7-(2,4-bis(hexyloxy)phenyl)-9,9-dimethyl-9H-fluoren-2-yl)amine (BBFA) groups respectively as donors. To encounter solubility problems associated with the fluorene derivatives, all the devices were made with a change in dipping solvent resulting in lower PCE (10.5%, J_{sc} : 16.67 mA/cm², V_{oc} : 840 mV., FF: 0.75) for **98** than previously reported. All the devices were found to exhibit improved performance when electrolyte was changed from iodide/triiodide to cobalt-based electrolyte ([Co(bpy)₃]^{+2/+3}) and in the presence of HC-A1 as the co-adsorbent. The alkoxy, as well as phenyloxy substituted fluorene derivatives (**100-102**), were found to be more effective both in red shifting the absorption spectrum as well as in preventing recombination, taking advantage of the electron-donating as well as the bulkiness of the donor groups, when compared to FA substituted dye **99**. This lead to higher current density and photocurrent for **100-102** resulting in higher PCE. Though **99** is not having additional alkoxy substitutions integrated on it, the absorption profile shows a redshift when compared to those of **98** having BBPA (bis(2',4'-bis(hexyloxy)-[1,1'-biphenyl]-4-yl)amino) as the donor. This absorption behaviour can be accredited to a lack of electronic communication between the alkoxy groups and the tertiary amine in BBPA based dye **98**. A higher molar extinction coefficient of **98** contributed towards higher current density compared to **99**. The bulkier BBPA also rendered **98** to have higher V_{oc} and hence higher PCE when compared to those of **99**. The device fabricated based on **102** showcased the highest efficiencies of 11.4 %, **99** delivered the least efficiency of 10.2 % .

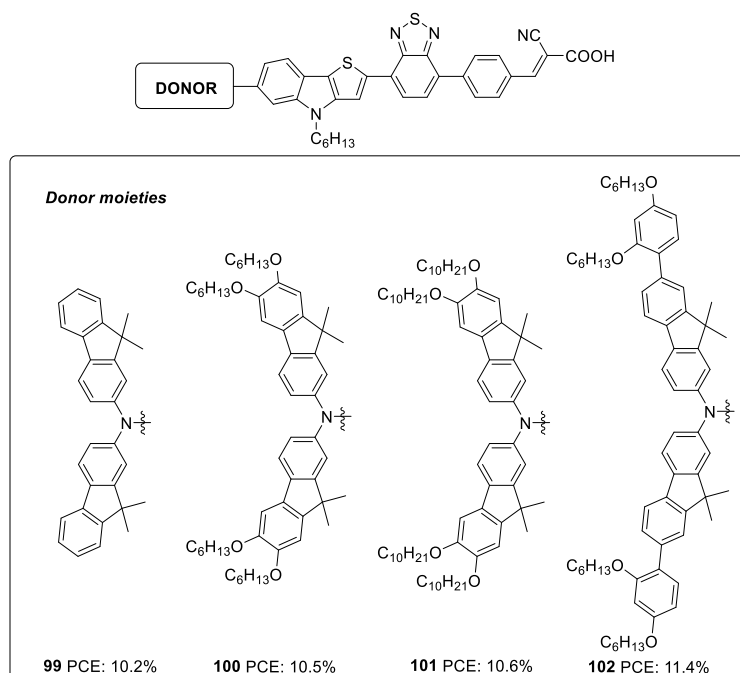


Figure 36. Photosensitizers **99-102** with thieno[3,2-*b*]indole moiety as π -spacer

The superior performance of TI over TAB as π -conjugator was again illustrated by Ji *et al.* (Figure 37).⁶⁶ To this end, two porphyrins based D- π -A dyes (D-ethynyl-zinc porphyrinyl-ethynyl-benzothiadiazole-acceptor) with extended conjugation at the donor sites were constructed. The dyes **104** and **105** differ in the auxiliary spacer between thieno[3,2-*b*]benzothiophene (TBT) and 4-hexyl-4H-thieno[3,2-*b*]indole, which were also subjected to a comparison with phenylethylene based dye **103** from earlier work.⁶⁷ The dihedral angle between donor part and π -spacer showed increment when the phenyl group in **103** was replaced with TI and TAB units with more conjugation. The trend observed in V_{oc} was following the increase in dihedral angle (**105**>**104**>**103**), which might have helped prevent the recombination effectively. The more electron-donating TI and TAB groups could also bring changes in the light-harvesting ability of dyes. In the Q-bands, significant changes were observed, having a more expansive and intensified absorption profile for **104-105**, leading to current densities in the order **105**>**104**>**103**. The more planar, electron-donating nature of the TI group along with the incorporated hexyl functionality contributed towards the best efficiency of 10.80% for **105** with higher J_{sc} (16.50 mA/cm²) and V_{oc} (0.847 V) in the presence of HC-A1 as the co-adsorbent, using [Co(bpy)₃]^{+2/+3} (bpy = 2,2'-bipyridine) redox electrolyte.

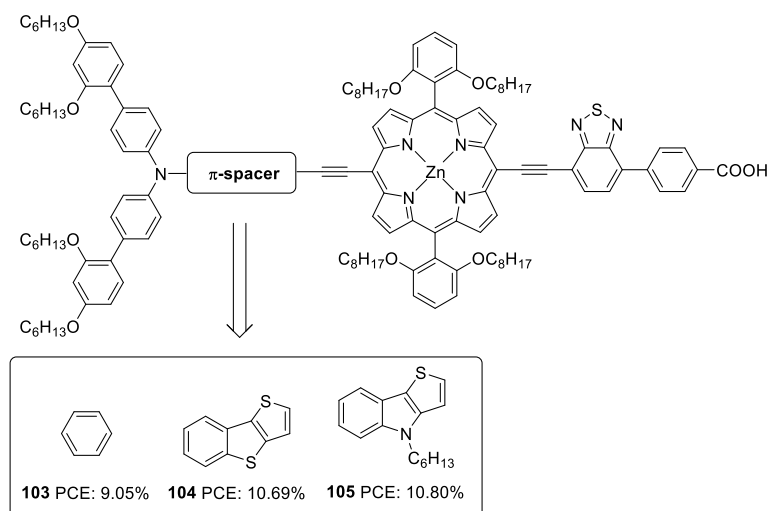


Figure 37. Molecular structures of photosensitizers **103-105** with different π -spacers

Thieno[2,3-*b*]indole was applied as a building block in DSSC for the first time by Irgashev *et al.* (Figure 38).⁶⁸⁻⁶⁹ They introduced a new synthetic route for constructing thieno[3,2-*b*]indole from 1-alkylisatin and 2-acetylthiophene. Among the dyes, **108** with thiophene as the π -bridge and ethyl hexyl as the alkyl group contributed towards the highest PCE of 6.3%. The bithiophene and terthiophene groups were entertaining aggregation of dyes which resulted in more recombination. Except for ethyl hexyl, other smaller alkyl groups like butyl and ethyl were not found to obstruct the dye aggregation, resulting in the downfall in efficiency using these spacers.

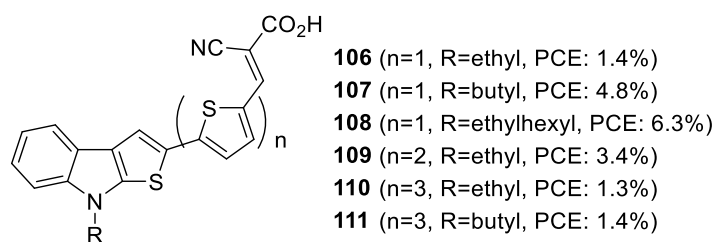


Figure 38. Photosensitizers **106-111** with thieno[3,2-*b*]indole moiety as the donor

Thienoindoles have proved to have the potential to function both as donor as well as π -spacer units. Systematic engineering of different π -spacers and auxiliary donors to this moiety could bring impressive PCE in the future. In this line, dye designs that incorporate TI unit with other indole fused systems open promising alternatives.

1.5.6 Tetraindole based sensitizers for DSSCs

The synthesis of tetraindole was first reported in 2006, which involved a one-pot tetramerization of indolin-2-one mediated by phosphoryl chloride.⁷⁰ This polyacene has four

indole units fused to cyclooctatetraene, which act as a promising donor motif for solar cell applications. In addition, the unique structural characteristics of this saddle-shaped scaffold will also prevent self-assembly of the dyes on the semiconductor surface.

Tetraindole found a place in DSSC through the work of Qian and co-workers.⁷¹ The D- π -A dyes **112** and **113** uses thiophene and bithiophene, respectively, as π -bridges (Figure 39). The dyes exhibit improved open-circuit potential benefitting from the saddle like structure with flanked octyl alkyl chains of the new donor moiety. The sensitizer **113** exhibited a broader ICT band and better light-harvesting ability, which is evident from the broader and enhanced response of the IPCE spectra. **113** delivered a maximum efficiency of 6.21% with the highest J_{sc} (13.0 mA/cm²) and V_{oc} (762 mV), whereas dye **112** could only deliver a PCE of 5.79% with J_{sc} of 12.1 mA/cm² and V_{oc} of 750 mV. The reduced aggregation behaviour of these dye was further illustrated by the co-adsorption experiments using CDCA. Both dyes exhibited lower efficiencies in the presence of CDCA, the reduction mainly aroused from lower J_{sc} values. Decreased dye loading in the presence of CDCA can be accounted for the decrease in photocurrent and hence the overall efficiency.

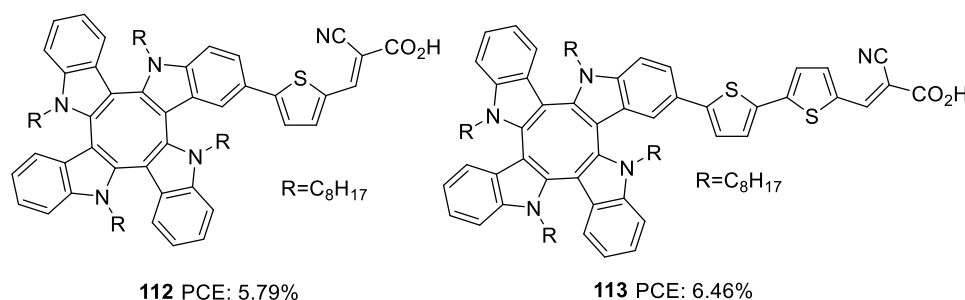


Figure 39. Photosensitizers **112-113** with tetraindole as the donor

1.6 Objective of the current work

Engineering sensitizers have got their prime importance when efficiency enhancement of DSSC is concerned. Electron rich fused heterocycles have proved their efficacy as donors as well as π -spacers in the sensitizer designs. The literature survey narrated in the previous section gives an impression on the extend of fused ring heterocycles being reported in literature. These systems were found to exhibit more electron-donating ability than indole in conjugation with expanded π -systems. Though the planarity could induce ICT in these molecules, a trade-off between light harvesting and dye aggregations lead to a shortfall of the power conversion efficiency in many instances. The strategic introduction of bulky substituents on the donor side and the π -conjugator helped abate these situations to some

extent. Another notable advantage is the ease of synthesising these fused indole heterocyclic motifs with functionalities required for further transformations. In addition, the stability of these fused heterocycles has contributed to enhancing device lifetime.

Keeping in view of the advantages of heteroaromatic indole-fused systems, in the upcoming chapters we have tried to carry out a detailed investigation of dyes which are based on indole fused systems as donor. Chapter 2 involves indoloindole donor based dyes. While chapter 2A deals with dyes **IID1-IID6** which are based on indolo[3,2-*b*]indole as donor, chapter 2B utilizes indolo[2,3-*b*]indole as donor to construct dyes **IID7-IID9**. Chapter 3 deals with dyes based on benzothienoindoles as donor unit. While Chapter 3A deals with **BID1-BID3** (benzothieno[3,2-*b*]indole as donor), the second part of the chapter deals with **BID4-BID6** (benzothieno[2,3-*b*]indole as donor). A di-branched di-anchoring approach was adopted in Chapter 4 to construct dyes **IID10-11D12**.

1.7 References

1. X. Chen, C. Li, M. Grätzel, R. Kostecki and S. S. Mao, Nanomaterials for Renewable Energy Production and Storage, *Chem. Soc. Rev.*, 2012, **41**, 7909–7937.
2. (a) N. Armaroli and V. Balzani, The Future of Energy Supply: Challenges and Opportunities., *Angew. Chemie - Int. Ed.*, 2007, **46**, 52–66; (b) R. Eisenberg and D. G. Nocera, Preface: Overview of the Forum on Solar and Renewable Energy, *Inorg. Chem.*, 2005, **44**, 6799–6801.
3. (a) W. A. Badawy, A Review on Solar Cells from Si-Single Crystals to Porous Materials and Quantum Dots, *J. Adv. Res.*, 2015, **6**, 123–132; (b) S. Sharma, K. K. Jain and A. Sharma, Solar Cells: In Research and Applications—A Review., *Mater. Sci. Appl.*, 2015, **06**, 1145–1155.
4. (a) M. Grätzel, Solar Energy Conversion by Dye-Sensitized Photovoltaic Cells, *Inorg. Chem.*, 2005, **44**, 6841–6851; (b) I. Chung, B. Lee, J. He, R. P. H. Chang and M. G. Kanatzidis, All-Solid-State Dye-Sensitized Solar Cells with High Efficiency, *Nature*, 2012, **485**, 486–489 (c) Y. Huang, E. J. Kramer, A. J. Heeger and G. C. Bazan, Bulk Heterojunction Solar Cells: Morphology and Performance Relationships, *Chem. Rev.*, 2014, **114**, 7006–7043; (d) I. Mora-Seró, Current Challenges in the Development of Quantum Dot Sensitized Solar Cells, *Adv. Energy Mater Adv. Energy Mater.*, 2020, **10**, 1–6. (e) O. E. Semonin, J. M. Luther and M. C. Beard, Quantum Dots for Next-Generation Photovoltaics, *Mater. Today*, 2012, **15**, 508–515; (f) M. A. Green, A. Ho-Baillie and H. J. Snaith, The Emergence of Perovskite Solar Cells, *Nat. Photonics*, 2014,

- 8, 506–514; (g) R. Rajeswari, M. Mrinalini, S. Prasanthkumar and L. Giribabu, Emerging of Inorganic Hole Transporting Materials For Perovskite Solar Cells, *Chem. Rec.*, 2017, **17**, 681–699.
5. G. Gokul, S. C. Pradhan and S. Soman, Dye Sensitized solar cells as potential candidates for Indoor/diffused light harvesting applications: from BIPV to self powered IoTs *Adv. Solar Energy Res.*, 2019, 281–316.
6. B. O'Regan and M. Grätzel, A low-cost, high-efficiency solar cell based on dye-sensitized colloidal TiO₂ films, *Nature*, **1991**, 353, 737-740.
7. (a) J. Gong, J. Liang and K. Sumathy, Review on Dye-Sensitized Solar Cells (DSSCs): Fundamental Concepts and Novel Materials, *Renew. Sustain. Energy Rev.*, 2012, **16**, 5848–5860; (b) Z. Ning, Y. Fu and H. Tian, Improvement of Dye-Sensitized Solar Cells: What We Know and What We Need to Know, *Energy Environ. Sci.*, 2010, **3**, 1170–1181; (c) T. Bessho, S. M. Zakeeruddin, C. Y. Yeh, E. W. G. Diau and M. Grätzel, Highly Efficient Mesoscopic Dye-Sensitized Solar Cells Based on Donor-Acceptor-Substituted Porphyrins, *Angew. Chemie - Int. Ed.*, 2010, **49**, 6646–6649. (d) A. Hagfeldt, G. Boschloo, L. Sun, L. Kloo and H. Pettersson, Dye-Sensitized Solar Cells, *Chem. Rev.*, 2010, **110**, 6595–6663; (e) H. S. Jung and J. K. Lee, Dye Sensitized Solar Cells for Economically Viable Photovoltaic Systems, *J. Phys. Chem. Lett.*, 2013, **4**, 1682–1693.
8. (a) H. Michaels, M. Rinderle, R. Freitag, I. Benesperi, T. Edvinsson, R. Socher, A. Gagliardi and M. Freitag, Dye-sensitized solar cells under ambient light powering machine learning: Towards autonomous smart sensors for the internet of things, *Chem. Sci.*, 2020, **11**, 2895–2906; (b) E. Tanaka, H. Michaels, M. Freitag and N. Robertson, Synergy of co-sensitizers in a copper bipyridyl redox system for efficient and cost-effective dye-sensitized solar cells in solar and ambient light, *J. Mater. Chem. A*, 2020, **8**, 1279–1287; (c) Y. Cao, Y. Liu, S. M. Zakeeruddin, A. Hagfeldt and M. Grätzel, *Joule*, 2018, **2**, 1108–1117; (d) S. Sasidharan, S. Soman, S. C. Pradhan, K. N. N. Unni, A. A. P. Mohamed, B. N. Nair and H. U. N. Saraswathy, *New J. Chem.*, 2017, **41**, 1007–1016; (e) M. Freitag, J. Teuscher, Y. Saygili, X. Zhang, F. Giordano, P. Liska, J. Hua, S. M. Zakeeruddin, J. E. Moser, M. Grätzel and A. Hagfeldt, Dye-sensitized solar cells for efficient power generation under ambient lighting, *Nat. Photonics*, 2017, **11**, 372–378; (f) S. Venkatesan, W. H. Lin, H. Teng and Y. L. Lee, High-Efficiency Bifacial Dye-Sensitized Solar Cells for Application under Indoor Light Conditions, *ACS Appl. Mater. Interfaces*, 2019, **11**, 42780–42789.

9. (a) Ji, J. M.; Zhou, H.; Kim, H. K. Rational Design Criteria for D- π -A Structured Organic and Porphyrin Sensitizers for Highly Efficient Dye-Sensitized Solar Cells. *J. Mater. Chem. A*, 2018, **6** (30), 14518–14545. (b) Wei, W.; Sun, K.; Hu, Y. H. An Efficient Counter Electrode Material for Dye-Sensitized Solar Cells - Flower-Structured 1T Metallic Phase MoS₂. *J. Mater. Chem. A*, 2016, **4** (32), 12398–12401. (c) Wei, W.; Sun, K.; Hu, Y. H. Direct Conversion of CO₂ to 3D Graphene and Its Excellent Performance for Dye-Sensitized Solar Cells with 10% Efficiency. *J. Mater. Chem. A*, 2016, **4** (31), 12054–12057. (d) Wang, D.; Wei, W.; Hu, Y. H. Highly Efficient Dye-Sensitized Solar Cells with Compositated Food Dyes. *Ind. Eng. Chem. Res.*, 2020, **59** (22), 10457–10463.
10. (a) Q. Huahmé, V. M. Mwalukuku, D. Joly, J. Liotier, Y. Kervella, P. Maldivi, S. Narbey, F. Oswald, A. J. Riquelme, J. A. Anta and R. Demadrille, Photochromic dye-sensitized solar cells with light-driven adjustable optical transmission and power conversion efficiency, *Nat. Energy*, 2020, **5**, 468–477; (b) A. Gopi, S. Lingamoorthy, S. Soman, K. Yoosaf, R. Haridas and S. Das, Modulating FRET in Organic-Inorganic Nanohybrids for Light Harvesting Applications, *J. Phys. Chem. C*, 2016, **120**, 26569–26578; (c) M. V. Vinayak, M. Yoosuf, S. C. Pradhan, T. M. Lakshmykanth, S. Soman and K. R. Gopidas, A detailed evaluation of charge recombination dynamics in dye solar cells based on starburst triphenylamine dyes, *Sustain. Energy Fuels*, 2018, **2**, 303–314; (d) H. Iftikhar, G. G. Sonai, S. G. Hashmi, A. F. Nogueira and P. D. Lund, Progress on electrolytes development in dye-sensitized solar cells, *Materials*, 2019, **12**, 1998–2065; (e) S. C. Pradhan, A. Hagfeldt and S. Soman, Resurgence of DSCs with copper electrolyte: a detailed investigation of interfacial charge dynamics with cobalt and iodine based electrolytes, *J. Mater. Chem. A*, 2018, **6**, 22204–22214; (f) S. Soman, Y. Xie and T. W. Hamann, Cyclometalated sensitizers for DSSCs employing cobalt redox shuttles, *Polyhedron*, 2014, **82**, 139–147; (g) S. Soman, M. A. Rahim, S. Lingamoorthy, C. H. Suresh and S. Das, Strategies for optimizing the performance of carbazole thiophene appended unsymmetrical squaraine dyes for dye-sensitized solar cells, *Phys. Chem. Chem. Phys.*, 2015, **17**, 23095–23103; (h) M. V. Vinayak, T. M. Lakshmykanth, M. Yoosuf, S. Soman and K. R. Gopidas, Effect of recombination and binding properties on the performance of dye sensitized solar cells based on propeller shaped triphenylamine dyes with multiple binding groups, *Sol. Energy*, 2016, **124**, 227–241; (i) Q. Wali, A. Fakharuddin and R. Jose, Tin oxide as a photoanode for dye-sensitised solar cells: Current progress and future challenges, *J. Power Sources*, 2015, **293**, 1039–1052.

11. (a) K. L. Wu, W. P. Ku, J. N. Clifford, E. Palomares, S. Te Ho, Y. Chi, S. H. Liu, P. T. Chou, M. K. Nazeeruddin and M. Grätzel, Harnessing the open-circuit voltage via a new series of Ru(ii) sensitizers bearing (iso-)quinolinyl pyrazolate ancillaries, *Energy Environ. Sci.*, 2013, **6**, 859–870; (b) Z. She, Y. Cheng, L. Zhang, X. Li, D. Wu, Q. Guo, J. Lan, R. Wang and J. You, Novel Ruthenium Sensitizers with a Phenothiazine Conjugated Bipyridyl Ligand for High-Efficiency Dye-Sensitized Solar Cells, *ACS Appl. Mater. Interfaces*, 2015, **7**, 27831–27837; (c) L. Han, A. Islam, H. Chen, C. Malapaka, B. Chiranjeevi, S. Zhang, X. Yang and M. Yanagida, High-efficiency dye-sensitized solar cell with a novel co-adsorbent, *Energy Environ. Sci.*, 2012, **5**, 6057–6060.
12. (a) Y. S. Yen, H. H. Chou, Y. C. Chen, C. Y. Hsu and J. T. Lin, Recent developments in molecule-based organic materials for dye-sensitized solar cells, *J. Mater. Chem.*, 2012, **22**, 8734–8747; (b) A. Mishra, M. K. R. Fischer and P. Büuerle, Metal-Free organic dyes for dye-Sensitized solar cells: From structure: Property relationships to design rules, *Angew. Chemie - Int. Ed.*, 2009, **48**, 2474–2499; (c) A. Carella, F. Borbone and R. Centore, Research progress on photosensitizers for DSSC, *Front. Chem.*, 2018, **6**, 1–24.
13. (a) J. J. Cid, J. H. Yum, S. R. Jang, M. K. Nazeeruddin, E. Martínez-Ferrero, E. Palomares, J. Ko, M. Grätzel and T. Torres, Molecular cosensitization for efficient panchromatic dye-sensitized solar cells, *Angew. Chemie - Int. Ed.*, 2007, **46**, 8358–8362; (b) N. V. Krishna, J. V. S. Krishna, M. Mrinalini, S. Prasanthkumar and L. Giribabu, Role of Co-Sensitizers in Dye-Sensitized Solar Cells, *ChemSusChem*, 2017, **10**, 4668–4689.
14. (a) B. Hemavathi, V. Jayadev, P. C. Ramamurthy, R. K. Pai, K. N. Narayanan Unni, T. N. Ahipa, S. Soman and R. G. Balakrishna, Variation of the donor and acceptor in D-A- π -A based cyanopyridine dyes and its effect on dye sensitized solar cells, *New J. Chem.*, 2019, **43**, 15673–15680.; (b) B. Hemavathi, V. Jayadev, S. C. Pradhan, G. Gokul, K. Jagadish, G. K. Chandrashekar, P. C. Ramamurthy, R. K. Pai, K. N. Narayanan Unni, T. N. Ahipa, S. Soman and R. Geetha Balakrishna, Aggregation induced light harvesting of molecularly engineered D-A- π -A carbazole dyes for dye-sensitized solar cells, *Sol. Energy*, 2018, **174**, 1085–1096.; (c) T. Maeda, T. V. Nguyen, Y. Kuwano, X. Chen, K. Miyanaga, H. Nakazumi, S. Yagi, S. Soman and A. Ajayaghosh, Intramolecular Exciton-Coupled Squaraine Dyes for Dye-Sensitized Solar Cells, *J. Phys. Chem. C*, 2018, **122**, 21745–21754; (d) V. Nikolaou, A. Charisiadis, S. Chalkiadaki, I. Alexandropoulos, S. C. Pradhan, S. Soman, M. K. Panda and A. G. Coutsolelos, Enhancement of the

- photovoltaic performance in D3A porphyrin-based DSCs by incorporating an electron withdrawing triazole spacer, *Polyhedron*, 2018, **140**, 9–18; (e) J. S. Panicker, B. Balan, S. Soman and V. C. Nair, Understanding structure-property correlation of metal free organic dyes using interfacial electron transfer measurements, *Sol. Energy*, 2016, **139**, 547–556; (f) S. Soman, S. C. Pradhan, M. Yoosuf, M. V. Vinayak, S. Lingamoorthy and K. R. Gopidas, Probing Recombination Mechanism and Realization of Marcus Normal Region Behavior in DSSCs Employing Cobalt Electrolytes and Triphenylamine Dyes, *J. Phys. Chem. C*, 2018, **122**, 14113–14127; (g) M. Yoosuf, S. C. Pradhan, S. Soman and K. R. Gopidas, Triple bond rigidified anthracene-triphenylamine sensitizers for dye-sensitized solar cells, *Sol. Energy*, 2019, **188**, 55–65.
15. (a) L. Zhang, X. Yang, W. Wang, G. G. Gurzadyan, J. Li, X. Li, J. An, Z. Yu, H. Wang, B. Cai, A. Hagfeldt and L. Sun, 13.6% Efficient organic dye-sensitized solar cells by minimizing energy losses of the excited state, *ACS Energy Lett.*, 2019, **4**, 943–951; (b) W. Zhang, Y. Wu, H. W. Bahng, Y. Cao, C. Yi, Y. Saygili, J. Luo, Y. Liu, L. Kavan, J. E. Moser, A. Hagfeldt, H. Tian, S. M. Zakeeruddin, W. H. Zhu and M. Grätzel, Comprehensive control of voltage loss enables 11.7% efficient solid-state dye-sensitized solar cells, *Energy Environ. Sci.*, 2018, **11**, 1779–1787; (c) Y. Cao, Y. Liu, S. M. Zakeeruddin, A. Hagfeldt, M. Grätzel, Direct contact of selective charge extraction layers enables high-efficiency molecular photovoltaics. *Joule*, 2018, **2**, 1108–1117; (d) K. Kakiage, Y. Aoyama, T. Yano, K. Oya, J. Fujisawa and M. Hanaya, Highly-efficient dye-sensitized solar cells with collaborative sensitization by silyl-anchor and carboxy-anchor dyes. *Chem. Commun.*, 2015, **51**, 15894–15897.
16. (a) L. Alibabaei, J. H. Kim, M. Wang, N. Postrakulchote, J. Teuscher, D. Di Censo, R. Humphry-Baker, J. E. Moser, Y. J. Yu, K. Y. Kay, S. M. Zakeeruddin and M. Grätzel, Molecular design of metal-free D- π -A substituted sensitizers for dye-sensitized solar cells, *Energy Environ. Sci.*, 2010, **3**, 1757–1764; (b) A. Yella, R. Humphry-Baker, B. F. E. Curchod, N. Ashari Astani, J. Teuscher, L. E. Polander, S. Mathew, J. E. Moser, I. Tavernelli, U. Rothlisberger, M. Grätzel, M. K. Nazeeruddin and J. Frey, Molecular engineering of a fluorene donor for dye-sensitized solar cells, *Chem. Mater.*, 2013, **25**, 2733–2739.
17. (a) J. Wang, K. Liu, L. Ma and X. Zhan, Triarylamine: Versatile Platform for Organic, Dye-Sensitized, and Perovskite Solar Cells, *Chem. Rev.*, 2016, **116**, 14675–14725; (b) K. Hara, K. Sayama, Y. Ohga, A. Shinpo, S. Suga and H. Arakawa, A coumarin-derivative dye sensitized nanocrystalline TiO₂solar cell having a high solar-energy conversion

- efficiency up to 5.6%, *Chem. Commun.*, 2001, 569–570; (c) Z. S. Wang, K. Hara, Y. Dan-oh, C. Kasada, A. Shinpo, S. Suga, H. Arakawa and H. Sugihara, Photophysical and (photo)electrochemical properties of a coumarin dye, *J. Phys. Chem. B*, 2005, **109**, 3907–3914.; (d) B. Liu, R. Wang, W. Mi, X. Li and H. Yu, Novel branched coumarin dyes for dye-sensitized solar cells: Significant improvement in photovoltaic performance by simple structure modification, *J. Mater. Chem.*, 2012, **22**, 15379–15387; (e) M. Marszalek, S. Nagane, A. Ichake, R. Humphry-Baker, V. Paul, S. M. Zakeeruddin and M. Grätzel, Tuning spectral properties of phenothiazine based donor- π -acceptor dyes for efficient dye-sensitized solar cells, *J. Mater. Chem.*, 2012, **22**, 889–894; (f) S. H. Kim, H. W. Kim, C. Sakong, J. Namgoong, S. W. Park, M. J. Ko, C. H. Lee, W. I. Lee and J. P. Kim, Effect of five-membered heteroaromatic linkers to the performance of phenothiazine-based dye-sensitized solar cells, *Org. Lett.*, 2011, **13**, 5784–5787; (g) K. Srinivas, C. R. Kumar, M. A. Reddy, K. Bhanuprakash, V. J. Rao and L. Giribabu, D- π -A organic dyes with carbazole as donor for dye-sensitized solar cells, *Synth. Met.*, 2011, **161**, 96–105.
18. (a) Y. Liu, J. He, L. Han and J. Gao, Influence of the auxiliary acceptor and π -bridge in carbazole dyes on photovoltaic properties, *J. Photochem. Photobiol. A Chem.*, 2017, **332**, 283–292; (b) K. Hara, Z. S. Wang, T. Sato, A. Furube, R. Katoh, H. Sugihara, Y. Dan-Oh, C. Kasada, A. Shinpo and S. Suga, Oligothiophene-containing coumarin dyes for efficient dye-sensitized solar cells, *J. Phys. Chem. B*, 2005, **109**, 15476–15482; (c) J. Liu, X. Yang, A. Islam, Y. Numata, S. Zhang, N. T. Salim, H. Chen and L. Han, Efficient metal-free sensitizers bearing circle chain embracing π -spacers for dye-sensitized solar cells, *J. Mater. Chem. A*, 2013, **1**, 10889–10897; (d) L. Huang, P. Ma, G. Deng, K. Zhang, T. Ou, Y. Lin and M. S. Wong, Novel electron-deficient quinoxalinedithienothiophene- and phenazinedithienothiophene-based photosensitizers: The effect of conjugation expansion on DSSC performance, *Dye. Pigment.*, 2018, **159**, 107–114.
19. (a) Y. Wu and W. Zhu, Organic sensitizers from D- π -A to D-A- π -A: Effect of the internal electron-withdrawing units on molecular absorption, energy levels and photovoltaic performances, *Chem. Soc. Rev.*, 2013, **42**, 2039–2058; (b) W. Zhu, Y. Wu, S. Wang, W. Li, X. Li, J. Chen, Z. S. Wang and H. Tian, Organic D-A- π -A solar cell sensitizers with improved stability and spectral response, *Adv. Funct. Mater.*, 2011, **21**, 756–763; (c) W. Li, Y. Wu, Q. Zhang, H. Tian and W. Zhu, D-A- π -A featured sensitizers bearing phthalimide and benzotriazole as auxiliary acceptor: effect on absorption and

- charge recombination dynamics in dye-sensitized solar cells, *ACS Appl. Mater. Interfaces*, 2012, **4**, 1822–1830; (d) Y. Wu, W. H. Zhu, S. M. Zakeeruddin and M. Grätzel, Insight into D-A- π -A structured sensitizers: A promising route to highly efficient and stable dye-sensitized solar cells, *ACS Appl. Mater. Interfaces*, 2015, **7**, 9307–9318; (e) J. He, Y. Liu, J. Gao and L. Han, New D-D- π -A triphenylamine-coumarin sensitizers for dye-sensitized solar cells, *Photochem. Photobiol. Sci.*, 2017, **16**, 1049–1056; (f) W. Sharmoukh, J. Cong, J. Gao, P. Liu, Q. Daniel and L. Kloo, Molecular Engineering of D-D- π -A-Based Organic Sensitizers for Enhanced Dye-Sensitized Solar Cell Performance, *ACS Omega*, 2018, **3**, 3819–3829; (g) V. Cuesta, M. Vartanian, P. de la Cruz, R. Singhal, G. D. Sharma and F. Langa, Comparative study on the photovoltaic characteristics of A-D-A and D-A-D molecules based on Zn-porphyrin; a D-A-D molecule with over 8.0% efficiency, *J. Mater. Chem. A*, 2017, **5**, 1057–1065; (h) K. S. V. Gupta, T. Suresh, S. P. Singh, A. Islam, L. Han and M. Chandrasekharam, Carbazole based A- π -D- π -A dyes with double electron acceptor for dye-sensitized solar cell, *Org. Electron.*, 2014, **15**, 266–275.
20. A. B. Muñoz-García, I. Benesperi, G. Boschloo, J. J. Concepcion, J. H. Delcamp, E. A. Gibson, G. J. Meyer, M. Pavone, H. Pettersson, A. Hagfeldt and M. Freitag, Dye sensitized solar cell strike back, *Chem. Soc. Rev.*, 2021, **50**, 12450-12550
 21. For the synthesis of indolo[2,3-*b*]quinoxaline see: G. M. Badger and P. J. Nelson, Polynuclear heterocyclic systems. Part XIV. Indoloquinoxalines, *J. Chem. Soc.*, 1962, 3926-3931.
 22. K. R. J. Thomas, P. Tyagi, Synthesis, Spectra, and Theoretical Investigations of the Triarylamines Based on 6H-Indolo[2,3-*b*]quinoxaline, *J. Org. Chem.*, 2010, **75**, 8100-8111.
 23. A. Venkateswararao, P. Tyagi, K. R. J. Thomas and P. Chen, Organic dyes containing indolo [2 , 3- b] quinoxaline as a donor : synthesis , optical and photovoltaic properties, *Tetrahedron*, 2014, **70**, 6318-6327.
 24. X. Qian, H. H. Gao, Y. Z. Zhu, L. Lu and J. Y. Zheng, 6H-Indolo[2,3-*b*]quinoxaline-based organic dyes containing different electron-rich conjugated linkers for highly efficient dye-sensitized solar cells, *J. Power Sources*, 2015, **280**, 573–580.
 25. X. Qian, X. Wang, L. Shao, H. Li, R. Yan and L. Hou, Molecular engineering of D–D– π –A type organic dyes incorporating indoloquinoxaline and phenothiazine for highly efficient dye-sensitized solar cells, *J. Power Sources*, 2016, **326**, 129–136

26. X. Qian, X. Lan, R. Yan, Y. He, J. Huang and L. Hou, T-shaped (D)2-A- π -A type sensitizers incorporating indoloquinoline and triphenylamine for organic dye-sensitized solar cells, *Electrochim. Acta*, 2017, **232**, 377–386.
27. R. Su, L. Lyu, M. R. Elmorsy and A. El-Shafei, Novel metal-free organic dyes constructed with the D-D|A- π -A motif: Sensitization and co-sensitization study, *Sol. Energy*, 2019, **194**, 400–414.
28. R. Su, S. Ashraf, L. Lyu and A. El-shafei, Tailoring dual-channel anchorable organic sensitizers with indolo [2 , 3- b] quinoxaline moieties : Correlation between structure and DSSC performance, *Sol. Energy*, 2020, **206**, 443–454.
29. R. Su, L. Lyu, M. R. Elmorsy and A. El-Shafei, Structural studies and photovoltaic investigation of indolo[2,3-: B] quinoxaline-based sensitizers/co-sensitizers achieving highly efficient DSSCs, *New J. Chem.*, 2020, **44**, 2797–2812.
30. (a) N. X. Hu, S. Xie, Z. Popovic, B. Ong, A. M. Hor and S. Wang, 5,11-Dihydro-5,11-di-1-naphthylindolo[3,2-*b*]carbazole: Atropisomerism in a Novel Hole-Transport Molecule for Organic Light-Emitting Diodes, *J. Am. Chem. Soc.*, 1999, **121**, 5097–5098; (b) S. Wakim, J. Bouchard, M. Simard, N. Drolet, Y. Tao and M. Leclerc, Organic Microelectronics: Design, Synthesis, and Characterization of 6,12-Dimethylindolo[3,2-*b*]Carbazoles, *Chem. Mater.*, 2004, **16**, 4386–4388; (c) Y. Li, Y. Wu, S. Gardner and B. S. Ong, Novel Peripherally Substituted Indolo[3,2-*b*]carbazoles for High-Mobility Organic Thin-Film Transistors, *Adv. Mater.*, 2005, **17**, 849–853; (d) Y. Wu, Y. Li, S. Gardner and B. S. Ong, Indolo[3,2-*b*]carbazole-Based Thin-Film Transistors with High Mobility and Stability, *J. Am. Chem. Soc.*, 2005, **127**, 614–618; (e) P. T. Boudreault, S. Wakim, N. Blouin, M. Simard, C. Tessier, Y. Tao, M. Leclerc and V. La, Synthesis, Characterization, and Application of Indolo[3,2-*b*]carbazole Semiconductors, *J. Am. Chem. Soc.* 2007, **129**, 9125-9136.
31. For the synthesis of indolocarbazole see: (a) B. Robinson, The Fischer indolisation of cyclohexane-1,4-dione bisphenylhydrazone, *J. Chem. Soc.* 1963, 3097-3099; (b) J. I. G Cadogan,, M. Carmeron-Wood, R. K. Makie, and R. I. J. Searle, The reactivity of organophosphorus compounds. Part XIX. Reduction of nitro-compounds by triethyl phosphite: a convenient new route to carbazoles, indoles, indazoles, triazoles, and related compounds. *J. Chem. Soc.*, 1965, 4831.
32. X. H. Zhang, Z. S. Wang, Y. Cui, N. Koumura, A. Furube and K. Hara, Organic sensitizers based on hexylthiophene-functionalized indolo[3, 2-*b*]carbazole for efficient dye-sensitized solar cells, *J. Phys. Chem. C*, 2009, **113**, 13409–13415.

33. S. Cai, G. Tian, X. Li, J. Su and H. Tian, Efficient and stable DSSC sensitizers based on substituted dihydroindolo[2,3-b]carbazole donors with high molar extinction coefficients, *J. Mater. Chem. A*, 2013, **1**, 11295–11305.
34. Y. Wu and W. Zhu, Organic sensitizers from D- π -A to D-A- π -A: Effect of the internal electron-withdrawing units on molecular absorption, energy levels and photovoltaic performances, *Chem. Soc. Rev.*, 2013, **42**, 2039–2058
35. S. Cai, X. Hu, G. Tian, H. Zhou, W. Chen, J. Huang, X. Li and J. Su, Photo-stable substituted dihydroindolo[2,3-b]carbazole-based organic dyes: Tuning the photovoltaic properties by optimizing the π structure for panchromatic DSSCs, *Tetrahedron*, 2014, **70**, 8122–8128.
36. X. Qian, L. Shao, H. Li, R. Yan, X. Wang and L. Hou, Indolo[3,2-b]carbazole-based multi-donor- π -acceptor type organic dyes for highly efficient dye-sensitized solar cells, *J. Power Sources*, 2016, **319**, 39–47.
37. Z. Xiao, Y. Di, Z. Tan, X. Cheng, B. Chen and J. Feng, Efficient organic dyes based on perpendicular 6,12-diphenyl substituted indolo[3,2-b] carbazole donor, *Photochem. Photobiol. Sci.*, 2016, **15**, 1514–1523.
38. Z. Xiao, B. Chen, Y. Di, H. Wang, X. Cheng and J. Feng, Effect of substitution position on photoelectronic properties of indolo[3,2-b]carbazole-based metal-free organic dyes, *Sol. Energy*, 2018, **173**, 825–833.
39. J. Y. Su, C. Y. Lo, C. H. Tsai, C. H. Chen, S. H. Chou, S. H. Liu, P. T. Chou and K. T. Wong, Indolo[2,3- b]carbazole synthesized from a double-intramolecular buchwald-hartwig reaction: Its application for a dianchor DSSC organic dye, *Org. Lett.*, 2014, **16**, 3176–3179.
40. H. Zhang, Z. E. Chen, J. Hu and Y. Hong, Novel metal-free organic dyes containing linear planar 11,12-dihydroindolo[2,3-a]carbazole donor for dye-sensitized solar cells: Effects of π spacer and alkyl chain, *Dye. Pigment.*, 2019, **164**, 213–221.
41. C. Luo, W. Bi, S. Deng, J. Zhang, S. Chen, B. Li, Q. Liu, H. Peng and J. Chu, Indolo [3 , 2 , 1-jk] carbazole Derivatives-Sensitized Solar Cells : E f f e c t of π - Bridges on the Performance of Cells, *J. Phys. Chem. C* , 2014, **118**, 14211–14217.
42. W. Cao, M. Fang, Z. Chai, H. Xu, T. Duan, Z. Li, X. Chen, J. Qin and H. Han, New D- π -A organic dyes containing a tert-butyl-capped indolo[3,2,1-jk]carbazole donor with bithiophene unit as π -linker for dye-sensitized solar cells, *RSC Adv.*, 2015, **5**, 32967–32975.

43. X. C. Li, C. Y. Wang, W. Y. Lai and W. Huang, Triazatruxene-based materials for organic electronics and optoelectronics, *J. Mater. Chem. C*, 2016, **4**, 10574-10587 and references cited therein.
44. For the synthesis of triazatruxene see: (a) J. Bergman and N. Eklund, Synthesis of 2,2'-biindolyls by coupling reactions, *Tetrahedron*, 1980, **36**, 1439-1443; (b) J. Bergman and N. Eklund, Synthesis and studies of tris-indolobenzenes and related compounds, *Tetrahedron*, 1980, **36**, 1445-1450; (c) M. A. Eissenstat, M. R. Bell, T. E. D'Ambra, E. J. Alexander, S. J. Daum, J. H. Ackerman, M. D. Gruett, V. Kumar, K. G. Estep, E. M. Olefirowicz, J. R. Wetzell, M. D. Alexander, J. D. Weaver, D. A. Haycock, D. A. Luttinger, F. M. Casiano, S. M. Chippari, J. E. Kuster, J. I. Stevenson and S. J. Ward, Aminoalkylindoles: Structure-Activity Relationships of Novel Cannabinoid Mimetics, *J. Med. Chem.*, 1995, **38**, 3094-3105.
45. X. Qian, Y. Z. Zhu, J. Song, X. P. Gao and J. Y. Zheng, New donor- π -acceptor type triazatruxene derivatives for highly efficient dye-sensitized solar cells, *Org. Lett.*, 2013, **15**, 6034-6037
46. X. Qian, L. Lu, Y. Z. Zhu, H. H. Gao and J. Y. Zheng, Triazatruxene-based organic dyes containing a rhodanine-3-acetic acid acceptor for dye-sensitized solar cells, *Dye. Pigment.*, 2015, **113**, 737-742.
47. B. Pan, Y. Z. Zhu, D. Ye, F. Li, Y. F. Guo and J. Y. Zheng, Effects of ethynyl unit and electron acceptors on the performance of triazatruxene-based dye-sensitized solar cells, *New J. Chem.*, 2018, **42**, 4133-4141.
48. X. Qian, R. Yan, L. Shao, H. Li, X. Wang and L. Hou, Triindole-modified push-pull type porphyrin dyes for dye-sensitized solar cells, *Dye. Pigment.*, 2016, **134**, 434-441.
49. P. Qin, P. Sanghyun, M. I. Dar, K. Rakstys, H. ElBatal, S. A. Al-Muhtaseb, C. Ludwig and M. K. Nazeeruddin, Weakly Conjugated Hybrid Zinc Porphyrin Sensitizers for Solid-State Dye-Sensitized Solar Cells, *Adv. Funct. Mater.*, 2016, **26**, 5550-5559.
50. L. Zhang, X. Yang, W. Wang, G. G. Gurzadyan, J. Li, X. Li, J. An, Z. Yu, H. Wang, B. Cai, A. Hagfeldt and L. Sun, 13.6% Efficient organic dye-sensitized solar cells by minimizing energy losses of the excited state, *ACS Energy Lett.*, 2019, **4**, 943-951.
51. L. Zhang, X. Yang, B. Cai, H. Wang, Z. Yu and L. Sun, Triazatruxene-based sensitizers for highly efficient solid-state dye-sensitized solar cells, *Sol. Energy*, 2020, **212**, 1-5.
52. L. Zhang, X. Yang, S. Li, Z. Yu, A. Hagfeldt and L. Sun, Electron-Withdrawing Anchor Group of Sensitizer for Dye-Sensitized Solar Cells, Cyanoacrylic Acid, or Benzoic Acid?, *Sol. RRL*, 2020, **4**, 1900436.

53. S. Li, X. Yang, L. Zhang, J. An, B. Cai and X. Wang, Effect of fluorine substituents on benzothiadiazole-based D- π -A'- π -A photosensitizers for dye-sensitized solar cells, *RSC Adv.*, 2020, **10**, 9203–9209.
54. Z. Yao, X. Liao, Y. Guo, H. Zhao, Y. Guo, F. Zhang, L. Zhang, Z. Zhu, L. Kloo, W. Ma, Y. Chen and L. Sun, Exploring Overall Photoelectric Applications by Organic Materials Containing Symmetric Donor Isomers, *Chem. Mater.* 2019, **31**, 8810–8819.
55. For the synthesis of indeno[1,2-*b*]indole see: D. W. Brown, M. F. Mahon, A. Ninan, M. Sainsbury and H. G. Shertzer, The Fischer indolisation reaction and the synthesis of dihydroindenoindoles. *Tetrahedron*, 1993, **49**, 8919-8932.
56. X. Qian, R. Yan, C. Xu, L. Shao, H. Li and L. Hou, New efficient organic dyes employing indeno[1,2-*b*]indole as the donor moiety for dye-sensitized solar cells, *J. Power Sources*, 2016, **332**, 103–110.
57. X. Qian, R. Yan, Y. Hang, Y. Lv, L. Zheng, C. Xu and L. Hou, Indeno[1,2-*b*]indole-based organic dyes with different acceptor groups for dye-sensitized solar cells, *Dye. Pigment.*, 2017, **139**, 274–282.
58. R. Yan, X. Qian, Y. Jiang, Y. He, Y. Hang and L. Hou, Ethynylene-linked planar rigid organic dyes based on indeno[1,2-*b*]indole for efficient dye-sensitized solar cells, *Dye. Pigment.*, 2017, **141**, 93–102.
59. P. P. Dai, Y. Z. Zhu, Q. L. Liu, Y. Q. Yan and J. Y. Zheng, Novel indeno[1,2-*b*]indole-spirofluorene donor block for efficient sensitizers in dye-sensitized solar cells, *Dye. Pigment.*, 2020, **175**, 108099.
60. P. P. Dai, J. Han, Y. Z. Zhu, Y. Q. Yan and J. Y. Zheng, Orientation-dependent effects of indeno[1,2-*b*]indole-spirofluorene donor on photovoltaic performance of D- π -A and D-D- π -A sensitizers, *J. Power Sources*, 2021, **481**, 228901-228907.
61. X. Zhou, J. Lu, H. Huang, Y. Yun, Z. Li and F. You, Dyes and Pigments Thieno [3 , 2-*b*] indole (TI) bridged A- π - D- π - A small molecules : Synthesis , characterizations and organic solar cell applications, *Dye. Pigment.*, 2019, **160**, 16–24.
62. X. Zhang, Y. Cui, R. Katoh, N. Koumura and K. Hara, Organic Dyes Containing Thieno [3 , 2- *b*] indole Donor for Efficient Dye-Sensitized Solar Cells, *J. Phys. Chem. C*, 2010, **114**, 18283–18290.
63. N. Koumura, Z. S. Wang, S. Mori, M. Miyashita, E. Suzuki and K. Hara, Alkyl-functionalized organic dyes for efficient molecular photovoltaics, *J. Am. Chem. Soc.*, 2006, **128**, 14256–14257

64. Y. K. Eom, S. H. Kang, I. T. Choi, Y. Yoo, J. Kim and H. K. Kim, Significant light absorption enhancement by a single heterocyclic unit change in the π -bridge moiety from thieno[3,2-b]benzothiophene to thieno[3,2-b]indole for high performance dye-sensitized and tandem solar cells, *J. Mater. Chem. A*, 2017, **5**, 2297–2308
65. J. M. Ji, H. Zhou, Y. K. Eom, C. H. Kim and H. K. Kim, 14.2% Efficiency Dye-Sensitized Solar Cells by Co-sensitizing Novel Thieno[3,2-b]indole-Based Organic Dyes with a Promising Porphyrin Sensitizer, *Adv. Energy Mater.*, 2020, **10**, 2000124
66. J. M. Ji, S. H. Kim, H. Zhou, C. H. Kim and H. K. Kim, D- π -A-Structured Porphyrins with Extended Auxiliary π -Spacers for Highly Efficient Dye-Sensitized Solar Cells, *ACS Appl. Mater. Interfaces*, 2019, **11**, 24067–24077.
67. S. H. Kang, S. Y. Jung, Y. W. Kim, Y. K. Eom and H. K. Kim, Exploratory synthesis and photovoltaic performance comparison of D- π -A structured Zn-porphyrins for dye-sensitized solar cells, *Dye. Pigment.*, 2018, **149**, 341–347
68. R. A. Irgashev, A. A. Karmatsky, S. A. Kozyukhin, V. K. Ivanov, A. Sadovnikov, V. V. Kozik, V. A. Grinberg, V. V. Emets, G. L. Rusinov and V. N. Charushin, A facile and convenient synthesis and photovoltaic characterization of novel thieno[2,3-b]indole dyes for dye-sensitized solar cells, *Synth. Met.*, 2015, **199**, 152–158
69. R. A. Irgashev, A. A. Karmatsky, G. A. Kim, A. A. Sadovnikov, V. V. Emets, V. A. Grinberg, V. K. Ivanov, S. A. Kozyukhin, G. L. Rusinov and V. N. Charushin, Novel push-pull thieno[2,3-b]indole-based dyes for efficient dye-sensitized solar cells (DSSCs), *Arkivoc*, 2017, **2017**, 34–50.
70. For the synthesis of tetraindole see: (a) H. Hiyoshi, T. Sonoda and S. Mataka, Synthesis of cyclic novel symmetric cyclic indole-tetramers, *Heterocycles*, 2006, **68**, 763-769; (b) F. Wang, X. C. Li, W. Y. Lai, Y. Chen, W. Huang and F. Wudl, Synthesis and characterization of symmetric cyclooctatetraindoles: Exploring the potential as electron-rich skeletons with extended π -systems, *Org. Lett.*, 2014, **16**, 2942–2945.
71. X. Qian, H. H. Gao, Y. Z. Zhu, B. Pan and J. Y. Zheng, Tetraindole-based saddle-shaped organic dyes for efficient dye-sensitized solar cells, *Dye. Pigment.*, 2015, **121**, 152–158

CHAPTER 2

Design, Synthesis and Characterization of Indoloindole Donor based Photosensitizers for DSSC Applications

Abstract

In part A of the chapter we detail the development of D- π -A dyes which utilizes indolo[3,2-*b*]indole as donor, cyanoacrylic acid as acceptor/anchoring group and varied the π -spacer employed with as benzene, thiophene and furan units to construct sensitizers **IID-1**, **IID-2** and **IID-3** respectively. To minimize dye aggregations, the two *N*-atoms of indolo[3,2-*b*]indole core was functionalized with hexyl chains. Though furan substituted dye was exhibiting higher light harvesting efficiency with wider absorption profile, **IID-1** having benzene as π -spacer outperformed the other two with higher photovoltage and current density. Optimization studies with co-adsorbent chenodeoxycholic acid (CDCA) further enhanced the performance with a maximum efficiency realized using 20 mM CDCA concentration. This indicated that significant dye aggregation was happening in the system and we concluded that the slightly twisted conformation of **IID-1** may be helping the system to alleviate dye aggregation and also the spatial approach of oxidized species in the electrolyte coming closer to semiconductor. Further we did molecular engineering by replacing the hexyl group with dodecyl chain as an approach towards reducing dye aggregation. The dyes thus developed are **IID-4**, **IID-5** and **IID-6** with π -spacer as benzene, thiophene and furan. By adopting this structural modification, all the dyes could outperform the previous set (**IID-1**, **IID-2**, and **IID-3**) even in the absence of any co-adsorbent. In the absence of aggregate formation, light harvesting efficiencies of the dyes improved contributing significantly towards improved power conversion efficiency (PCE) and furan substituted dye exhibited maximum PCE of 4.4% and the minimum was delivered by the benzene substituted dye **IID-4**. In Part B dodecyl chain incorporated indolo[2,3-*b*]indole was used as donor to synthesize **IID-7**, **IID-8**, and **IID-9** with benzene, thiophene and furan respectively as π -spacer. Like in the previous case, light harvesting efficiency dominated the overall PCE and thus furan spacer showcased superior performance followed by thiophene and benzene.

2.1 Introduction

The sustainable development in harnessing conventional energy sources has always got utmost importance due to its economic and eco-friendly nature.¹ Photovoltaic technology is one of the strategies to this line that is undergoing continuous improvement towards higher performance to cost ratio.² Dye sensitized solar cells (DSSC) being one of the third generation techniques has many merits such as environmental benignity, cost-effectiveness in terms of raw materials and fabrication processes, good indoor light harvesting efficiency etc.³⁻⁴ A plethora of studies have been carried out in the last three decades in a view to improve the power conversion efficiency (PCE) of DSSC. Much of these efforts are oriented towards photosensitizer and counter electrode engineering. Designing of dye sensitizer with intensified absorption profile from visible to NIR region is a critical factor for light harvesting. The sensitizers are also supposed to have features to prevent any kind of dark current generation.⁵ The quest for good dye sensitizers resulted in new molecular architectures, D- π -A being the most investigated one.⁶⁻⁷

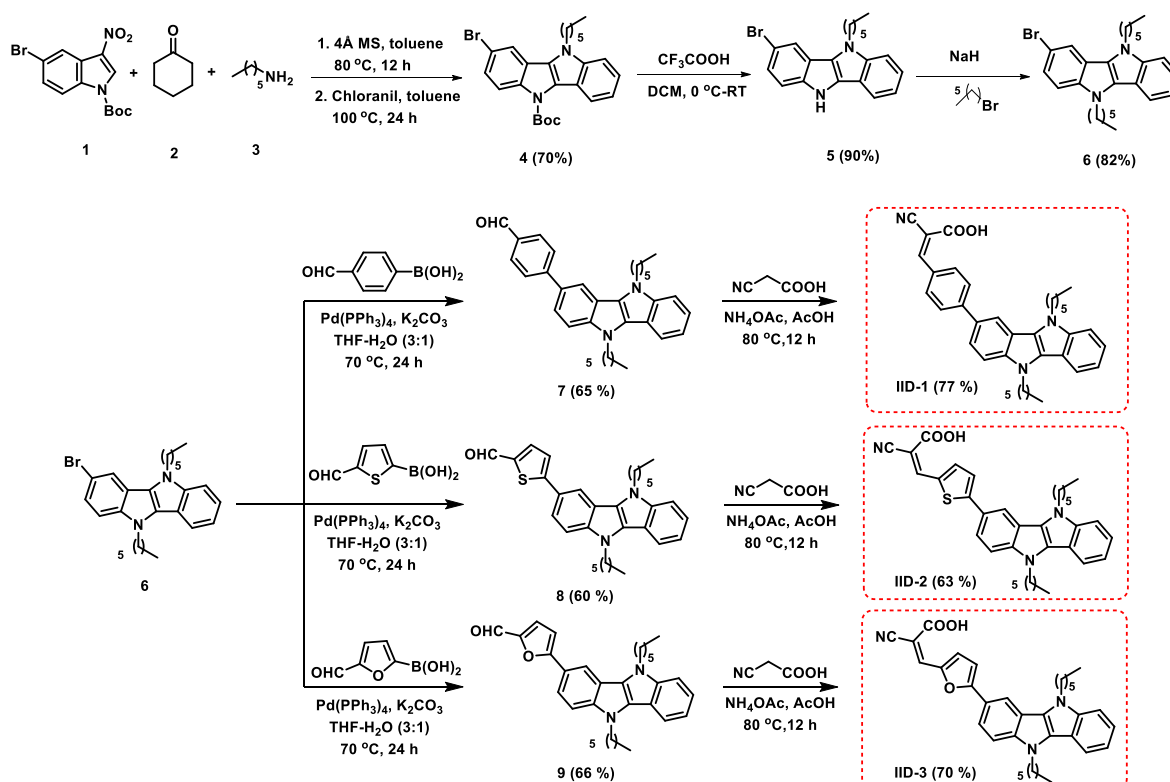
Molecular engineering of photosensitizer deals with optimization of each fragments of the system such as donor, π -spacer and acceptor.⁸ In addition to the ability for tuning the energy levels of the dye; donor unit is also capable of modulating the current generation and recombination reactions. Though this technology was initiated with metal complex based sensitizers, metal free organic sensitizers are paving new trajectories with their tunability and performance.⁹ Triphenylamine, carbazole, coumarines, indolines are some of the donors generally encountered in DSSC.¹⁰ Along with the development of new design strategies with the existing donors, development and employment of new donors especially fused heterocycles has also got importance in view of their light harvesting ability and stability when employed in devices. Indole fused heterocycles are one such class of donors which has already demonstrated their capability due to their electron rich planar systems coupled with arylation/alkylation sites to create hydrophobic barrier to prevent aggregate formations and back electron transfer reactions.¹¹ A notable example for the utilization of indole fused heterocycles in DSSC was reported by Zhang and co-workers in which a single photosensitizer based on triazatruxene/triindole donor using cobalt based redox electrolyte could realize a PCE of 13.6 %.¹² Another interesting report utilized thieno[2,3-*b*]indole based dyes that reached an efficiency of 14.2% with co-sensitization strategy.¹³

In 2017, our group introduced a facile route involving a sequential MCR-oxidation approach towards the synthesis of these fused indole heteroacenes.¹⁴ The methodology involves an initial MCR of an enolizable ketone (cyclohexanone), a 1° amine, and *N*-tosyl-3-nitroindole furnishing the intermediate pyrrolo[3,2-*b*]indole which on further oxidation with chloranil affords indolo[3,2-*b*]indole moieties in good yields. The advantage of our method with existing ones was clearly demonstrated by the generation of symmetrical and unsymmetrical indolo[3,2-*b*]indoles; highly relevant for material applications. Indoloindoles are an interesting class of *N*-heteroacenes among which indolo[3,2-*b*]indoles are considered to be good electron donors. This donor character of indolo[3,2-*b*]indole moiety can be attributed to the small atomic radius of *N*-atom which in turn would result in a more dense assembly of molecules. In addition, these molecules are also known to possess better charge carrier mobility due to the bidirectional electronic coupling enabled by NH- π interactions. These fused *N*-heteroacenes have been used in the development of organic photovoltaics, organic field-effect transistors, core donors in heterojunction solar cells and high-spin organic polymers. Followed by the establishment of new synthetic strategies for the construction of indolo[3,2-*b*]indole, we initiated the development of sensitizers which are based on indolo[3,2-*b*]indole donor. Part A of the second chapter (2A) deals with the development of D- π -A dyes which utilizes hexyl group incorporated indolo[3,2-*b*]indole as donor, cyanoacrylic acid as acceptor/anchoring group and varied the π -spacers such as benzene, thiophene and furan to construct sensitizers **IID-1**, **IID-2** and **IID-3** respectively. Further we did molecular engineering by replacing the hexyl group with dodecyl chain as an approach towards reducing dye aggregation. The dyes thus developed are **IID-4**, **IID-5** and **IID-6** with π -spacer as benzene, thiophene and furan respectively. The work was also extended to another class of donors which is indolo[2,3-*b*]indole. Detailed investigations of the performance of these sensitizers are explained in the coming sections.

Chapter 2A: Investigation of Indolo[3,2-*b*]indole Donor based D- π -A Dyes for DSSC

2.2 Synthesis and Characterization of IID-1, IID-2, and IID-3

The synthesis of the indolo[3,2-*b*]indole based dyes following the D- π -A approach commenced with the one-pot MCR/oxidation of *N*-Boc-5-bromo-3-nitro-indole **1**, cyclohexanone **2** and hexylamine **3**. The Boc-group on the indoloindole **4** was easily removed by treating with trifluoroacetic acid in DCM furnishing the intermediate **5** in 90% yield. This fused indole moiety **5** was then subjected to *N*-alkylation with hexylbromide to afford the donor dihexylindoloindole **6** in excellent yield. The π -spacer was attached to the donor moiety by Suzuki reaction of **6** with formyl-aryl/heteroaryl boronic acids such as 4-formyl phenyl boronic acid, (5-formylthiophen-2-yl)boronic acid and (5-formylfuran-2-yl)boronic acid to afford the molecules **7**, **8** and **9** respectively. Finally, the acceptor part was attached to **7**, **8** and **9** via Knoevenagel condensation with cyanoacetic acid furnishing the dyes **IID-1**, **IID-2**, and **IID-3** respectively. The entire synthetic route is shown in Scheme 2.1.



Scheme 2.1. Synthetic route adopted for indolo[3,2-*b*]indole based dyes **IID-1**, **IID-2** and **IID-3**

2. 3 Photophysical and Electrochemical properties

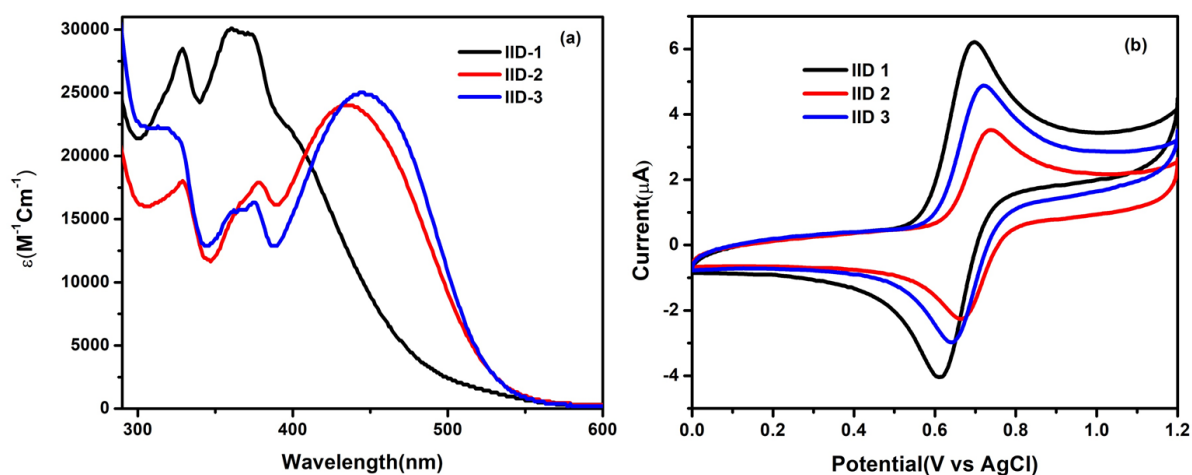


Figure 2.1 (a) Absorption spectra of dyes in THF. (b) Cyclic voltammogram of dyes

The absorption spectra for all the three dyes were recorded in tetrahydrofuran and are shown in Figure 2.1 (a). Availing the benefit from D- π -A architecture, all the above sensitizers (**IID-1**, **IID-2**, and **IID-3**) exhibited absorption in the range of 300-600 nm. The bands observed at shorter wavelengths correspond to π - π^* transitions and the ones at longer wavelengths are attributed to intramolecular charge transfer (ICT) transitions. All the three dyes can be clearly distinguished by analysing its characteristic intramolecular charge transfer band. The dyes **IID-1**, **IID-2**, and **IID-3** displayed an absorption maximum at 360 nm, 434 nm and 443 nm respectively. The variation in absorption spectra is attributed to the presence of different π -spacers and the dihedral angle between the indolo[3,2-*b*]donor and the π -spacers which played a key role in determining the absorption maxima and shift in absorption spectra. The role of hetero-atomic π -spacers like thiophene and furan in **IID-2** and **IID-3** decreased the energy band gap of these dyes which resulted in a bathochromic as well as a hyperchromic shift in absorption spectra compared to the non-heteroatomic π spacer like benzene present in **IID-1**. Hence both the dyes **IID-2** and **IID-3** showed a red-shifted absorption in comparison to **IID-1**.

To investigate in detail the feasibility of electron injection from the excited state of the dye to the semiconductor (TiO_2) conduction band (CB) and regeneration of the oxidized dye ground state by the electrolyte, cyclic voltammetry was used to study the electrochemical properties of the sensitizers (Figure 2.1 (b)). Cyclic voltammetry was performed for all the three dyes employing dichloromethane as the solvent in 0.1 M tetrabutylammonium

hexafluorophosphate as supporting electrolyte and ferrocene as an internal standard, glassy carbon was used as the anode, platinum wire as cathode and Ag/AgCl as the reference electrode. The oxidation potentials of **IID-1**, **IID-2**, and **IID-3** were calculated with respect to ferrocene and was converted to NHE using the equation, $E_{\text{HOMO}} = [E_{\text{ox}} + 0.63\text{V}]$. The LUMO of these dyes were calculated by taking the difference between E_{HOMO} and E_{0-0} band gap of the dyes obtained from the intersection of absorption and emission spectra. All photophysical and electrochemical values are tabulated in Table 2.1 As shown in Table 2.1, the HOMO levels for **IID-1**, **IID-2**, and **IID-3** were 0.82, 0.87 and 0.85 V vs. NHE, respectively which is placed at a more positive potential in comparison to the iodide/triiodide redox system (0.4 V vs. NHE). The excited state potential of the dyes was estimated to be -1.77, -1.48 and -1.51 V, respectively which is more negative than the TiO_2 conduction band energy level (-0.5 V vs. NHE), affirming smooth electron injection from the dye excited states for all the three dyes.

Table 2.1 Photophysical and electrochemical data of **IID** dyes.

Sensitizer	λ_{max} , nm (ϵ , $\text{M}^{-1}\text{cm}^{-1}$)	$E_{\text{ox}}(\text{Fc}/\text{Fc}^+)$ (V)	E_{HOMO} (vs NHE) (V)	E_{0-0} eV	E_{LUMO} (vs NHE) (V)
IID-1	360 (30090)	0.19	0.82	2.59	-1.77
IID-2	434 (24000)	0.24	0.87	2.35	-1.48
IID-3	443 (25030)	0.22	0.85	2.36	-1.51

2.4 Computational Studies

The ability of dyes to exhibit better photovoltaic properties predominantly rely on their photophysical, electrochemical and detailed pre-experimental information about the molecular geometry, electron density distribution and spectroscopic properties. An adept knowledge of the above-mentioned parameters will help us to understand the electron transfer in more detail which in turn acts as a useful tool for further modifications to improve the performance. In addition to this, the degree of π -conjugation, which determines how efficiently the donor-acceptor interactions take place in these molecular systems, is judged by the dihedral angle between the donor, π -spacer and terminal acceptor groups. Keeping this in mind, geometrical optimizations in the gas phase were carried out for all the three **IID** dyes under study. The density functional theory (DFT) calculation was performed at B3LYP exchange-correlation functional level theory with 6-311g(d, p) basis set using a Gaussian

G09 package. All the optimized structures were subjected to vibrational analysis to check for imaginary frequencies. Gaussview 5.0 was used for the visualization of structures and has been given in Figure 2. 2. In π -conjugated system analogous to **IID** dyes having D- π -A architecture, charge transport occurs between donor and the terminal acceptor *via* π -spacer units and is directly dependent on the corresponding dihedral angles (Figure 2. 2). It is quite clear from Figure 2. 2 that the introduction of different spacers into D- π -A type **IID** systems lead to a different twists between the indolo[3,2-*b*]indole donor unit and the π -spacer. The dihedral angle between indolo[3,2-*b*]indole donor and phenyl unit in **IID-1** was calculated to be around 34.48° while in the case of thiophene (**IID-2**), a dihedral angle of 21.99° was obtained. On the other hand, for **IID-3**, indolo[3,2-*b*]indole-furan moieties are more or less aligned in the same plane and the dihedral angle was found to be 1.66° . The terminal cyanoacrylic acid is found to be almost coplanar with respective π -conjugated spacers displaying dihedral angle between 0.48 – 2.22° . An increased dihedral angle retards the electronic communication between the donor and acceptor which led to a red-shifted absorption ongoing from **IID-1** to **IID-2** to **IID-3**. The alkyl substituents grafted on to the indolo[3,2-*b*]indole donor do not seem to appear to be affecting the planarity of the dye molecules.

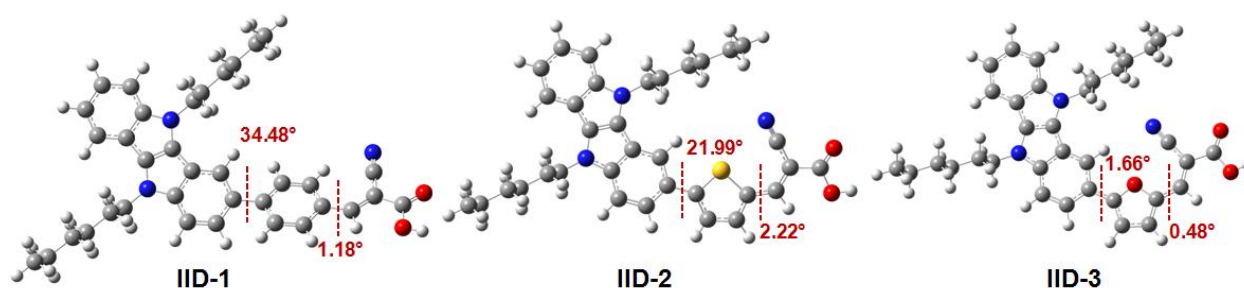


Figure 2. 2 Energy minimized structures of **IID** dyes and the corresponding dihedral angles between the indolo[3,2-*b*]indole donor and the neighbouring fragments.

To simulate experimental UV/Vis spectra of the dyes, these optimized geometries were subjected to single-point time-dependent DFT (TDDFT) calculations. The isodensity plots of frontier molecular orbitals and the energy levels of the **IID** dyes have been depicted in Figure 2.3. The HOMO of all the **IID** dyes is largely localized over indolo[3,2-*b*]indole and a very small amount is located over the π -spacer, while LUMO is predominantly localized on the acceptor cyanoacrylic acid unit with a slight overlap on the π -spacer fragments. From the ground and excited state electron density distribution shown in Figure 2.3, it is quite evident that there is sufficient charge separation between the donor and acceptor and the LUMO

electron density is localized over the cyanoacrylic acid functionality leading to better injection of the excited state charge carriers. The HOMO–LUMO gaps were calculated to be between 2.45 to 2.53 eV. The HOMO of all the dyes was found to be in between -5.09 to -5.22 eV. These results are matching with what we observed from the photophysical and electrochemical studies with the corresponding **IID** dyes.

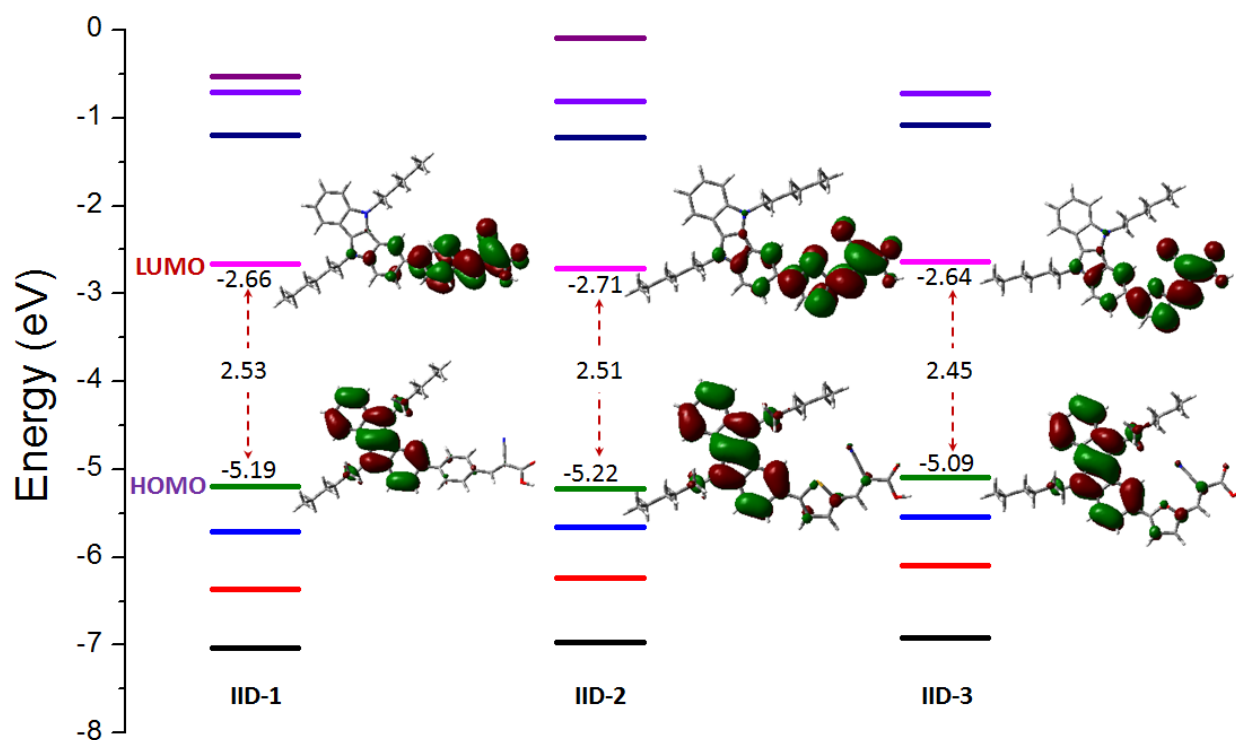


Figure 2.3 Schematic representation of electronic distributions observed in frontier orbitals (HOMO and LUMO) of **IID** dyes using DFT/B3LYP/6-311G(d, p) with band gap values.

Further, to gain a deeper insight into the electron density distribution in each dye, partial electron density contribution from the respective frontier orbitals have been calculated and data is provided in Table 2.2. As can be seen from the Table 2.2, the major low energy transition is contributed by the excitation of charge carriers from HOMO, HOMO-1, and HOMO-2 of the **IID** dyes to the LUMO, which is basically the charge transfer from the indolo[3,2-*b*]indole donor to the cyanoacrylic acid acceptor.

Table 2.2 Comparison of absorption properties of the dyes with the simulated excitation energy, oscillator strength, percentage contributions of the orbital density for different transitions and dipole moments.

Dyes	Experimental		Theoretical (B3LYP-6311g**)			μ (Debye)
	λ_{\max} (nm)	ε ($M^{-1}cm^{-1}$)	λ (nm)	f	composition	
IID-1	357	20620	364 (3.40 eV)	0.56	HOMO→LUMO (99.16%) HOMO-1→LUMO (99.66%) HOMO-2→LUMO (89.60)	8.0
IID-2	385	32960	383 (3.24 eV)	0.43	HOMO→LUMO (98.37%) HOMO-1→LUMO (96.38%) HOMO-2→LUMO (93.73%)	7.4
IID-3	447	35703	471 (2.63 eV)	0.36	HOMO→LUMO (98.24%) HOMO-1→LUMO (95.12%) HOMO-2→LUMO (93.56%)	6.5

2.5 Photovoltaic Performance

To explore the potential of the newly synthesized indolo[3,2-*b*]indole dyes [**IID-1**, **IID-2** and **IID-3**] to be used as sensitizers in dye solar cells, devices were fabricated and the photovoltaic performance was evaluated using standard (AM 1.5G, 100 mWcm⁻²) simulated solar spectrum employing an electrolyte composed of 0.3M BMII, 0.1M LiI, 0.05M I₂ and 0.5M tbp in acetonitrile. Detailed optimizations were carried out by fabricating devices with and without co-adsorbant (Chenodeoxycholic acid, CDCA), and also by systematically varying the co-adsorbent concentrations (5mM, 10mM & 20mM), in a way to study the effect of aggregation on photovoltaic performance. All the three dyes displayed their best performance in presence of 20mM CDCA. From the results, it is quite clear that the dyes are

prone to aggregation and the best performance was obtained in presence of co-adsorbant CDCA (20mM).

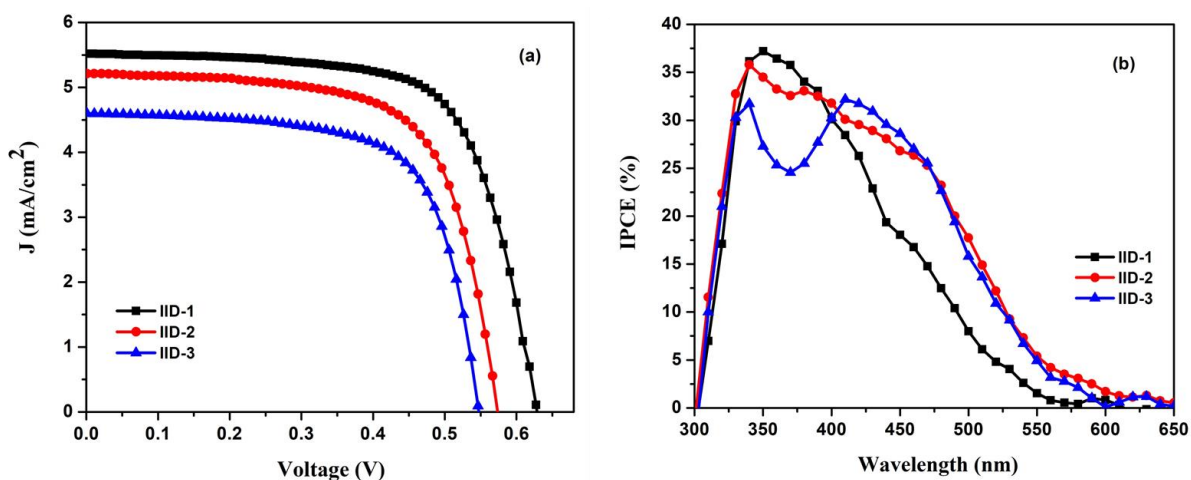


Figure 2. 4 (a) Current density-voltage characteristics of DSSCs based on **IID-1**, **IID-2**, and **IID-3** under one sun illumination (AM 1.5G). (b) Spectra of incident photon-to-current conversion efficiency (IPCE) for DSCs based on **IID-1**, **IID-2**, and **IID-3**

The current density versus voltage (J - V) results for the optimized solar cells fabricated using **IID-1**, **IID-2**, and **IID-3** as sensitizers are shown in Figure 2.4 (a) and the tabulated values are compiled in Table 2.3. The benzene substituted dye, **IID-1** outperformed the other dyes (**IID-2** and **IID-3**) giving a power conversion efficiency of 2.38% ($J_{sc} = 5.51 \text{ mAcm}^{-2}$, $V_{oc} = 620 \text{ mV}$, and $FF = 0.69$) whereas **IID-2** showed a power conversion efficiency of 2.0% ($J_{sc} = 5.22 \text{ mAcm}^{-2}$, $V_{oc} = 570 \text{ mV}$ and $FF = 0.67$) and **IID-3** displayed a power conversion efficiency of 1.71% ($J_{sc} = 4.6 \text{ mAcm}^{-2}$, $V_{oc} = 540 \text{ mV}$ and $FF = 0.68$) respectively. It is quite interesting to note that even though **IID-2** and **IID-3** exhibited a much broader absorption profile and higher molar extinction coefficient in comparison to **IID-1**, the smaller dihedral angle of **IID-2** and **IID-3** resulted in better conjugation and improved interaction between the donor and acceptor units and thus the J_{sc} for both the dyes were less in comparison to **IID-1**. The furan substituted dye, **IID-3** imparted the least current density and voltage among the series as a result of more recombination. Figure 2.4 (b) shows the IPCE spectra of **IID-1**, **IID-2**, and **IID-3**. IPCE results are in accordance with the J - V data. Even though there is an extended absorption in IPCE spectra for **IID-2** and **IID-3** from 400 to 600 nm with higher molar extinction coefficients, the device fabricated with **IID-1** showed better current, voltage and fill factor leading to improved photovoltaic performance.

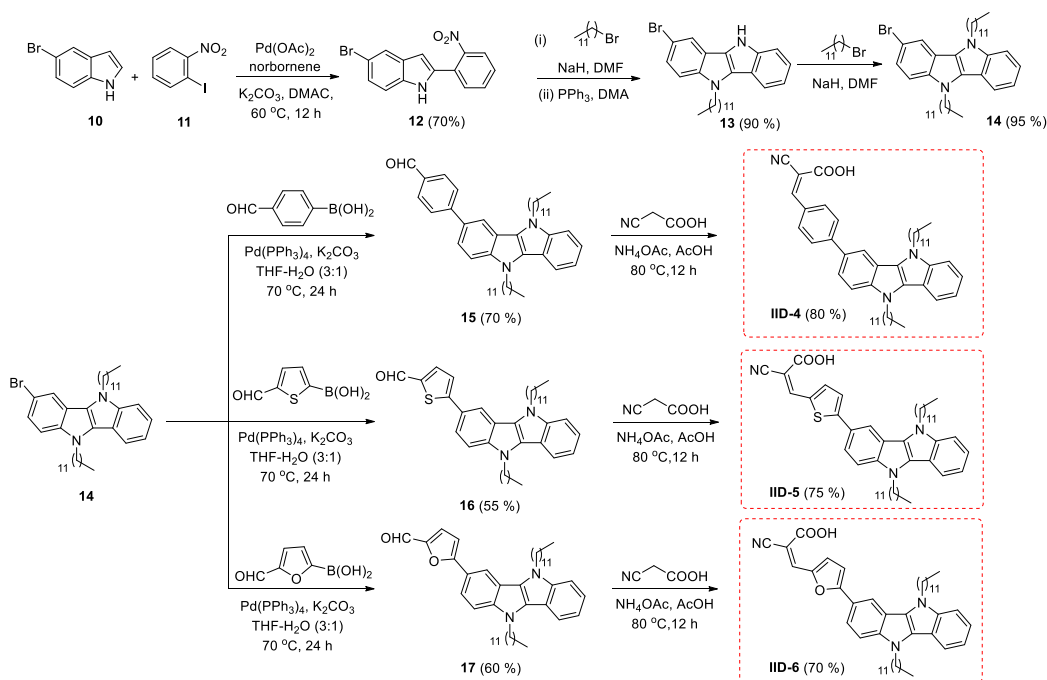
Table 2.3 Solar cell characteristics of DSSCs based on **IID-1**, **IID-2**, and **IID-3**.

Sensitizer	V _{OC} (mV)	J _{SC} (mA/cm ²)	FF (%)	Efficiency
IID-1	620 ± 2	5.51 ± 0.33	69 ± 0.9	2.38 ± 0.11
IID-2	570 ± 8	5.22 ± 0.21	67 ± 0.5	2.00 ± 0.07
IID-3	540 ± 6	4.60 ± 0.32	69 ± 0.5	1.71 ± 0.12

In the current set of dyes, the hexyl group was not found to be effective in preventing back electron transfer reaction. Hence we planned to increase the alkyl chain length to dodecyl in a view to prevent recombination reactions and to tap the light harvesting ability of dyes to its fullest. The dyes thus developed are **IID-4**, **IID-5** and **IID-6** with π -spacer as benzene, thiophene and furan respectively.

2.6 Synthesis and Characterization of **IID-4**, **IID-5**, and **IID-6**

We commenced our studies with the synthesis of indolo[3,2-*b*]indole based dyes with dodecyl-groups as the *N*-substituent by following the D- π -A approach. We initiated the synthesis of the core with the norbornene mediated palladium catalysed C-2 arylation of indole with 1-iodo-2-nitrobenzene to yield intermediate **12**. *N*-alkylation of **12** with dodecylbromide followed by PPh₃ mediated annulation reaction afforded **13**. The halogenated donor didodecylindoloindole **14** was then made by subjecting the fused indole moiety **13** to *N*-alkylation with dodecylbromide. Having the donor moiety in hand, our next task was to attach the π -spacers by Suzuki reaction of **14** with formyl-aryl/heteroaryl boronic acids. The coupling products **15**, **16** and **17** were obtained from the reaction of **14** with 4-formyl phenyl boronic acid, (5-formylthiophen-2-yl)boronic acid and (5-formylfuran-2-yl)boronic acid respectively. The dyes **IID-4**, **IID-5** and **IID-6** were finally made by attaching the acceptor part to **15**, **16** and **17** via Knoevenagel condensation with cyanoacetic acid.



Scheme 2.2 Synthetic route adopted for indolo[3,2-*b*]indole based dyes **IID-4**, **IID-5**, **IID-6**.

2. 7 Photophysical and Electrochemical properties

The absorption measurements were done in THF and the data obtained are presented in Figure 2.5 (a) and Table 2.4. The change in alkyl chain length could not bring significant differences in the absorption properties of these dyes. The solid state absorption spectra of the compounds on TiO_2 are presented in Figure 2.5 (b). According to this, furan substituted dye **IID-6** was showing higher and broader absorption profile than the rest of the compounds. While **IID-4** was having higher absorption value, **IID-6** showcased wider and red-shifted absorption profile. The cyclic voltammogram of these dyes are shown in Figure 2. 6 and the data deduced from these experiments are summarized in Table 2.4. The energetics of the current set of dyes are almost similar to their hexyl incorporated counterparts.

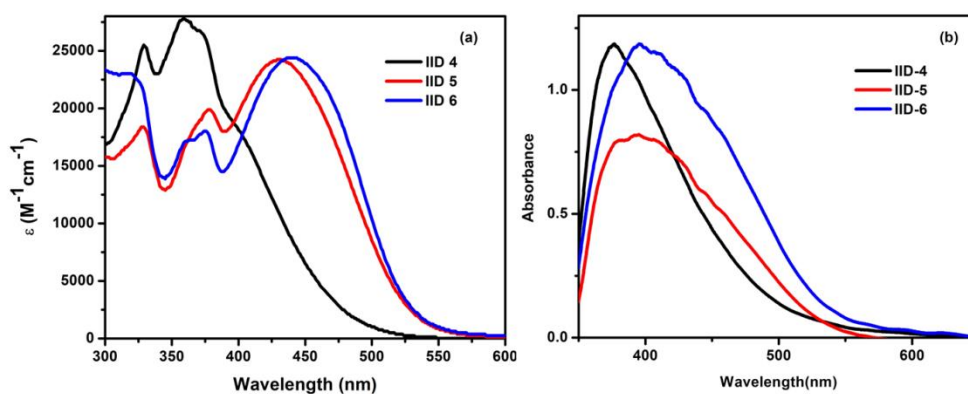


Figure 2.5 (a) Absorption spectra of dyes in THF. (b) Absorption spectra of dyes on TiO_2

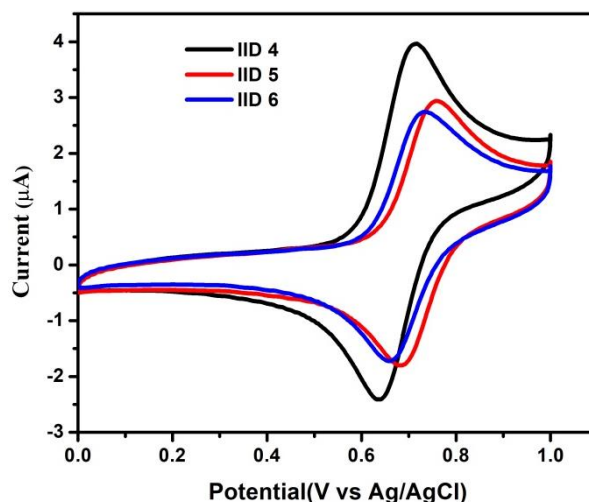


Figure 2.6 Cyclic voltammogram of **IID-4**, **IID-5** and **IID-6**

Table 2.4 Photophysical and electrochemical data of **IID-4** to **IID-6** dyes

Sensitizer	λ_{\max} , nm (ϵ , $M^{-1}cm^{-1}$)	$E_{ox}(Fc/Fc^+)$ (V)	E_{HOMO} (vs NHE) (V)	E_{0-0} eV	E_{LUMO} (vs NHE) (V)
IID-4	360 (27750)	0.21	0.84	2.58	-1.74
IID-5	432 (24250)	0.25	0.88	2.34	-1.46
IID-6	444 (24375)	0.23	0.86	2.32	-1.46

2. 8 Computational Studies

The molecular structure and electronic distribution of the dyes were investigated by with Gaussian 09 program. DFT studies at B3LYP level of theory with valence double-zeta polarisation basis set, viz 6-31G* was used for all the calculations in gas phase. Figure 2.7 shows the frontier molecular orbital of the dyes. All the dyes are having HOMO electron density mostly located on the donor unit and LUMO is located on the acceptor unit/cyanoacrylic acid and extended to π -spacer also. These results show good HOMO-LUMO overlap and possibility of strong coupling of semiconductor conduction band with the sensitizer. This can in turn make sure efficient electron injection to conduction band of TiO_2 which is essential for the current generation in the device.

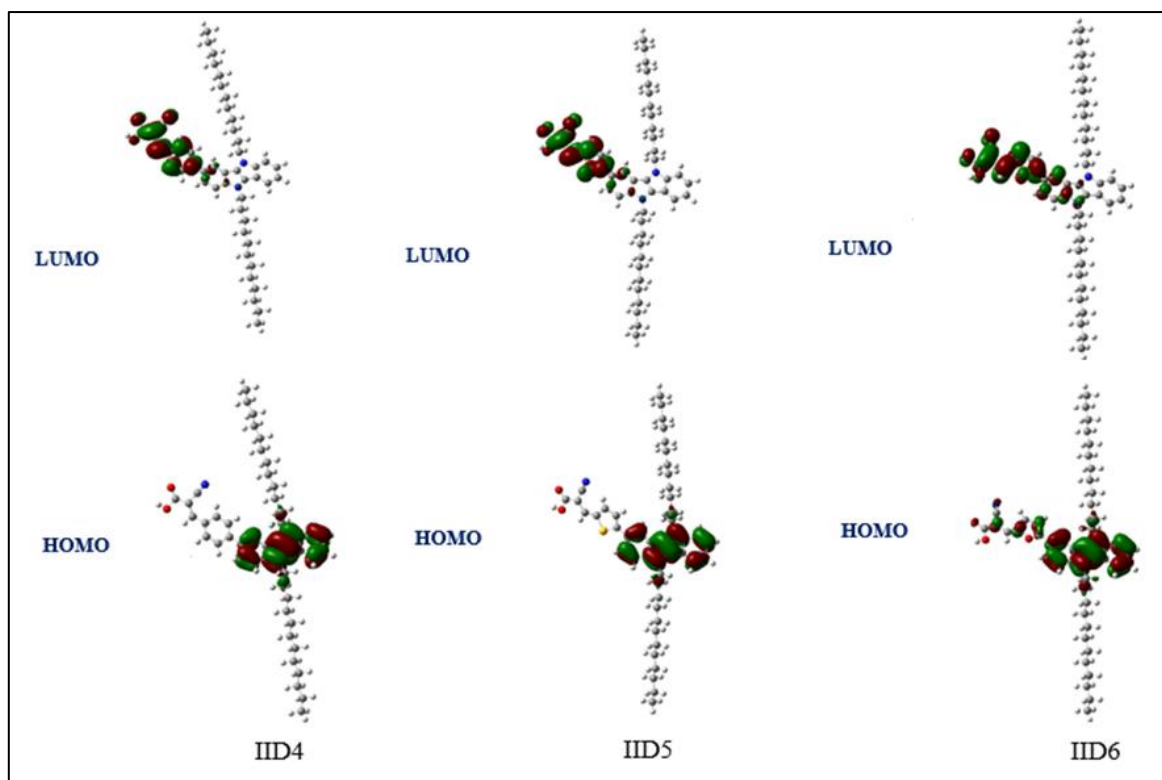


Figure 2.7 Frontier molecular orbital distributions of the dyes **IID-4**, **IID-5** and **IID-6**

Further the energy minimized structures (Figure 2.8) gives idea about the effect of different spacers on the performance.

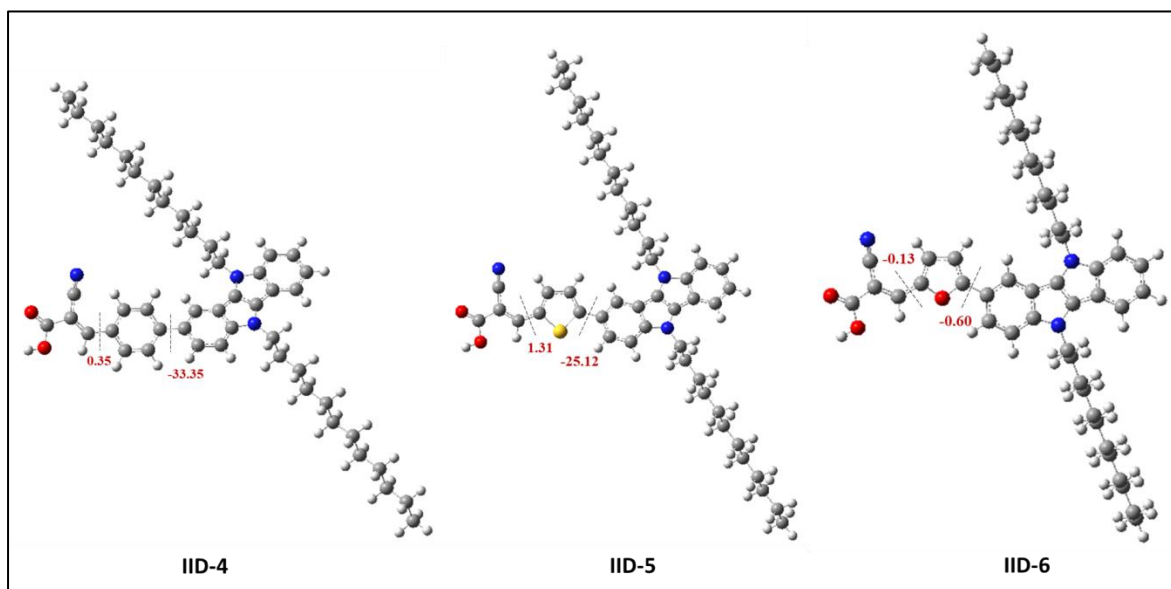


Figure 2.8 Energy minimized structure of the dyes **IID-4**, **IID-5** and **IID-6**

All the dyes were having almost coplanar conformation with respect to angle between spacer and anchoring group. But changes in the structure induced by the angle between donor and π -spacer. Benzene substituted dye **IID-4** was having more twisted conformation which is evident from their blue shifted absorption spectra with less prominent ICT bands. Furan substituted dye **IID-6** was more planar with lowest dihedral angle between donor and furan unit.

2.9 Photovoltaic Performance

The current-voltage (J-V) curves of DSSCs based on dyes **IID-4** to **IID-6** obtained under AM 1.5 solar simulator illumination (100 mWcm^{-2}) are shown in Figure 2.9 (a) and the corresponding photovoltaic parameters are listed in Table 2.5. All the devices showcased improved performance compared to their hexyl group incorporated counterparts even in the absence of co-adsorbent. This illustrated the significant role played by the longer alkyl chain (dodecyl group) in minimizing the back electron transfer reactions. In this scenario, The **IID-6** sensitized device showcased maximum power conversion efficiency of 4.46% ($J_{sc} = 9.09 \text{ mAcm}^{-2}$, $V_{oc} = 670 \text{ mV}$, and $FF = 73.25$). Under the same conditions **IID-4** and **IID-5** sensitized cells gave J_{sc} values of 6.93 mAcm^{-2} and 8.15 mAcm^{-2} , V_{oc} of 678 mV and 672 mV and FF of 74.03 and 74.34 corresponding to PCE of 3.44% and 4.06% respectively.

Table 2.5 Solar cell characteristics of DSSCs based on **IID-4**, **IID-5**, and **IID-6**

Sensitizer	V_{oc} (mV)	J_{sc} (mA/cm^2)	FF (%)	Efficiency (%)
IID-4	678 ± 2	6.93 ± 0.18	74.03 ± 0.32	3.44 ± 0.12
IID-5	672 ± 4	8.15 ± 0.22	74.34 ± 0.29	4.06 ± 0.11
IID-6	670 ± 3	9.09 ± 0.27	73.25 ± 0.38	4.46 ± 0.08

No significant shift was observed in the voltage of the devices. It was the current density which contributed to the significant differences in PCE for devices which lead to higher PCE for **IID-6**. **IID-4** was delivering the least efficiency among all the three dyes. The incident photon-to-current conversion efficiency (IPCE) of the cells are shown in Figure 2.9 (b) which was in accordance with the current density measured during J-V measurements. The solar cells based on **IID-4** showed blue shifted as well as lower IPCE value compared to other two

dyes. Even though **IID-5** and **IID-6** were having similar absorption behaviour, the onset extended up to 650 nm. The IPCE value of **IID-6** could manage to have higher absorption in visible region value exceeding 80%. This lead to higher current density for **IID-6** compared to **IID-5**.

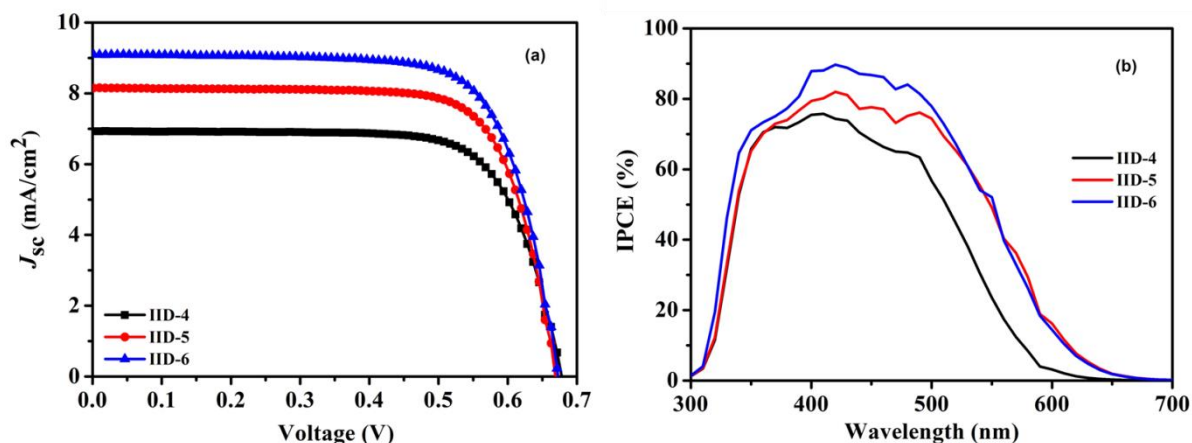


Figure 2.9 (a) J-V curve & (b) IPCE spectra of DSSCs based on the dyes

To understand further on recombination reactions in these solar cells, we carried out lifetime measurements using transient photovoltage decay and the graph obtained is shown in Figure 2.10 (a). All the three devices were having similar lifetime which implies that the rate of back electron reactions of the injected electrons also followed similar trend. In accordance with the similar voltages, the charge extraction measurements are presented in Figure 2.10 (b) which showed no significant shift in the conduction band edge of TiO_2 for any of the dyes. Both the lifetime and charge extraction measurements suggested similar voltage for the devices which is in agreement with the voltage measured. Further we performed transient photocurrent decay measurements to obtain the transport time of the solar cells. According to the data shown in Figure 2.11, **IID-5** and **IID-6** were having almost similar transport time which is lesser than that of **IID-4**. Transport time along with the recombination time/lifetime can give valuable information on charge collection efficiency of devices. Since there was not much change in the voltage for the current set of compounds, transport time can be taken as the limiting factor in determining the collection efficiency. This indicates that charge collection efficiency followed the trend in transport time leaving **IID-4** sensitized devices with lowest value.

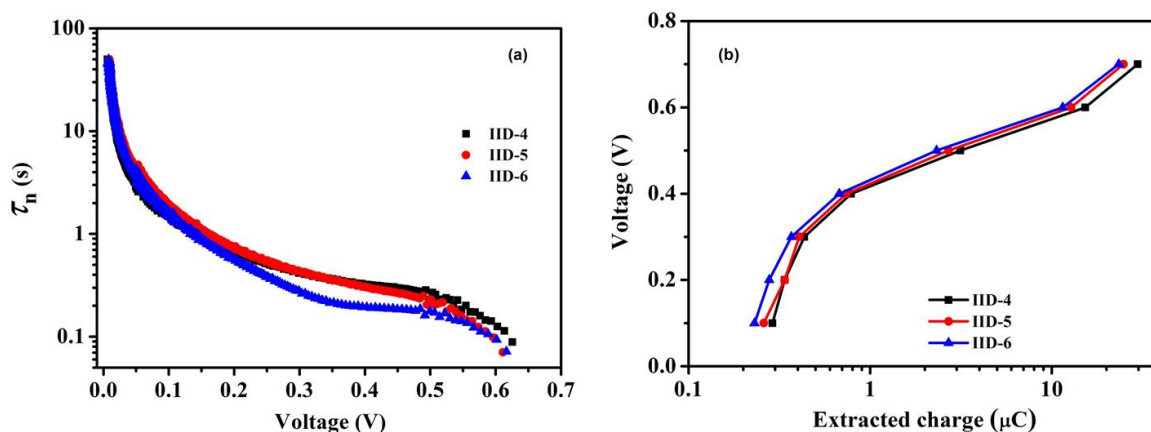


Figure 2.10 (a) Lifetime as a function of light intensity measured using TPV technique and (b) Extracted charge versus voltage from charge extraction measurement

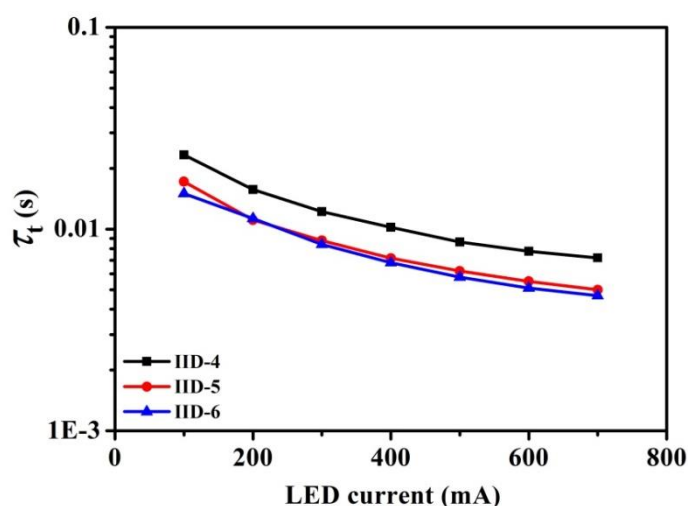


Figure 2.11 Transport time as a function of light intensity measured using TPC technique

2.10 Conclusion

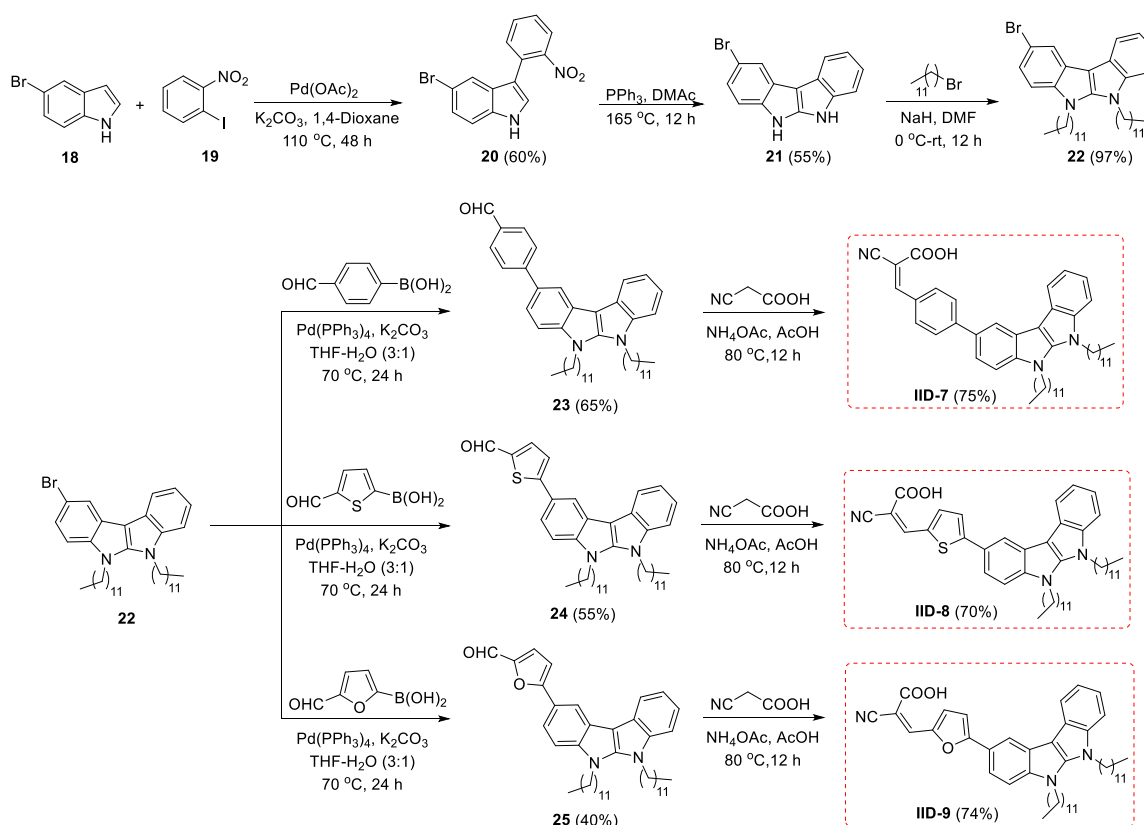
In summary, we initiated with development of D- π -A dyes which utilizes indolo[3,2-*b*]indole as donor, cyanoacrylic acid as acceptor/anchoring group and varied the π -spacer employed such as benzene, thiophene and furan to construct sensitizers **IID-1**, **IID-2** and **IID-3** respectively. To minimize dye aggregations, the two *N*-atoms of indolo[3,2-*b*]indole core was functionalized with hexyl chains. Though furan substituted dye was exhibiting higher light harvesting efficiency with wider absorption profile, **IID-1** having benzene as π -spacer outperformed the other two with higher photovoltage and current density. Optimization studies with co-adsorbent chenodeoxycholic acid (CDCA) further enhanced the performance with maximum efficiency realized using 20 mM CDCA concentration. This indicated

significant dye aggregations happening in the system and we concluded that the slightly twisted conformation of **IID-1** may be helping the system to alleviate dye aggregation and also the approach of oxidized species in the electrolyte coming closer to semiconductor. Further we did molecular engineering by replacing the hexyl group with dodecyl chain as an approach towards reducing dye aggregation. The dyes thus developed are **IID-4**, **IID-5** and **IID-6** with π -spacers as benzene, thiophene and furan respectively. By adopting this structural modification, all the dyes could outperform the previous set even in the absence of any co-adsorbent. This indicates the added advantage of dodecyl chains in inhibiting aggregate formation than hexyl chain and thus preventing the back electron transfer reactions. In the absence of aggregate formation, light harvesting efficiencies of dyes improved contributing significantly towards the power conversion efficiency (PCE) and furan substituted dye exhibited maximum PCE of 4.4 % and the benzene substituted dye **IID-4** delivered an efficiency of 3.44%.

Chapter 2B: Investigation of Indolo[2,3-*b*]indole Donor based D- π -A Dyes for DSSC

2.11 Synthesis and Characterization of IID-7, IID-8, and IID-9

The indolo[2,3-*b*]indole core was synthesized *via* a three step synthetic route starting from 5-bromoindole **18**. The first step involved a Pd-catalyzed C-3 arylation of 5-bromo-indole **18** with 1-iodo-2-nitrobenzene **19** affording the C-3 arylated indole **20** in 60% yield.¹⁸ The indolo[2,3-*b*]indole core **21** was then generated by the Cadogen reaction of **20** in presence of triphenylphosphine in DMAc at 165 °C. The final alkylation of **21** with 1-bromododecane afforded the halogenated didodecyl-substituted indolo[2,3-*b*]indole **22** in 97% yield. The attachment of the π -spacer was effected by the Suzuki reaction of brominated indolo[2,3-*b*]indole **22** with formyl-aryl/heteroaryl boronic acids to afford **23** (benzene as π -spacer), **24** (thiophene as π -spacer) and **25** (furan as π -spacer) respectively. From the Suzuki coupling products, the dyes **IID-7**, **IID-8** and **IID-9** were synthesized by Knoevenagel condensation with cyanoacetic acid (Scheme 2.3).



Scheme 2.3 Synthetic route adopted for indolo[2,3-*b*]indole based dyes **IID-7**, **IID-8** and **IID-9**

2.12 Photophysical and Electrochemical properties

The absorption spectra of the dyes **IID-7**, **IID-8** and **IID-9** in tetrahydrofuran and on TiO₂ are shown in Figure 2.12 (a) and Figure 2.12 (b) respectively and the relevant data are documented in Table 2B.1. Both the spectra showed improved and red shifted absorption behavior for **IID-8** and **IID-9** compared to benzene substituted dye **IID-7**. The dyes **IID-8** and **IID-9** with thiophene and furan π -linker were showing almost similar molar absorption coefficient (27875 and 28500 M⁻¹cm⁻¹) and absorption maximum (436 and 441 nm) and their absorption onsets in solution state were extended up to 505 nm. The solid state absorption spectra of all the compounds were broader and exhibited bathochromic shift compared to solution state spectra. This indicated the predominant formation of aggregates when compounds were sensitized on TiO₂. The cyclic voltammogram of the dyes are shown in Figure 2.13 and the energetics calculated is presented in Table 2.6. According to this data, the dyes were proved to be potential candidates for device making with TiO₂ as semiconductor and iodide/triiodide as redox mediator.

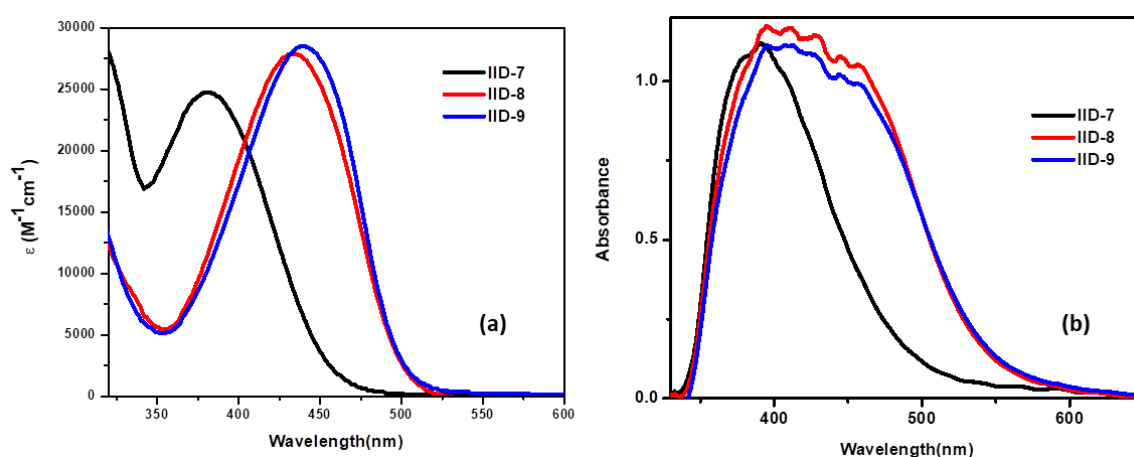


Figure 2.12 (a) Solution state absorption spectra of dyes in THF. (b) Solid state absorption spectra of dyes on TiO₂

Table 2.6 Photophysical and electrochemical data of **IID-7** to **IID-9** dyes

Sensitizer	λ_{\max} , nm (ϵ , M ⁻¹ cm ⁻¹)	$E_{\text{ox}}(\text{Fc}/\text{Fc}^+)$ (V)	E_{HOMO} (vs NHE) (V)	E_{0-0} eV	E_{LUMO} (vs NHE) (V)
IID-7	383 (24750)	0.29	0.92	2.74	-1.82
IID-8	436 (27875)	0.35	0.98	2.46	-1.48
IID-9	441 (28500)	0.33	0.96	2.45	-1.49

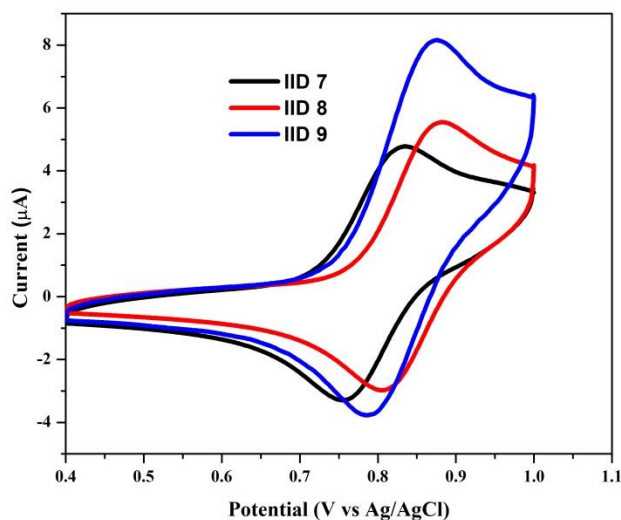


Figure 2.13 Cyclic voltammogram of IID-7, IID-8, and IID-9 dyes in dichloromethane

2. 13 Computational Studies

To investigate the molecular structure and electronic distribution of the three organic dyes, these were optimized using DFT calculations with Gaussian 09 program. The calculations were performed with the B3LYP exchange correlation functional under cc-PVDZ basis set. The absence of imaginary frequencies was confirmed with vibration analysis. The electronic distribution of frontier molecular orbitals is shown in Figure 2.14 and the energy minimized structures are shown in Figure 2.15.

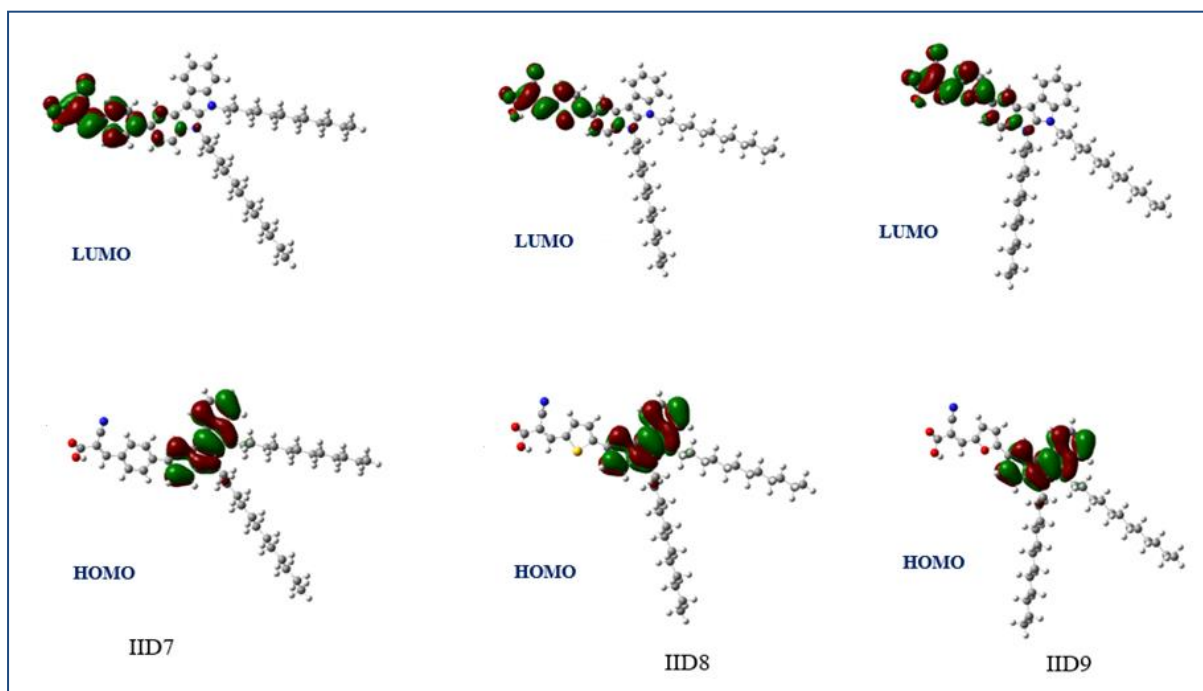


Figure 2.14 Frontier molecular orbital distributions of the dyes IID-7, IID-8 and IID-9

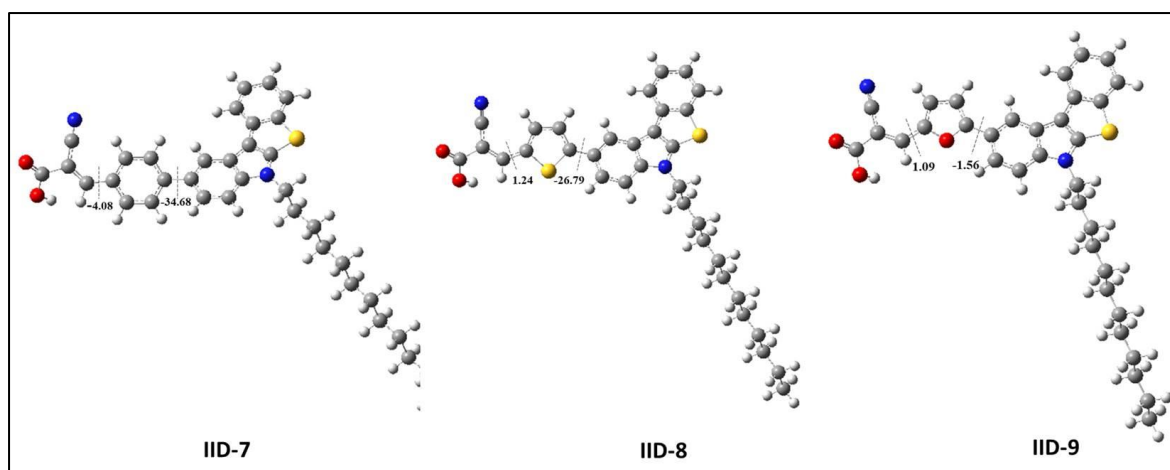


Figure 2.15 Energy minimized structure of the dyes **IID-7**, **IID-8** and **IID-9**

All the dyes are having HOMO electron density mostly located on the donor unit and the LUMO located on acceptor unit/cyanoacrylic acid and extended to π -spacer also. These results show good HOMO-LUMO overlap and possibility of strong coupling of semiconductor conduction band with the sensitizer. This can in turn make sure of efficient electron injection to conduction band of TiO_2 which is essential for the current generation in the device. According to the energy minimized structure of compounds, **IID-9** with furan as π -spacer exhibited maximum planarity with least dihedral angle value of 0.60° between the donor and π -spacer fragments. The dye **IID-7** was having a twisted conformation with a dihedral value of 33.35° . These results are also in agreement with the experimental absorption spectra, absorption of **IID-7** was blue shifted compared to those of **IID-9**.

2.14 Photovoltaic Performance

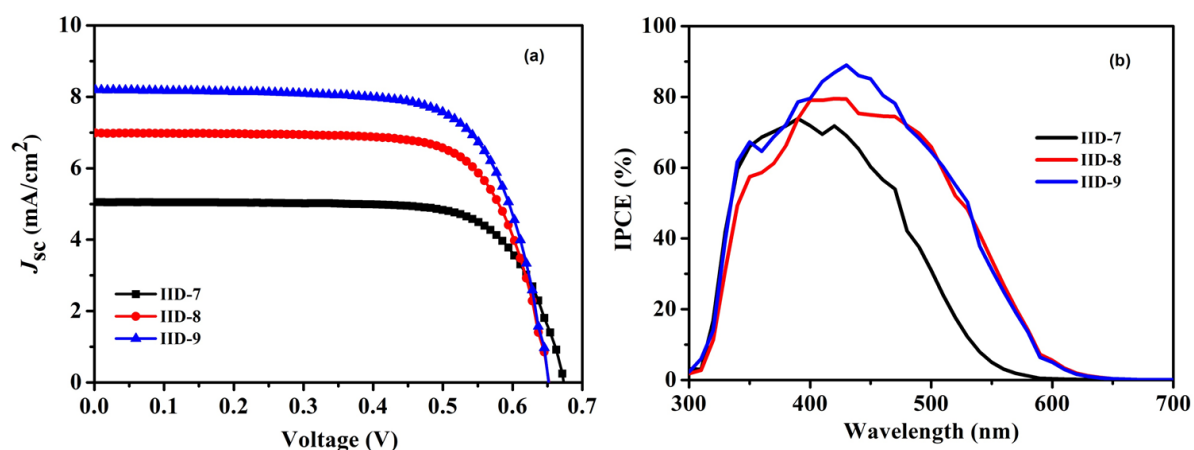
The photovoltaic performance of DSSCs fabricated with the dyes **IID-7**, **IID-8** and **IID-9** were evaluated under full sun AM 1.5G (100 mW cm^{-2}) conditions. The current density-voltage (J - V) and incident-photon-to-current conversion efficiency (IPCE) curves are shown in Figure 2.16. The J - V parameters are summarized in Table 2.7.

The furan substituted dye, **IID-9** outperformed the other dyes (**IID-7** and **IID-8**) giving a power conversion efficiency of 3.81% ($J_{\text{sc}} = 8.19 \text{ mAcm}^{-2}$, $V_{\text{oc}} = 651 \text{ mV}$, and $\text{FF} = 71.62$) whereas **IID-8** showed a power conversion efficiency of 3.32% ($J_{\text{sc}} = 6.98 \text{ mAcm}^{-2}$, $V_{\text{oc}} = 651 \text{ mV}$ and $\text{FF} = 73.18$) and **IID-7** displayed a power conversion efficiency of 2.48% ($J_{\text{sc}} = 5.05 \text{ mAcm}^{-2}$, $V_{\text{oc}} = 673 \text{ mV}$ and $\text{FF} = 73.42$) respectively.

Table 2.7 Solar cell characteristics of DSSCs based on **IID-7**, **IID-8**, and **IID-9**

Sensitizer	V_{OC} (mV)	J_{SC} (mA/cm ²)	FF (%)	Efficiency (%)
IID-7	673 ± 3	5.05 ± 0.21	73.42 ± 0.42	2.48 ± 0.11
IID-8	651 ± 4	6.98 ± 0.31	73.18 ± 0.55	3.32 ± 0.13
IID-9	651 ± 3	8.19 ± 0.33	71.62 ± 0.57	3.81 ± 0.09

The efficiencies of devices were in parallel to their current generation. Though **IID-7** with benzene π -linker outperformed other dyes in terms of photovoltage, lowest current density generated resulted in its inferior performance compared to the rest of the dyes. This observation is also reflected in the IPCE spectra. According to this, **IID-7** showed blue shifted as well as lower IPCE value compared to **IID-8** and **IID-9**. The devices sensitized with **IID-8** and **IID-9** are having same absorption on set but the IPCE value of **IID-9** was able to exceed 80% and reached a maximum value of 89% at 429 nm. Accordingly, **IID-9** showed slight increment in current density compared to that of **IID-8**.

**Figure 2.16** (a) Current-voltage characteristics of DSSCs with **IID-7**, **IID-8**, and **IID-9** under 1.5G. (b) Spectra of incident photon-to-current conversion efficiency (IPCE) for DSSCs

The data obtained for transient photovoltage decay measurements, charge extraction measurements and transient photocurrent decay measurements are shown in Figure 2.17. While the charge extraction measurements showed similar shift in the conduction band of TiO₂ (Figure 2.17 (a)), lifetime of the devices exhibited deviations (Figure 2.17 (b)). **IID-7** sensitized cells showed better lifetime which was also translated into better photovoltage compared to the rest of the dyes. Devices based on furan and thiophene substituted dyes **IID-**

8 and **IID-9** were showcasing almost similar lifetime as well as photovoltage. Further we measured transient photocurrent decay to understand the trends in transport time which is presented in (Figure 2.17 4(c)). The transport time of the devices was not in favour of **IID-7** which exhibited higher transport time compared to **IID-8** and **IID-9**.

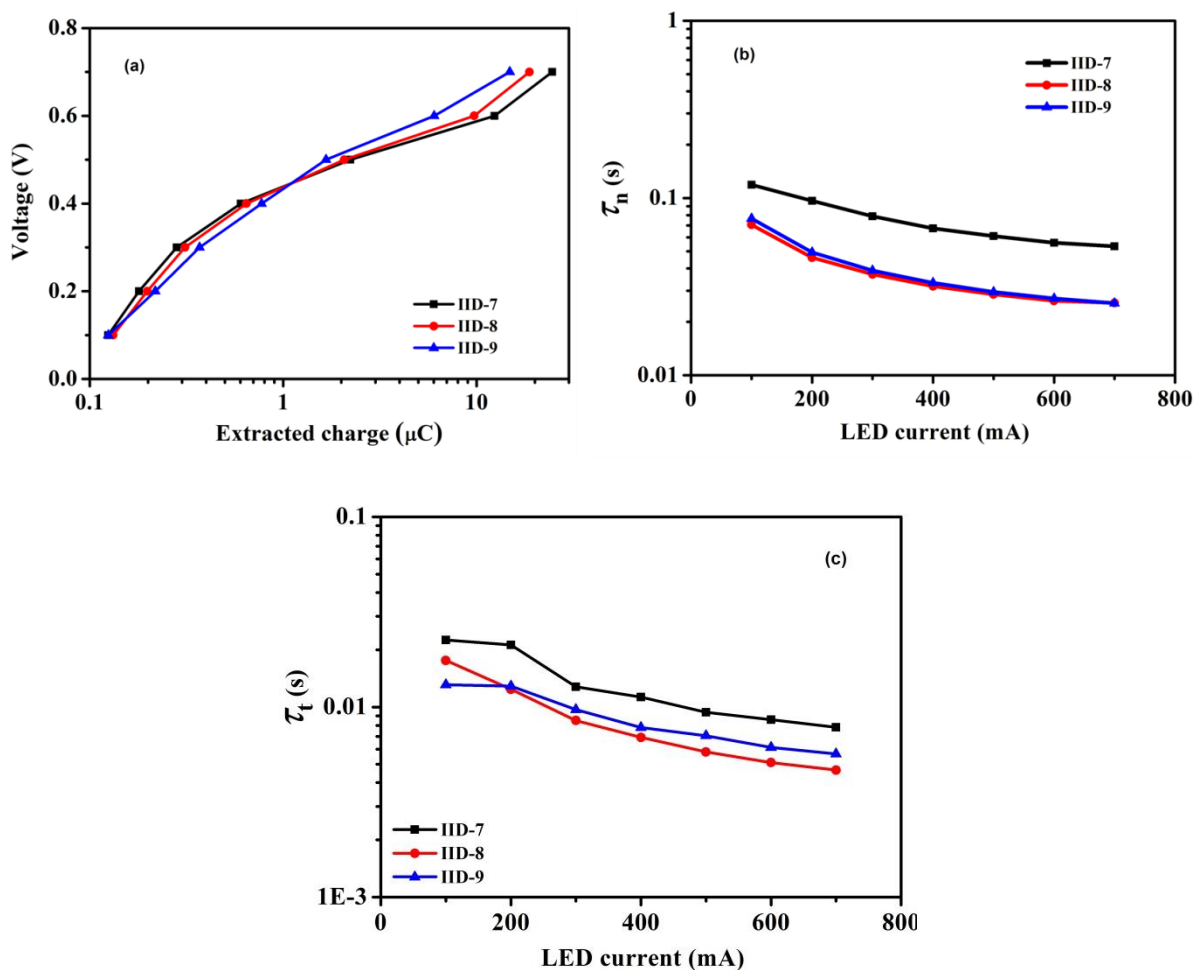


Figure 2.17 (a) Extracted charge versus voltage from charge extraction measurement (b) Lifetime as a function of light intensity measured using TPV technique and (c) Transport time as a function of light intensity measured using TPC technique

2.15 Conclusion

In summary, we successfully synthesized three new D- π -A organic dyes based on indolo[2,3-*b*]indole as donor and by varying the π -spacer unit with benzene (**IID-7**), thiophene (**IID-8**) and furan (**IID-9**). Here also we incorporated dodecyl group on the donor moiety to minimize the back electron reactions. The performances of the devices were evaluated in the absence of any co-adsorbent. Furan substituted dye, **IID-9** showcased the best performance with a PCE of 3.81% and least PCE was delivered by **IID-7** with 2.48%. The changes in current density brought changes in PCE among the devices. Though **IID-7** was having higher photovoltage,

there was significant decrease in its current density as evident from the IPCE spectra. This can be attributed to its lower light harvesting ability which is evident from both solution as well as solid state absorption of **IID-7** dye.

2.16 Experimental Section

General procedure for the synthesis of indolo[3,2-*b*]indole:

The enolizable ketone, cyclohexanone (2.0 equiv.) and primary amine, *n*-hexylamine (2.0 equiv.) were weighed into a dry reaction tube. Dry toluene along with 4 Å MS (50 mg) was added and allowed to stir at 60 °C for 1 hour, after which 3-nitro-*N*-tosyl indole (1.0 equiv.) was added into it and again kept it for stirring at the same temperature for 11 hours. After the complete consumption of 3-nitro-*N*-tosyl indole, Chloranil (3.0 equiv.) along with toluene was added and kept at 100 °C for 10 hours. The solvent was evaporated in vacuo and the residue on activated neutral alumina column chromatography yielded indolo[3,2-*b*]indole with hexanes and ethyl acetate as eluent.

Synthesis of *tert*-Butyl 8-bromo-10-hexylindolo[3,2-*b*]indole-5(10H)-carboxylate (4**):** The reaction was performed according to general procedure with 5-bromo-3-nitro-*N*-Boc indole (500 mg, 1.47 mmol), *n*-hexylamine (297 mg, 2.94 mmol) and cyclohexanone (288 mg, 2.94 mmol) and chloranil (1084 mg, 4.41 mmol). The crude product was purified by activated neutral alumina column chromatography (2% ethyl acetate in hexane) to afford the desired product as a pale yellow viscous liquid (483 mg, 70%). TLC (SiO₂): *R_f*; 0.71 (7% ethyl acetate in hexane); ¹H NMR (500 MHz, CDCl₃, TMS): δ 8.44-8.43 (m, 1H), 8.14-8.13 (m, 1H), 7.78 (s, 1H), 7.41-7.35 (m, 2H), 7.29-7.24 (m, 1H), 7.16 (t, *J* = 8 Hz, 1H), 4.38 (t, *J* = 8 Hz, 2H), 1.92-1.86 (m, 2H), 1.79 (s, 9H), 1.38-1.25 (m, 6H), 0.85 (t, *J* = 7 Hz, 3H); ¹³C NMR (125 MHz, CDCl₃): δ 150.4, 140.7, 126.9, 126.5, 122.9, 121.9, 120.4, 119.9, 119.2, 118.3, 116.0, 115.8, 109.5, 84.3, 44.9, 31.6, 30.3, 28.6, 26.7, 22.5, 14.0; HRMS (ESI-Orbitrap) *m/z*: (M+Na)⁺ calcd for C₂₅H₂₉BrN₂O₂Na: 491.1305; found: 491.1320.

Synthesis of 3-bromo-5-ethyl-5,10-dihydroindolo[3,2-*b*]indole (5**):** To a stirred solution of **4** (400 mg, 0.85 mmol) in DCM (15 mL), TFA (10%) was added portion wise under nitrogen atmosphere at 0 °C. The reaction mixture was then warmed to room temperature and stirred for 3 hours. Upon completion, the reaction mixture was concentrated under reduced pressure and water was added, and then extracted with EtOAc. The organic layer washed successively with brine and the combined organic layer was dried over anhydrous Na₂SO₄ and concentrated under reduced pressure to yield the deprotected compound **5** as colourless solid

(282 mg, 90%). m.p. 145-148 °C; ¹H NMR (500 MHz, Acetone): δ 10.42 (s, 1H), 7.90 (s, 1H), 7.65 (d, *J* = 8.0 Hz, 1H), 7.42 (d, *J* = 8.5 Hz, 1H), 7.36 (d, *J* = 8.5 Hz, 1H), 7.17-7.16 (m, 1H), 7.14 – 7.11 (m, 1H), 6.97-6.94 (m, 1H), 4.43 (t, *J* = 7.0 Hz, 2H), 1.81-1.75 (m, 2H), 1.28-1.23 (m, 2H), 1.18-1.02 (m, 4H), 0.67 (t, *J* = 7.5 Hz, 3H); ¹³C NMR (125 MHz, Acetone): δ 141.1, 139.4, 126.1, 125.6, 124.0, 122.3, 119.7, 118.1, 116.4, 114.4, 113.8, 110.8, 110.0, 44.7, 31.4, 30.2, 29.4, 29.3, 29.1, 29.0, 28.8, 28.7, 28.5, 26.4, 22.3, 13.4; HRMS (ESI-Orbitrap) *m/z*: (M+H)⁺ calcd for C₂₀H₂₂N₂Br: 369.0961; Found: 369.0972.

Synthesis of 3-bromo-5,10-dihexyl-5,10-dihydroindolo[3,2-*b*]indole (6): To a stirred solution of **5** (250 mg, 0.68 mmol) in a mixture of THF: DMF (8: 2, 5 mL), NaH (41 mg, 1.62 mmol) was added portion wise under nitrogen atmosphere at 0 °C. The reaction mixture was then warmed to room temperature and stirred for 30 minutes. The reaction mixture was cooled again to 0 °C and 1-bromohexane (134.7 mg, 0.82 mmol) was added dropwise and stirred at room temperature for 8 hours. Upon completion, the reaction mixture was concentrated under reduced pressure and water was added, and then extracted with EtOAc. The organic layer washed successively with brine and the combined organic layer was dried over anhydrous Na₂SO₄ and concentrated under reduced pressure and the residue on activated neutral alumina column chromatography (2% ethyl acetate in hexane) yielded the compound **6** as colourless solid (252 mg, 82%). m.p. 70 °C; ¹H NMR (500 MHz, CDCl₃) δ 7.88 (s, 1H), 7.79 (d, *J* = 7.5 Hz, 1H), 7.43 (d, *J* = 8.5 Hz, 1H), 7.34-7.25 (m, 3H), 7.15 (t, *J* = 7.5 Hz, 1H), 4.46-4.43 (m, 4H), 1.98-1.92 (m, 4H), 1.41-1.30 (m, 4H), 1.27-1.25 (m, 8H), 0.87-0.83 (m, 6H); ¹³C NMR (125 MHz, CDCl₃): δ 140.9, 139.0, 124.0, 122.2, 120.0, 118.2, 117.8, 114.3, 110.9, 109.8, 45.3, 31.6, 30.2, 26.8, 22.5, 14.0; HRMS (ESI-Orbitrap) *m/z*: (M+H)⁺ calcd for C₂₆H₃₄N₂Br: 453.1900; found: 453.1907.

Synthesis of 4-(5,10-diethyl-5,10-dihydroindolo[3,2-*b*]indol-3-yl)benzaldehyde (7): A mixture of indoloindole **6** (250 mg, 0.551 mmol), 4-formyl phenyl boronic acid (124 mg, 0.83 mmol), Pd(PPh₃)₄ (64 mg, 0.055 mmol), K₂CO₃ (380 mg, 2.75 mmol) were weighed into a Schlenk tube and degassed for 10 minutes. Degassed THF (5 mL) and water (1.5 mL) was added then, the reaction mixture was purged with argon and allowed to stir at 65 °C for 24 hours. The solvent was evaporated in vacuum and the residue on activated neutral alumina column chromatography (3% ethyl acetate in hexane) yielded the product **7** as colourless amorphous solid (171 mg, 65%). TLC (SiO₂): R_f: 0.38 (7% ethyl acetate in hexane); ¹H NMR (500 MHz, CDCl₃): δ 10.07 (s, 1H), 8.08-8.04 (m, 1H), 7.98 (d, *J* = 8 Hz, 2H), 7.87 (d, *J* = 8 Hz, 2H), 7.58-7.53 (m, 2H), 7.50-7.42 (m, 2H), 7.33 (t, *J* = 7.5 Hz, 1H), 7.20 (t, *J* = 7.5 Hz, 1H), 4.54-4.52 (m, 4H), 2.03- 1.99 (m, 4H), 1.46-1.43 (m, 4H), 1.35-1.25 (m, 8H), 0.87-0.83

(m, 6H); ^{13}C NMR (126 MHz, CDCl_3): δ 192.0, 148.7, 140.7, 140.5, 134.4, 130.4, 129.6, 127.6, 122.0, 121.1, 118.3, 117.8, 116.6, 115.2, 110.2, 109.9, 45.5, 45.4, 31.6, 30.3, 29.7, 26.8, 22.6, 14.0; HRMS (ESI-Orbitrap) m/z : $(\text{M}+\text{H})^+$ calcd for $\text{C}_{33}\text{H}_{39}\text{N}_2\text{O}$: 479.3057; found: 479.3043.

Synthesis of 2-cyano-3-(4-(5,10-dihexyl-5,10-dihydroindolo[3,2-*b*]indol-3-yl)phenyl)acrylic acid (IID-1): A mixture of aldehyde **7** (150 mg, 0.31 mmol), cyanoacetic acid (80 mg, 0.94 mmol), ammonium acetate (119 mg, 1.55 mmol) in acetic acid (3.0 mL) was heated at reflux overnight under argon atmosphere. After cooling to room temperature, it was precipitated by pouring into water. The precipitate was washed with water and dried in vacuum oven. The product **IID-1** was obtained as a red solid (130 mg, 77%). m.p. 180-183 °C; ^1H NMR (500 MHz, Acetone) δ 8.38 (s, 2H), 8.23 (d, $J = 8.5$ Hz, 2H), 8.04 (d, $J = 8.5$ Hz, 2H), 7.94 (d, $J = 8.0$ Hz, 1H), 7.74 (s, 2H), 7.63 (d, $J = 8.0$ Hz, 1H), 7.30 (t, $J = 7.0$ Hz, 1H), 7.16 (t, $J = 7.5$ Hz, 1H), 4.71 (t, $J = 7.0$ Hz, 2H), 4.65 (t, $J = 7.0$ Hz, 2H), 2.05-1.98 (m, 4H), 1.45-1.42 (m, 4H), 1.36- 1.23 (m, 8H), 0.84-0.79 (m, 6H); ^{13}C NMR (125 MHz, Acetone) δ 162.4, 153.7, 146.6, 145.6, 140.4, 140.3, 131.2, 129.1, 128.8, 126.8, 126.0, 125.3, 121.4, 120.3, 117.7, 117.3, 116.1, 115.4, 114.8, 114.0, 110.1, 109.6, 103.8, 101.3, 44.4, 44.2, 30.9, 30.9, 29.6, 28.9, 26.0, 21.8, 21.8, 12.8, 12.8; HRMS (ESI-Orbitrap) m/z : $(\text{M})^+$ calcd for $\text{C}_{36}\text{H}_{39}\text{N}_3\text{O}_2$: 545.3037; Found: 545.3033.

Synthesis of 5-(5,10-dihexyl-5,10-dihydroindolo[3,2-*b*]indol-3-yl)thiophene-2-carbaldehyde (8): A mixture of indoloindole **6** (250 mg, 0.551 mmol), (5-formylthiophene-2-yl)boronic acid (129 mg, 0.83 mmol), $\text{Pd}(\text{PPh}_3)_4$ (64 mg, 0.055 mmol), K_2CO_3 (380 mg, 2.75 mmol) were weighed into a Schlenk tube and degassed for 10 minutes. Degassed THF (5 mL) and water (1.5 mL) was added then, the reaction mixture was purged with argon and allowed to stir at 65 °C for 24 hours. The solvent was evaporated under vacuum and the residue on activated neutral alumina column chromatography (3% ethyl acetate in hexane) yielded the product **8** as a white amorphous solid (160 mg, 60%). TLC (SiO_2): R_f : 0.39 (7% ethyl acetate in hexane); ^1H NMR (500 MHz, CDCl_3): δ 9.89 (s, 1H), 8.13 (s, 1H), 7.84 (d, $J = 7$ Hz, 1H), 7.77-7.76 (m, 1H), 7.62-7.60 (m, 1H), 7.49-7.47 (m, 2H), 7.43-7.42 (m, 1H), 7.33 (t, $J = 7.5$ Hz, 1H), 7.20 (t, $J = 7.5$ Hz, 1H), 4.53-4.49 (m, 4H), 2.00-1.99 (m, 4H), 1.48-1.42 (m, 4H), 1.34-1.26 (m, 8H), 0.86-0.84 (m, 6H); ^{13}C NMR (126 MHz, CDCl_3): δ 182.6, 157.0, 141.1, 140.8, 137.9, 127.0, 125.8, 123.3, 122.7, 122.2, 120.1, 118.4, 117.8, 116.0, 115.0, 114.4, 110.2, 109.9, 45.6, 45.4, 31.6, 31.6, 30.3, 30.2, 26.9, 26.8, 22.6, 22.5; HRMS (ESI-Orbitrap) m/z : $(\text{M}+\text{H})^+$ calcd for $\text{C}_{31}\text{H}_{37}\text{N}_2\text{OS}$: 485.2621; Found: 485.2634.

Synthesis of 2-cyano-3-(5-(5,10-dihexyl-5,10-dihydroindolo[3,2-*b*]indol-3-yl)thiophen-2-yl) acrylic acid (IID-2): A mixture of aldehyde **8** (150 mg, 0.31mmol), cyanoacetic acid (80 mg, 0.94mmol), ammonium acetate (119 mg, 1.55mmol) in acetic acid (3.0 mL) was heated at reflux for overnight under argon atmosphere. After cooling to room temperature, it was precipitated by pouring in to water. Precipitate was washed with water and dried in vacuum oven. The product **IID-2** was obtained as a red solid (108 mg, 63%). m.p. 240-242 °C; ¹H NMR (500 MHz, CDCl₃) δ 8.30 (s, 1H), 8.13-8.07 (m, 1H), 7.83-7.75 (m, 2H), 7.70-7.66 (m, 1H), 7.61-7.59 (m, 1H), 7.49-7.47 (m, 1H), 7.45-7.42 (m, 1H), 7.35 – 7.32 (m, 1H), 7.20 (t, *J* = 7.5 Hz) 4.51 (t, *J* = 7Hz, 2H), 4.47 (t, *J* = 7 Hz, 2H), 2.01-1.97 (m, 4H), 1.46-1.40 (m, 4H), 1.31-1.25 (m, 8H), 0.87- 0.82 (m, 6H); ¹³C NMR (126 MHz, CDCl₃) δ 158.7, 147.7, 141.0, 140.9, 140.2, 139.5, 133.5, 129.3, 126.6, 123.3, 123.0, 122.3, 120.5, 118.5, 117.9, 116.1, 110.4, 110.0, 45.6, 31.6, 30.3, 30.2, 29.7, 26.8, 26.8, 22.5, 14.0; HRMS (ESI-Orbitrap) *m/z*: (M)⁺ calcd for C₃₄H₃₇N₃O₂S: 551.2601; found: 551.2610.

Synthesis of 5-(5,10-dihexyl-5,10-dihydroindolo[3,2-*b*]indol-3-yl)furan-2-carbaldehyde (9): A mixture of indoloindole **6** (250 mg, 0.551 mmol), (5-formylfuran-2-yl)boronic acid (116 mg, 0.83 mmol), Pd(PPh₃)₄ (64 mg, 0.055 mmol), K₂CO₃ (380 mg, 2.75 mmol) were weighed into a Schlenk tube and degassed for 10 minutes. Degassed THF (5 mL) and water (1.5 mL) was then added and the reaction mixture was purged with argon and allowed to stir at 65 °C for 24 hours. The solvent was evaporated under vacuum and the residue on activated neutral alumina column chromatography (3% ethyl acetate in hexane) yielded the product **9** as a white amorphous solid (170 mg, 66%). TLC (SiO₂): R_f: 0.37 (7% ethyl acetate in hexane); ¹H NMR (500 MHz, CDCl₃): δ 9.63 (s, 1H), 8.29 (s, 1H), 7.83 (d, *J* = 8 Hz, 1H), 7.73 (d, *J* = 8.5 Hz, 1H), 7.50 – 7.46 (m, 2H), 7.36 (d, *J* = 3.5 Hz, 1H), 7.31 (t, *J* = 8 Hz, 1H), 7.21-7.18 (m, 1H), 6.82 (d, *J* = 4 Hz, 1H), 4.54 (t, *J* = 7 Hz, 2H), 4.49 (t, *J* = 7.5 Hz, 2H), 2.00-1.97 (m, 4H), 1.46-1.43 (m, 4H), 1.34-1.25 (m, 8H), 0.84-0.82 (m, 6H); ¹³C NMR (125 MHz, CDCl₃): δ 161.8, 151.5, 149.8, 144.9, 140.9, 140.8, 129.2, 128.1, 126.8, 125.9, 125.3, 123.2, 122.1, 119.3, 118.4, 117.8, 115.9, 115.2, 114.8, 114.4, 112.6, 110.1, 110.0, 106.0, 45.5, 45.4, 31.6, 31.5, 30.9, 30.4, 30.2, 29.7, 26.8, 22.5, 14.0; HRMS (ESI-Orbitrap) *m/z*: (M+H)⁺ calcd for C₃₁H₃₇N₂O₂: 469.2850; Found: 469.2863.

Synthesis of 2-cyano-3-(5-(5,10-dihexyl-5,10-dihydroindolo[3,2-*b*]indol-3-yl)furan-2-yl) acrylic acid (IID-3): A mixture of aldehyde **9** (150 mg, 0.32mmol), cyanoacetic acid (82 mg, 0.96mmol), ammonium acetate (123 mg, 1.6 mmol) in acetic acid (3.0 mL) was heated at reflux for overnight under argon atmosphere. After cooling to room temperature, it was precipitated by pouring in to water. Precipitate was washed with water and dried in vacuum

oven. The product **IID-3** was obtained as a red solid (120 mg, 70%). m.p. 190-193 °C; ¹H NMR (500 MHz, Acetone): δ 8.73 (s, 1H), 8.09 (s, 1H), 7.95 (d, *J* = 8.0 Hz, 1H), 7.92 (d, *J* = 8.5 Hz, 1H), 7.76 (d, *J* = 9 Hz, 1H), 7.66 (d, *J* = 8.0 Hz, 1H), 7.57 (d, *J* = 3.5 Hz, 1H), 7.33 (t, *J* = 7.5 Hz, 1H), 7.26 (d, *J* = 7.5 Hz, 1H), 7.18 (t, *J* = 7.5 Hz, 1H), 4.71 – 4.67 (m, 4H), 2.03-1.97 (m, 4H), 1.49-1.43 (m, 4H), 1.36-1.21 (m, 8H), 0.85-0.79 (m, 6H); ¹³C NMR (125 MHz, CDCl₃): δ 163.8, 162.2, 147.4, 141.0, 137.5, 127.1, 121.9, 119.0, 118.5, 116.5, 110.7, 110.4, 107.5, 95.1, 44.9, 31.5, 31.4, 26.4, 26.2, 22.3, 13.3, 13.3; HRMS (ESI-Orbitrap) *m/z*: (M+H)⁺ calcd for C₃₄H₃₇N₃O₃: 535.2829; found: 535.2820.

Synthesis of 5-bromo-2-(2-nitrophenyl)-1H-indole (12): To a 100 mL schlenck flask were added 5-bromoaniline (2 g, 10.2 mmol), compound 1-iodo-2-nitrobenzene (3 g, 12.2 mmol), Pd(OAc)₂ (114 mg, 5 mol%), K₂CO₃ (2.8 g, 20.2 mmol), and norbornene (1.9 g, 20.2 mmol). The reaction vessel was degassed using vacuum pump and back filled with argon. This procedure was repeated three times which was followed by addition of 0.5 molar solution of H₂O in DMA as solvent under argon atmosphere. The reaction mixture was stirred at 70 °C for 48 h. The crude reaction mixture was then filtered through celite and extracted with ethyl acetate. The organic layer was washed successively with water and brine which was then dried over Na₂SO₄. Solvent removal was followed by column purification on silica gel to obtain **12** as red coloured solid (2.2 g, 7.0 mmol, 70%). m.p. 134-136 °C; ¹H NMR (500 MHz, CDCl₃): 8.48 (s, 1H), 7.78 (d, *J* = 8 Hz, 1H), 7.70 (s, 1H), 7.62-7.57 (m, 2H), 7.45 (t, *J* = 7 Hz, 1H), 7.25 (d, *J* = 9 Hz, 1H), 7.19 (d, *J* = 4.5 Hz, 1H), 6.57 (s, 1H) ppm; ¹³C NMR (125 MHz, (CDCl₃) : 149.0, 135.5, 133.6, 132.4, 131.8, 129.9, 129.1, 126.5, 126.1, 124.5, 123.4, 113.6, 112.7, 103.9 ppm. HRMS (ESI-Orbitrap) *m/z*: (M-H)⁺ calcd for C₁₄H₈BrN₂O₂: 314.9775, found: 314.9765.

Synthesis of 3-bromo-10-dodecyl-5,10-dihydroindolo[3,2-*b*]indole (13): To a stirred solution of **12** (2 g, 6.30 mmol) in dry DMF was added NaH (2.26 g, 9.45 mmol) under nitrogen atmosphere at 0 °C. The reaction mixture was then warmed to room temperature and stirred for 30 minutes. The reaction mixture was cooled again to 0 °C and 1-bromododecane (1.8 g, 7.56 mmol) was added dropwise and stirred at room temperature for 8 hours. Upon completion, the reaction mixture was quenched by adding water slowly and then extracted with EtOAc. The organic layer was washed successively with water and brine which was then dried over anhydrous Na₂SO₄. After solvent removal, column purification was done on silica gel to isolate the alkylated product as red coloured viscous oil (2.9 g, 5.29 mmol, 98%). Rf: 0.48 (5% ethyl acetate in hexane) ¹H NMR (500 MHz, CDCl₃): 7.98 (d, *J* = 8.5 Hz, 1H),

7.66 (s, 1H), 7.62 (t, $J = 7.5$ Hz, 1H), 7.56 (t, $J = 7.5$ Hz, 1H), 7.45 (d, $J = 7$ Hz, 1H), 7.24 (d, $J = 8.5$ Hz, 1H), 7.18-7.15 (m, 1H), 6.32 (s, 1H), 3.83 (t, $J = 7$ Hz, 2H), 1.54-1.51 (m, 2H), 1.22-1.04 (m, 18H), 0.81 (t, $J = 7$ Hz, 3H)) ppm; ^{13}C NMR (125 MHz, CDCl_3) : 150.0, 136.3, 135.6, 133.4, 132.6, 129.9, 127.3, 124.8, 124.4, 123.3, 113.0, 111.5, 102.0, 44.4, 31.9, 29.6, 29.6, 29.6, 29.5, 29.3, 29.0, 26.7, 22.7, 14.1 ppm. HRMS (ESI-Orbitrap) m/z : $(\text{M}+\text{H})^+$ calcd for $\text{C}_{26}\text{H}_{34}\text{BrN}_2\text{O}_2$: 485.1804, found: 485.1802.

To this alkylated intermediate (2.9 g, 5.90 mmol) in DMA was added PPh_3 (3.86 g, 14.7 mmol) and stirred the reaction mixture for 24 h at 165°C . After completion of the reaction, the reaction mixture was extracted with ethyl acetate and washed successively with water and brine. After solvent removal, column purification was done on silica gel to isolate the product **13** as colourless solid (2.4 g, 5.29 mmol, 90%). m.p. $74-76^\circ\text{C}$; ^1H NMR (500 MHz, $(\text{CD}_3\text{CO})_2$): 10.38 (s, 1H), 7.95-7.92 (m, 2H), 7.59-7.56 (m, 2H), 7.34 (d, $J = 8.5$ Hz, 1H), 7.26 (t, $J = 7.5$ Hz, 1H), 7.16 (t, $J = 7.5$ Hz, 1H), 4.62 (t, $J = 7$ Hz, 2H), 2.01-1.96 (m, 2H), 1.44-1.39 (m, 2H) 1.35-1.22 (m, 16H), 0.88 (t, $J = 7.5$ Hz, 3H) ppm; ^{13}C NMR (125 MHz, CDCl_3) : 141.3, 139.2, 127.9, 123.7, 123.6, 122.4, 120.2, 118.6, 117.7, 116.1, 114.8, 112.4, 111.6, 110.3, 44.8, 31.7, 30.2, 26.6, 22.4, 13.4 ppm. HRMS (ESI-Orbitrap) m/z : $(\text{M})^+$ calcd for $\text{C}_{26}\text{H}_{33}\text{BrN}_2$: 452.1827, found: 452.1839.

Synthesis of 3-bromo-5,10-didodecyl-5,10-dihydroindolo[3,2-*b*]indole (14): To a stirred solution of **13** (2.3 g, 5.07 mmol) in dry DMF was added NaH (182 mg, 7.60 mmol) under nitrogen atmosphere at 0°C . The reaction mixture was then warmed to room temperature and stirred for 30 minutes. The reaction mixture was cooled again to 0°C and 1-bromododecane (1.51 g, 6.08 mmol) was added dropwise and stirred at room temperature for 8 hours. Upon completion, the reaction mixture was quenched by adding water slowly and then extracted with EtOAc. The organic layer was washed successively with water and brine which was then dried over anhydrous Na_2SO_4 . After solvent removal, column purification was done on silica gel to isolate the alkylated product **14** as colourless solid (2.9 g, 4.66 mmol, 95%). m.p. $80-84^\circ\text{C}$; ^1H NMR (500 MHz, CDCl_3): 7.86 (s, 1H), 7.78 (d, $J = 8$ Hz, 1H), 7.41 (d, $J = 8$ Hz, 1H), 7.31-7.25 (m, 3H), 7.13 (t, $J = 7.5$ Hz, 1H), 4.41-4.37 (m, 4H), 1.92-1.87 (m, 4H), 1.38-1.18 (m, 36H), 0.82 (t, $J = 7$ Hz, 6H) ppm; ^{13}C NMR (125 MHz, CDCl_3) : 140.8, 139.0, 126.8, 124.7, 124.0, 122.2, 120.0, 118.2, 117.9, 115.8, 114.3, 111.0, 110.8, 109.8, 45.5, 45.3, 31.9, 30.2, 29.6, 29.5, 29.5, 29.5, 29.4, 29.4, 29.3, 27.1, 22.7, 14.1 ppm. HRMS (ESI-Orbitrap) m/z : $(\text{M})^+$ calcd for $\text{C}_{38}\text{H}_{57}\text{BrN}_2$: 620.3705, found: 620.3683.

Synthesis of 4-(5,10-didodecyl-5,10-dihydroindolo[3,2-*b*]indol-3-yl)benzaldehyde (15): A mixture of **14** (100 mg, 0.16 mmol.), 4-formylphenylboronic acid (28 mg, 0.19 mmol), Pd(PPh₃)₄ (18 mg, 10 mol%), K₂CO₃ (110 mg, 0.8 mmol) were weighed into a Schlenk tube and degassed for 10 minutes. Degassed THF and water in a 3:1 ratio was then added and the reaction mixture was purged with argon and allowed to stir at 70 °C for 24 hours. The solvent was evaporated under vacuum and the residue on activated neutral alumina column chromatography (with mixtures of ethyl acetate in hexane as eluent) yielded the product **15** as a yellow coloured solid (72 mg, 0.11 mmol, 70%). m.p. 75-77 °C; ¹H NMR (500 MHz, CDCl₃): 10.06 (s, 1H), 8.08 (s, 1H), 7.98 (t, *J* = 8.5 Hz, 2H), 7.88-7.84 (m, 3H), 7.59-7.57 (m, 1H), 7.54 (d, *J* = 9 Hz, 1H), 7.48 (d, *J* = 8 Hz, 1H), 7.33 (t, *J* = 8 Hz, 1H), 7.19 (t, *J* = 7.5 Hz, 1H), 4.56-4.50 (m, 4H), 2.02-1.97 (m, 14H), 1.46-1.41 (m, 4H), 1.38-1.32 (m, 4H), 1.28-1.19 (m, 28H), 0.88-0.84 (m, 6H) ppm. ¹³C NMR (125 MHz, (CDCl₃): 191.9, 148.7, 140.8, 140.5, 134.4, 130.4, 129.8, 127.6, 126.7, 126.0, 121.9, 121.0, 118.3, 117.8, 116.6, 115.2, 114.5, 110.2, 109.8, 45.5, 45.4, 31.9, 31.9, 30.3, 30.3, 29.6, 29.5, 29.4, 29.4, 29.4, 29.3, 27.2, 27.2, 22.7, 14.1 ppm. HRMS (ESI-Orbitrap) *m/z*: (M)⁺ calcd for C₄₅H₆₂N₂O: 646.4862, found: 646.4881.

Synthesis of 2-cyano-3-(4-(5,10-didodecyl-5,10-dihydroindolo[3,2-*b*]indol-3-yl)phenyl)acrylic acid (IID-4): A mixture of aldehyde **15** (50 mg, 0.077 mmol), cyanoacetic acid (20 mg, 0.23 mmol), ammonium acetate (30 mg, 0.38 mmol) in acetic acid was heated at reflux overnight under argon atmosphere. After cooling to room temperature, it was precipitated by pouring into water. The precipitate was washed with water and dried in vacuum oven. The product **IID-4** was obtained as orange colored solid (44 mg, 0.062 mmol, 80%). m.p. 98-100 °C; ¹H NMR (500 MHz, CDCl₃): 8.27 (s, 1H), 8.09 (d, *J* = 8.5 Hz, 2H), 8.04 (s, 1H), 7.82-7.77 (m, 3H), 7.54 (d, *J* = 8.5 Hz, 1H), 7.48 (d, *J* = 9 Hz, 1H), 7.42 (d, *J* = 8.5 Hz, 1H), 7.26 (t, *J* = 8 Hz, 1H), 7.13 (t, *J* = 8 Hz, 1H), 4.49-4.42 (m, 4H), 1.97-1.93 (m, 4H), 1.39-1.34 (m, 4H), 1.30-1.13 (m, 32H), 0.81-0.77 (m, 6H) ppm. ¹³C NMR (125 MHz, (CDCl₃): 166.7, 156.2, 148.2, 140.8, 140.6, 132.3, 129.2, 129.0, 127.6, 126.8, 125.9, 122.0, 120.8, 118.3, 117.8, 116.6, 115.6, 115.2, 114.4, 110.3, 109.9, 100.1, 45.6, 45.4, 31.9, 30.3, 29.6, 29.5, 29.5, 29.4, 29.3, 27.2, 27.2, 22.7, 14.1 ppm. HRMS (ESI-Orbitrap) *m/z*: (M)⁺ calcd for C₄₈H₆₃N₃O₂: 713.4920, found: 713.4953.

Synthesis of 5-(5,10-didodecyl-5,10-dihydroindolo[3,2-*b*]indol-3-yl)thiophene-2-carbaldehyde (16): A mixture of **14** (100 mg, 0.16 mmol.), 5-Formyl-2-thiopheneboronic acid (30 mg, 0.19 mmol), Pd(PPh₃)₄ (18 mg, 10 mol%), K₂CO₃ (110 mg, 0.8 mmol) were

weighed into a Schlenk tube and degassed for 10 minutes. Degassed THF and water in a 3:1 ratio was then added and the reaction mixture was purged with argon and allowed to stir at 70 °C for 24 hours. The solvent was evaporated under vacuum and the residue on activated neutral alumina column chromatography (with mixtures of ethyl acetate in hexane as eluent) yielded the product **16** as a yellow coloured solid (57 mg, 0.087 mmol, 55%). m.p. 58-60 °C; ¹H NMR (500 MHz, CDCl₃): 9.81 (s, 1H), 8.06 (s, 1H), 7.76 (d, *J* = 8 Hz, 1H), 7.68 (d, *J* = 4 Hz, 1H), 7.54-7.52 (m, 1H), 7.42-7.39 (m, 2H), 7.35 (d, *J* = 4 Hz, 1H), 7.23 (t, *J* = 8 Hz, 1H), 7.12 (t, *J* = 7.5 Hz, 1H), 4.46-4.41 (m, 4H), 1.95-1.88 (m, 4H), 1.39-1.14 (m, 36H), 0.81-0.77 (m, 6H) ppm. ¹³C NMR (125 MHz, (CDCl₃): 181.6, 155.9, 140.1, 139.8, 136.8, 128.2, 125.9, 124.7, 122.3, 121.6, 121.1, 119.1, 117.3, 116.8, 115.0, 113.9, 113.4, 109.2, 108.9, 44.5, 44.4, 30.8, 29.3, 29.2, 28.6, 28.5, 28.5, 28.4, 28.3, 28.3, 26.2, 26.1, 21.7, 13.1 ppm. HRMS (ESI-Orbitrap) *m/z*: (M+H)⁺ calcd for C₄₃H₆₁BrN₂OS: 653.4505, found: 653.4517

Synthesis of (2-cyano-3-(5-(5,10-didodecyl-5,10-dihydroindolo[3,2-*b*]indol-3-yl)thiophen-2-yl)acrylic acid (IID-5): A mixture of aldehyde **16** (50 mg, 0.076 mmol), cyanoacetic acid (20 mg, 0.23 mmol), ammonium acetate (30 mg, 0.38 mmol) in acetic acid was heated at reflux overnight under argon atmosphere. After cooling to room temperature, it was precipitated by pouring into water. The precipitate was washed with water and dried in vacuum oven. The product **IID-5** was obtained as red coloured solid (38 mg, 0.053 mmol, 75%) m.p. 140-142 °C; ¹H NMR (500 MHz, (CD₃)₂CO): 8.32 (s, 1H), 8.27 (s, 1H), 7.88 (d, *J* = 4 Hz, 1H), 7.81 (d, *J* = 7.5 Hz, 1H), 7.61-7.60 (m, 3H), 7.50 (d, *J* = 8 Hz, 1H), 7.18 (t, *J* = 7.5 Hz, 1H), 7.03 (t, *J* = 7.5 Hz, 1H), 4.57-4.51 (m, 4H), 1.89-1.86 (m, 4H), 1.35-1.29 (m, 4H), 1.25-1.04 (m, 32H), 0.73-0.69 (m, 6H) ppm. ¹³C NMR (125 MHz, (CD₃)₂CO): 165.3, 156.4, 146.5, 141.0, 140.7, 133.7, 126.8, 125.7, 123.4, 123.2, 122.2, 120.3, 118.4, 118.0, 116.0, 115.0, 114.4, 110.8, 110.1, 45.0, 44.8, 31.7, 30.1, 30.0, 29.7, 26.7, 26.7, 22.4, 13.5 ppm. HRMS (ESI-Orbitrap) *m/z*: (M+H)⁺ calcd for C₄₆H₆₂N₃O₂S: 720.4563, found: 720.4572.

Synthesis of 5-(5,10-didodecyl-5,10-dihydroindolo[3,2-*b*]indol-3-yl)furan-2-carbaldehyde (17): A mixture of **14** (100 mg, 0.16 mmol.), 5-Formyl-2-furanylboronic acid (22 mg, 0.19 mmol), Pd(PPh₃)₄ (18 mg, 10 mol%), K₂CO₃ (110 mg, 0.8 mmol) were weighed into a Schlenk tube and degassed for 10 minutes. Degassed THF and water in a 3:1 ratio was then added and the reaction mixture was purged with argon and allowed to stir at 70 °C for 24 hours. The solvent was evaporated under vacuum and the residue on activated neutral alumina column chromatography (with mixtures of ethyl acetate in hexane as eluent) yielded

the product **17** as a yellow coloured solid (61 mg, 0.096 mmol, 60%). m.p. 62-64 °C; ¹H NMR (500 MHz, CDCl₃): 9.57 (s, 1H), 8.22 (s, 1H), 7.76 (d, *J* = 7.5 Hz, 1H), 7.67 (d, *J* = 9 Hz, 1H), 7.42 (d, *J* = 8.5 Hz, 2H), 7.30 (d, *J* = 3.5 Hz, 1H), 7.26 (t, *J* = 8 Hz, 1H), 7.12 (t, *J* = 7.5 Hz, 1H), 6.72 (d, *J* = 4 Hz, 1H), 4.49-4.42 (m, 4H), 1.95-1.90 (m, 14H), 1.37-1.31 (m, 4H), 1.27-1.13 (m, 32H), 0.81-0.77 (m, 6H) ppm. ¹³C NMR (125 MHz, (CDCl₃)): 161.8, 151.6, 140.9, 140.7, 126.8, 125.9, 122.1, 119.3, 118.4, 117.8, 115.1, 114.8, 114.3, 110.0, 110.0, 106.0, 45.5, 45.4, 31.9, 30.3, 0.2, 29.6, 29.5, 29.5, 29.5, 29.4, 29.4, 29.4, 29.3, 27.1, 22.6, 14.1 ppm. HRMS (ESI-Orbitrap) *m/z*: (M+H)⁺ calcd for C₄₃H₆₁N₂O₂: 637.473, found: 637.4736.

Synthesis of 2-cyano-3-(5-(5,10-didodecyl-5,10-dihydroindolo[3,2-*b*]indol-3-yl)furan-2-yl)acrylic acid (IID-6): A mixture of aldehyde **17** (50 mg, 0.078 mmol), cyanoacetic acid (20 mg, 0.23 mmol), ammonium acetate (30 mg, 0.39 mmol) in acetic acid was heated at reflux overnight under argon atmosphere. After cooling to room temperature, it was precipitated by pouring into water. The precipitate was washed with water and dried in vacuum oven. The product **IID-6** was obtained as red coloured solid (35 mg, 0.056 mmol, 70%). m.p. 168-170 °C; ¹H NMR (500 MHz, (CD₃)₂SO): 8.56 (s, 1H), 8.05 (s, 1H), 7.90 (d, *J* = 7.5 Hz, 1H), 7.83 (d, *J* = 8.5 Hz, 1H), 7.75 (d, *J* = 9 Hz, 1H), 7.64 (d, *J* = 8 Hz, 1H), 7.56 (d, *J* = 3 Hz, 1H), 7.34 (d, *J* = 3.5 Hz, 1H), 7.28 (t, *J* = 7.5 Hz, 1H), 7.14 (t, *J* = 7.5 Hz, 1H), 7.14 (t, *J* = 7.5 Hz, 1H), 4.60-4.58 (m, 4H), 1.88-1.82 (m, 4H), 1.25-1.05 (m, 36H), 0.82-0.79 (m, 6H) ppm. ¹³C NMR (125 MHz, (CD₃)₂SO): 164.8, 161.6, 147.2, 141.1, 140.9, 137.7, 126.6, 126.0, 122.5, 119.5, 119.2, 118.8, 118.3, 117.6, 115.6, 114.7, 114.4, 111.5, 110.9, 108.6, 45.2, 44.8, 31.7, 30.1, 29.4, 29.3, 29.2, 29.2, 29.1, 29.1, 29.0, 29.0, 26.5, 26.3, 22.5, 14.4 ppm. HRMS (ESI-Orbitrap) *m/z*: (M)⁺ calcd for C₄₆H₆₁N₃O₃: 703.4713, found: 703.4704.

Synthesis of 5-bromo-3-(2-nitrophenyl)-1H-indole (20): A solution of 5-bromoindole (2 g, 10.2 mmol), 2-iodonitrobenzene (3 g, 12.24 mmol), Pd(OAc)₂ (229 mg., 10 mol%), K₂CO₃ (2.1 g, 15.3 mmol) in dioxane was degassed and the reaction mixture was stirred at 110°C for 72 hour. It was then cooled and passed through celite, extracted with ethyl acetate. Organic layer was washed with water, dried over sodium sulphate and evaporated the solvent. The residue obtained was subjected to column chromatography to obtain **20** as red coloured solid (1.94 g, 6.11 mmol, 60%). m.p. 100-102 °C. ¹H NMR (500 MHz, CDCl₃): 8.44 (s, 1H), 7.87 (d, *J* = 8.5 Hz, 1H), 7.68-7.63 (m, 3H), 7.51-7.32 (m, 3H) ppm. ¹³C NMR (125 MHz, (CDCl₃)): 150.0, 134.6, 132.5, 132.1, 128.3, 128.2, 127.7, 125.8, 124.5, 124.1, 121.6, 114.1,

113.0, 112.1 ppm. HRMS (ESI-Orbitrap) m/z : (M+H)⁺ calcd for C₁₄H₁₀BrN₂O₂: 316.9926, found: 316.9935.

Synthesis of 2-bromo-5,6-dihydroindolo[2,3-*b*]indole (21): To compound **20** (1.5 g, 4.72 mmol) in DMA was added PPh₃ (3.09 g, 11.82 mmol) and stirred the reaction mixture for 24 h at 165 °C. After completion of the reaction, the reaction mixture was extracted with ethyl acetate and washed successively with water and brine. After solvent removal, column purification was done on silica gel to isolate the product **21** as colourless solid (737 mg, 2.59 mmol, 55%). m.p. > 240 °C. ¹H NMR (500 MHz, (CD₃CO)₂): 10.44 (s, 1H), 10.34 (s, 1H), 7.86 (s, 1H), 7.77 (d, *J* = 7.5 Hz, 1H), 7.31 (d, *J* = 8 Hz, 1H), 7.26 (d, *J* = 8 Hz, 1H), 7.06-7.01 (m, 2H) ppm. ¹³C NMR (125 MHz, (CDCl₃)): 145.2, 139.2, 137.7, 124.2, 122.2, 121.6, 120.0, 119.9, 118.0, 113.0, 112.3, 111.6, 100.3 ppm. HRMS (ESI-Orbitrap) m/z : (M)⁺ calcd for C₁₄H₉BrN₂: 283.9949, found: 283.9954.

Synthesis of 2-bromo-5,6-didodecyl-5,6-dihydroindolo[2,3-*b*]indole (22): To a stirred solution of **21** (700 mg, 2.46 mmol) in dry DMF was added NaH (88 mg, 3.69 mmol) under nitrogen atmosphere at 0 °C. The reaction mixture was then warmed to room temperature and stirred for 30 minutes. The reaction mixture was cooled again to 0 °C and 1-bromododecane (735 mg, 2.95 mmol) was added dropwise and stirred at room temperature for 8 hours. Upon completion, the reaction mixture was quenched by adding water slowly and then extracted with EtOAc. The organic layer was washed successively with water and brine which was then dried over anhydrous Na₂SO₄. After solvent removal, column purification was done on silica gel to isolate the alkylated product **22** as colourless solid (1.4 g, 2.25 mmol, 97%). m.p. 68-70 °C. ¹H NMR (500 MHz, CDCl₃): 7.98 (s, 1H), 7.86 (d, *J* = 7 Hz, 1H), 7.38 (d, *J* = 8 Hz, 1H), 7.29-7.22 (m, 4H), 1.46-1.27 (m, 36H), 1.93-1.84 (m, 4H), 1.46-1.27 (m, 36H), 0.92-0.89 (m, 6H) ppm. ¹³C NMR (125 MHz, (CDCl₃)): 144.6, 139.6, 138.2, 123.6, 121.8, 121.7, 120.7, 120.3, 120.0, 118.3, 113.1, 110.5, 109.3, 100.4, 44.4, 44.2, 31.9, 30.4, 30.4, 29.6, 29.6, 29.5, 29.5, 29.4, 27.0, 22.7, 14.1 ppm. HRMS (ESI-Orbitrap) m/z : (M)⁺ calcd for C₃₈H₅₇BrN₂: 620.3705, found: 620.3714.

Synthesis of 4-(5,6-didodecyl-5,6-dihydroindolo[2,3-*b*]indol-2-yl)benzaldehyde (23): A mixture of **22** (100 mg, 0.16 mmol.), 4-formylphenylboronic acid (28 mg, 0.19 mmol), Pd(PPh₃)₄ (18 mg, 10 mol%), K₂CO₃ (110 mg, 0.8 mmol) were weighed into a Schlenk tube and degassed for 10 minutes. Degassed THF and water in a 3:1 ratio was then added and the reaction mixture was purged with argon and allowed to stir at 70 °C for 24 hours. The solvent

was evaporated under vacuum and the residue on activated neutral alumina column chromatography (with mixtures of ethyl acetate in hexane as eluent) yielded the product **23** as a yellow coloured solid (68 mg, 0.10 mmol, 65%). m.p. 64-66 °C. ¹H NMR (500 MHz, CDCl₃): 10.0 (s, 1H), 8.06 (d, *J* = 1.5 Hz, 1H), 7.91 (d, *J* = 8 Hz, 2H), 7.86-7.83 (m, 3H), 7.41 (dd, *J*₁ = 8.5 Hz, *J*₂ = 2 Hz, 1H), 7.36 (d, *J* = 8.5 Hz, 1H), 7.31 (d, *J* = 8 Hz, 1H), 7.21-7.14 (m, 2H), 4.3-4.28 (m, 4H), 1.86-1.81 (m, 4H), 1.38-1.18 (m, 36H), 0.82-0.79 (m, 6H) ppm. ¹³C NMR (125 MHz, (CDCl₃)): 192.2, 148.9, 144.7, 139.7, 139.6, 134.4, 131.8, 130.0, 127.8, 122.6, 121.9, 120.2, 119.8, 118.9, 118.3, 117.1, 109.6, 109.4, 101.1, 44.4, 44.3, 31.9, 30.5, 30.5, 29.6, 29.6, 29.5, 29.4, 29.4, 27.1, 22.7, 14.1 ppm. HRMS (ESI-Orbitrap) *m/z*: (M+H)⁺ calcd for C₄₅H₆₃N₂O: 647.4940, found: 647.4943.

Synthesis of 2-cyano-3-(4-(5,6-didodecyl-5,6-dihydroindolo[2,3-*b*]indol-2-yl)phenyl)acrylic acid (IID-7): A mixture of aldehyde **23** (50 mg, 0.077 mmol), cyanoacetic acid (20 mg, 0.23 mmol), ammonium acetate (30 mg, 0.38 mmol) in acetic acid was heated at reflux overnight under argon atmosphere. After cooling to room temperature, it was precipitated by pouring into water. The precipitate was washed with water and dried in vacuum oven. The product **IID-7** was obtained as orange coloured solid (38 mg, 0.053 mmol, 75%). m.p. 142-144 °C. ¹H NMR (500 MHz, (CD₃CO)₂): 8.25 (d, *J* = 10 Hz, 2H), 8.10 (d, *J* = 8 Hz, 2H), 7.94 (d, *J* = 8 Hz, 2H), 7.89 (d, *J* = 7 Hz, 1H), 7.53-7.48 (m, 2H), 7.40 (d, *J* = 8 Hz, 1H), 7.09-7.03 (m, 2H), 4.46-4.39 (m, 4H), 1.86-1.80 (m, 4H), 1.39-1.13 (m, 36H), 0.75-0.72 (m, 6H) ppm. ¹³C NMR (125 MHz, ((CD₃CO)₂): 154.3, 148.1, 147.4, 144.8, 140.1, 139.8, 131.7, 131.0, 129.6, 127.4, 122.7, 121.9, 119.9, 119.7, 118.6, 118.2, 116.6, 110.2, 109.7, 101.0, 44.1, 44.0, 31.7, 30.2, 30.2, 26.6, 22.4, 13.4 ppm. HRMS (ESI-Orbitrap) *m/z*: (M+H)⁺ calcd for C₄₈H₆₄N₃O₂: 714.4999, found: 714.5001.

Synthesis of 5-(5,6-didodecyl-5,6-dihydroindolo[2,3-*b*]indol-2-yl)thiophene-2-carbaldehyde (24): A mixture of **22** (100 mg, 0.16 mmol.), 5-Formyl-2-thiopheneboronic acid (30 mg, 0.19 mmol), Pd(PPh₃)₄ (18 mg, 10 mol%), K₂CO₃ (110 mg, 0.8 mmol) were weighed into a Schlenk tube and degassed for 10 minutes. Degassed THF and water in a 3:1 ratio was then added and the reaction mixture was purged with argon and allowed to stir at 70 °C for 24 hours. The solvent was evaporated under vacuum and the residue on activated neutral alumina column chromatography (with mixtures of ethyl acetate in hexane as eluent) yielded the product **24** as a yellow coloured solid (58 mg, 0.089 mmol, 55%). m.p. 88-90 °C. ¹H NMR (500 MHz, CDCl₃): 9.82 (s, 1H), 8.09 (s, 1H), 7.85 (d, *J* = 7.5 Hz, 1H), 7.70 (d, *J* = 3.5 Hz, 1H), 7.45 (d, *J* = 7.5 Hz, 1H), 7.40 (d, *J* = 3.5 Hz, 1H), 7.32-7.30 (m, 2H), 7.23-7.15

(m, 2H), 4.32-4.28 (m, 4H), 1.86-1.80 (m, 4H), 1.39-1.17 (m, 36 H), 0.82-0.79 (m, 6H) ppm. ^{13}C NMR (125 MHz, CDCl_3): 182.7, 157.2, 144.8, 141.2, 140.2, 139.6, 137.9, 125.2, 123.0, 122.5, 121.7, 120.3, 120.0, 118.4, 118.2, 116.2, 109.7, 109.4, 101.0, 44.5, 44.3, 31.9, 30.5, 29.6, 29.6, 29.5, 29.4, 29.3, 27.1, 22.7, 14.1 ppm. ^{13}C NMR (125 MHz, CDCl_3): 176.9, 161.8, 151.6, 144.7, 140.1, 139.6, 122.2, 121.7, 121.1, 120.4, 120.0, 118.6, 117.3, 115.5, 109.5, 109.4, 106.3, 101.2, 44.5, 44.3, 31.9, 30.5, 29.6, 29.6, 29.5, 29.4, 29.3, 27.1, 27.1, 22.7, 14.1 ppm. HRMS (ESI-Orbitrap) m/z : $(\text{M}+\text{H})^+$ calcd for $\text{C}_{43}\text{H}_{61}\text{N}_2\text{OS}$: 653.4505, found: 653.4506.

Synthesis of 2-cyano-3-(5-(5,6-didodecyl-5,6-dihydroindolo[2,3-*b*]indol-2-yl)thiophen-2-yl)acrylic acid (IID-8): A mixture of aldehyde **24** (50 mg, 0.076 mmol), cyanoacetic acid (20 mg, 0.23 mmol), ammonium acetate (30 mg, 0.38 mmol) in acetic acid was heated at reflux overnight under argon atmosphere. After cooling to room temperature, it was precipitated by pouring into water. The precipitate was washed with water and dried in vacuum oven. The product **IID-8** was obtained as red coloured solid (39 mg, 0.054 mmol, 70%). m.p. 154-156 °C. ^1H NMR (500 MHz, $(\text{CD}_3\text{CO})_2$): 8.32 (s, 1H), 8.23 (s, 1H), 7.88-7.85 (m, 2H), 7.65 (d, $J = 4$ Hz, 1H), 7.52-7.47 (m, 2H), 7.40 (d, $J = 7.5$ Hz, 1H), 7.10-7.04 (m, 2H), 4.45-4.38 (m, 4H), 1.87-1.78 (m, 4H), 1.39-1.13 (m, 36H), 0.75-0.72 (m, 6H) ppm. ^{13}C NMR (125 MHz, $(\text{CD}_3\text{CO})_2$): 157.1, 146.7, 145.0, 140.8, 140.7, 140.0, 133.7, 124.9, 123.5, 122.5, 121.7, 120.1, 120.0, 118.2, 118.2, 115.8, 110.5, 109.8, 100.8, 44.1, 43.9, 31.7, 30.3, 30.2, 26.7, 22.4, 13.5 ppm. HRMS (ESI-Orbitrap) m/z : $(\text{M}+\text{H})^+$ calcd for $\text{C}_{46}\text{H}_{62}\text{BrN}_3\text{O}_2\text{S}$: 720.4563, found: 720.4581.

Synthesis of 5-(5,6-didodecyl-5,6-dihydroindolo[2,3-*b*]indol-2-yl)furan-2-carbaldehyde (25): A mixture of **22** (100 mg, 0.16 mmol.), 5-Formyl-2-furanylboronic acid (22 mg, 0.19 mmol), $\text{Pd}(\text{PPh}_3)_4$ (18 mg, 10 mol%), K_2CO_3 (110 mg, 0.8 mmol) were weighed into a Schlenk tube and degassed for 10 minutes. Degassed THF and water in a 3:1 ratio was then added and the reaction mixture was purged with argon and allowed to stir at 70 °C for 24 hours. The solvent was evaporated under vacuum and the residue on activated neutral alumina column chromatography (with mixtures of ethyl acetate in hexane as eluent) yielded the product **25** as a yellow coloured solid (41 mg, 0.064 mmol, 40%). m.p. 74-76 °C. ^1H NMR (500 MHz, CDCl_3): 9.58 (s, 1H), 8.26 (s, 1H), 7.90 (d, $J = 7.5$ Hz, 1H), 7.61 (d, $J = 8.5$ Hz, 1H), 7.33-7.30 (m, 3H), 7.23-7.15 (m, 2H), 6.81 (d, $J = 3$ Hz, 1H), 4.30 (q, $J = 8.5$ Hz, 4H), 1.84-1.81 (m, 4H), 1.38-1.17 (m, 36H), 0.80 (t, $J = 7$ Hz, 3H), HRMS (ESI-Orbitrap) m/z : $(\text{M}+\text{H})^+$ calcd for $\text{C}_{43}\text{H}_{61}\text{N}_2\text{O}_2$: 637.4728, found: 637.4723.

Synthesis of (2-cyano-3-(5-(5,6-didodecyl-5,6-dihydroindolo[2,3-*b*]indol-2-yl)furan-2-yl)acrylic acid (IID-9): A mixture of aldehyde **25** (50 mg, 0.078 mmol), cyanoacetic acid (20 mg, 0.23 mmol), ammonium acetate (30 mg, 0.39 mmol) in acetic acid was heated at reflux overnight under argon atmosphere. After cooling to room temperature, it was precipitated by pouring into water. The precipitate was washed with water and dried in vacuum oven. The product **IID-9** was obtained as red coloured solid (41 mg, 0.058 mmol, 74%). m.p. 190-192 °C. ¹H NMR (500 MHz, (CD₃CO)₂): 8.52 (s, 1H), 7.94 (s, 1H), 7.86 (d, *J* = 7.5 Hz, 1H), 7.70 (d, *J* = 8.5 Hz, 1H), 7.52 (d, *J* = 8.5 Hz, 1H), 7.43-7.40 (m, 2H), 7.15 (d, *J* = 3 Hz, 1H), 7.10-7.04 (m, 2H), 4.46-4.43 (m, 4H), 1.86-1.80 (m, 4H), 1.38-1.13 (m, 36H), 0.74-0.72 (m, 6H) ppm. ¹³C NMR (125 MHz, (CD₃CO)₂): 163.6, 162.2, 147.1, 144.8, 140.6, 140.0, 137.5, 122.2, 121.7, 120.9, 120.2, 119.9, 118.2, 117.1, 116.5, 115.6, 110.3, 109.8, 107.8, 101.0, 95.3, 44.1, 43.9, 31.8, 30.3, 30.3, 26.7, 22.4, 13.5 ppm. HRMS (ESI-Orbitrap) *m/z*: (M+H)⁺ calcd for C₄₆H₆₂N₃O₃: 704.4791, found: 704.4816.

2.17 References:

1. Armaroli, N.; Balzani, V. The Future of Energy Supply: Challenges and Opportunities. *Angew. Chemie - Int. Ed.* **2007**, *46* (1–2), 52–66.
2. (a) Badawy, W. A. A Review on Solar Cells from Si-Single Crystals to Porous Materials and Quantum Dots. *J. Adv. Res.* **2015**, *6* (2), 123–132. (b) Mohammad Bagher, A. Types of Solar Cells and Application. *Am. J. Opt. Photonics* **2015**, *3* (5), 94.
3. (a) Hardin, B. E.; Snaith, H. J.; McGehee, M. D. The Renaissance of Dye-Sensitized Solar Cells. *Nat. Photonics* **2012**, *6* (3), 162–169 (b) Gong, J.; Sumathy, K.; Qiao, Q.; Zhou, Z. Review on Dye-Sensitized Solar Cells (DSSCs): Advanced Techniques and Research Trends. *Renew. Sustain. Energy Rev.* **2017**, *68*, 234–246.
4. (a) Michaels, H.; Rinderle, M.; Freitag, R.; Benesperi, I.; Edvinsson, T.; Socher, R.; Gagliardi, A.; Freitag, M. Dye-Sensitized Solar Cells under Ambient Light Powering Machine Learning: Towards Autonomous Smart Sensors for the Internet of Things. *Chemical Science.* **2020**, *11*, 2895–2906. (b) G. Gokul, S. C. Pradhan and S. Soman, Dye sensitized solar cells as potential candidates for indoor/diffused light harvesting applications: From BIPV to self powered IoTs, *Adv. Sol. Energy Res.*, **2019**, 281 — 316

5. (a) Kim, B. G.; Chung, K.; Kim, J. Molecular Design Principle of All-Organic Dyes for Dye-Sensitized Solar Cells. *Chem. - A Eur. J.* **2013**, *19* (17), 5220–5230 (b) Błaszczuk, A. Strategies to Improve the Performance of Metal-Free Dye-Sensitized Solar Cells. *Dye. Pigment.* **2018**, *149* (November 2017), 707–718.
6. (a) Baldoli, C.; Bertuolo, S.; Licandro, E.; Viglianti, L.; Mussini, P.; Marotta, G.; Salvatori, P.; Angelis, F. De; Manca, P.; Abbotto, A. SC. Benzodithiophene Based Organic Dyes for DSSC: Effect of Alkyl Chain Substitution on Dye Efficiency *Dye. Pigment.* **2015**, *121*, 351-362.
7. (a) Kumar, D.; Wong, K. T. Organic Dianchor Dyes for Dye-Sensitized Solar Cells. *Mater. Today Energy* **2017**, *5*, 243–279. (b) Wu, Y.; Zhu, W. Organic Sensitizers from D- π -A to D-A- π -A: Effect of the Internal Electron-Withdrawing Units on Molecular Absorption, Energy Levels and Photovoltaic Performances. *Chem. Soc. Rev.* **2013**, *42* (5), 2039–2058. (c) Qian, X.; Wang, X.; Shao, L.; Li, H.; Yan, R.; Hou, L. Molecular Engineering of D-D- π -A Type Organic Dyes Incorporating Indoloquinoxaline and Phenothiazine for Highly Efficient Dye-Sensitized Solar Cells. *J. Power Sources* **2016**, *326*, 129–136. (d) Qian, X.; Lan, X.; Yan, R.; He, Y.; Huang, J.; Hou, L. T-Shaped (D)₂-A- π -A Type Sensitizers Incorporating Indoloquinoxaline and Triphenylamine for Organic Dye-Sensitized Solar Cells. *Electrochim. Acta* **2017**, *232* (D), 377–386.
8. (a) Zhang, L.; Cole, J. M. Anchoring Groups for Dye-Sensitized Solar Cells. *ACS Appl. Mater. Interfaces* **2015**, *7*, 6, 3427–3455. (b) Sivanadanam, J.; Ganesan, P.; Madhumitha, R. Effect of π -Spacers on the Photovoltaic Properties of D - π - A Based Organic Dyes. "Journal Photochem. Photobiol. A Chem. **2015**, *299*, 194–202. (C) Hemavathi, B.; Jayadev, V.; Ramamurthy, P. C.; Pai, R. K.; Narayanan Unni, K. N.; Ahipa, T. N.; Soman, S.; Balakrishna, R. G. Variation of the Donor and Acceptor in D-A- π -A Based Cyanopyridine Dyes and Its Effect on Dye Sensitized Solar Cells. *New J. Chem.* **2019**, *43* (39), 15673–15680.
9. Carella, A.; Borbone, F.; Centore, R. Research Progress on Photosensitizers for DSSC. *Front. Chem.* **2018**, *6*, 1–24.
10. (a) Yoosuf, M.; Pradhan, S. C.; Soman, S.; Gopidas, K. R. Triple Bond Rigidified Anthracene-Triphenylamine Sensitizers for Dye-Sensitized Solar Cells. *Sol. Energy* **2019**, *188* (May), 55–65. (b) Liu, B.; Wang, R.; Mi, W.; Li, X.; Yu, H. Novel Branched Coumarin Dyes for Dye-Sensitized Solar Cells: Significant Improvement in

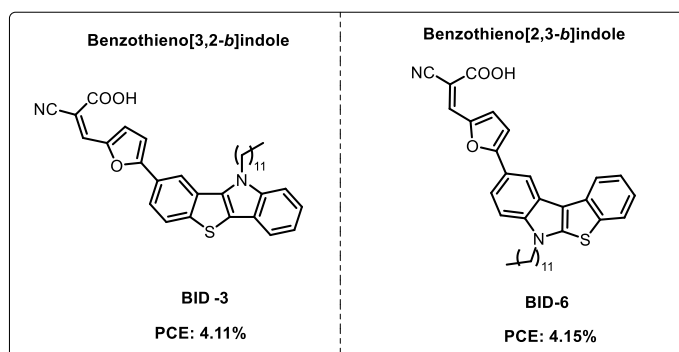
- Photovoltaic Performance by Simple Structure Modification. *J. Mater. Chem.* **2012**, 22 (30), 15379–15387. (c) Zhu, W.; Wu, Y.; Wang, S.; Li, W.; Li, X.; Chen, J.; Wang, Z. S.; Tian, H. Organic D-A- π -A Solar Cell Sensitizers with Improved Stability and Spectral Response. *Adv. Funct. Mater.* **2011**, 21 (4), 756–763. (d) Hemavathi, B.; Jayadev, V.; Pradhan, S. C.; Gokul, G.; Jagadish, K.; Chandrashekhara, G. K.; Ramamurthy, P. C.; Pai, R. K.; Narayanan Unni, K. N.; Ahipa, T. N.; et al. Aggregation Induced Light Harvesting of Molecularly Engineered D-A- π -A Carbazole Dyes for Dye-Sensitized Solar Cells. *Sol. Energy* **2018**, 174 (May), 1085–1096.
11. Nitha, P. R.; Soman, S.; John, J. Indole Fused Heterocycles as Sensitizers in Dye-Sensitized Solar Cells: An Overview. *Materials Advances*. **2021**, 2, 6136–6168.
 12. Zhang, L., Yang, X., Wang, W., Gurzadyan, G. G., Li, J., Li, X., An, J., Yu, Z., Wang, H., Cai, B., Hagfeldt, A., & Sun, L. 13.6% Efficient organic dye-sensitized solar cells by minimizing energy losses of the excited state. *ACS Energy Letters*, **2019**, 4(4), 943–951.
 13. Ji, J. M., Zhou, H., Eom, Y. K., Kim, C. H., & Kim, H. K. 14.2% Efficiency Dye-Sensitized Solar Cells by Co-sensitizing Novel Thieno[3,2-b]indole-Based Organic Dyes with a Promising Porphyrin Sensitizer. *Advanced Energy Materials*, **2020**, 2000124, 1–12.
 14. (a) Santhini, P. V.; Babu, S. A.; Krishnan, A. R.; Suresh, E.; John, J. Heteroannulation of 3-Nitroindoles and 3-Nitrobenzo[b]thiophenes: A Multicomponent Approach toward Pyrrole-Fused Heterocycles. *Org. Lett.*, **2017**, 19, 2458–2461

CHAPTER 3

Design, Synthesis and Characterization of Benzothienoindole Donor based Photosensitizers for DSSC Applications

Abstract

Herein, we tried to explore the potential of benzothienoindole unit as donor in development of sensitizers for DSSC application. In chapter 3A, we successfully synthesized three new D- π -A organic dyes based on benzothieno[3,2-*b*]indole as donor and by varying the π -spacer unit with benzene (**BID-1**), thiophene (**BID-2**) and furan (**BID-3**). With judicious selection of the π -spacer, optical properties can be controlled in a way to realize improved photovoltaic performance. Furan substituted dye; **BID-3** showcased the best performance with a PCE of 4.11%. The efficiency value increased in the order **BID-1** (1.16%) < **BID-2** (3.10%) < **BID-3** (4.11%). Detailed interfacial electrical measurements along with theoretical calculations were performed to disclose the mechanism of back electron transfer and improvement in photovoltaic performance with respect to variation in both donor and π -spacer. A similar investigation approach was adopted for benzothieno[2,3-*b*]indole donor based D- π -A dyes. The dyes thus constructed **BID-4**, **BID-5**, and **BID-6** with benzene, thiophene and furan spacers respectively are included in chapter 3B. Here also the dye **BID-6** with furan as the spacer outperformed the rest with PCE of 4.15% and the least efficiency was delivered by **BID-4** with 2.29%.



3.1 Introduction

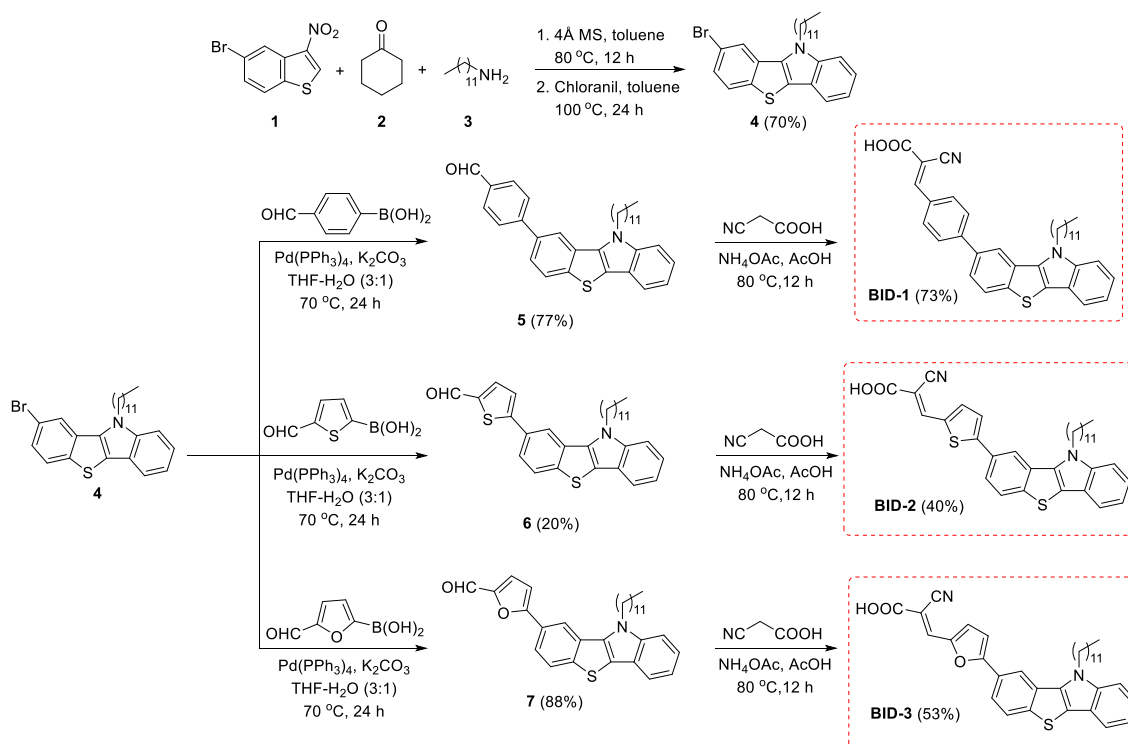
A plethora of reports on different aspects of dye sensitizer development is available owing to the importance of sensitizer as a key component in DSSC. The list extends from the development of novel molecular architecture to the strategical incorporation/assembling of sensitizer components either explored/novel in an established molecular architecture.¹ Exploration of novel scaffolds as sensitizer components has always got its own relevance. Aryl amines, carbazoles and indoles are the commonly used donors in high performing DSSCs.²⁻⁴ There is a need to develop alternate units with higher donor strength, more capability to reduce aggregation and to prevent recombination and which can be made with simple synthetic routes. In the previous chapter we reported dyes based on indoloindoles as donors. We could devise methods for the facile synthesis of indolo[3,2-*b*]indole as well as indolo[2,3-*b*]indole and could demonstrate the use of these fused indole motifs as donor units in donor- π spacer-acceptor molecular architecture. A systematic investigation of π -spacer as well as alkyl chain length could provide new insights towards balanced current-voltage scenario which could lead to improved device performance. As a continuation of our quest for new donor motifs, specifically indole fused heteroacenes, we decided to investigate another heteroacene which is benzothienoindole. When our developed synthetic methodology *via* sequential multicomponent reaction-oxidation strategy helped us to construct benzothieno[3,2-*b*]indole units, reported strategies were adopted for the construction of benzothieno[2,3-*b*]indole which is the another isomer of the former.

Benzothieno[3,2-*b*]indole, is an electron rich fused ring planar system which can serve as a good donor functionality in metal free organic sensitizers. Very recently, Lee and Hong reported the use of benzothieno[3,2-*b*]indole as a hole transport unit in the fabrication of OLEDs.⁵ Unlike indolo[3,2-*b*]indole, benzothieno[3,2-*b*]indole is an under explored tetracene and to the best of our knowledge, this moiety has not been explored till date for photovoltaic applications. Similar is the case with its another isomer, benzothieno[2,3-*b*]indole. Apart from the work done by Lee *et al.* in 2019, where they developed TADF emitters utilizing benzothieno[2,3-*b*]indole core, significant exploration of these systems in material side or photovoltaic field is not explored to date.⁶ Here we attempted to utilize these systems in sensitizer development by employing a donor- π -spacer-acceptor molecular architecture with systematic detailed investigations on the effect of different π -linker on device performance.

Chapter 3A Investigation of Benzothieno[3,2-*b*]indole Donor based D- π -A Dyes for DSSC

3.2 Synthesis and Characterization

The target molecules **BID-1**, **BID-2**, and **BID-3** were synthesized by following a five-step synthetic strategy. We commenced the synthesis with the nitration of 5-bromobenzothiophene by following reported protocols. Compound **1** was subjected to a one-pot MCR/oxidation process to afford benzothieno[3,2-*b*]indole (**4**) in 70% yield. The π -spacer was then attached to the donor moiety **4** by Suzuki reaction of 4-formyl phenyl boronic acid, (5-formylthiophen-2-yl)boronic acid and (5-formylfuran-2-yl)boronic acid to afford the molecules **5**, **6** and **7** respectively. Finally, the acceptor part was attached to **5**, **6** and **7** via Knoevenagel condensation with cyanoacetic acid furnishing the dyes **BID-1**, **BID-2**, and **BID-3** respectively. The entire synthetic route for **BID-1**, **BID-2**, and **BID-3** starting from **4** is given in Scheme 3.1. We have drawn the terminal double bonds of BID dyes in *E*-configuration by following the DFT results.



Scheme 3.1 Synthetic route adopted for benzothieno[3,2-*b*]indole based dyes **BID-1**, **BID-2** and **BID-3**

3.3 Computational Studies

A better knowledge on molecular geometry along with electron density distribution will pave the way towards deeper understanding of interfacial electron transfer dynamics in dye-sensitized solar cells. Additionally, the dihedral angle between the donor and π -spacer determines the dipole moment which is critical in determining the extend of donor-acceptor interactions in D- π -A organic dyes. The minimum energy structures of **BID-1**, **BID-2**, and **BID-3** are determined by density functional theory (DFT) calculations at B3LYP/cc-pVDZ level and are given in Figure 3.1. These structures show large variation in the twist angle (θ) between the aromatic moieties; **BID-3** with furan as π -spacer has the lowest θ (7.0°) followed by **BID-2** with thiophene (17.6°) and **BID-1** with phenyl (35.4°) moieties as π -spacers. The large variation in θ can significantly influence the π -electron distribution along the D- π -A framework. **BID-3** with a larger dipole moment of 3.8D clearly provides improved charge separation in comparison to **BID-2** (2.2D) and **BID-1** (1.9D). Further, a highly twisted structure such as **BID-1** is expected to show large difference in molecular packing compared to a nearly planar **BID-3**. Additionally, it also hampers efficient donor-acceptor interactions.

The absorption spectra of **BID-1**, **BID-2**, and **BID-3** are calculated with the TD-DFT approach using the CAM-B3LYP/cc-pVDZ method in conjunction with the self-consistent reaction field method to include solvation effect of dichloromethane. The calculated λ_{\max} 345 and 397 nm for **BID-1** and **BID-2** respectively agrees well with their corresponding experimental values of 350 and 406 nm. In the case of **BID-3**, the calculated λ_{\max} 399 nm is in reasonable agreement with the experimental value 420 nm. Good agreement between the trends in extinction coefficient and trends in the calculated oscillator strength is also observed (Table 3.1). Schematic representation of electronic distributions observed in frontier orbitals of benzothieno[3,2-*b*]indole based dyes at B3LYP/cc-pVDZ level along with MO energy and band gap values in eV are depicted in Figure 3.2. The molecular orbital (MO) composition corresponding to λ_{\max} indicates that the HOMO-1 to LUMO contribution is dominating π - π^* transition for **BID-2** and **BID-3** whereas in **BID-1** with phenyl as the π -spacer, the contributions from HOMO, HOMO-1 and HOMO-2 to LUMO are almost equal. In all cases, HOMO is distributed exclusively on the donor site while the LUMO is distributed largely on the π -spacer and acceptor unit which helps in efficient charge injection from dye excited state to semiconductor. The HOMO-1 of **BID-1** is more expressed at donor site than the π -A region compared to **BID-2** and **BID-3** dyes. The HOMO-2 of all the three molecules show a

more delocalized distribution over the D- π -A region. The frontier MO analysis suggests that the electronic transition corresponding to the absorption peak possess significant charge transfer character as the ground state electron density is mostly localized in the donor site is promoted to the π -A region in the excited state.

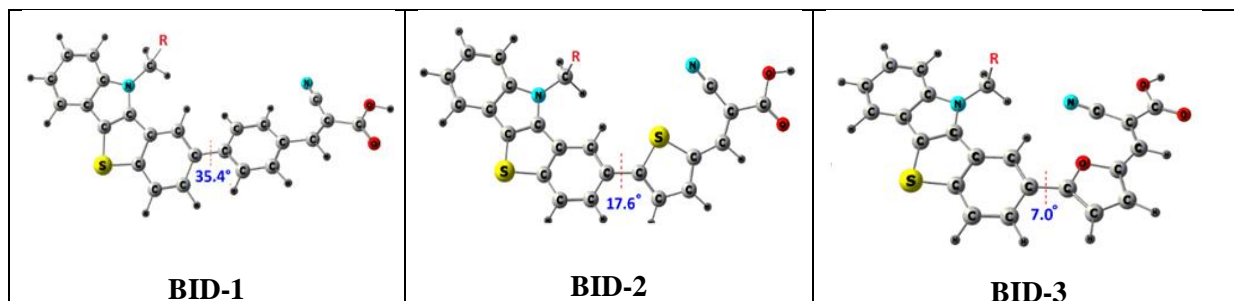


Figure 3.1 Energy minimized structures of benzothieno[3,2-*b*]indole based dyes with corresponding dihedral angles between the donor and π -spacers.

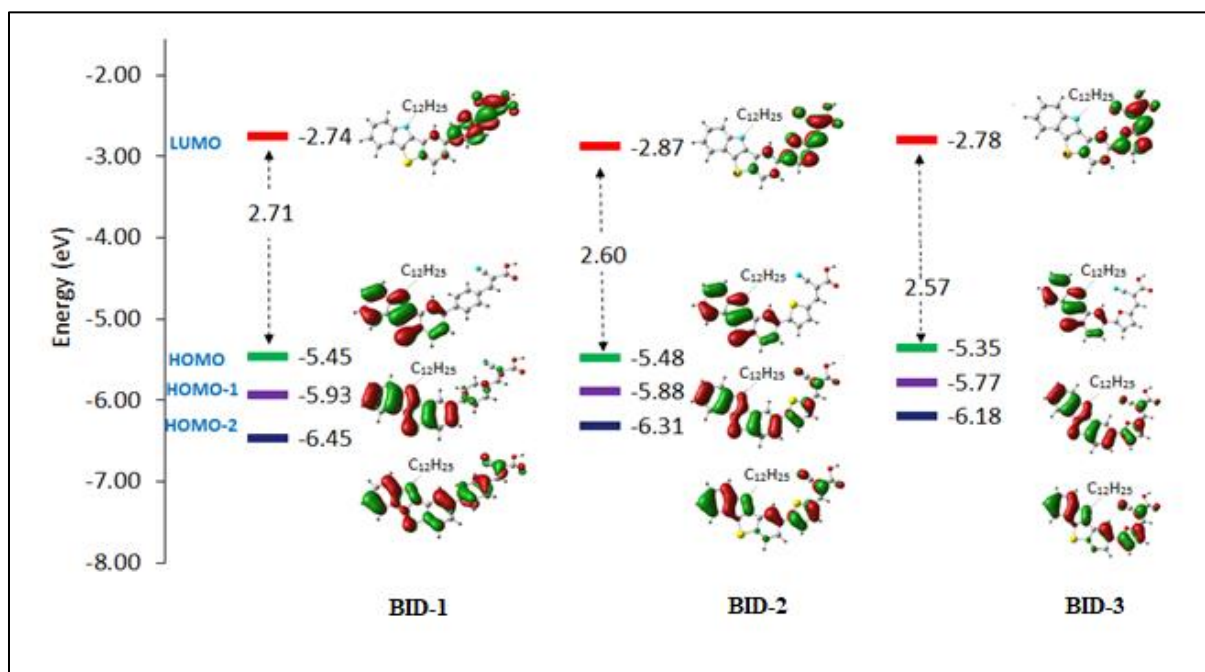


Figure 3.2 Schematic representation of electronic distributions observed in frontier orbitals of benzothieno[3,2-*b*]indole based dyes at B3LYP/cc-pVDZ level. MO energy and band gap values in eV are also depicted.

Table 3.1 Absorption maxima, oscillator strength, percentage contributions of orbital density, and dipole moments calculated at CAM-B3LYP/cc-pVDZ level

Dyes	λ_{\max} (nm)	f	Composition	μ (Debye)
BID-1	345 (3.59 eV)	1.18	HOMO \rightarrow LUMO (23.62%) HOMO-1 \rightarrow LUMO (25.86%) HOMO-2 \rightarrow LUMO (29.44%)	1.9
BID-2	397 (3.12 eV)	0.99	HOMO \rightarrow LUMO (23.62%) HOMO-1 \rightarrow LUMO (51.13%) HOMO-2 \rightarrow LUMO (19.87%)	2.2
BID-3	399 (3.12 eV)	0.74	HOMO \rightarrow LUMO (24.89%) HOMO-1 \rightarrow LUMO (55.46%) HOMO-2 \rightarrow LUMO (15.23%)	3.8

3.4 Photophysical Properties

The absorption spectra of dyes **BID-1**, **BID-2** and **BID-3** in CHCl_3 are shown in Figure 3.3 (a) and the corresponding data is listed in Table 3.2. All the three sensitizers exhibited absorption in the range of 300-520 nm. The absorption profile of **BID-2** and **BID-3** consists of three prominent bands. The bands at 300-360 nm wavelength is attributed to localized $\pi-\pi^*$ transitions and the bands positioned at lower energy wavelength regions can be attributed to the intramolecular charge transfer (ICT) transitions between donor and terminal acceptor units, respectively. In case of **BID-2** and **BID-3**, the ICT bands exhibited molar extinction coefficient of $31060 \text{ M}^{-1}\text{cm}^{-1}$ and $28560 \text{ M}^{-1}\text{cm}^{-1}$ respectively. The absorption spectrum of **BID-1** is blue shifted compared to that of the other two dyes and is also not exhibiting significant intramolecular charge transfer band, which can be an indication of the interrupted delocalization between donor and acceptor moieties. The absorption spectra got red shifted on changing the π -spacer from benzene to furan *via* thiophene which is augmented by the dihedral angle between the donor and π -spacer unit which got decreased in the order 35.4° (benzene) $>$ 17.6° (thiophene) $>$ 7.0° (furan). With a more planar geometry in thiophene and furan substituted dyes, **BID-2** and **BID-3** showcased improved charge transfer properties leading to enhanced light harvesting. Absorption spectra of the compounds on TiO_2 are

shown in Figure 3.3 (b). The trend observed in the solution state absorption is also followed in the absorption spectra on TiO₂, thiophene substituted dye **BID-2** leading the trend with improved light harvesting and lower absorption capability was showcased by **BID-1** with much blue shifted absorption.

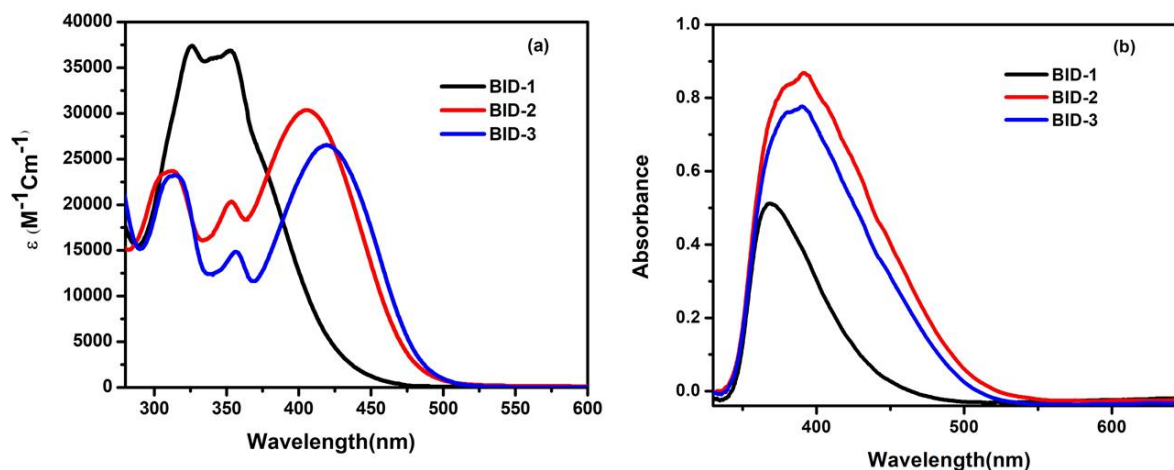


Figure 3.3 (a) Absorption spectra of dyes in THF. (b) Absorption spectra of dyes on TiO₂.

Table 3.2 Photophysical and electrochemical data of **BID** dyes V vs. NHE

Sensitizer	λ_{max} , nm (ϵ , M ⁻¹ cm ⁻¹)	$E_{\text{ox}}(\text{Fc}/\text{Fc}^+)$ (V)	E_{HOMO} (V)	E_{0-0} (eV)	E_{LUMO} (V)
BID-1	350 (37660)	0.61	1.24	2.90	-1.66
BID-2	406 (31060)	0.65	1.28	2.58	-1.30
BID-3	420 (28560)	0.62	1.25	2.54	-1.29

3.5 Electrochemical Properties

To investigate the molecular energy levels, cyclic voltammetry measurements were performed in CH₂Cl₂, using tetrabutylammonium hexafluorophosphate (0.1 M) as the supporting electrolyte, Ag/AgCl as reference electrode, Pt as working and counter electrode and ferrocene as internal standard at 0.63 V vs. NHE (Figure 3.4). The oxidation potentials of **BID-1**, **BID-2**, and **BID-3** were calculated with respect to ferrocene and were converted to NHE using the equation, $E_{\text{HOMO}} = [E_{\text{ox}}(\text{Fc}/\text{Fc}^+) + 0.63 \text{ V}]$. LUMO level (E_{LUMO}) was calculated

as the difference $E_{\text{HOMO}} - E_{0-0}$. E_{0-0} (band gap) was determined from the tangent intercept of absorption edges. All photophysical and electrochemical values are tabulated in Table 3A.2. The HOMO level of **BID-1**, **BID-2** and **BID-3** were observed to be 1.24 V, 1.28 V and 1.25 V vs. NHE. In all the three dyes, the donor unit being the same (benzothieno[3,2-*b*]indole) and HOMO being exclusively distributed on the donor site, very less change in the ground state oxidation potential was observed.

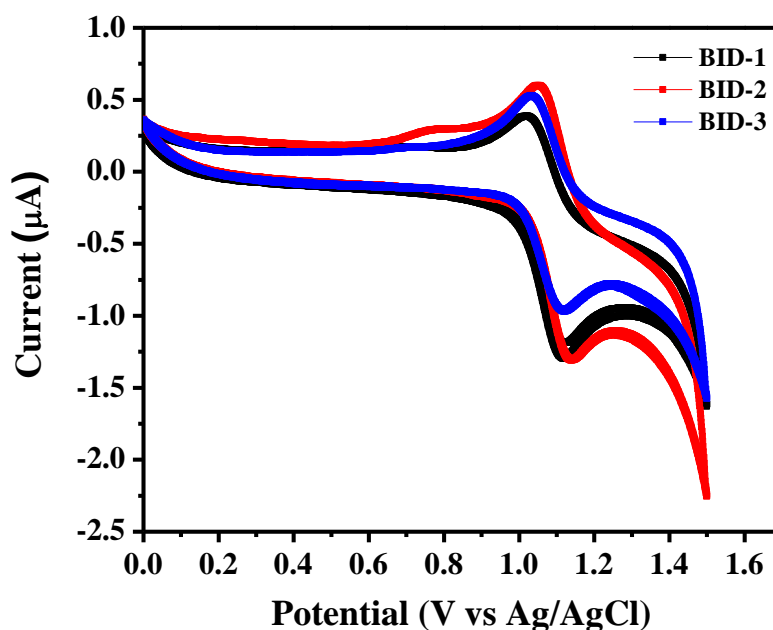


Figure 3.4 Cyclic voltammogram of **BID-1**, **BID-2**, and **BID-3** dyes in dichloromethane.

The schematic representation of dye energy levels along with TiO_2 conduction band and electrolyte redox potential are represented in Figure 3.5. The ground state redox potentials for all the BID dyes were substantially more positive than that of iodide/triiodide redox potential (0.4 V vs. NHE), indicating that regeneration is energetically favorable in all the three dyes. The optical transition energies (E_{0-0}) of **BID-1**, **BID-2** and **BID-3** were 2.9 eV, 2.58 eV and 2.54 eV respectively. The LUMO energy levels were determined by subtracting E_{0-0} from HOMO energy level which gave values of, -1.66, -1.30 and -1.29 V for **BID-1**, **BID-2** and **BID-3** respectively. The LUMO energy levels are relatively negative with respect to the position of the TiO_2 conduction band (-0.5 V vs. NHE) in a way to allow efficient electron injection.

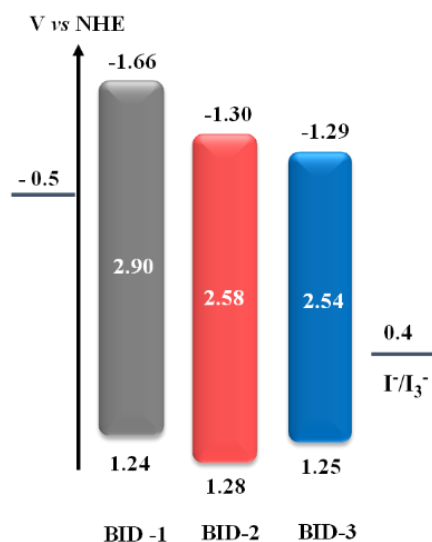


Figure 3.5 Energy level diagram of **BID** dyes

3.6 Photovoltaic Performance

The photovoltaic performance of DSSCs fabricated with the newly synthesized benzothieno[3,2-*b*]indole donor unit attached dyes (**BID-1**, **BID-2** and **BID-3**) were evaluated under full sun AM 1.5G (100 mW cm^{-2}) conditions. The current density-voltage (J - V) and incident-photon-to-current conversion efficiency (IPCE) curves are shown in Figure 3.6. The J - V parameters are summarized in Table 3.3.

Table 3.3 Solar Cell Characteristics of DSSCs based on **BID-1**, **BID-2**, and **BID-3**

Sensitizer	V_{oc} (mV)	J_{sc} (mA/cm^2)	FF (%)	Efficiency (%)
BID-1	590 ± 2	2.86 ± 0.13	68.86 ± 1.2	1.16 ± 0.10
BID-2	652 ± 5	6.51 ± 0.16	73.27 ± 0.95	3.10 ± 0.25
BID-3	671 ± 8	8.38 ± 0.25	73.15 ± 0.56	4.11 ± 0.14

The sensitizer **BID-3** with furan as π -spacer outperformed both **BID-1** and **BID-2** dyes having benzene and thiophene spacers displaying a power conversion efficiency of $4.11 \pm 0.14\%$ ($J_{sc} = 8.38 \pm 0.25 \text{ mA cm}^{-2}$, $V_{oc} = 671 \pm 8 \text{ mV}$, and $FF = 73.15 \pm 0.56$) which is highest among the series, followed by **BID-2** with power conversion efficiency of $3.1 \pm 0.25\%$ ($J_{sc} = 6.51 \pm 0.16 \text{ mA cm}^{-2}$, $V_{oc} = 652 \pm 5 \text{ mV}$, and $FF = 73.27 \pm 0.95$), and an efficiency of $1.16 \pm 0.10\%$ ($J_{sc} = 2.86 \pm 0.13 \text{ mA cm}^{-2}$, $V_{oc} = 590 \pm 2 \text{ mV}$, and $FF = 68.86 \pm 1.2$)

was realized for **BID-1**. The sensitizer with furan as π -spacer (**BID-3**) showcased an improvement in both short-circuit current density (J_{sc}) and open-circuit voltage (V_{oc}) than with benzene and thiophene spacers. The increase in J_{sc} is attributed to the increase in light harvesting ability of **BID-3** sensitizer which is clearly seen from the extended absorption profile in the IPCE spectra. J - V results are in accordance with the IPCE data for all the three **BID** dyes. Lower dihedral angle between the donor and π -spacer in **BID-3** (7°) compared with **BID-1** (35.4°) and **BID-2** (17.6°) along with a larger dipole moment of 3.8D for **BID-3** in comparison to 2.2D for **BID-2** and 1.9D for **BID-1** helped **BID-3** in achieving better donor- π -spacer interactions and enhanced charge separation leading to improved photovoltaic performance. Devices fabricated with **BID-3** sensitizer showed a broad absorption peak from 350 nm to 550 nm as evident from IPCE spectra with a maximum value of 88% at 460 nm, leading to a J_{sc} of $8.38 \pm 0.25 \text{ mA cm}^{-2}$. **BID-2** showed highest EQE of 75% at 400 nm and **BID-1** showed 75% at 350nm respectively. The red shifted absorption spectra of both **BID-2** and **BID-3** compared to **BID-1** (Figure 3.3 (a)) contributed towards significant improvement in IPCE for both the dyes, leading to improvement in J_{sc} . Even though **BID-2** exhibited higher absorption coefficient in comparison to **BID-3**, it failed to achieve higher absorption in action spectra as IPCE involves contribution from other electron transfer process such as injection, regeneration and collection which again depends on transport and lifetime of electrons in these devices

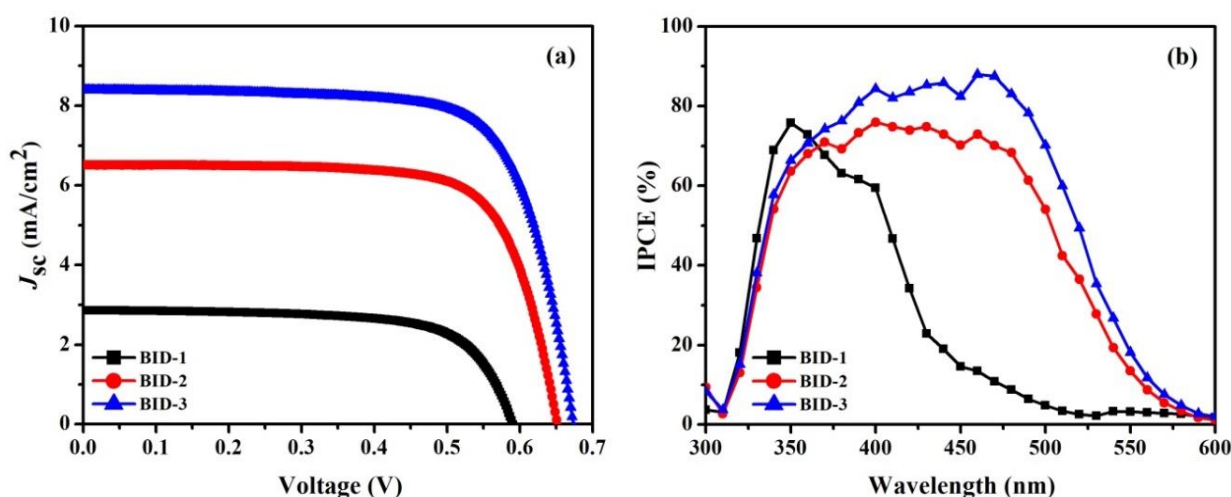


Figure 3.6 (a) Current-voltage characteristics of DSSCs with **BID-1**, **BID-2**, and **BID-3** under 1.5G. (b) Spectra of incident photon-to-current conversion efficiency (IPCE) for DSSCs

To get an in-depth understanding of the variation in photovoltaic performance, both electrical and light perturbation measurements were carried out involving Charge Extraction (CE),

Intensity Modulated Photovoltage Spectroscopy (IMVS), and Electrochemical Impedance Spectroscopy (EIS). CE measurement provides the distribution of trap states and the position of conduction band. Figure 3.7(a) shows charge extraction as a function of applied voltage for devices fabricated with three newly synthesized BID sensitizers. There is a positive shift in the conduction band (CB) for **BID-3** compared to **BID-1** and **BID-2**. The positive shift in TiO₂ CB resulted in efficient electron injection, contributing to improved light harvesting efficiency for **BID-3**. Additionally, a positive shift in CB will lead to less recombination driving force, contributing towards lower electron lifetime. The average time injected electrons stays in the energy states of TiO₂ (lifetime, τ_n) was calculated using IMVS technique using the equation, $\tau_n = 1/(2\pi f_{\max})$, where f_{\max} is the frequency corresponding to the highest value in Bode curve obtained from IMVS plot. Lifetime as a function of light intensity is shown in Figure 3.7(b). The lifetime plot shows almost similar lifetime for **BID-3** and **BID-1** (furan and benzene π -spacers) sensitizers and both exhibits longer lifetime than **BID-2**. Improved lifetime is an indication of less recombination at TiO₂/dye/electrolyte interface. Even with a more negative shift in CB which contributes to higher recombination driving force, the added advantage of having a twisted conformation might have rendered **BID-1** the capability to prevent the approach of oxidized species in electrolyte coming closer to TiO₂ and thereby achieving a lifetime similar to that of **BID-3**. The less rate of recombination along with the broad visible absorption helped **BID-3** in achieving better open-circuit potential in comparison to other dyes. For all three sensitizers, LUMO levels are placed at potentials with more than 800 mV of driving force for electron injection.

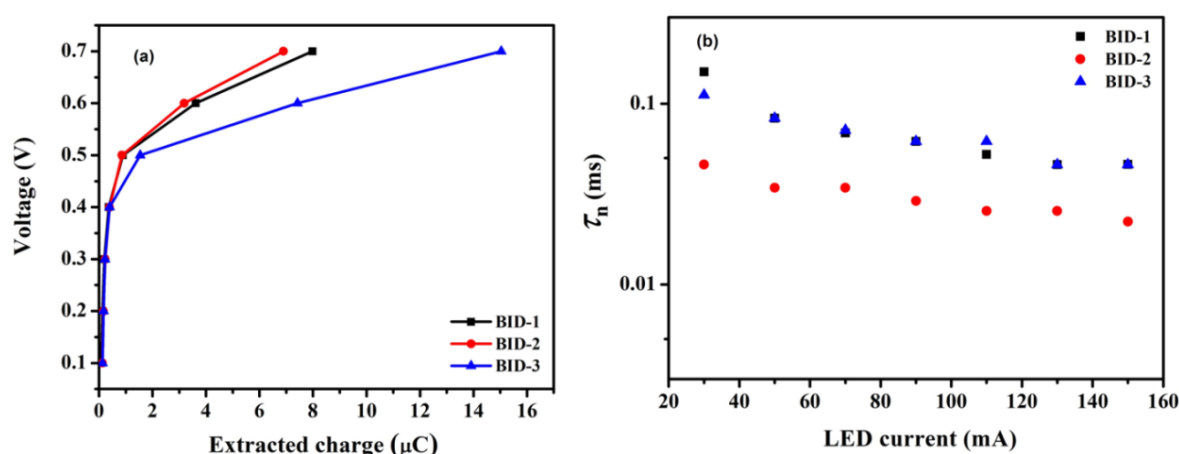
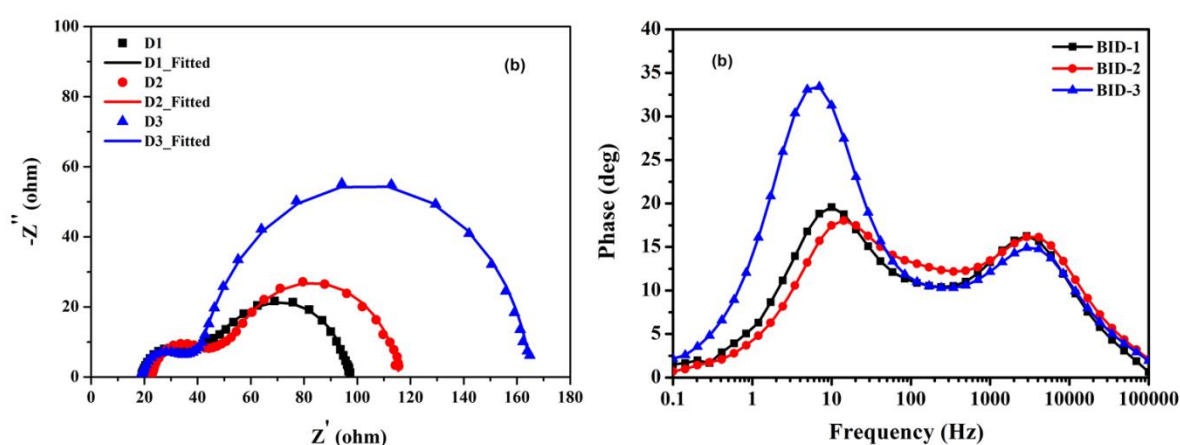


Figure 3.7 (a) Extracted charge versus voltage from charge extraction measurement and (b) Lifetime as a function of light intensity measured using IMVS technique for **BID** dyes

To probe the charge transfer processes under dark conditions bypassing the contribution of charge recombination from the injected electrons in TiO_2 to the overall lifetime, EIS was carried out at -0.66 V under forward bias in dark. Figure 3.8(a) shows the Nyquist plot of the devices measured using EIS technique at -0.66 V under forward bias. The frequency response of typical DSSC consists of three different semicircles in the complex plane plot due to the different time constants at various interfaces. The semicircles at high frequency, middle frequency and low frequency regions correspond to platinum/electrolyte interface, TiO_2 /dye/electrolyte interface and the diffusion of ions in the electrolyte respectively. Generally, while employing iodide/triiodide electrolyte, due to faster diffusion of ions in iodide electrolyte, the third semicircle is rarely seen. Herein, we observed two semicircles which correspond to charge transfer at platinum/electrolyte interface and TiO_2 /dye/electrolyte interface. Nyquist plot was fitted using equivalent circuit with transmission line model. The Transport Resistance (R_t), Charge-Transfer Resistance (Recombination Resistance, R_{ct}) and Chemical Capacitance (C_{μ}) were derived by fitting the Nyquist plots with equivalent circuit model and lifetime (τ_n) is calculated using the equation $\tau_n = C_{\mu} \times R_{ct}$. All the fitted, derived and calculated parameters are summarized in Table 3.4. **BID-3** sensitizer showcased a larger semicircle in the middle frequency region indicating a higher recombination resistance (131.3 Ω) followed by **BID-1** and **BID-2** with R_{ct} 63.25 Ω and 49.08 Ω respectively. For **BID** dyes the radii of the second semicircle increases in the order **BID-2** < **BID-1** < **BID-3** Figure 3.8(a) indicating that the electron recombination rate increased in the order of **BID-3** < **BID-1** < **BID-2** in dark. The Bode phase plot is given in (Figure 3.8 (b)). The recombination process of injected electrons in TiO_2 is represented by the peak at higher frequency. A shift of higher frequency peak to lower frequency suggest the possibility of lower charge recombination rate which leads to a longer electron lifetime. The reciprocal of this frequency peak is regarded as electron lifetime, where $\tau_n = (1/2\pi f_n)$ where f_n is the frequency corresponding to the highest value in Bode plot. As seen in Table 3A.4, **BID-3** showed highest lifetime in **BID** series of dyes derived from EIS measurement which is in accordance with the lifetime data obtained from IMVS measurement. Apart from the red shifted absorption, lower transport resistance and higher recombination resistance, longer lifetime favored **BID-3** in achieving higher photovoltaic performance among **BID** dye series.

Table 3.4 Transport Resistance (R_t), Recombination Resistance (R_{ct}), Chemical Capacitance (C_{μ}) and Lifetime (τ_n) calculated from EIS at -0.66 V for **BID** dyes

Sensitizer	Transport Resistance (R_t), Ω	Recombination Resistance (R_{ct}), Ω	Chemical Capacitance (C_{μ}), mF	Lifetime (τ_n), ms
BID-1	48.77	63.25	666	42.12
BID-2	58.54	49.08	644	31.61
BID-3	27.93	131.3	687	90.20

**Figure 3.8** (a) Nyquist plot and (b) Bode plot measured using EIS technique for DSSCs at -0.66 V under forward bias for **BID** dyes

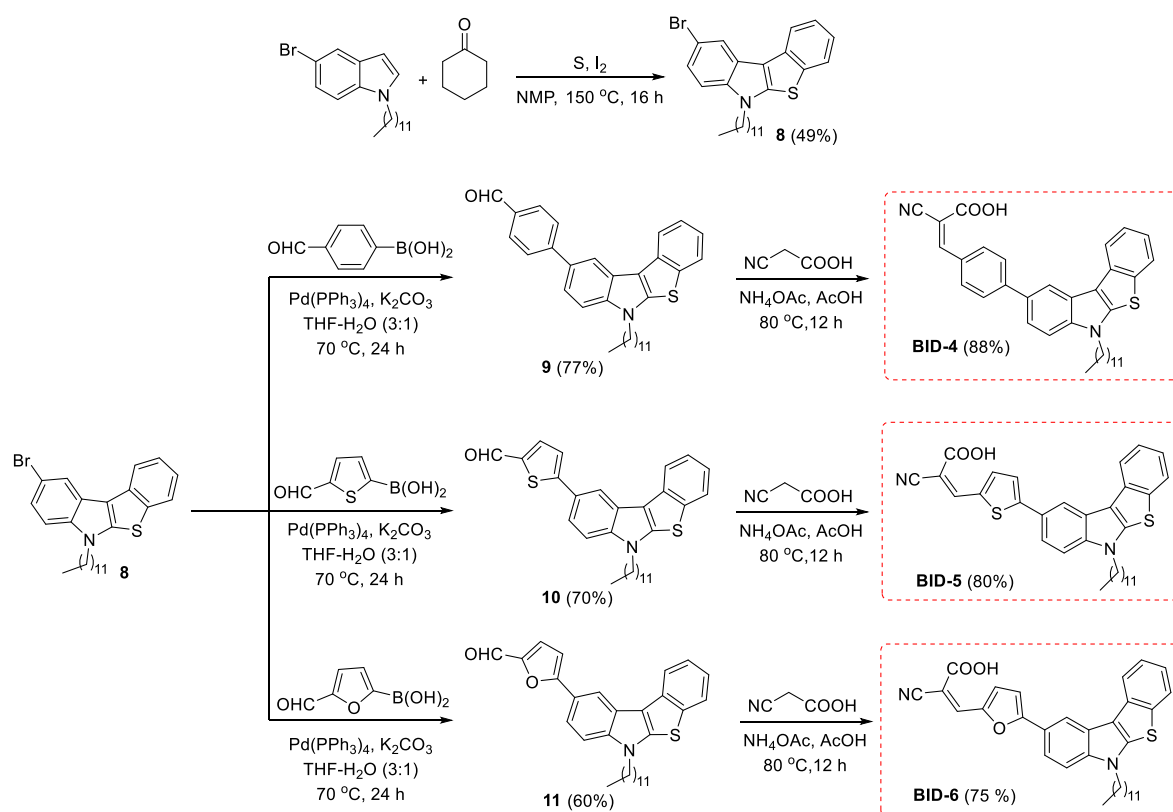
3.7 Conclusion

In summary, we successfully synthesized three new D- π -A organic dyes based on benzothieno[3,2-*b*]indole as donor and by varying the π -spacer unit with benzene (**BID-1**), thiophene (**BID-2**) and furan (**BID-3**). With judicious selection of π -spacer, the optical properties were controlled in a way to realize improved photovoltaic performance. Furan substituted dye, **BID-3** showcased the best performance with a PCE of 4.11%. The efficiency value increased in the order **BID-1** (1.16%) < **BID-2** (3.10%) < **BID-3** (4.11%). Better planarity of the molecular backbone helped **BID-3** in achieving improved donor-acceptor interactions and superior charge separation leading to larger dipole moment thereby realizing improved light harvesting and photovoltaic performance. Additionally, lower driving force for recombination attained with a positive CB shift also helped **BID-3** in achieving enhanced lifetime as evident from both IMVS and EIS measurements.

Chapter 3B: Investigation of Benzothieno[2,3-*b*]indole Donor based D- π -A Dyes for DSSC

3.8 Synthesis and Characterization

The dyes with benzothieno[2,3-*b*]indole as the donor moiety was synthesized as shown in scheme 3.2. The benzothieno[2,3-*b*]indole core was accessed by following an iodine mediated three-component annulative arylation involving *N*-dodecyl-5-bromo-indole, cyclohexanone as the arylating agent and elemental sulphur. The π -spacer was attached to the benzothieno[2,3-*b*]indole donor moiety by Suzuki reaction of **8** with formyl-aryl/heteroaryl boronic acids to afford the molecules **9** (benzene as π -spacer), **10** (thiophene as π -spacer) and **11** (furan as π -spacer) respectively. Finally, Knoevenagel condensation of **9**, **10** and **11** with cyanoacetic acid introduced the acceptor functionality furnishing the dyes **BID-4**, **BID-5**, and **BID-6** respectively.



Scheme 3.2 Synthetic route adopted for benzothieno[2,3-*b*]indole based dyes **BID-4**, **BID-5** and **BID-6**.

3.9 Computational Studies

The molecular structure and electronic distribution of the dyes were investigated by with Gaussian 09 program. DFT studies at B3LYP level of theory with valance double-zeta polarisation basis set, viz 6-31G* was used for all the calculations in gas phase. Figure 3.9 shows the frontier molecular orbital of the dyes. All the dyes are having HOMO electron density mostly located on the donor unit and LUMO is located on the acceptor unit/cyanoacrylic acid and extended to π -spacer also. These results show good HOMO-LUMO overlap and possibility of strong coupling of semiconductor conduction band with the sensitizer. This can in turn make sure of efficient electron injection to the conduction band of TiO_2 which is essential for the current generation in the device.

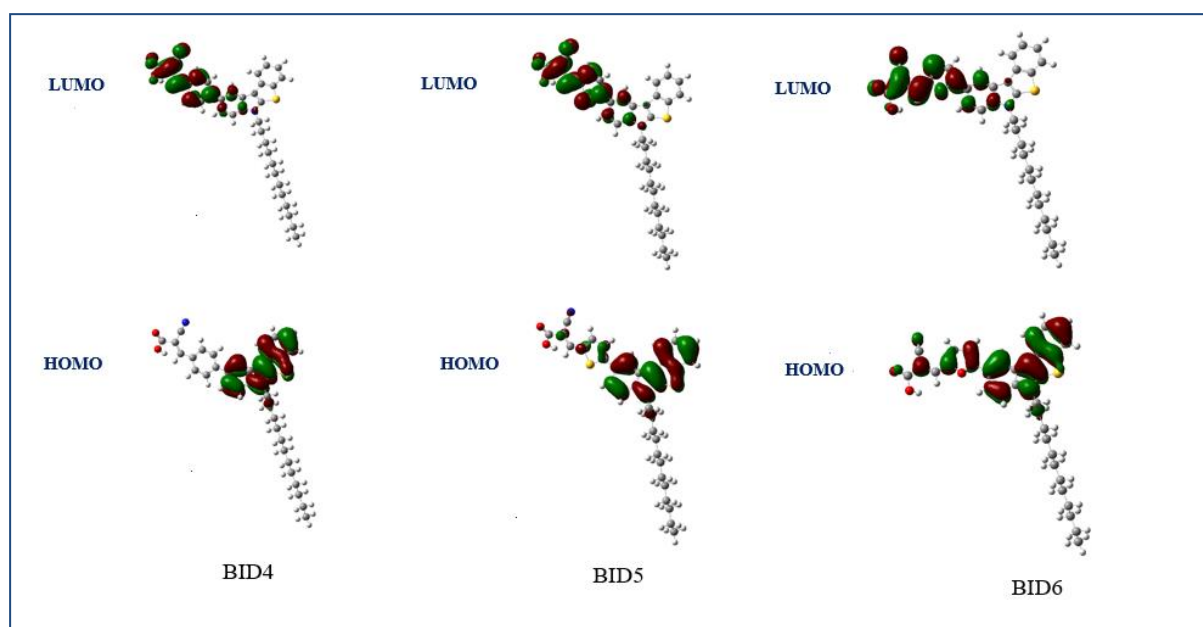


Figure 3.9 Frontier molecular orbital distributions of the dyes **BID-4**, **BID-5** and **BID-6**

According to the energy minimized structure of compounds (Figure 3.10), all the three dyes were having almost coplanar conformation with respect to angle between spacer and anchoring group. But changes in the structure were induced by the angle between donor and π -spacer. While benzene substituted dye **BID-4** exhibited blue shifted absorption with a twisted conformation, the twist being originated from the larger angle between benzene and donor (34.68°), **BID-6** with furan as π -spacer exhibited maximum planarity with least dihedral angle value of 1.56° between the donor and π -spacer fragments.

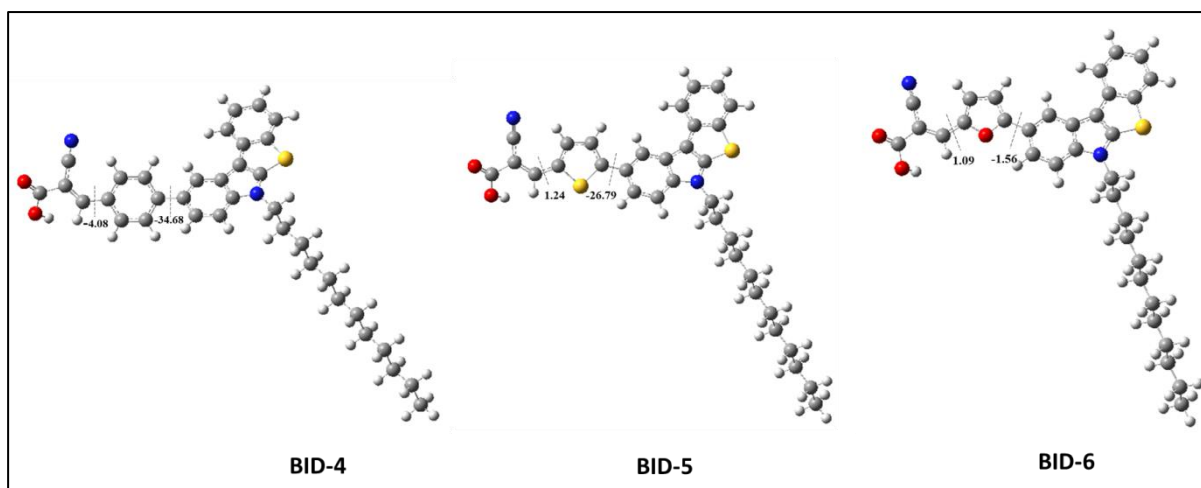


Figure 3.10 Energy minimized structure of the dyes **BID-4**, **BID-5** and **BID-6**

3.10 Photophysical and Electrochemical Studies

Figure 3.11 (a) and 3.11 (b) present absorption spectra of the compounds in THF and on TiO₂ respectively and the corresponding data are summarised in Table 3.5. In the solution state absorption spectra, **BID-4** dyes which are having benzene as the π -spacer exhibited blue shifted absorption spectra (λ_{max} at 375 nm) with lower molar extinction coefficient ($24,625 \text{ mol}^{-1} \text{ cm}^{-1}$) compared to **BID-5** and **BID-6**. Though there is slight difference in the absorption maxima of **BID-5** and **BID-6** with furan π -linker slightly shifting the absorption maximum of **BID-6** to longer wavelength region, the two are having almost same absorption onset. The factors which can influence the absorption spectra of dyes on TiO₂ are the formation of H- or J- aggregates and deprotonation of carboxyl group on semiconductor. While H- aggregates and deprotonation of carboxyl group can lead to blue shifted absorption, bathochromically shifted absorption can be resulted from the formation of J- aggregates. Compared to the solution state, the dyes showed broad and red-shifted absorption spectra on TiO₂. This suggested significant formation of J- kind aggregates on TiO₂. While **BID-6** showed more bathochromically shifted spectra, **BID-4** was showing least light harvesting as observed in the solution state absorption spectra.

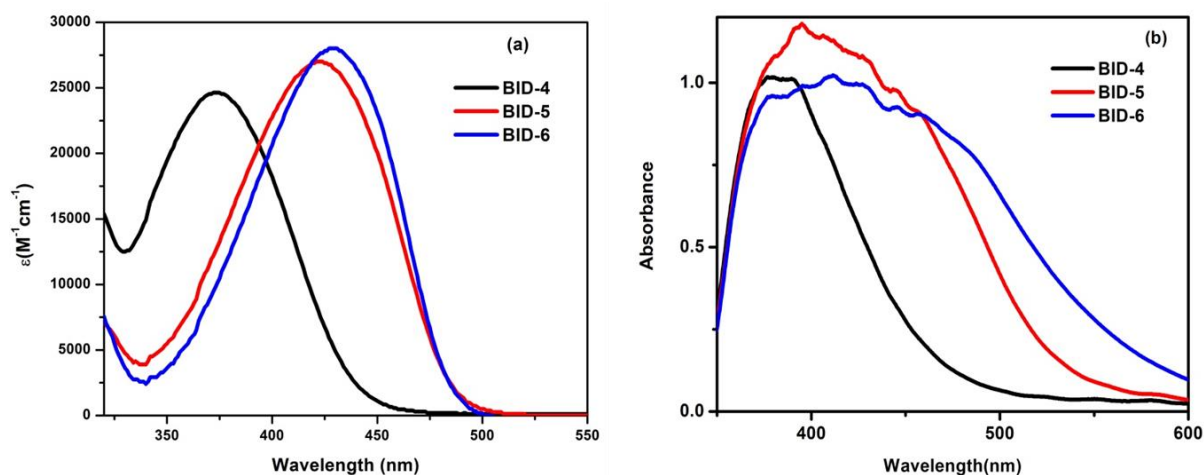


Figure 3.11 (a) Solution state absorption spectra of dyes in THF. (b) Solid state absorption spectra of dyes on TiO₂

Table 3.5 Photophysical and electrochemical data of BID dyes V vs. NHE

Sensitizer	λ_{max1} nm ($\epsilon, \text{M}^{-1} \text{cm}^{-1}$)	$E_{\text{ox}}(\text{Fc}/\text{Fc}^+)$ (V)	E_{HOMO} (V)	E_{0-0} (eV)	E_{LUMO} (V)
BID-4	375 (24625)	0.64	1.27	2.84	-1.57
BID-5	424 (27750)	0.69	1.32	2.56	-1.24
BID-6	431 (28000)	0.66	1.29	2.56	-1.27

Cyclic voltammetry measurements of the dyes were performed in dichloromethane solutions, using tetrabutylammonium hexafluorophosphate (0.1 M) as the supporting electrolyte, Ag/AgCl as reference electrode, glassy carbon as working electrode and Pt as counter electrode and ferrocene as internal standard (Figure 3.12). The HOMO level was calculated from the first oxidation potential of the dyes. The band gap which was estimated from the onset wavelength of the absorption spectrum was subtracted from the HOMO level to obtain LUMO energy level. All the three BID dyes were having energy levels which are optimum for electron injection into TiO₂ conduction band and dye regeneration from iodide triiodide redox couple.

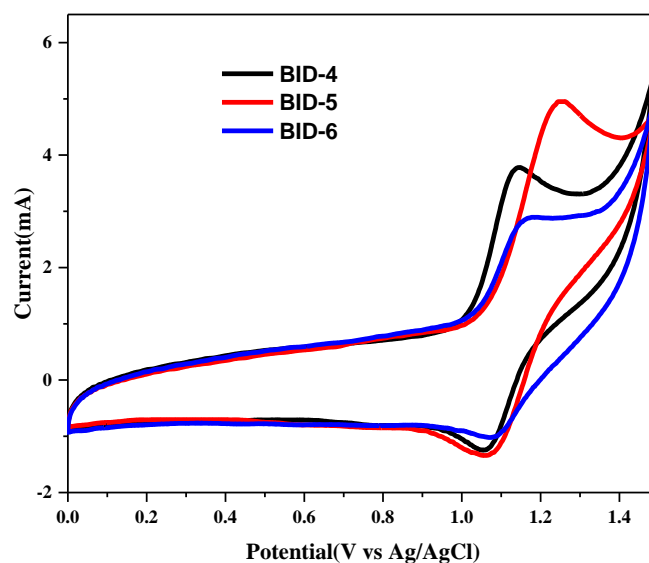


Figure 3.12 Cyclic voltammogram of **BID-4**, **BID-5** and **BID-6** in dichloromethane.

3.11 Photovoltaic Studies

We employed **BID-4**, **BID-5** and **BID-6** as sensitizers to construct DSSCs and to evaluate the PV performance. The photocurrent density-photovoltage (J - V) curves of DSSCs based on **BID-1**, **BID-2** and **BID-3** under AM 1.5G (100 mWcm^{-2}) illumination is shown in Figure 3.13 (a) and the related photovoltaic parameters obtained are presented in Table 3.6. Here, the highest performance was delivered by the furan substituted dye **BID-6** with a PCE of 4.15% and least performance was showcased by benzene substituted dye **BID-4** with a PCE of 2.29%. The current density generated followed the trend as **BID-6** (9.28 mA/cm^2) > **BID-5** (8.16 mA/cm^2) > **BID-4** (5.32 mA/cm^2). This trend in current generation is in parallel with the absorption behaviour of dyes on TiO_2 . Lower light harvesting ability of **BID-4** with benzene π -linker which showed significantly blue shifted absorption behaviour might have caused its inferior performance in current generation. The other two dyes were showing slight difference in their J_{sc} value which is also in tune with absorption behaviour observed. **BID-6** with furan π -linker exhibited slightly broader and bathochromically shifted absorption on TiO_2 . The solution state absorption of dyes also follows the same trend with molar absorptivity in the order **BID-6** > **BID-5** > **BID-4**. The incident photon to current conversion efficiencies (IPCE) of the DSSCs against different irradiation wavelength are shown in Figure 3.13 (b). The data obtained was also in accordance with the previous observation. While **BID-4** showed a plateau region of 350 nm to 415 nm in the IPCE curve, other two dyes could exhibit wider absorption whose onset of absorption is extended to $\sim 620 \text{ nm}$ region. **BID-6**

dyes also excelled with higher photovoltage of 627 mV which was followed by **BID-4** (616 mV) and **BID-5** (607 mV) in order.

Table 3.6 Solar Cell Characteristics of DSSCs based on **BID-4**, **BID-5**, and **BID-6**

Sensitizer	V_{oc} (mV)	J_{sc} (mA/cm ²)	FF (%)	Efficiency (%)
BID-4	616 ± 3	5.32 ± 0.17	69.47 ± 0.38	2.29 ± 0.08
BID-5	607 ± 5	8.16 ± 0.20	71.63 ± 0.22	3.57 ± 0.12
BID-6	627 ± 4	9.28 ± 0.18	70.89 ± 0.33	4.15 ± 0.11

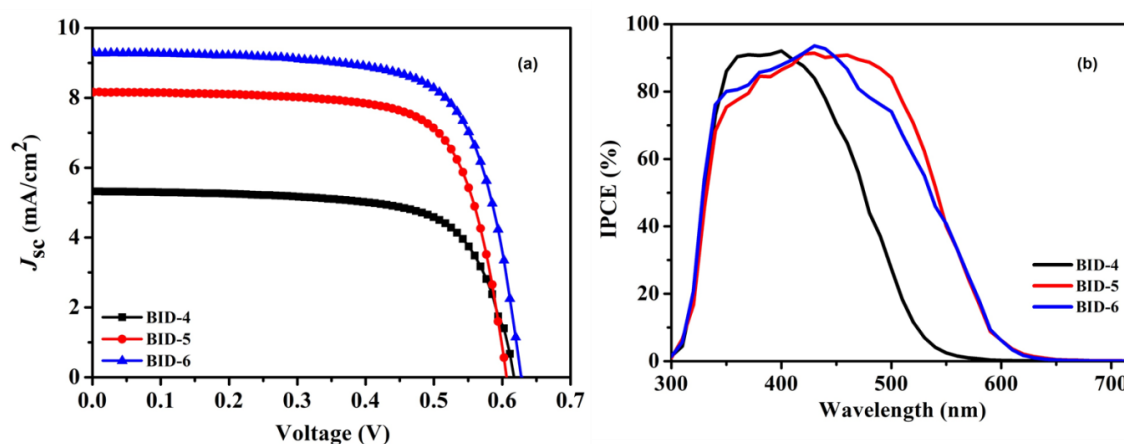


Figure 3.13 (a) Current-voltage characteristics of DSSCs with **BID-1**, **BID-2**, and **BID-3** under 1.5G. (b) Spectra of incident photon-to-current conversion efficiency (IPCE) for DSSCs

To get a deeper understanding on the device performance, we carried out transient photovoltage decay and charge extraction measurements of the devices (Figure 3.14). The energy level of conduction band edge of TiO₂ was almost same in case of all the dyes which was estimated from the charge extraction measurements shown in Figure 3.14 (a). The lifetime measurements conducted indicated the increased recombination resistance for **BID-4** and least value is observed for **BID-5** with thiophene as π -linker. This observation can be credited to the ability of **BID-4** in preventing back electron transfer reactions owing to its twisted conformation.

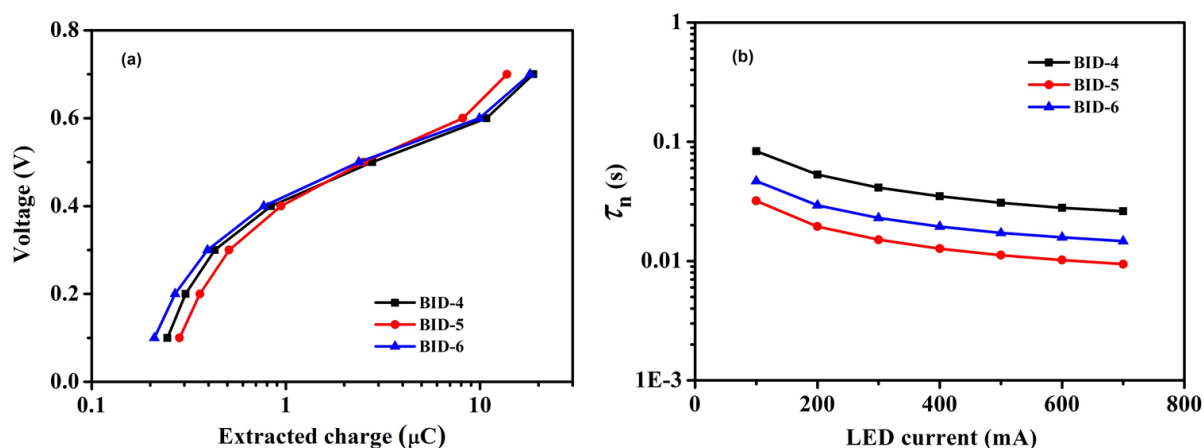


Figure 3.14 (a) Extracted charge versus voltage from charge extraction measurement and (b) Lifetime as a function of light intensity measured using TPV technique

Further we measured transient photo current decay to get the trends in transport time of devices (Figure 3.15). Lesser transport time could lead to efficient charge collection and current generation. Among the dyes, **BID-4** was having larger transport time and the rest of the dyes showcased almost similar transport time.

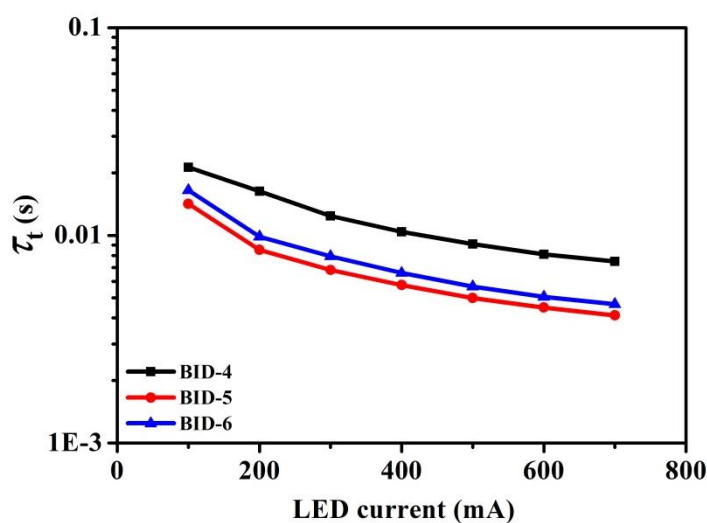


Figure 3.15 Transport time as a function of light intensity measured using TPC technique

3.12 Conclusion

In summary, donor- π -acceptor (D- π -A) dyes abbreviated as **BID-4**, **BID-5** and **BID-6** were designed, synthesized and evaluated for their performance in DSSC. All the dyes were having dodecyl group incorporated benzothieno[2,3-*b*]indole and cyanoacrylic acid respectively as donor and acceptor units. The dyes **BID-4**, **BID-5** and **BID-6** differ in the π -linker attached as benzene, thiophene and furan respectively. Among these, **BID-6** based devices showed a

higher overall power conversion efficiency of 4.15% under simulated AM 1.5G solar irradiation (100 mW/cm^2). The device excelled with both higher current density and photovoltage. The major factor which influenced the PCE of the devices was the light harvesting ability of dyes. While furan substituted dye **BID-6** exhibited higher light harvesting ability both in solution state as well as on TiO_2 , significantly low absorption profile of **BID-4** lead to much decrease in current density. Though **BID-4** was managed to have higher photovoltage than thiophene substituted dye **BID-5** due to its twisted conformation, lowest current density obtained in the former case lead to its inferior performance with 2.29%.

3.13 Experimental Section

General Methods

All chemicals were of the best grade commercially available and were used without further purification. All solvents were purified according to standard procedure; dry solvents were obtained according to the literature methods and stored over molecular sieves. Gravity column chromatography was performed using neutral alumina and mixtures of hexane-ethyl acetate were used for elution. Melting points were determined on a Buchi melting point apparatus and are uncorrected. Proton nuclear magnetic resonance spectra (^1H NMR) were recorded on a Bruker AMX 500 spectrophotometer (CDCl_3 and Acetone- d_6 as solvents). Chemical shifts for ^1H NMR spectra are reported as δ in units of parts per million (ppm) downfield from SiMe_4 (δ 0.0) and relative to the signal of chloroform- d (δ 7.25ppm) Acetone- d_6 (2.05 ppm). Multiplicities were given as: s (singlet); d (doublet); t (triplet); q (quartet); dd (double doublet); m (multiplet). Coupling constants are reported as J value in Hz. Carbon nuclear magnetic resonance spectra (^{13}C NMR) are reported as δ in units of parts per million (ppm) downfield from SiMe_4 (δ 0.0) and relative to the signal of chloroform- d (δ 77.03 ppm) and Acetone- d_6 (29.84 and 206.26 ppm). Mass spectra were recorded under ESI/HRMS at 60,000 resolution using Thermo Scientific Exactive mass spectrometer. The UV-visible absorbance was studied using a SCHIMADZU UV-1800 UV-Visible spectrophotometer, using commercially available 1 cm quartz cuvette purchased from Sigma-Aldrich.

Synthesis of 8-Bromo-10-dodecyl-10H-benzo[4,5]thieno[3,2-*b*]indole (4): The enolizable ketone, cyclohexanone (760 mg, 7.75 mmol) and primary amine, dodecylamine (1.43 g, 7.75 mmol) were weighed into a dry reaction tube. Dry toluene along with 4\AA MS was added and

allowed to stir at 80 °C for 1 hour, after which 5-bromo-3-nitrobenzothiophene (1 g, 3.87 mmol) was added into it and kept again for stirring at the same temperature for 11 hours. After the complete consumption of 5-bromo-3-nitrobenzothiophene, chloranil (2.8 g, 11.6 mmol.) along with toluene was added and kept at 100 °C for 24 hours. The solvent was evaporated in vacuo and the residue on activated neutral alumina column chromatography yielded 8-bromo-10-dodecyl-10H-benzo[4,5]thieno[3,2-*b*]indole **4** as colourless solid, Yield: 1.27 g, 70% ; mp (65-67 °C); ¹H NMR (500 MHz, CDCl₃): δ 8.09 (d, *J* = 1.5 Hz, 1H) 7.78-7.76 (m, 2H) 7.49 (d, *J* = 8 Hz, 1H) 7.44 (dd, *J*₁ = 8.5 Hz, *J*₂ = 2 Hz, 1H) 7.39-7.35 (m, 1H) 7.24-7.21(m, 1H) 4.54 (t, *J* = 7.5 Hz, 2H) 1.98-1.93(m, 2H) 1.47-1.41(m, 2H) 1.37-1.24(m, 16 H) 0.87(t, *J* = 7Hz, 3H) ppm; ¹³C NMR (125 MHz, CDCl₃) : δ 141.7, 141.7, 136.2, 128.5, 126.5, 125.7, 123.4, 122.6, 121.3, 119.6, 118.1, 116.8, 110.0, 45.0, 31.9, 30.4, 29.6, 29.6, 29.6, 29.5, 29.4, 29.3, 27.0, 22.7, 14.1 ppm; HRMS (ESI) *m/z*: (M+H)⁺ calcd for C₂₆H₃₃BrNS 470.1512, found 470.1583.

Synthesis of 4-(10-Dodecyl-10H-benzo[4,5]thieno[3,2-*b*]indol-7-yl)benzaldehyde (5): A mixture of **4** (200 mg, 0.43 mmol.), 4-formylphenylboronic acid (76 mg, 0.51 mmol), Pd(PPh₃)₄ (49 mg, 0.42 mmol), K₂CO₃ (294 mg, 2.1 mmol) were weighed into a Schlenk tube and degassed for 10 minutes. Degassed THF and water in a 3:1 ratio was then added and the reaction mixture was purged with argon and allowed to stir at 70 °C for 24 hours. The solvent was evaporated under vacuum and the residue on activated neutral alumina column chromatography (with mixtures of ethyl acetate in hexane as eluent) yielded the product **5** as a yellow coloured solid. Yield 162 mg, 77 %; mp (85-87 °C); ¹H NMR (500 MHz, CDCl₃): δ 10.10 (1H, S), 8.21-8.20 (m, 1H), 8.03-8.01 (m, 3H), 7.86 (d, *J* = 8.5 Hz, 2H), 7.80 (d, *J* = 8 Hz, 1H), 7.64-7.62 (m, 1H), 7.51 (d, *J* = 8.5 Hz, 1H) 7.40-7.36 (m, 1H), 7.26-7.22 (m, 1H), 4.63 (t, *J* = 7.5 Hz, 2H) 2.05-1.99 (m, 2H), 1.51-1.45 (m, 2H), 1.40-1.34 (m, 2H), 1.27-1.21 (m, 14 H), 0.86 (t, *J* = 7 Hz, 3H) ppm ¹³C NMR (125 MHz, CDCl₃) : 191.9, 147.5, 143.4, 137.1, 136.2, 135.2, 130.4, 127.9, 127.6, 125.0, 123.2, 123.1, 121.5, 119.6, 119.5, 118.6, 110.0, 45.2, 31.9, 30.5, 29.7, 29.6, 29.6, 29.5, 29.4, 29.3, 27.1, 22.7, 14.1 ppm; HRMS (ESI) *m/z*: (M+Na)⁺ calcd for C₃₃H₃₇NNaOS 518.2488, found 518.2422.

Synthesis of 2-Cyano-3-(4-(10-dodecyl-10H-benzo[4,5]thieno[3,2-*b*]indol-7yl)phenyl) acrylic acid (BID-1): A mixture of aldehyde **5** (150 mg, 0.3 mmol), cyanoacetic acid (77 mg, 0.9 mmol), ammonium acetate (116 mg, 1.5 mmol) in acetic acid was heated at reflux overnight under argon atmosphere. After cooling to room temperature, it was precipitated by pouring into water. The precipitate was washed with water and dried in vacuum oven. The

product **BID-1** was obtained as an orange coloured solid. Yield: 124 mg, 73 %; mp: 160-165 °C; ¹H NMR (500 MHz, (CD₃)₂CO): δ 8.37 (d, *J* = 1.5 Hz, 1H), 8.26 (s, 1H), 8.12 (d, *J* = 8.5 Hz, 2H) 8.02(d, *J* = 8.5 Hz, 1H) 7.94-7.92 (m, 2H), 7.70-7.68 (m, 2H), 7.58 (d, *J* = 8.5 Hz, 1H), 7.26-7.23 (m, 1H) 7.10-7.08 (m, 1H), 4.70 (t, *J* = 7 Hz, 2H) 1.90-1.87 (m, 2H) 1.37-1.32 (m, 2H) 1.26-1.22 (m, 2H) 1.14-1.04 (m, 14H) 0.71 (t, *J* = 7 Hz, 3H) ppm ¹³C NMR (125 MHz, (CD₃)₂CO) : 162.9, 153.7, 145.5, 143.2, 141.8, 137.2, 136.0, 131.6, 130.8, 127.9, 127.8, 125.1, 123.2, 123.2, 121.4, 119.6, 119.1, 118.8, 115.8, 115.7, 110.6, 103.2, 44.6, 31.7, 30.3, 29.4, 29.3, 29.2, 29.2, 29.1, 26.6, 22.4, 13.4 ppm; HRMS (ESI) m/z: (M-CO₂)⁻ calcd for C₃₅H₃₇N₂S 517.2683, found 517.2686.

Synthesis of 5-(10-dodecyl-10H-benzo[4,5]thieno[3,2-*b*]indol-8-yl)thiophene-2-carbaldehyde (6): A mixture of **4** (200 mg, 0.43 mmol), 5-Formyl-2-thiopheneboronic acid (80 mg, 0.51 mmol), Pd(PPh₃)₄ (49 mg, 0.042 mmol), K₂CO₃ (294 mg, 2.1 mmol) were weighed into a Schlenk tube and degassed for 10 minutes. Degassed THF and water in a 3:1 ratio was then added and the reaction mixture was purged with argon and allowed to stir at 70 °C for 24 hours. The solvent was evaporated under vacuum and the residue on activated neutral alumina column chromatography (with mixtures of ethyl acetate in hexane as eluent) yielded the product **6** as a yellow coloured solid. Yield: 43 mg, 20 % ; mp (80-83 °C); ¹H NMR (500 MHz, CDCl₃): δ 9.93 (1H, s), 8.25-8.20 (m, 1H), 7.96-7.94 (m, 1H), 7.79-7.78 (m, 2H) 7.70-7.64 (m, 1H), 7.51-7.48 (m, 2H), 7.38 (t, *J* = 7.5 Hz, 1H), 7.24-7.19 (m, 1H) 4.60-4.52 (m, 2H), 2.01-1.95 (m, 2H), 1.52-1.47 (m, 2H), 1.42-1.35 (m, 2H) 1.27-1.21 (m, 14H) 0.86 (t, *J* = 7 Hz, 3H) ppm; ¹³C NMR (125 MHz, CDCl₃) : 182.7, 154.7, 144.2, 141.6, 137.6, 136.8, 125.1, 124.1, 124.0, 123.4, 122.0, 121.8, 121.4, 120.4, 119.6, 119.6, 117.7, 116.6, 109.9, 45.2, 31.9, 30.5, 30.1, 29.5, 29.3, 27.2, 27.1, 22.7, 14.1 ppm; HRMS (ESI) m/z: (M + H)⁺ calcd for C₃₁H₃₆NOS₂ 502.2233, found 502.2233.

2-Cyano-3-(5-(10-dodecyl-10H-benzo[4,5]thieno[3,2-*b*]indol-8-yl)thiophen-2-yl)acrylic acid (BID-2): A mixture of aldehyde **6** (151 mg, 0.30 mmol), cyanoacetic acid (77 mg, 0.90 mmol), ammonium acetate (116 mg, 1.5 mmol) in acetic acid was heated at reflux overnight under argon atmosphere. After cooling to room temperature, it was precipitated by pouring into water. The precipitate was washed with water and dried in vacuum oven. The product **BID-2** was obtained as red coloured solid. Yield: 68 mg, 40%; mp: 203-205 °C; ¹H NMR (500 MHz, (CD₃)₂CO): δ 8.40 (d, *J* = 1.5 Hz, 1H) 8.37 (s, 1H), 8.03 (d, *J* = 8.5 Hz, 1H), 7.93 (d, *J* = 4 Hz, 1H), 7.74-7.72 (m, 2H) 7.70 (d, *J* = 8 Hz, 1H) 7.60 (d, *J* = 8 Hz, 1H) 7.27-7.24 (m, 1H) 7.10 (t, *J* = 7.5 Hz, 1H), 4.69 (t, *J* = 7.5 Hz, 2H) 1.90-1.87 (m, 2H), 1.46-1.40 (m,

2H) 1.15-1.07 (m, 14 H) 0.72 (t, $J = 7.5$ Hz, 3H)ppm; ^{13}C NMR (125 MHz, $(\text{CD}_3)_2\text{CO}$) :163.0, 154.3, 145.3, 146.4, 143.9, 141.8, 140.2, 136.8, 135.0, 129.4, 127.5, 125.3, 125.0, 123.4, 122.0, 121.2, 119.6, 119.1, 117.8, 116.1, 116.1, 110.6, 98.6, 44.8, 31.6, 30.1, 26.5, 22.4, 13.5 ppm; HRMS (ESI) m/z : $(\text{M}-\text{CO}_2)^-$ calcd for $\text{C}_{33}\text{H}_{35}\text{N}_2\text{S}_2$ 523.2242, found 523.2232.

Synthesis of 5-(10-Dodecyl-10H-benzo[4,5]thieno[3,2-*b*]indol-8-yl)furan-2-carbaldehyde (7): A mixture of **4** (200 mg, 0.43 mmol), 5-Formyl-2-furanylboronic acid (71 mg, 0.51 mmol), $\text{Pd}(\text{PPh}_3)_4$ (49 mg, 0.42 mmol), K_2CO_3 (294 mg, 2.1 mmol) were weighed into a Schlenk tube and degassed for 10 minutes. Degassed THF and water in a 3:1 ratio was then added and the reaction mixture was purged with argon and allowed to stir at 70 °C for 24 hours. The solvent was evaporated under vacuum and the residue on activated neutral alumina column chromatography (with mixtures of ethyl acetate in hexane as eluent) yielded the product **7** as a yellow coloured solid. Yield: 182 mg, 88 % ; mp: 100-103 °C; ^1H NMR (500 MHz, CDCl_3): δ 9.71 (1H, s), 8.43 (1H, S), 7.98 (d, $J = 8$ Hz, 1H), 7.79 (t, $J = 7$ Hz, 2H) 7.52 (d, $J = 8.5$ Hz, 1H) 7.40-7.37 (m, 2H) 7.26-7.22 (m, 1H) 6.93 (d, $J = 4$ Hz, 1H) 4.65 (t, $J = 7.5$ Hz, 2H) 2.05-1.99 (m, 2H) 1.53-1.47 (m, 2H) 1.41-1.36 (m, 2H) 1.27-1.20 (m, 14H) 0.86 (t, $J = 7$ Hz, 3H) ppm ^{13}C NMR (125 MHz, CDCl_3) : 177.1, 159.7, 152.0, 144.3, 141.6, 136.9, 127.3, 125.4, 124.9, 123.3, 121.3, 120.6, 119.6, 119.6, 116.4, 110.1, 107.6, 45.2, 31.9, 30.4, 29.6, 29.6, 29.6, 29.5, 29.4, 29.3, 27.1, 22.7, 14.1 ppm. HRMS (ESI) m/z : $(\text{M} + \text{H})^+$ calcd for $\text{C}_{31}\text{H}_{36}\text{NO}_2\text{S}$ 486.2461, found 486.2479.

Synthesis of 2-Cyano-3-(5-(10-dodecyl-10H-benzo[4,5]thieno[3,2-*b*]indol-8-yl)furan-2-yl)acrylic acid (BID-3): A mixture of aldehyde **7** (146 mg, 0.30 mmol), cyanoacetic acid (77 mg, 0.90 mmol), ammonium acetate (116 mg, 1.5 mmol) in acetic acid was heated at reflux overnight under argon atmosphere. After cooling to room temperature, it was precipitated by pouring into water. The precipitate was washed with water and dried in vacuum oven. The product **BID-3** was obtained as red coloured solid. Yield: 88 mg, 53 %; mp: 190-193 °C; ^1H NMR (500 MHz, $(\text{CD}_3)_2\text{CO}$): 8.69 (s, 1H), 8.03 (d, $J = 8.5$ Hz, 1H), 8.01 (s, 1H), 7.87 (dd, $J_1 = 8.5$ Hz, $J_2 = 1.5$ Hz, 1H), 7.70 (d, $J = 7$ Hz, 1H), 7.60 (d, $J = 8.5$ Hz, 1H), 7.46 (d, $J = 4$ Hz, 1H), 7.30 (d, $J = 3.5$ Hz, 1H), 7.27-7.24 (m, 1H), 7.11-7.08 (m, 1H), 4.72 (t, $J = 7$ Hz, 2H) 1.88-1.83 (m, 2H), 1.32-1.26 (m, 2H), 1.69-1.02 (m, 16 H), 0.71 (t, $J = 7.5$ Hz, 3H)ppm; ^{13}C NMR (125 MHz, $(\text{CD}_3)_2\text{CO}$) : 163.3, 159.8, 148.0, 144.2, 142.0, 137.9, 137.2, 127.5, 126.3, 125.5, 125.2, 123.4, 121.3, 120.9, 119.6, 119.1, 116.7, 116.4, 115.9, 110.9, 109.6, 97.2, 44.4,

31.7, 30.3, 26.3, 22.4, 13.4 ppm; HRMS (ESI) m/z : $(M + H)^+$ calcd for $C_{34}H_{36}N_2O_3S$ 553.2519, found 553.2526.

Synthesis of 9-bromo-6-dodecyl-6H-benzo[4,5]thieno[2,3-*b*]indole (8): Sulfur powder (4 equiv.), 5-bromo-1-dodecyl-1H-indole (**1**, 1.5 equiv.), cyclohexanone (1 equiv.), iodine (1 equiv.), NMP were added to a reaction vessel (10 mL). The sealed reaction vessel under air atmosphere was stirred at 150 °C for 16 h. After cooling to room temperature, the reaction was diluted with ethyl acetate and washed with saturated salt water. The organic layer was separated, and the aqueous layer was extracted with ethyl acetate for three times. The combined organic layer was dried over sodium sulphate, the volatiles were removed under reduced pressure. The residue was purified by column chromatography on silica gel to yield the desired product **8** as colourless viscous liquid. Yield: 49 % ; R_f : 0.4 (hexane); 1H NMR (500 MHz, $CDCl_3$): δ 8.05 (s, 1H), 7.96 (d, $J = 7.5$ Hz, 1H), 7.73 (d, $J = 8$ Hz, 1H), 7.41 (t, $J = 7.5$ Hz, 1H), 7.31-7.30 (m, 1H), 7.22-7.20 (m, 2H), 4.15 (t, $J = 7$ Hz, 2H), 1.88-1.83(m, 2H), 1.25-1.15 (m, 18H), 0.80 (t, $J = 6$ Hz, 3H) ppm; ^{13}C NMR (125 MHz, $CDCl_3$) : 143.8, 139.9, 138.0, 132.7, 125.3, 124.1, 124.0, 123.7, 122.4, 121.5, 120.6, 116.2, 113.1, 110.8, 46.5, 31.9, 29.6, 29.5, 29.4, 29.3, 29.2, 29.0, 27.0, 22.7, 14.1 δ ppm; HRMS (ESI) m/z : $(M)^+$ calcd for $C_{26}H_{32}BrNS$ 469.1439, found 469.1443.

Synthesis of 4-(6-dodecyl-6H-benzo[4,5]thieno[2,3-*b*]indol-9-yl)benzaldehyde (9): A mixture of benzothienoindole **8** (1 equiv.), 4-formylphenylboronic acid (1.2 equiv.), $Pd(PPh_3)_4$ (10 mol%), K_2CO_3 (5 equiv.) were weighed into a schlenk tube and degassed for 10 minutes. Degassed THF and water in a 3:1 ratio was then added and the reaction mixture was purged with argon and allowed to stir at 70 °C for 24 hours. The solvent was evaporated under vacuum and the residue on activated neutral alumina column chromatography yielded the product as a yellow coloured solid. Yield: 77 % ; mp (82-84 °C); 1H NMR (500 MHz, $CDCl_3$): δ 10.08 (s, 1H), 8.27 (s, 1H), 8.15(d, $J = 8$ Hz, 1H), 8.00 (d, $J = 8$ Hz, 2H), 7.90(d, $J = 7.5$ Hz, 2H), 7.84 (d, $J = 8$ Hz, 1H), 7.59(d, $J = 7.5$ Hz, 1H), 7.52-7.49 (m, 2H), 7.30-7.27 (m, 1H), 4.49 (t, $J = 7$ Hz, 2H), 2.00-1.97 (m, 2H), 1.41-1.23 (m, 18H), 0.87 (t, $J = 7$ Hz, 3H)ppm; ^{13}C NMR (125 MHz, $CDCl_3$) : 192.1, 148.5, 143.7, 142.3, 138.2, 134.6, 133.0, 131.8, 130.4, 127.9, 125.3, 123.7, 123.2, 122.3, 121.0, 120.6, 117.9, 117.1, 110.0, 46.6, 31.9, 29.6, 29.5, 29.4, 29.3, 29.2, 29.1, 27.0, 22.7, 14.1 ppm; HRMS (ESI) m/z : $(M+H)^+$ calcd for $C_{33}H_{38}NOS$ 496.2669, found 496.2681.

Synthesis 2-cyano-3-(4-(6-dodecyl-6H-benzo[4,5]thieno[2,3-*b*]indol-9-yl)phenyl)acrylic acid (BID-1): A mixture of aldehyde **9** (1 equiv.), cyanoacetic acid (3 equiv.), ammonium

acetate (5 equiv.) in acetic acid was heated at reflux overnight under argon atmosphere. After cooling to room temperature, it was precipitated by pouring into water. The precipitate was washed with water and dried in vacuum oven. The product **BID-1** was obtained as an orange coloured solid. Yield: 88 %; mp: 157-160 °C; ¹H NMR (500 MHz, CDCl₃): δ 8.46 (s, 1H), 8.26-8.26 (m, 2H), 8.12 (d, *J* = 8 Hz, 2 H), 7.98 (d, *J* = 8 Hz, 2 H), 7.83 (d, *J* = 8 Hz, 2H), 7.64 (s, 2 H), 7.39 (t, *J* = 7 Hz, 1 H), 7.18 (t, *J* = 7.5 Hz, 1 H), 4.32 (t, *J* = 7 Hz, 2H), 1.90-1.87(m, 2H), 1.31-1.23 (m, 4H), 1.15-1.10 (m, 14 H), 0.72 (t, *J* = 7 Hz, 3H) ppm; ¹³C NMR (125 MHz, CDCl₃) : 163.0, 154.1, 146.7, 143.4, 141.7, 138.2, 133.0, 131.7, 131.3, 130.1, 127.7, 125.3, 123.8, 123.1, 122.4, 121.0, 117.6, 117.1, 116.0, 110.6, 46.1, 31.7, 26.6, 22.4, 13.5 ppm; HRMS (ESI) *m/z*: (M+H)⁺ calcd for C₃₆H₃₉N₂O₂S 563.2727, found 563.2736.

Synthesis of 5-(6-dodecyl-6H-benzo[4,5]thieno[2,3-*b*]indol-9-yl)thiophene-2-carbaldehyde (10): A mixture of benzothienoindole **8** (1 equiv.), (5-formylthiophene-2-yl)boronic acid (1.2 equiv.), Pd(PPh₃)₄ (10 mol%), K₂CO₃ (5 equiv.) were weighed into a schlenk tube and degassed for 10 minutes. Degassed THF and water in a 3:1 ratio was then added and the reaction mixture was purged with argon and allowed to stir at 70 °C for 24 hours. The solvent was evaporated under vacuum and the residue on activated neutral alumina column chromatography yielded the product **10** as a yellow coloured solid. Yield: 70 %; mp (82-84 °C); ¹H NMR (500 MHz, CDCl₃): δ 9.90 (s, 1H), 8.31 (s, 1H), 8.13(d, *J* = 7.5 Hz, 1H), 7.83(d, *J* = 8 Hz, 1H), 7.80-7.83 (m, 1H), 7.62 (d, *J* = 8 Hz), 7.54-7.45(m, 3H), 7.30 (t, *J* = 7.5 Hz, 1H), 4.28 (t, *J* = 7 Hz, 2H), 1.20-1.94 (m, 2 H), 1.41-1.23 (m, 18 Hz), 0.87(t, *J* = 6 Hz, 3 H) ppm; ¹³C NMR (125 MHz, CDCl₃) : 182.7, 156.4, 141.8, 141.5, 138.3, 137.9, 132.8, 125.4, 125.2, 123.7, 123.2, 123.1, 122.6, 120.8, 120.2, 117.1, 110.0, 46.6, 32.5, 31.9, 30.3, 29.6, 29.5, 29.3, 29.2, 28.3, 27.0, 22.7, 10.6 ppm; HRMS (ESI) *m/z*: (M+H)⁺ calcd for C₃₁H₃₆NOS₂ 563.2727, found 563.2736.

Synthesis of 2-cyano-3-(5-(6-dodecyl-6H-benzo[4,5]thieno[2,3-*b*]indol-9-yl)thiophen-2-yl)acrylic acid (BID-2): A mixture of aldehyde **10** (1 equiv.), cyanoacetic acid (3 equiv.), ammonium acetate (5 equiv.) in acetic acid was heated at reflux overnight under argon atmosphere. After cooling to room temperature, it was precipitated by pouring into water. The precipitate was washed with water and dried in vacuum oven. The product **BID-2** was obtained as red coloured solid. Yield: 80 %; mp: 210-212 °C; ¹H NMR (500 MHz, CDCl₃): δ 8.49 (s, 1H), 8.34 (s, 1H), 8.22 (d, *J* = 8 Hz, 1H), 7.91(d, *J* = 4 Hz, 1 H), 7.84(d, *J* = 8 Hz, 1 H), 7.74 (d, *J* = 4 Hz, 1 H), 7.64 (s, 2H), 7.41 (t, *J* = 7.5 Hz, 1 H), 7.20 (t, *J* = 7.5 Hz, 1 H),

4.33(t, $J = 7$ Hz, 2 H), 1.88-1.87 (m, 2H), 1.31-1.10 (m, 18 H), 0.72 (t, $J = 7$ Hz, 3 H) ppm; ^{13}C NMR (125 MHz, CDCl_3) : 163.3, 156.1, 146.5, 143.8, 142.1, 140.7, 138.1, 134.1, 132.9, 125.4, 125.1, 124.1, 123.8, 122.9, 122.7, 120.9, 120.4, 117.0, 116.8, 116.2, 111.0, 97.2, 46.1, 31.7, 26.6, 22.4, 13.5 ppm; HRMS (ESI) m/z : ($\text{M}+\text{H}$) $^+$ calcd for $\text{C}_{34}\text{H}_{37}\text{N}_2\text{O}_2\text{S}_2$ 569.2291, found 569.2300.

Synthesis of 5-(6-dodecyl-6H-benzo[4,5]thieno[2,3-*b*]indol-9-yl)furan-2-carbaldehyde (11): A mixture of benzothienoindole **8** (1 equiv.), (5-formylfuran-2-yl)boronic acid (1.2 equiv.), $\text{Pd}(\text{PPh}_3)_4$ (10 mol%), K_2CO_3 (5 equiv.) were weighed into a schlenk tube and degassed for 10 minutes. Degassed THF and water in a 3:1 ratio was then added and the reaction mixture was purged with argon and allowed to stir at 70 °C for 24 hours. The solvent was evaporated under vacuum and the residue on activated neutral alumina column chromatography yielded the product **11** as a yellow coloured viscous liquid. Yield: 60 % ; R_f : 0.44 (20 % ethyl acetate in hexane); ^1H NMR (500 MHz, CDCl_3): δ 9.59 (s, 1H), 8.40 (s, 1H), 8.12 (d, $J = 8$ Hz, 1H), 7.75 (d, $J = 8$ Hz, 1 H), 7.69-7.67 (m, 1H), 7.45 (t, $J = 7$ Hz, 1H), 7.38-7.37 (m, 1H), 7.30 (d, $J = 4$ Hz, 1 H), 7.22 (t, $J = 7$ Hz, 1 H), 6.81(d, 3.5, $J = \text{Hz}$, 1H), 4.18 (t, $J = 7$ Hz, 2 H), 1.91-1.86 (m, 2H), 1.32-1.26 (m, 4 H), 1.18-1.15 (m, 14 H), 0.79 (t, $J = 7.5$ Hz, 3H) ppm ^{13}C NMR (125 MHz, CDCl_3) : 161.4, 151.7, 143.9, 141.8, 138.2, 132.8, 125.4, 123.7, 122.8, 122.5, 121.1, 120.9, 119.2, 117.3, 116.2, 109.9, 106.6, 46.6. 31.9, 29.6, 29.5, 29.4, 29.3, 29.2, 29.0, 27.0, 22.7, 14.1 ppm; HRMS (ESI) m/z : ($\text{M}+\text{H}$) $^+$ calcd for $\text{C}_{34}\text{H}_{37}\text{N}_2\text{O}_3\text{S}$ 553.2539, found 553.2519.

Synthesis of 2-cyano-3-(5-(6-dodecyl-6H-benzo[4,5]thieno[2,3-*b*]indol-9-yl)furan-2-yl) acrylic acid (BID-3): A mixture of aldehyde **11** (1 equiv.), cyanoacetic acid (3 equiv.), ammonium acetate (5 equiv.) in acetic acid was heated at reflux overnight under argon atmosphere. After cooling to room temperature, it was precipitated by pouring into water. The precipitate was washed with water and dried in vacuum oven. The product was obtained as red coloured solid. Yield: 75 %; mp: 173-175 °C; ^1H NMR (500 MHz, CDCl_3): 8.72 (S, 1H), 8.24 (d, $J = 7.5$ Hz, 1H), 7.97(s, 1H), 7.82(t, $J = 9$ Hz, 2H), 7.62 (d, $J = 9$ Hz, 1H), 7.42-7.38 (m, 2H), 7.21-7.18 (m, 2H), 1.29-1.22 (m, 6.5 Hz, 4H), 1.15-1.09 (m, 14H), 0.72(t, $J = 6.5$ Hz, 3H) ppm; ^{13}C NMR (125 MHz, CDCl_3) : 161.5, 147.4, 143.8, 142.1, 138.4, 137.6, 132.8, 125.4, 123.8, 122.7, 122.6, 121.2, 121.0, 119.1, 117.3, 116.5, 110.7, 108.1, 46.1, 31.7, 26.6, 22.4, 13.4 ppm; HRMS (ESI) m/z : (M) $^+$ calcd for $\text{C}_{34}\text{H}_{36}\text{N}_2\text{O}_3\text{S}$ 552.2446, found 552.2373.

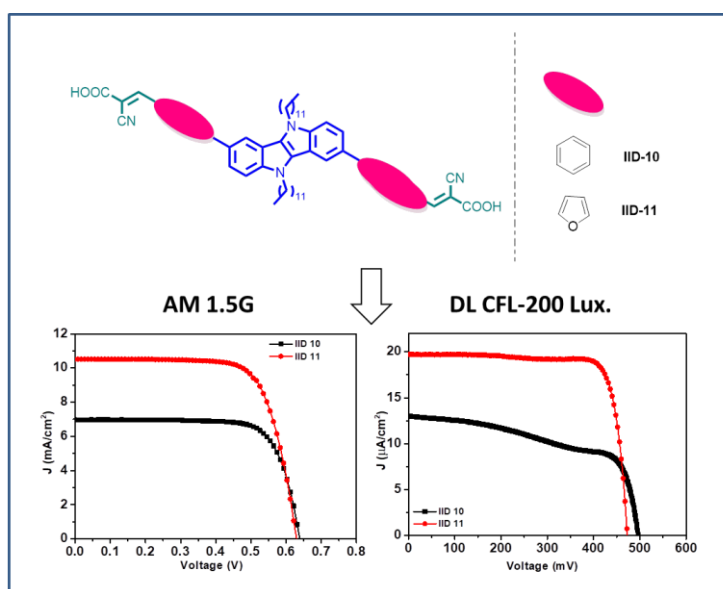
3.14 References:

1. (a) Z. Wang, Q. Chen, Y. Zou, J. Chen, Y. Luo, Y. Liu, S. Ding, P. Cai, J. Yuan and M. Liang, *Dye. Pigment.*, 2021, **187**, 109134 (b) A. Baumann, C. Curiac and J. H. Delcamp, *ChemSusChem*, 2020, **13**, 2503–2512 (c) Z. Yao, Y. Guo, L. Wang, Y. Hao, Y. Guo, D. Franchi, F. Zhang, L. Kloo and L. Sun, *Sol. RRL*, 2019, **3**, 1–9 (d) A. F. Buene, D. M. Almenningen, A. Hagfeldt, O. R. Gautun and B. H. Hoff, *Sol. RRL* (e) A. K. Singh, M. F. Mele Kavungathodi and J. Nithyanandhan, *ACS Appl. Mater. Interfaces*, 2020, **12**, 2555–2565 (f) R. Bisht, F. K. Munavvar, A. K. Singh and J. Nithyanandhan, *J. Org. Chem.*, 2017, **82**, 1920–1930
2. (a) L. Giribabu, V. K. Singh, C. V. Kumar, Y. Soujanya, P. Y. Reddy and M. L. Kantam, *Sol. Energy*, **2011**, 85, 1204–1212 (b) J. Tang, W. Wu, J. Hua, J. Li, X. Li and H. Tian, *Energy Environ. Sci.*, **2009**, 2, 982–990 (c) M. V. Vinayak, T. M. Lakshmykanth, M. Yoosuf, S. Soman and K. R. Gopidas, *Sol. Energy*, **2016**, 124, 227–241 (d) J. Wang, K. Liu, L. Ma and X. Zhan, *Chem. Rev.*, **2016**, 116, 14675–14725 (e) M. Liang, J. Chen, *Chem. Soc. Rev.* **2013**, 42, 3453.
3. (a) K. Hara, Z. S. Wang, Y. Cui, A. Furube and N. Koumura, *Energy Environ. Sci.*, **2009**, 2, 1109–1114 (b) G. Marotta, M. A. Reddy, S. P. Singh, A. Islam, L. Han, F. De Angelis, M. Pastore and M. Chandrasekharam, *ACS Appl. Mater. Interfaces*, **2013**, 5, 9635–9647 (c) P. Naik, A. Planchat, Y. Pellegrin, F. Odobel and A. Vasudeva Adhikari, *Sol. Energy*, **2017**, 157, 1064–1073.
4. (a) D. D. Babu, S. R. Gachumale, S. Anandan and A. V. Adhikari, *Dye. Pigment.*, **2015**, 112, 183–191 (b) D. D. Babu, R. Su, A. El-Shafei and A. V. Adhikari, *Electrochim. Acta*, **2016**, 198, 10–21 (c) Y. Hong, Z. Iqbal, X. Yin and D. Cao, *Tetrahedron*, **2014**, 70, 6296–6302
5. R. K. Konidena, K. hyung Lee, J. Y. Lee and W. P. Hong, *Org. Electron.*, **2019**, 70, 211–218.
6. R. K. Konidena, K. H. Lee and J. Y. Lee, *J. Mater. Chem. C*, **2019**, 7, 13912–13919.

CHAPTER 4

An Investigation into the Photovoltaic Performance of Indolo[3,2-*b*]indole and Indolo[2,3-*b*]indole based $D(\pi-A)_2$ Dyes

Abstract



Herein, we present the synthesis, detailed photophysical as well as photovoltaic evaluation of DSSCs based on three di-branched, di-anchoring dyes **IID-10**, **IID-11** and **IID-12**. The superiority of indolo[3,2-*b*]indole over indolo[2,3-*b*]indole was further illustrated in the new molecular architecture of $D(\pi-A)_2$. The sensitizer **IID-12** which is having indolo[2,3-*b*]indole as donor moiety showcased poor performance in both indoor as well as outdoor conditions. Among the indolo[3,2-*b*]indole based dyes, **IID-11** with furan as π -spacer delivered highest efficiency of 4.80% and least PCE was delivered by **IID-10** with 3.34%. Further evaluation of indoor light harvesting revealed **IID-11** as the best performer with 13.40% under 200 lux illumination when day light CFL was used as light source. To probe the trend in voltage and current generated detailed investigations were carried out on the absorption behaviour, energetics and adsorption nature of dyes along with computational approach. Lifetime as well as charge extraction measurements were also performed to get insight into the photovoltaic behaviour of dyes.

4.1 Introduction

Since dye sensitizer being a key player in DSSC, engineering of molecular architecture was always been a topic of utmost importance. Dye designs always target at obtaining enhanced absorption in the higher photon flux region in solar irradiance spectra with strategies to prevent back electron transfer reactions.¹⁻² It was the D- π -A architecture which brought major breakthrough in this area with its charge transfer properties. Though D- π -A architecture is still the most widely used strategy, many different approaches have been explored in recent years for the construction of sensitizers. Incorporation of more than one anchoring group/multianchoring approach is one among these new strategies developed.³ Compared to the mono-anchoring dyes, multianchoring dyes carry a number of added advantages. Increased π -conjugation in the latter case can ensure bathochromically shifted absorption with enhanced absorptivity. Since the adsorption rates are likely to increase with extra anchoring group, similar increment in dye loading and resultant absorption can be expected. An effective surface coverage of semiconductor will also be beneficial to minimize the recombination of injected electrons with the electrolyte. Further, an effective electronic communication between the dye and semiconductor will be possible with the enhanced binding strength of dye on semiconductor surface. This can in turn lead to better electron injection and current generation. Since there are less chances of dye desorption, long term stability of DSSC can also be targeted.

Bi-anchoring dyes can be classified into different classes based on the connector/connectivity of two dipolar D- π -A branches (Figure. 4.1).⁴ Two D- π -A branches are connected at the donor part with (i) π -unit or (ii) σ unit; linked at the π -spacer part with (iii) π -unit or (iv) σ unit ; (v) donor-acceptor back bone directly connected at π -linker; and (vi) different acceptor units are bridged via a common donor unit. First report of di-branched di-anchoring organic sensitizer was made in 2009 by Abbotto *et al.* They synthesized **DB-1** and **DB-2** which employs cyanoacetic acid and conjugated rhodanine respectively as π -spacer. A comparative investigation was also made with **D5** which is a monoanchored version of **DB-1** (Figure 4.2). Along with demonstrating the efficiency of dianchoring molecular architecture, this work could also illustrate the superiority of cyanoacrylic acid as the anchoring group over conjugated rhodanine. Due to severe recombination happening in the system, **DB-2** showcased least performance with lowest current density and photovoltage compared to the rest of the dyes. Though **DB-1** was having lower photovoltage, higher current density

produced in the devices helped it to showcase best PCE. Light soaking measurements conducted also reveals the improved lifetime and stability of di-anchoring approach over the corresponding mono-anchored version.

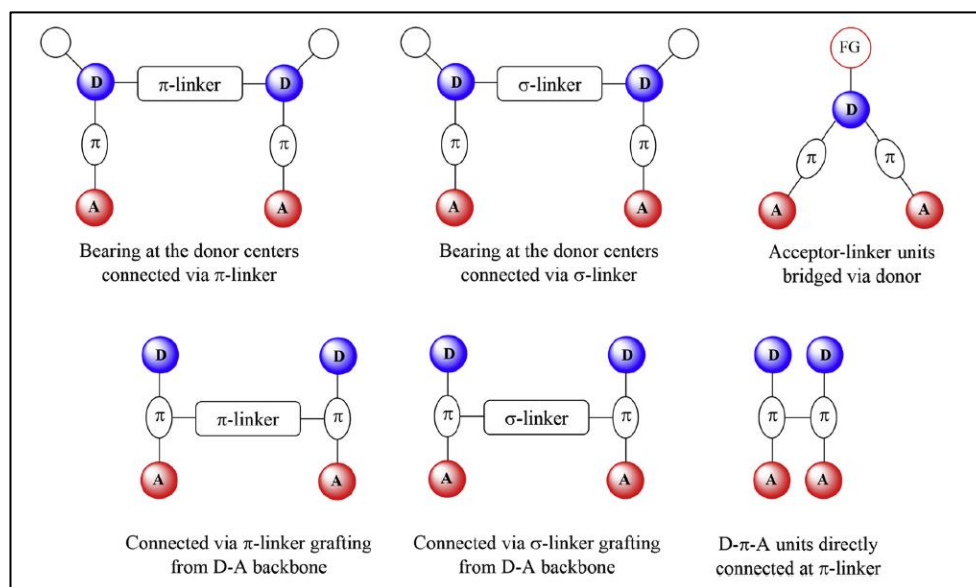


Figure 4.1 Di-anchoring dyes with different geometries

Since the first application of this multianchoring concept, it has undergone much development in design as well as efficiency by incorporating novel structural units. The concept of *concerted companion dye* introduced by Yongshu and co-workers is the latest advancement in this area.⁵⁻⁶ In this approach two complementary dye components are linked through covalent chains to target intramolecular co-sensitization. Along with achieving panchromatic absorption with higher efficiency, simple optimization procedures and stability are added advantages associated with this approach.

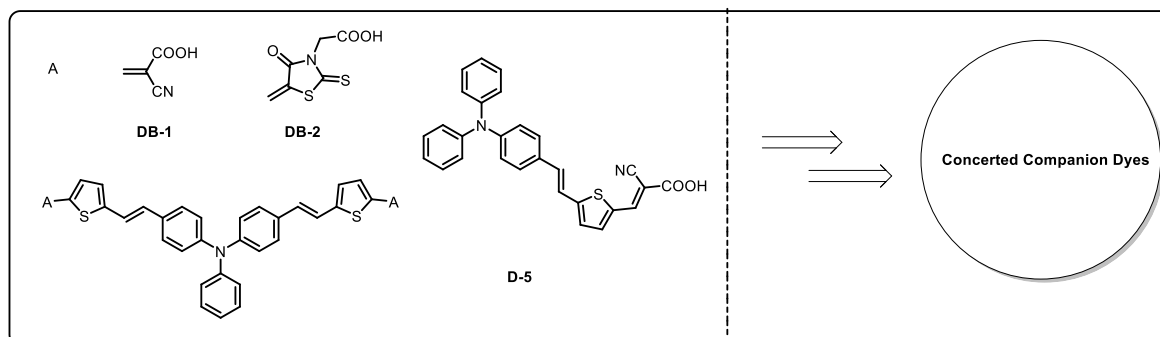
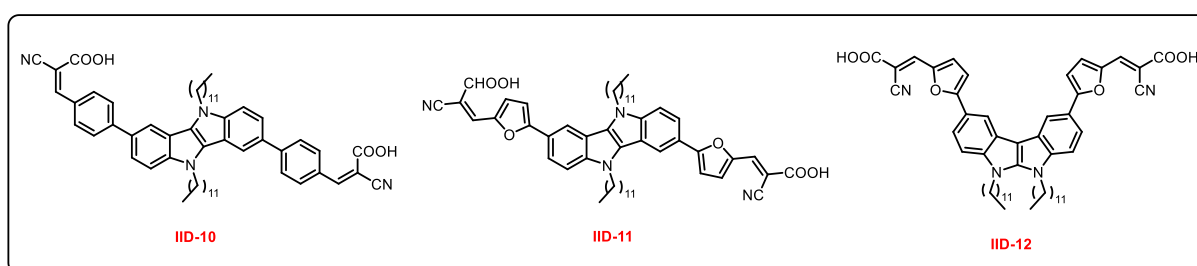


Figure 4.2 Molecular structures of sensitizers **D5**, **DB-1** and **DB-2**

4.2 Design Strategy

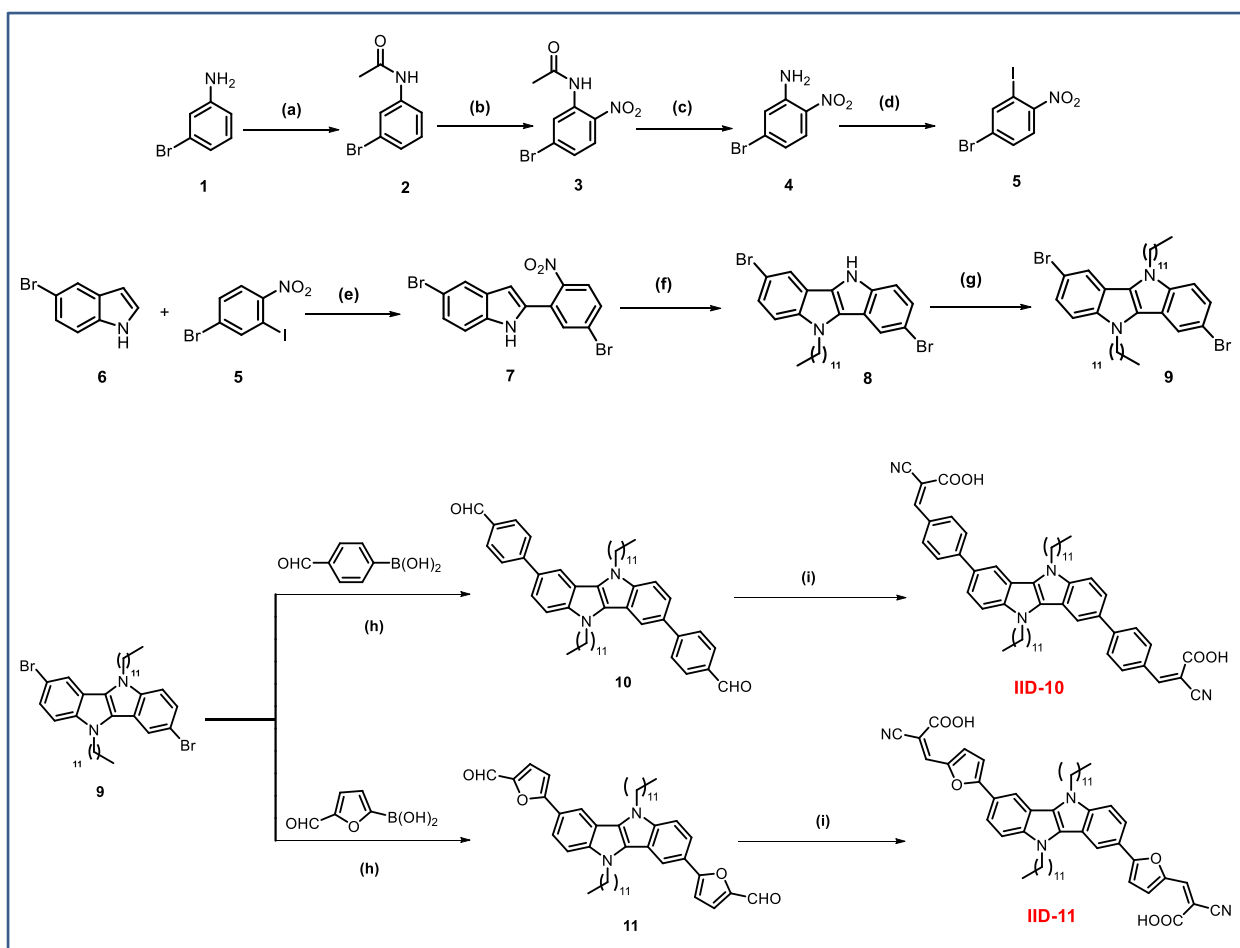
In the present work, we adopted the innovative molecularly engineered bifunctional $D(\pi-A)_2$ architecture taking dodecyl group incorporated indolo[3,2-*b*]indole as donor which is the best optimized system we obtained from our previous investigations. We changed the π -spacer as benzene (**IID-10**) and furan (**IID-11**) keeping the acceptor/anchoring group fixed as cyanoacrylic acid. Next, we synthesized dye **IID-12** with the same molecular architecture utilizing indolo[2,3-*b*]indole as donor, furan as π -spacer and cyanoacrylic acid as the anchoring/acceptor group (Scheme 4.1).



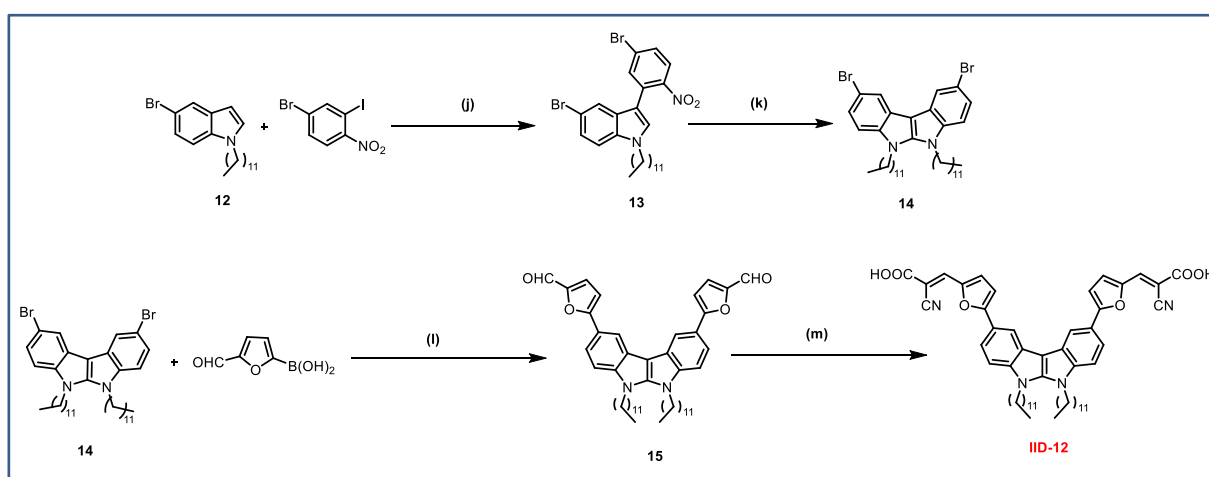
Scheme 4.1 Molecular structure of sensitizers **IID-10** to **IID-12**

4.3 Synthetic Strategy

Our first step was the synthesis of starting material 4-bromo-2-iodo-1-nitrobenzene. We could successfully synthesize the starting material in gram scale from 3-bromoaniline *via* a four-step synthetic route (Scheme 4.2). The amino group of 3-bromoaniline was acylated using acetic anhydride in presence of catalytic amount of H_2SO_4 to obtain **2**. Compound **2** was then nitrated predominantly at the *ortho*-position of acetanilide using $Bi(NO_3)_3$ in acetic anhydride. The compound **3** thus obtained was subjected to acetyl-deprotection of and subsequent diazotization. During diazotization, PTSA was employed as the proton source in presence of KI as the source of the nucleophile iodide. Using this starting material **5**, the dibrominated indoloindole and the dyes **IID-10** and **IID-11** were synthesized by adopting the strategies discussed in the first chapter. Similar methodology was adopted for the synthesis of **IID-12** after obtaining compound **13** with palladium catalysed C-3 arylation of alkylated 5-bromoindoloindole with **5** using AgO as the additive in HFIP (Scheme 4.3).



Scheme 4.2 (a) Ac_2O , H_2SO_4 , RT (b) $\text{Bi}(\text{NO}_3)_3$, Ac_2O , RT (c) KOH , DMSO , $60\text{ }^\circ\text{C}$ (d) PTSA , NaNO_2 , KI , ACN , $0\text{ }^\circ\text{C}$ -RT (e) $\text{Pd}(\text{OAc})_2$, K_2CO_3 , norbornene, DMA , $60\text{ }^\circ\text{C}$ (f) (i) 1-bromododecane, NaH , DMF , $0\text{ }^\circ\text{C}$ -RT (ii) PPh_3 , DMA , $165\text{ }^\circ\text{C}$ (g) 1-bromohexane, NaH , DMF , $0\text{ }^\circ\text{C}$ -RT (h) $\text{Pd}(\text{PPh}_3)_4$, K_2CO_3 , $\text{THF}/\text{H}_2\text{O}(4:1)$, $70\text{ }^\circ\text{C}$ (i) Cyanoacetic acid, Piperidine, ACN , $80\text{ }^\circ\text{C}$



Scheme 4.3 (j) $\text{Pd}(\text{OAc})_2$, NaOAc , AgO , HFIP , RT (k) (i) PPh_3 , DMA , $165\text{ }^\circ\text{C}$ (ii) 1-bromododecane, NaH , DMF , $0\text{ }^\circ\text{C}$ -RT (l) $\text{Pd}(\text{PPh}_3)_4$, K_2CO_3 , $\text{THF}/\text{H}_2\text{O}(4:1)$, $70\text{ }^\circ\text{C}$ (m) Cyanoacetic acid, Piperidine, ACN , $80\text{ }^\circ\text{C}$

4.4 Photophysical Properties

The absorption spectra of dyes, **IID-10** to **IID-12**, in THF and on TiO₂ film are shown in Figure 4.3 and the corresponding data are documented in Table 1.

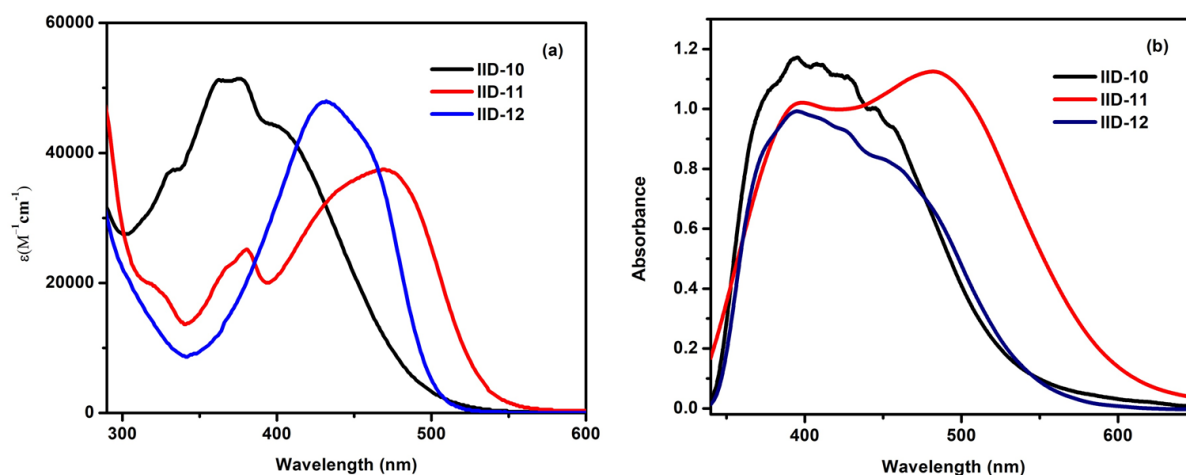


Figure 4.3 (a) Solution state absorption spectra of dyes in THF. (b) Solid state absorption spectra of dyes on TiO₂

Among indolo[3,2-*b*]indole donor based dyes, furan substituted dye **IID-11** showcased a bathochromically shifted spectra with an absorption maximum at 470 nm and least planar **IID-10** with benzene as π -spacer is having absorption maximum at 376 nm. Though **IID-12** which is having indolo[2,3-*b*]indole as donor is having higher molar extinction coefficient compared to its indolo[3,2-*b*]indole counterpart **IID-11**, the former has a blue shifted absorption profile with absorption maximum at 434 nm. The absorption spectra of all the molecules on TiO₂ were taken by following the conditions adopted during device fabrication (TiO₂ electrodes were soaked in 0.2 mM solutions of dye in 1:1 tert-Butanol: Acetonitrile mixture for 15 hour). Compared to solution state spectra, broadened and red shifted absorption is exhibited by the dyes in solid state. Among the three dyes, **IID-11** is showcasing better absorption followed by **IID-10** and **IID-12** in order.

4.5 Electrochemical properties

Cyclic voltammetry was performed to find out the energy levels of the dyes which can in turn be used to check the feasibility of electron injection as well as the regeneration of dyes. The measurements were carried out in THF using tetrabutyl ammonium hexafluorophosphate (0.1M) as the supporting electrolyte. While glassy carbon was employed as working electrode, Ag/AgCl was used as reference electrode. The oxidation potentials of **IID-10**, **IID-**

IID-11, and **IID-12** were calculated with respect to ferrocene and were converted to NHE using the equation, $E_{\text{HOMO}} = [E_{\text{ox}}(\text{Fc}/\text{Fc}^+) + 0.63 \text{ V}]$. LUMO level (E_{LUMO}) was calculated as the difference $E_{\text{HOMO}} - E_{0-0}$. E_{0-0} (band gap) was determined from the tangent intercept of absorption edges. The obtained values for HOMO and LUMO are compiled in Table 1 which shows that electron injection into TiO_2 conduction band (-0.5 V vs NHE) and dye regeneration by iodide (0.4 V vs NHE) are thermodynamically feasible. Higher energy HOMO of **IID-11** compared to **IID-12** also indicates the more electron donating nature of **IID-11** over **IID-12** (Figure 4.4).

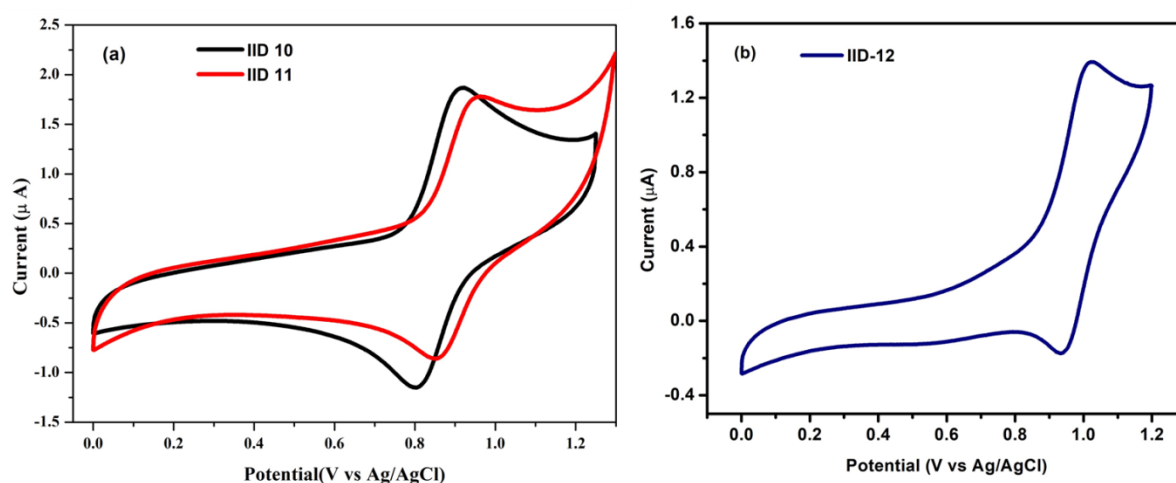


Figure 4.4 Cyclic voltammogram of (a) **IID-10** and **IID-11**. (b) **IID-12**

Table 1 Photophysical and electrochemical parameters of dyes

Sensitizer	λ_{max} , nm (ϵ , $\text{M}^{-1}\text{cm}^{-1}$)	$E_{\text{ox}}(\text{Fc}/\text{Fc}^+)$ (V)	E_{HOMO} (vs NHE) (V)	E_{0-0} eV	E_{LUMO} (vs NHE) (V)
IID-10	376(51400)	0.296	0.93	2.5	-1.57
IID-11	470(37450)	0.334	0.97	2.27	-1.30
IID-12	434(47800)	0.419s	1.04	2.47	-1.42

4.6 Infrared spectroscopic studies

The sensitizer dyes are adsorbed onto TiO_2 for DSSC fabrication. The FTIR spectra of the three dyes and their TiO_2 adsorbed version are shown in Figure 4.5. The C=O stretching band of carboxylic acid functional group of dyes were at 1696 cm^{-1} for **IID-10**, 1688 cm^{-1} for **IID-**

11, and 1679 cm^{-1} for IID-12. When the compounds were adsorbed onto TiO_2 , the absorption intensity of C=O band was significantly reduced suggesting coordination of both carboxylic acid group with TiO_2 for binding.

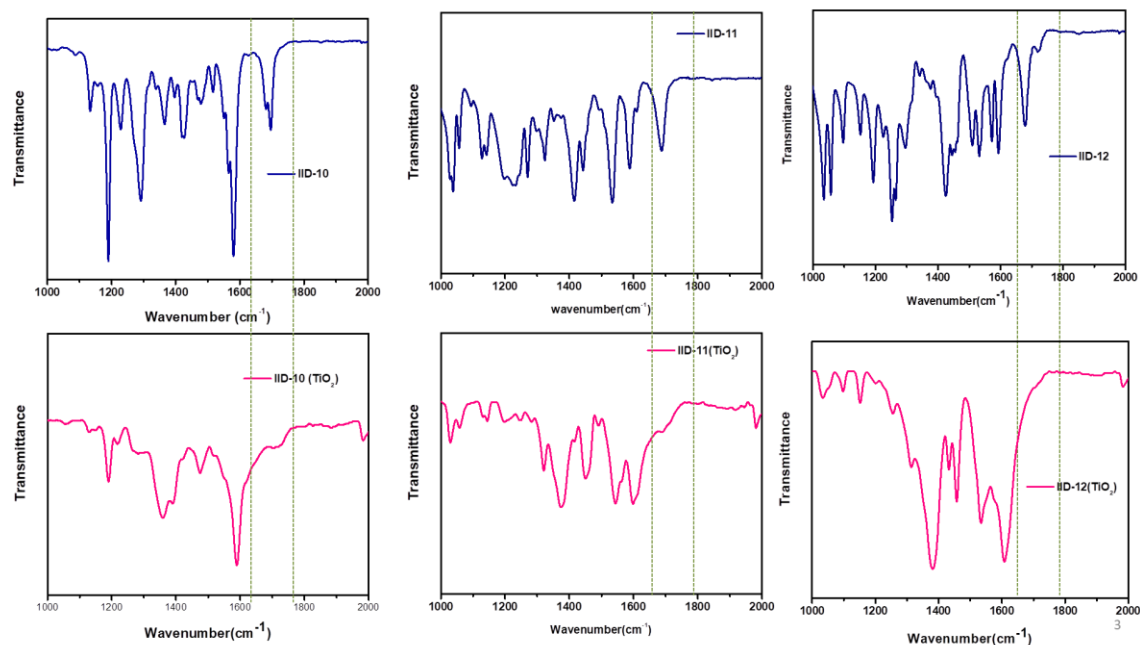


Figure 4.5 Infrared spectra of dye and that of dyes coated on TiO_2

The dye can be adsorbed onto semiconductor surface through three possible coordination bonds, (a) unidentate, (b) bidentate chelating and (c) bidentate bridging (Figure 4.6). To find out the binding modes of dyes in our case, we adopted the empirical rule proposed by Decon and Philips. According to which, the mode of binding can be deduced by comparing the carboxylic acid stretching frequencies in the anionic and adsorbed forms of the dye. If the difference between antisymmetric and symmetric vibrations ($\Delta\nu$) in TiO_2 adsorbed version is lower than the carboxylate form, the mode of binding can be bidentate chelating. If $\Delta\nu$ is same in both cases, then the mode of binding will be bidentate bridging, and if $\Delta\nu$ is higher the binding will be unidentate. In all the three cases, antisymmetric stretching frequencies for the carboxylate and adsorbed versions were almost same and significant changes were seen in the case of symmetric stretching frequencies of the dyes. The required data to lead to the binding mode are recorded in Table 4.2 and according to which all the dyes prefer to bind with TiO_2 in a bidentate chelating mode.

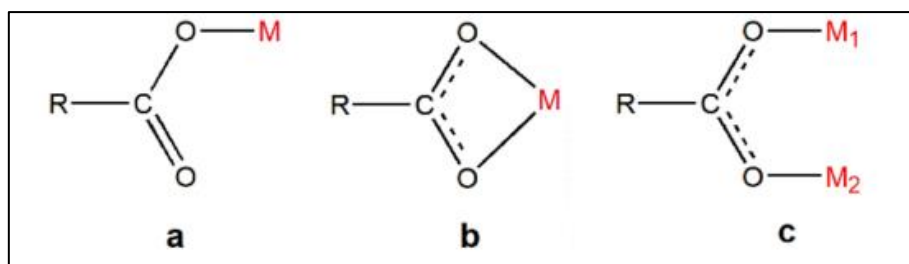


Figure 4.6 Different possible binding modes of dyes with TiO_2 , M represent Ti metal atom

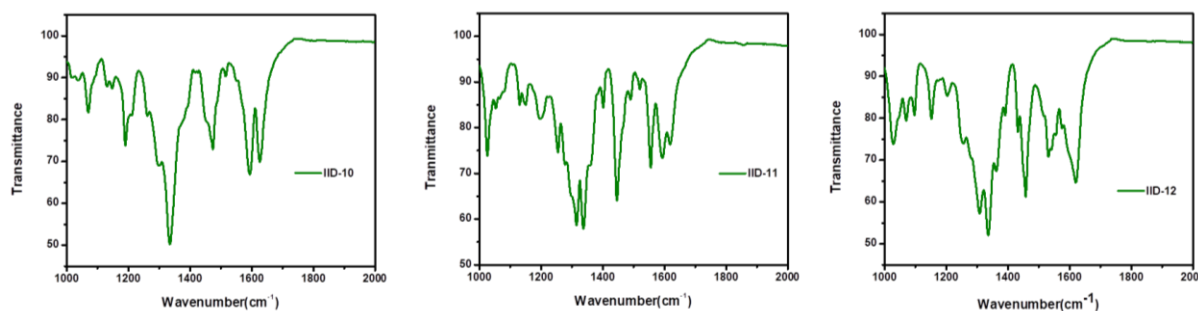


Figure 4.7: IR spectra of dyes in the carboxylate form

Table 4.2 IR frequencies of dyes in carboxylate form and TiO_2 adsorbed form

Compound	Antisymmetric stretching vibration (AS) (cm^{-1})	Symmetric stretching vibration (SS) (cm^{-1})	Difference between AS and SS (cm^{-1})
IID-10 (TiO_2)	1589	1386	203
IID-10 (Carboxylate)	1594	1335	259
IID-11 (TiO_2)	1598	1372	226
IID-11 (Carboxylate)	1594	1337	257
IID-12 (TiO_2)	1608	1381	227
IID-12 (Carboxylate)	1580	1337	243

4.7 Computational Studies

To investigate the molecular structure and electronic distribution of the three organic dyes, the three dyes have been optimized using DFT calculations with Gaussian 09 program. The

calculations were performed with the B3LYP exchange correlation functional under cc-PVDZ basis set. The absence of imaginary frequencies was confirmed with vibration analysis. The electronic distribution of frontier molecular orbitals is shown in Figure 4.8. The HOMO of the dyes was mainly composed of the donor, indoloindole core in all the three cases. While in the case of **IID-12**, the LUMO was localized on both acceptor groups, **IID-10** and **IID-11** were having LUMO located on only one acceptor part.

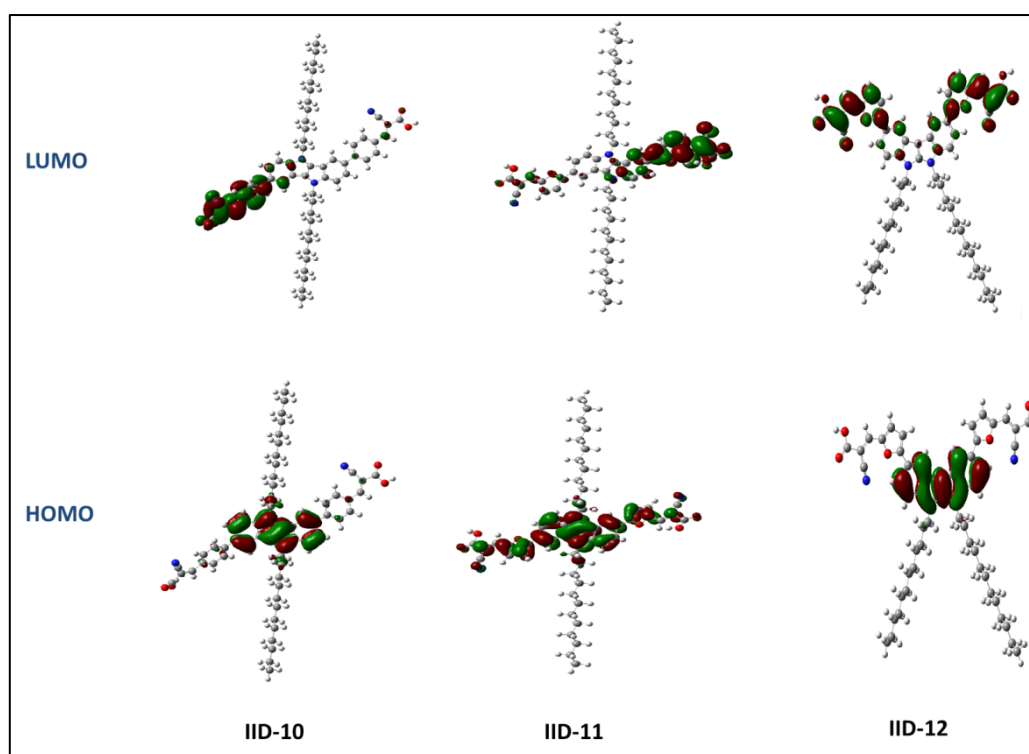


Figure 4.8 Electronic distributions of frontier molecular orbitals of **IID-10**, **IID-11** and **IID-12** dyes.

4.8 Photovoltaic properties

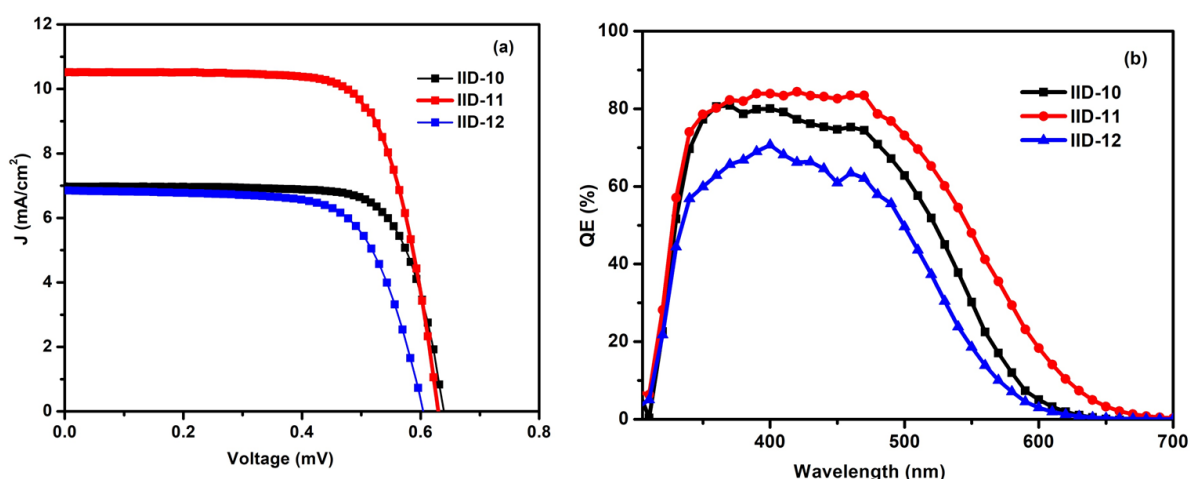
4.8.1 J-V and IPCE measurements

We fabricated devices based on dyes **IID-10**, **IID-11**, and **IID-12** by following the procedures adopted in the previous sections. To circumvent the solubility issues of the dyes, 1:1 mixture of tert-butanol and acetonitrile were used as the dye bath. Photoanode was made by soaking electrodes in 0.2 mM dye solutions for 15 hour. The photovoltaic parameters of devices obtained under AM 1.5 G illumination is shown in Table 4.3.

Table 4.3 Photovoltaic parameters of dyes

Sensitizer	V _{oc} (mV)	J _{sc} (mA/cm ²)	FF (%)	Efficiency
IID-10	0.64±0.00085	6.97±0.024	74.95±0.05	3.34±0.007
IID-11	0.63±0.00164	10.51±0.113	72.62±0.29	4.81±0.050
IID-12	0.60±0.009	6.86±0.262	69.13±0.13	2.87±0.940

Among the indolo[3,2-*b*]indole based dyes **IID-11** with furan as π -spacer was showcasing best PCE of 4.81% with $J_{sc} = 10.51 \text{ mA/cm}^2$, $V_{oc} = 0.63 \text{ mV}$ and $FF = 72.62\%$. Though benzene substituted dye **IID-10** was having slightly higher voltage, it lagged behind in performance with an efficiency of 3.34% ($J_{sc} = 6.97 \text{ mA/cm}^2$, $V_{oc} = 0.64 \text{ mV}$ and $FF = 74.95\%$). Significantly higher current density generated in the solar cells based on **IID-11** made it to outperform **IID-10**. **IID-12** delivered the lowest efficiency of 2.87% with both lower current density and photovoltage ($J_{sc} = 6.86 \text{ mA/cm}^2$, $V_{oc} = 0.60 \text{ mV}$ and $FF = 69.13\%$). The trend in current density observed is reflected in the IPCE curve which is represented in Figure 4.9. **IID-11** display higher plateau region than rest of the molecules with IPCE value >80% from 350 nm to 480 nm region and it has maximum IPCE value of 84% at 421 nm.

**Figure 4.9** (a) J-V curve & (b) IPCE spectra of DSSCs based on **IID-10**, **IID-11** & **IID-12** dyes

4.8.2 Electron lifetime studies and charge extraction measurements

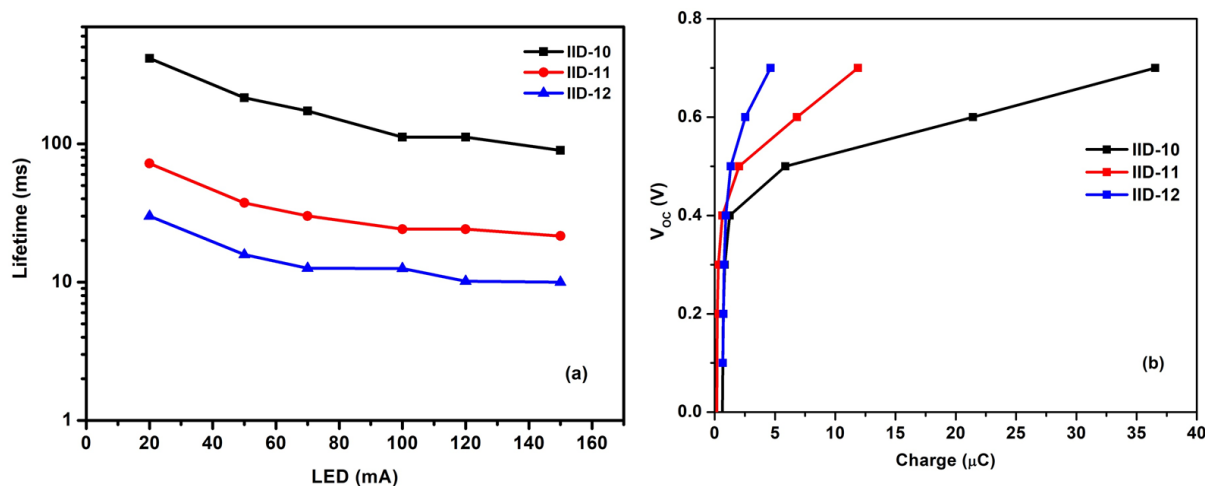


Figure 4.10 (a) IMVS & (b) Charge extraction measurements of DSSCs

The open circuit potential of a device depends on its electron recombination resistance which can in turn be probed by measuring the lifetime of devices. Here we have studied the lifetime by IMVS technique which is a plot of lifetime as a function of light intensity (Figure 4.10). The electron lifetime (τ_n) can be calculated from the expression $\tau_n = 1/2\pi f_n$ where f_n is the frequency minima of the IMVS imaginary component. According to the plot, higher lifetime is observed for **IID-10** than **IID-11**. The twisted conformation of benzene substituted dye **IID-10** may be helping to minimize the interaction between electrolyte and semiconductor surface.

We also conducted charge extraction measurements to estimate the shift in conduction band of TiO_2 for these dyes (Figure 4.9). A decreased V_{oc} for constant Q indicates a positive shift of conduction band edge. In the current set of compounds, at constant Q value, V_{oc} was found to increase in the order **IID-12**>**IID-11**>**IID-10** suggesting more positively shifted conduction band edge results for **IID-10** and more negatively shifted conduction band in the case of devices based on **IID-12**. The positively shifted conduction band for **IID-10** could also suggest less electron recombination driving force and can also contribute towards improved injection. This is evident from its higher V_{oc} value which can be attributed to its retarded charge recombination. Severe recombination happening in **IID-12** resulted in lower V_{oc} value for the same.

4.9 Indoor light measurements

The remarkable feature of DSSC which makes it competitive to other PV technologies is its ability to harvest artificial light sources such as light emitting diodes (LED) bulbs, halogen lamps, and fluorescent lamp. So far different classes of dyes such as ruthenium complexes, Zn porphyrin and organic dyes have been utilized for indoor light harvesting. Among these the highest efficiency obtained is for a metal free dye CX22 (Figure 4.11). The dye which is having a bis-anthracene π -bridge was reported by Chen *et al.* in 2022 and it could realize an efficiency of 37% under 6000 lux illumination for T5 fluorescent lamp.

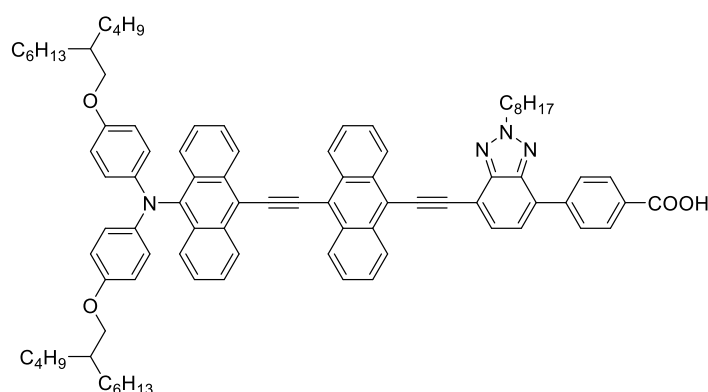


Figure 4.11 Molecular structure of CX22

Since all the three sensitizers developed was having steady absorption in the IPCE spectra, we subjected them for indoor light measurements using day light CFL as light source and recorded the performance for various light intensities from 1000 lux to 200 lux. The photovoltaic parameters obtained are listed in Table 4.4. Except dye **IID-12**, the other two dyes were delivering improved performance when compared to those of outdoor condition. While **IID-10** maintained almost similar performance at all irradiance levels, **IID-11** was showcasing improvement in performance with decrease of light intensity. **IID-11** could outperform **IID-10** with a PCE of 13.4% under 200 lux irradiation.

Table 4.4 Photovoltaic parameters for indoor light measurements

(a) 1000 lux illumination

Sensitizer	Voc (V)	Jsc (μAcm^{-2})	FF (%)	Efficiency (%)
IID-10	539 ± 1	56.57 ± 0.01	72.5 ± 0.5	6.92 ± 0.02
IID-11	510 ± 1	77.71 ± 0.01	78.6 ± 0.03	9.72 ± 0.07
IID-12	0.42 ± 0.02	47.12 ± 1.12	42.2 ± 2.9	2.70 ± 0.375

(b) 500 lux illumination

Sensitizer	Voc (V)	Jsc (mAcm^{-2})	FF (%)	Efficiency (%)
IID-10	514 ± 3	27.42 ± 0.003	66.8 ± 0.6	6.13 ± 0.02
IID-11	495 ± 3	39.88 ± 0.002	80.4 ± 0.5	10.32 ± 0.05
IID-12	0.31 ± 0.025	24.90 ± 2.73	34.80 ± 2.1	1.76 ± 0.239

(c) 200 lux illumination

Sensitizer	Voc (V)	Jsc (mAcm^{-2})	FF (%)	Efficiency (%)
IID-10	496 ± 1	12.98 ± 0.01	59.3 ± 0.5	6.70 ± 0.03
IID-11	475 ± 2	19.73 ± 0.003	80.8 ± 0.5	13.4 ± 0.08
IID-12	0.20 ± 0.005	10.45 ± 0.28	33.40 ± 0.6	1.21 ± 0.003

4.10 Conclusion

In summary, we constructed 3 dyes adopting di-branched and di-anchoring architecture. The dyes **IID-10** and **IID-11** are having indolo[3,2-*b*]indole as donor and differ in the π -spacer being employed. While furan was utilized in **IID-11**, **IID-10** incorporated benzene as π -spacer. Indolo[2,3-*b*]indole was also utilized as the donor to furnish the dye **IID-12** which is

having furan as π -spacer. Due to the higher light harvesting ability of **IID-11**, it could generate significantly higher current density which helped it to outperform **IID-10** even when it was having slightly lower photovoltage. Due to severe recombination and inferior light harvesting ability, **IID-12** based devices showcased least current density and photovoltage leading to poor performance compared to the rest of the dyes. Indoor light measurements under DL CFL revealed superior performance of **IID-11** with 13.4% under 200 lux illumination.

4.11 Experimental section

General Methods

All chemicals were of the best grade commercially available and were used without further purification. All solvents were purified according to standard procedure; dry solvents were obtained according to the literature methods and stored over molecular sieves. Gravity column chromatography was performed using neutral alumina and mixtures of hexane-ethyl acetate were used for elution. Melting points were determined on a Buchi melting point apparatus and are uncorrected. Proton nuclear magnetic resonance spectra (^1H NMR) were recorded on a Bruker AMX 500 spectrophotometer (CDCl_3 and Acetone- d_6 as solvents). Chemical shifts for ^1H NMR spectra are reported as δ in units of parts per million (ppm) downfield from SiMe_4 (δ 0.0) and relative to the signal of chloroform- d (δ 7.25ppm) Acetone- d_6 (2.05 ppm). Multiplicities were given as: s (singlet); d (doublet); t (triplet); q (quartet); dd (double doublet); m (multiplet). Coupling constants are reported as J value in Hz. Carbon nuclear magnetic resonance spectra (^{13}C NMR) are reported as δ in units of parts per million (ppm) downfield from SiMe_4 (δ 0.0) and relative to the signal of chloroform- d (δ 77.03 ppm) and Acetone- d_6 (29.84 and 206.26 ppm). Mass spectra were recorded under ESI/HRMS at 60,000 resolution using Thermo Scientific Exactive mass spectrometer. The UV-visible absorbance was studied using a SCHIMADZU UV-1800 UV-Visible spectrophotometer, using commercially available 1 cm quartz cuvette purchased from Sigma-Aldrich.

The starting material **5** was synthesized from 3-bromoaniline *via* a four step synthetic strategy by adopting reported procedures.⁷

Synthesis of 5-bromo-2-(5-bromo-2-nitrophenyl)-1H-indole (7): To a 100 mL schlenk flask were added compound **5** (1 g, 5.1 mmol), compound **6** (2.5 g, 6.12 mmol), Pd(OAc)₂ (57 mg, 5 mol%), K₂CO₃ (1.4 g, 10.2 mmol), and norbornene (1 g, 10.2 mmol). The reaction vessel was degassed using vacuum pump and back filled with argon. This procedure was repeated three times which was followed by addition of 0.5 molar solution of H₂O in DMA as solvent under argon atmosphere. The reaction mixture was stirred at 70 °C for 48 h. The crude reaction mixture was then filtered through celite and extracted with ethyl acetate. The organic layer was washed successively with water and brine which was then dried over Na₂SO₄. Solvent removal was followed by column purification on silica gel to obtain **7** as red coloured solid (400 mg, 1.01 mmol, 20%). mp 158-160 °C. ¹H NMR (500 MHz, CDCl₃): 8.54 (s, 1H), 7.77 (d, *J* = 1.5 Hz, 1H), 7.70 (s, 1H), 7.67 (d, *J* = 8.5 Hz, 1H), 7.58-7.56 (m, 1H), 7.28-7.26 (m, 1H), 7.19 (d, *J* = 4 Hz, 1H), 6.60 (s, 1H) ppm; ¹³C NMR (125 MHz, (CDCl₃) : 147.3, 135.6, 134.6, 132.2, 132.0, 129.7, 128.4, 127.1, 126.6, 126.0, 123.6, 113.9, 112.8, 104.7 ppm. HRMS (ESI) *m/z*: (M + H)⁺ calcd for C₁₄H₉Br₂N₂O₂ 394.9025, found 394.9034.

Synthesis of 3,8-dibromo-5-dodecyl-5,10-dihydroindolo[3,2-*b*]indole (8): To a stirred solution of **7** (1 g, 2.52 mmol) in dry DMF was added NaH (90 mg, 3.78 mmol) under nitrogen atmosphere at 0 °C. The reaction mixture was then warmed to room temperature and stirred for 30 minutes. The reaction mixture was cooled again to 0 °C and 1-bromododecane (755 mg, 3 mmol) was added dropwise and stirred at room temperature for 8 hours. Upon completion, the reaction mixture was quenched by adding water slowly and then extracted with EtOAc. The organic layer was washed successively with water and brine which was then dried over anhydrous Na₂SO₄. After solvent removal, column purification was done on silica gel to isolate the alkylated product as red coloured viscous oil (1.4 g, 2.48 mmol, 98%). *R_f*: 0.5 (5% EtOAc in hexane). ¹H NMR (500 MHz, CDCl₃): 7.87 (d, *J* = 9 Hz, 1H), 7.69-7.67 (m, 2H), 7.62 (s, 1H), 7.26 (d, *J* = 9 Hz, 1H), 7.18-7.16 (m, 1H), 6.34 (s, 1H), 3.83 (t, *J* = 7 Hz, 2H), 1.55-1.52 (m, 2H), 1.22-1.05 (m, 18H), 0.80 (t, *J* = 7Hz, 3H) ppm; ¹³C NMR (125 MHz, (CDCl₃) : 148.2, 136.2, 135.7, 134.9, 133.0, 129.4, 129.2, 127.3, 125.9, 125.3, 123.5, 113.2, 111.5, 102.6, 44.5, 31.9, 29.7, 29.6, 29.5, 29.4, 29.3, 29.0, 26.8, 22.7, 14.1 ppm. HRMS (ESI) *m/z*: (M + H)⁺ calcd for C₂₆H₃₃Br₂N₂O₅ 563.0909, found 563.0917.

To this alkylated intermediate (1.4 g, 2.48 mmol) in DMA was added PPh₃ (1.62 g, 6.2 mmol) and stirred the reaction mixture for 24 h at 165 °C. After completion of the reaction,

the reaction mixture was extracted with ethyl acetate and washed successively with water and brine. After solvent removal, column purification was done on silica gel to isolate the product **8** as colourless solid (1 g, 1.88 mmol). mp 74-76 °C. ¹H NMR (500 MHz, (CD₃)₂CO): 10.41 (s, 1H), 7.93 (s, 1H), 7.83 (s, 1H), 7.46-7.40 (m, 2H), 7.24-7.21 (m, 2H), 4.48-4.46 (m, 2H), 1.83-1.81 (m, 2H), 1.24-1.07 (m, 18H), 0.73 (t, *J* = 7 Hz, 3H) ppm; ¹³C NMR (125 MHz, ((CD₃)₂CO) : 139.5, 126.8, 124.8, 124.5, 120.5, 120.0, 116.1, 115.7, 114.0, 111.8, 111.0, 110.5, 44.8, 31.7, 30.1, 26.7, 22.4, 13.4 ppm. HRMS (ESI) *m/z*: (M)⁺ calcd for C₂₆H₃₂Br₂N₂ 530.0932, found 530.0926.

Synthesis of 3,8-dibromo-5,10-didodecyl-5,10-dihydroindolo[3,2-*b*]indole (9): To a stirred solution of **8** (1 g, 1.88 mmol) in dry DMF was added NaH (68 mg, 2.82 mmol) under nitrogen atmosphere at 0 °C. The reaction mixture was then warmed to room temperature and stirred for 30 minutes. The reaction mixture was cooled again to 0 °C and 1-bromododecane (563 mg, 2.26 mmol) was added dropwise and stirred at room temperature for 8 hours. Upon completion, the reaction mixture was quenched by adding water slowly and then extracted with EtOAc. The organic layer was washed successively with water and brine which was then dried over anhydrous Na₂SO₄. After solvent removal, column purification was done on silica gel to isolate the alkylated product **9** as colourless solid (1.26 g, 1.78 mmol, 95%). mp 110-114 °C. ¹H NMR (500 MHz, CDCl₃): δ 7.83 (2H, s), 7.30 (d, *J* = 9 Hz, 2H), 7.25 (d, *J* = 9 Hz, 2H), 4.34 (t, *J* = 7 Hz, 4H), 1.89-1.82 (m, 4H), 1.30-1.15 (m, 36H), 0.81-0.79 (m, 6H) ppm; ¹³C NMR (125 MHz, (CDCl₃) : 139.3, 125.7, 124.7, 120.3, 115.5, 111.2, 111.1, 45.4, 1.9, 30.2, 29.6, 29.6, 29.4, 29.3, 29.3, 27.0, 22.7, 14.2 ppm. HRMS (ESI) *m/z*: (M)⁺ calcd for C₃₈H₅₆Br₂N₂ 698.2810, found 698.2791.

Synthesis of 4,4'-(5,10-didodecyl-5,10-dihydroindolo[3,2-*b*]indole-3,8-diyl)dibenzaldehyde (10): A mixture of **9** (100 mg, 0.14 mmol), (4-formylphenyl)boronic acid (64 mg, 0.42 mmol), Pd₂(dba)₃ (6 mg, 5 mol%), P(*o*-tolyl)₃ (4 mg, 5 mol%), KF (24 mg, 0.42 mmol) were weighed into a Schlenk tube and degassed for 10 minutes. Degassed DMF and toluene in a 1:1 ratio was then added and the reaction mixture was purged with argon and allowed to stir at 110 °C for 24 hours. The reaction mixture was extracted with ethyl acetate. The combined organic layer was washed with brine and dried over Na₂SO₄. Solvent was evaporated under pressure and the residue on silica gel column chromatography yielded the product **10** as a yellow coloured solid (50 mg, 0.066 mmol, 47%). mp 110-114 °C. ¹H NMR (500 MHz, CDCl₃): 10.01 (s, 2H), 8.02-9.58 (s, 2H), 7.92 (d, *J* = 8 Hz, 4H), 7.80 (d, *J* = 8 Hz,

4H), 7.55 (d, $J = 8.5$ Hz, 2H), 7.50 (d, $J = 8.5$ Hz, 2H), 4.51 (t, $J = 6.5$ Hz, 4H), 2.0-1.95 (m, 4H), 1.40-1.13 (m, 36H), 0.78 (t, $J = 7$ Hz, 6H) ppm; ^{13}C NMR (125 MHz, CDCl_3): 192.0, 148.6, 140.7, 134.4, 130.4, 130.1, 127.6, 126.8, 121.5, 116.7, 115.1, 110.4, 45.6, 31.9, 30.3, 29.6, 29.5, 29.4, 29.3, 27.2, 22.7, 14.1 ppm. HRMS (ESI) m/z : $(\text{M})^+$ calcd for $\text{C}_{52}\text{H}_{66}\text{N}_2\text{O}_2$ 750.5124, found 750.5138.

Synthesis of 3-(4-(8-(4-((E)-2-carboxy-2-cyanovinyl)phenyl)-5,10-didodecyl-5,10-dihydroindolo[3,2-*b*]indol-3-yl)phenyl)-2-cyanoacrylic acid (IID-10): A mixture of aldehyde **10** (50 mg, 0.066 mmol), cyanoacetic acid (28 mg, 0.33 mmol) and 12 μL of piperidine in acetonitrile were heated at reflux overnight under argon atmosphere. After cooling to room temperature, the product was precipitated by pouring into water. It was then washed with dilute hydrochloric acid followed by water and dried in vacuum oven. The product **IID-10** was obtained as orange coloured solid (43 mg, 0.049 mmol, 74%). mp 264-266 $^\circ\text{C}$. ^1H NMR (500 MHz, DMF-d_7 : $(\text{CD}_3)_2\text{CO}$): 9.29 (s, 2H), 9.23 (s, 2H), 9.09 (d, $J = 8$ Hz, 4H), 8.93 (d, $J = 8$ Hz, 4H), 8.84 (s, 1H), 8.65 (s, 3H), 5.64-5.62 (m, 3H), 2.30-2.0 (m, 36H), 1.70-1.67 (m, 6H) ppm. ^{13}C NMR (125 MHz, DMF-d_7 : $(\text{CD}_3)_2\text{CO}$): 152.4, 141.4, 140.9, 131.2, 129.5, 127.2, 126.8, 121.2, 116.5, 115.1, 110.7, 45.0, 31.8, 26.7, 22.4, 13.4 ppm. HRMS (ESI) m/z : $(\text{M})^+$ calcd for $\text{C}_{58}\text{H}_{68}\text{N}_2\text{O}_4$ 884.5241, found 884.5291.

Synthesis of 5,5'-(5,10-didodecyl-5,10-dihydroindolo[3,2-*b*]indole-3,8-diyl)bis(furan-2-carbaldehyde) (11): A mixture of **9** (100 mg, 0.14 mmol), 5-Formyl-2-furanylboronic acid (59 mg, 0.42 mmol), $\text{Pd}_2(\text{dba})_3$ (6 mg, 5 mol%), $\text{P}(o\text{-tolyl})_3$ (4 mg, 5 mol%), KF (24 mg, 0.42 mmol) were weighed into a Schlenk tube and degassed for 10 minutes. Degassed DMF and toluene in a 1:1 ratio was then added and the reaction mixture was purged with argon and allowed to stir at 110 $^\circ\text{C}$ for 24 hours. The reaction mixture was extracted with ethyl acetate. The combined organic layer was washed with brine and dried over Na_2SO_4 . Solvent was evaporated under pressure and the residue on silica gel column chromatography yielded the product **11** as a yellow coloured solid (52 mg, 0.071 mmol, 51%). mp 130-132 $^\circ\text{C}$. ^1H NMR (500 MHz, CDCl_3): 9.58 (s, 2H), 8.23 (s, 2H), 7.70 (d, $J = 8.5$ Hz, 2H), 7.45 (d, $J = 8.5$ Hz, 2H), 7.31 (d, $J = 3.5$ Hz, 2H), 6.77 (d, $J = 3.5$ Hz, 2H), 4.50 (t, $J = 7$ Hz, 4H), 1.98-1.95 (m, 4H), 1.37-1.12 (m, 36H), 0.78 (t, $J = 7$ Hz, 6H) ppm; ^{13}C NMR (125 MHz, CDCl_3): 176.7, 161.3, 151.8, 141.0, 127.2, 119.7, 119.6, 115.3, 114.4, 110.7, 106.1, 45.6, 31.9, 30.2, 29.6, 29.6, 29.6, 29.5, 29.4, 29.3, 27.1, 22.7, 14.1 ppm. HRMS (ESI) m/z : $(\text{M})^+$ calcd for $\text{C}_{48}\text{H}_{62}\text{N}_2\text{O}_4$ 730.4710, found 730.4713.

Synthesis of 3,3'-((5,10-didodecyl-5,10-dihydroindolo[3,2-*b*]indole-3,8-diyl)bis(furan-5,2-diyl))bis(2-cyanoacrylic acid) (IID-11): A mixture of aldehyde **11** (50 mg, 0.068 mmol), cyanoacetic acid (29 mg, 0.34 mmol) and 14 μ L of piperidine in acetonitrile were heated at reflux overnight under argon atmosphere. After cooling to room temperature, the product was precipitated by pouring into water. It was then washed with dilute hydrochloric acid followed by water and dried in vacuum oven. The product **IID-11** was obtained as red coloured solid (40 mg, 0.046 mmol, 68%). mp 258-260 °C. ^1H NMR (500 MHz, $(\text{CD}_3)_2\text{SO}$): 8.57 (s, 2H), 8.07 (s, 2H), 7.89 (d, $J = 9$ Hz, 2H), 7.82 (d, $J = 9$ Hz, 2H), 7.59 (d, $J = 3.5$ Hz, 2H), 7.38 (d, $J = 4$ Hz, 2H), 4.66 (t, $J = 6$ Hz, 4H), 1.90-1.87 (m, 4H), 1.26-1.02 (m, 36H), 0.79 (t, $J = 7$ Hz, 6H) ppm; ^{13}C NMR (125 MHz, $(\text{CD}_3)_2\text{SO}$) : 164.9, 161.4, 147.3, 141.4, 137.7, 126.8, 120.0, 119.6, 117.6, 115.7, 114.4, 111.7, 108.8, 70.0, 45.0, 31.6, 30.1, 29.4, 29.1, 29.1, 28.9, 22.5, 14.4 ppm. HRMS (ESI) m/z : $(\text{M})^+$ calcd for $\text{C}_{54}\text{H}_{64}\text{N}_4\text{O}_6$ 864.4826, found 864.4931.

Synthesis of 5-bromo-3-(5-bromo-2-nitrophenyl)-1-dodecyl-1H-indole (13): A mixture of 4-bromo-2-iodo-1-nitrobenzene (2 g, 6.0 mmol), **12** (4.4 g, 12 mmol), $\text{Pd}(\text{OAc})_2$ (4 mol%), NaOAc (246 mg, 3 mmol) and Ag_2O (1.4 g, 6 mmol) in HFIP was stirred at room temperature for 36 hour. The reaction mixture was then filtered through a short pad of celite and solvent was removed under reduced pressure. The residue obtained was then subjected to column chromatography on silica gel to obtain the product **13** as red coloured viscous oil (1g, 1.77 mmol, 30%). R_f : 0.56 (5% EtOAc in hexane). ^1H NMR (500 MHz, CDCl_3): 7.67 (s, 1H), 7.63 (d, $J = 8.5$ Hz, 1H), 7.53 (s, 1H), 7.48-7.46 (m, 1H), 7.26 (d, $J = 9$ Hz, 1H), 7.18-7.15 (m, 2H), 4.03 (t, $J = 7$ Hz, 2H), 1.77-1.74 (m, 2H), 1.22-1.67 (m, 18H), 0.80 (t, $J = 7$ Hz, 3H) ppm; ^{13}C NMR (125 MHz, CDCl_3): 148.4, 135.1, 134.9, 130.7, 130.2, 128.5, 128.2, 126.4, 125.7, 125.4, 121.4, 114.0, 111.6, 109.1, 46.9, 31.9, 30.1, 29.6, 29.6, 29.5, 29.4, 29.2, 26.9, 22.7, 14.2 ppm. HRMS (ESI) m/z : $(\text{M} + \text{Na})^+$ calcd for $\text{C}_{26}\text{H}_{32}\text{Br}_2\text{N}_2\text{NaO}_2$ 585.0728, found 587.0737.

Synthesis of 2,9-dibromo-5,6-didodecyl-5,6-dihydroindolo[2,3-*b*]indole (14): To a mixture of **13** (1 g, 1.77 mmol) in DMA was added PPh_3 (1.15 g, 4.42 mmol) and stirred the reaction mixture for 24 h at 165 °C. After completion of the reaction, the reaction mixture was extracted with ethyl acetate and washed successively with water and brine. After solvent removal, column purification was done on silica gel to isolate the desired product as colourless solid (650 mg, 1.22 mmol, 69%). mp 84-86 °C. ^1H NMR (500 MHz, $(\text{CD}_3)_2\text{CO}$):

10.78 (s, 1H), 7.98 (d, $J = 6.5$ Hz, 2H), 7.33 (d, $J = 8.5$ Hz, 1H), 7.23 (d, $J = 8$ Hz, 1H), 7.14 (d, $J = 8.5$ Hz, 1H), 7.09 (d, $J = 8.5$ Hz, 1H), 4.26 (t, $J = 7$ Hz, 2H), 1.83-1.78 (m, 2H), 1.26-1.08 (m, 18H), 0.73 (t, $J = 7$ Hz, 3H) ppm; ^{13}C NMR (125 MHz, $(\text{CD}_3)_2\text{CO}$): 146.7, 137.9, 137.8, 124.0, 123.4, 122.2, 122.0, 120.7, 120.5, 113.1, 112.8, 112.5, 111.3, 98.7, 43.8, 31.7, 26.6, 22.4, 13.5 ppm. HRMS (ESI) m/z : $(M + 2)^+$ calcd for $\text{C}_{26}\text{H}_{32}\text{Br}_2\text{N}_2$ 532.0932, found 532.0928.

To a stirred solution of this intermediate (500 mg, 0.94 mmol) in dry DMF was added NaH (34 mg, 1.41 mmol) under nitrogen atmosphere at 0 °C. The reaction mixture was then warmed to room temperature and stirred for 30 minutes. The reaction mixture was cooled again to 0 °C and 1-bromododecane (282 mg, 1.13 mmol) was added dropwise and stirred at room temperature for 8 hours. Upon completion, the reaction mixture was quenched by adding water slowly and then extracted with EtOAc. The organic layer was washed successively with water and brine which was then dried over anhydrous Na_2SO_4 . After solvent removal, column purification was done on silica gel to isolate the alkylated product **14** as colourless solid (550 mg, 0.78 mmol, 83%). mp 66-68 °C. ^1H NMR (500 MHz, CDCl_3): 7.85 (s, 2H), 7.21-7.19 (m, 2H), 7.12 (d, $J = 8.5$ Hz, 2H), 4.21 (t, $J = 7$ Hz, 4H), 1.78-1.74 (m, 4H), 1.32-1.17 (m, 36H), 0.80 (t, $J = 7$ Hz, 6H) ppm; ^{13}C NMR (125 MHz, CDCl_3): 145.0, 138.3, 123.1, 122.4, 120.8, 113.4, 110.6, 99.8, 44.4, 32.0, 30.4, 29.6, 29.5, 29.3, 27.0, 22.7, 14.1 ppm. HRMS (ESI) m/z : $(M + \text{H})^+$ calcd for $\text{C}_{38}\text{H}_{57}\text{Br}_2\text{N}_2$ 699.2883, found 699.2887.

Synthesis of 5-(5,6-didodecyl-9-(4-formylfuran-2-yl)-5,6-dihydroindolo[2,3-*b*]indol-2-yl)furan-2-carbaldehyde (15): A mixture of **14** (100 mg, 0.14 mmol), 5-Formyl-2-furanylboronic acid (59 mg, 0.42 mmol), $\text{Pd}_2(\text{dba})_3$ (6 mg, 5 mol%), $\text{P}(o\text{-tolyl})_3$ (4 mg, 5 mol%), KF (24 mg, 0.42 mmol) were weighed into a Schlenk tube and degassed for 10 minutes. Degassed DMF and toluene in a 1:1 ratio was then added and the reaction mixture was purged with argon and allowed to stir at 110 °C for 24 hours. The reaction mixture was extracted with ethyl acetate. The combined organic layer was washed with brine and dried over Na_2SO_4 . Solvent was evaporated under pressure and the residue on silica gel column chromatography yielded the product **15** as a yellow coloured solid (40 mg, 0.055 mmol, 39%). mp 92-94 °C. ^1H NMR (500 MHz, CDCl_3): 9.59 (s, 2H), 8.33 (s, 2H), 7.65 (d, $J = 8.5$ Hz, 2H), 7.34-7.32 (m, 4H), 6.90 (d, $J = 3.5$ Hz, 2H), 4.29 (t, $J = 7$ Hz, 4H), 1.85-1.82 (m, 4H), 1.38-1.17 (m, 36H), 0.80 (t, $J = 7$ Hz, 6H) ppm. ^{13}C NMR (125 MHz, CDCl_3): 176.8, 161.8, 151.7, 145.2, 140.4, 122.0, 121.5, 117.9, 115.9, 109.8, 106.7, 44.5, 31.9, 30.6, 29.6,

29.5, 29.3, 27.1, 22.7, 14.1 ppm. HRMS (ESI) m/z: (M + Na)⁺ calcd for C₄₈H₆₂N₂NaO₄ 753.4602, found 753.4627.

Synthesis of 3-(5-(9-(4-(-2-carboxy-2-cyanovinyl)furan-2-yl)-5,6-didodecyl-5,6-dihydroindolo[2,3-b]indol-2-yl)furan-2-yl)-2-cyanoacrylic acid (IID-12): A mixture of aldehyde **15** (50 mg, 0.068 mmol), cyanoacetic acid (29 mg, 0.34 mmol) and 14 μ L of piperidine in acetonitrile were heated at reflux overnight under argon atmosphere. After cooling to room temperature, the product was precipitated by pouring into water. It was then washed with dilute hydrochloric acid followed by water and dried in vacuum oven. The product **IID-12** was obtained as red colored solid (45 mg, 0.052 mmol, 76%). mp 216-220 °C. ¹H NMR (500 MHz, (CD₃)₂SO): 8.50 (s, 2H), 8.00 (s, 2H), 7.83-7.76 (m, 4H), 7.65 (s, 2H), 7.30 (s, 2H), 4.49 (s, 4H), 1.83 (s, 4H), 1.38-1.18 (m, 36H), 0.82 (s, 6H) ppm. ¹³C NMR (125 MHz, (CD₃)₂SO): 164.6, 161.3, 147.2, 140.6, 137.6, 121.5, 121.1, 117.4, 117.2, 115.4, 111.2, 108.3, 100.9, 96.0, 70.3, 31.8, 31.0, 29.5, 29.3, 29.2, 29.1, 27.1, 26.6, 22.5, 14.4 ppm. HRMS (ESI) m/z: (M)⁺ calcd for C₅₄H₆₄N₄O₆ 864.4826, found 864.4885.

4.12 References:

1. B. G. Kim, K. Chung and J. Kim, Molecular design principle of all-organic dyes for dye-sensitized solar cells, *Chem. - A Eur. J.*, 2013, **19**, 5220–5230.
2. A. B. Muñoz-García, I. Benesperri, G. Boschloo, J. J. Concepcion, J. H. Delcamp, E. A. Gibson, G. J. Meyer, M. Pavone, H. Pettersson, A. Hagfeldt and M. Freitag, Dye-sensitized solar cells strike back, *Chem. Soc. Rev.*, 2021, **50**, 12450–12550.
3. (a) X. X. Dai, H. L. Feng, W. J. Chen, Y. Yang, L. Bin Nie, L. Wang, D. Bin Kuang, H. Meier and D. Cao, Synthesis and photovoltaic performance of asymmetric di-anchoring organic dyes, *Dye. Pigment.*, 2015, **122**, 13–21. (b) Q. Li, J. Shi, H. Li, S. Li, C. Zhong, F. Guo, M. Peng, J. Hua, J. Qin and Z. Li, Novel pyrrole-based dyes for dye-sensitized solar cells: From rod-shape to ‘h’ type, *J. Mater. Chem.*, 2012, **22**, 6689–6696. (c) R. Yeh-Yung Lin, F. L. Wu, C. H. Chang, H. H. Chou, T. M. Chuang, T. C. Chu, C. Y. Hsu, P. W. Chen, K. C. Ho, Y. H. Lo and J. T. Lin, Y-shaped metal-free D- π -(A)₂ sensitizers for high-performance dye-sensitized solar cells, *J. Mater. Chem. A*, 2014, **2**, 3092–3101. (d) G. Wu, F. Kong, Y. Zhang, X. Zhang, J. Li, W. Chen, W. Liu, Y. Ding, C. Zhang, B. Zhang, J. Yao and S. Dai, Multiple-anchoring triphenylamine dyes for dye-sensitized solar cell application, *J. Phys. Chem. C*, 2014, **118**, 8756–8765

4. S. Kumar, K. R. J. Thomas, M. S. Fan and K. C. Ho, Dithienopyrrole-based dianchoring dyes: Effect of molecular design and donors on the optical and photovoltaic properties, *J. Lumin.*, 2021, **230**, 117727.
5. A. Abboto, N. Manfredi, C. Marinzi, F. De Angelis, E. Mosconi, J. H. Yum, Z. Xianxi, M. K. Nazeeruddin and M. Grätzel, Di-branched di-anchoring organic dyes for dye-sensitized solar cells, *Energy Environ. Sci.*, 2009, **2**, 1094–1101.
6. (a) K. Zeng, Y. Chen, W. H. Zhu, H. Tian and Y. Xie, Efficient Solar Cells Based on Concerted Companion Dyes Containing Two Complementary Components: An Alternative Approach for Cosensitization, *J. Am. Chem. Soc.*, 2020, **142**, 5154–5161. (b) H. Jia, K. Shen, X. Ju, M. Zhang and H. Zheng, Enhanced performance of dye-sensitized solar cells with Y-shaped organic dyes containing di-anchoring groups, *New J. Chem.*, 2016, **40**, 2799–2805.
7. (a) I. Kalvet, K. Deckers, I. Funes-Ardoiz, G. Magnin, T. Sperger, M. Kremer and F. Schoenebeck, Selective ortho-Functionalization of Adamantylarenes Enabled by Dispersion and an Air-Stable Palladium(I) Dimer, *Angew. Chemie - Int. Ed.*, 2020, **59**, 7721–7725. (b) Y. Lu, Y. Li, R. Zhang, K. Jin and C. Duan, Regioselective ortho-nitration of N-phenyl carboxamides and primary anilines using bismuth nitrate/acetic anhydride, *Tetrahedron*, 2013, **69**, 9422–9427. (c) D. V. Kosynkin and J. M. Tour, Phenylene ethynylene diazonium salts as potential self-assembling molecular devices, *Org. Lett.*, 2001, **3**, 993–995. (d) N. L. Sloan, S. K. Luthra, G. McRobbie, S. L. Pimlott and A. Sutherland, A one-pot radioiodination of aryl amines: Via stable diazonium salts: Preparation of ¹²⁵I-imaging agents, *Chem. Commun.*, 2017, **53**, 11008–11011.

ABSTRACT

Name of the Student: **Ms. Nitha P. R.**
Faculty of Study: Chemical Sciences
AcSIR academic centre/CSIR Lab: CSIR-
National Institute for Interdisciplinary
Science and Technology (CSIR-NIIST)

Registration No.: 10CC15A39009
Year of Submission: 2022
Name of the Supervisor(s):
Dr. Jubi John (Supervisor)
Dr. Suraj Soman (Co-supervisor)

Title of the thesis: **Development of Indole Fused Heteroacene based Sensitizers for Dye Sensitized Solar Cell Applications**

Dye sensitized solar cells which belong to the third generation photovoltaic has got many attractive features which can ensure this technology as an emerging alternative to conventional energy sources like fossil fuels. Among the different components of a DSSC cell, dye sensitizer plays a key role. Exploration of novel scaffolds as sensitizer components has always got its own relevance. As a part of the thesis work, we tried to explore the potential of different indole fused heterocycles as sensitizer. **Chapter 1** gives a brief introduction to the background literature where indole fused heterocycles were used either as a donor or as a π -spacer to construct photosensitizers for DSSC applications. **Chapter 2** which is divided into two parts deals with the utilization of indoloindole as donor to develop D- π -A dyes for DSSC. Part A of the chapter deals with indolo[3,2-*b*]indole donors. Optimization of alkyl chain length (hexyl and dodecyl) as well as π -spacers (benzene, thiophene, furan) revealed the significant role played by dodecyl chain in preventing back electron transfer reactions. In this scenario, the dyes with better LHE (Furan spacer, **IID-6**) could showcase better PV performance. In the second part we did similar optimization studies utilizing indolo[2,3-*b*]indole as donor keeping the alkyl chain fixed as dodecyl. The LHE played major role in regulating the PCE of dyes which lead to maximum for furan substituted dye (**IID-9**) and minimum for benzene substituted one (**IID-7**). **Chapter 3** deals with benzothienoindole donor based dyes with optimization of π -spacers. While Chapter 3A deals with **BID1-BID3** (benzothieno[3,2-*b*]indole as donor), the second part of the chapter deals with **BID4-BID6** (benzothieno[2,3-*b*]indole as donor). In both the set of dyes, furan substituted dyes outperformed the rest and least was delivered by benzene based sensitizers. The systematic investigations of donors in the previous sections revealed the superiority of indolo[3,2-*b*]indole in device performance. Hence, in **Chapter 4** we adopted a bifunctional D(π -A)₂ architecture taking indolo[3,2-*b*]indole as the donor. We changed the π -spacer as benzene (**IID-10**) and furan (**IID-11**) keeping the acceptor/anchoring group fixed as cyanoacrylic acid. Another dye **IID-12** with the same molecular architecture utilizing indolo[2,3-*b*]indole as donor, furan as π -spacer and cyanoacrylic acid as the anchoring/acceptor group was also subjected to performance evaluation. The former set of compounds outperformed the latter both in indoor and outdoor conditions. Among the indolo[3,2-*b*]indole donor based dyes, **IID-11** with higher absorption and recombination resistance exhibited better efficiency under both indoor and outdoor conditions.

Details of the publications emanating from the thesis work

1. **P. R. Nitha**, V. Jayadev, S. Pradhan, V. V. Divya, C. H. Suresh, J. John, S. Soman, A. Ajayaghosh, *Regulating Back Electron Transfer through Donor and p-Spacer Alterations in Benzothieno[3,2-b]indole-based Dye-sensitized Solar Cells*, *Chem. Asian J.* **2020**, *15*, 3503.
2. **P. R. Nitha**, S. Soman and J. John, Indole Fused Heterocycles as Sensitizers in Dye-Sensitized Solar Cells: An Overview. *Materials Advances.* **2021**, *2*, 6136–6168.
3. **P. R. Nitha**, V. Jayadev, S. Soman and J. John, Indole fused Heterocycles as Donor in DSC: Investigation on the Effect of Interplay between Donors with Different p-Spacer on Photovoltaic Parameters (Manuscript to be submitted).
4. **P. R. Nitha**, S. Andrew, S. Soman and J. John, An investigation on the effect of different π -spacers on the efficiency of DSSC based on indolo[3,2-b]indole based dibranched, dianchoring sensitizers (Manuscript to be submitted).

List of publications from other related works

1. **P. R. Nitha**, Manu M. Joseph, Greeshma Gopalan, K. K. Maiti, K. V. Radhakrishnan and Parthasarathi Das, Chloroform as a carbon monoxide source in palladium-catalyzed synthesis of 2-amidoimidazo[1,2-a]pyridines. *Org. Biomol. Chem.*, **2018**, *16*, 6430.
2. P. Rahul, **P. R. Nitha**, V. K. Omanakuttan, S. A. Babu, P. Sasikumar, V. K. Praveen, H. Hopf and J. John, *Superbase-Mediated Indirect Friedländer Reaction: A Transition Metal-Free Oxidative Annulation toward Functionalized Quinolines* *European J. Org. Chem.*, **2020**, 308.
3. A. Krishnan R, S. A. Babu, **P. R. Nitha**, J. Krishnan and J. John, *Synthesis of Benzothienobenzofurans via Annulation of Electrophilic Benzothiophenes with Phenols* *Org. Lett.*, **2021**, *23*, 1814.
4. S. A. Babu, A. R. Rajalekshmi, **P. R. Nitha**, V. K. Omanakuttan, P. Rahul, S. Varughese and J. John, *Unprecedented Access of Functionalized Pyrrolo[2,1-a]isoquinolines from the Domino Reaction of Isoquinolinium Ylides and Electrophilic Benzannulated Heterocycles* *Org. Biomol. Chem.*, **2021**, *19*, 1807.
5. M. Shimi, Vandana Sankar, M. K. Abdul Rahim, **P. R. Nitha**, Suresh Das, K. V. Radhakrishnan and K. G. Raghu, Novel glycoconjugated squaraine dyes for selective optical imaging of cancer cells. *Chem. Commun.*, **2017**, *53*, 5433.

List of posters presented in conferences

1. **P. R. Nitha**, Manu M. Joseph, Greeshma Gopalan, K. V. Radhakrishnan, and Parthasarathi Das

Chloroform as carbon monoxide source in Palladium-catalyzed synthesis of 2-amidoimidazo[1,2-a]pyridines

XIV J-NOST Conference for research scholars, CSIR-indian institute of chemical Technology, Hyderabad (28 November- 1st December 2018).

2. **P. R. Nitha.**, V. Jayadev , Suraj Soman and Jubi John

Regulating back electron transfer through donor and π -spacer alterations in dye-sensitized solar cells using indole fused dyes

International Conference series on Materials for the Millennium-“MATCON 2021”, Cochin University of Science and Technology (15-19 March 2021).

CHEMISTRY

AN **ASIAN** JOURNAL

www.chemasianj.org

Accepted Article

Title: Regulating back electron transfer through donor and π -spacer alterations in benzothieno[3,2-b]indole based dye-sensitized solar cells

Authors: Nitha P Ravi, V. Jayadev, Sourava C. Pradhan, Velayudhan V. Divya, Cherumuttathu H. Suresh, Jubi John, Suraj Soman, and Ayyappanpillai Ajayaghosh

This manuscript has been accepted after peer review and appears as an Accepted Article online prior to editing, proofing, and formal publication of the final Version of Record (VoR). This work is currently citable by using the Digital Object Identifier (DOI) given below. The VoR will be published online in Early View as soon as possible and may be different to this Accepted Article as a result of editing. Readers should obtain the VoR from the journal website shown below when it is published to ensure accuracy of information. The authors are responsible for the content of this Accepted Article.

To be cited as: *Chem. Asian J.* 10.1002/asia.202000808

Link to VoR: <https://doi.org/10.1002/asia.202000808>

A Journal of



A sister journal of *Angewandte Chemie*
and *Chemistry – A European Journal*

WILEY-VCH

Regulating back electron transfer through donor and π -spacer alterations in benzothieno[3,2-b]indole based dye-sensitized solar cells

Nitha P. R.,^{[a],[b]} Jayadev V.,^{[a],[b]} Sourava C. Pradhan,^{[a],[b]} Velayudhan V. Divya,^{[a],[b]} Cherumuttathu H. Suresh,^{[a],[b]} Jubi John,*^{[a],[b]} Suraj Soman*^{[a],[b]} and Ayyappanpillai Ajayaghosh*^{[a],[b]}

[a] Chemical Sciences and Technology Division, CSIR-National Institute for Interdisciplinary Science and Technology (CSIR-NIIST), Thiruvananthapuram 695019, India.

[b] Academy of Scientific and Innovative Research (AcSIR), Ghaziabad-201002, India.
E-mail: jubijohn@niist.res.in; suraj@niist.res.in; ajayaghosh@niist.res.in

Supporting information for this article is given via a link at the end of the document.

Abstract: Three metal free organic D- π -A dyes with benzothieno[3,2-b]indole as electron donor, cyanoacrylic acid as both electron acceptor and anchoring group with benzene (**BID-1**), thiophene (**BID-2**) and furan (**BID-3**) as π -spacers were designed and synthesized for application in dye-sensitized solar cells (DSSCs). Planar and electron rich heterocycle such as benzothieno[3,2-b]indole offers better backbone rigidity and improved charge transport properties in comparison to indolo[3,2-b]indole donor, previously reported from our group. Additionally, we synthesized benzothieno[3,2-b]indole donor grafted with longer alkyl chains which efficiently prevented the approach of oxidized species in electrolyte coming closer to semiconductor thereby arresting recombination. Power conversion efficiency of 4.11% was achieved for dye-sensitized solar cells based on furan π -spacer benzothieno[3,2-b]indole dye **BID-3** in comparison to the corresponding indolo[3,2-b]indole dye (**IID-3**) having an efficiency of 1.71%. Detailed interfacial electrical measurements along with theoretical calculations disclosed the mechanism of back electron transfer and improvement in photovoltaic performance with respect to variation in both donor and π -spacer.

Introduction

The dependence on renewable energy sources are growing exponentially, out of which harvesting solar energy occupies a prominent position. For the past three decades, research on development of technologies for effective conversion and utilization of sunlight were given utmost importance globally.¹ Even with the requirement of high purity materials and high production cost, silicon based photovoltaics are the market leading technology and are used extensively for outdoor light harvesting. The need for a more promising, inexpensive and low cost alternative to silicon triggered research on developing new generation of molecular photovoltaics.² In 1991, Brian O' Regan and Michael Grätzel introduced one of the most prominent class of molecular photovoltaic technology, dye-sensitized solar cells (DSSCs) which mimics natural photosynthesis.³ This innovation received wide attention in both academic and industrial sector with the added advantage of its low cost, colour tunability, flexibility to use both on rigid and flexible substrates, ease of fabrication and high efficiency in indoor/ambient light conditions.⁴ DSSC consists of three main components, a mesoporous semiconductor, sensitizer and redox electrolyte.⁵ The photovoltaic performance of DSSC depends on each of these

components along with the complex interactions that takes place in between these components at the various interfaces. Out of these components, sensitizer harness the light and occupies a prominent position.⁶ Sensitizers are mainly classified into metal complex and metal free dyes. Ruthenium (Ru) and Zinc (Zn) porphyrins are the two major class of highly efficient and well-studied metal complex sensitizers.⁷ The drawbacks of conventional metal complexes such as high cost, scarcity of materials, difficulty in ligand structural modifications and moderate light absorption have prompted the search for metal free organic dyes.⁸ The most common organic dye architectures follow D- π -A, D- π - π -A, D-D- π -A and D-A- π -A designs.⁹ Cyanoacrylic acid group being the best acceptor and linker functionality, novel design strategies for metal free organic sensitizers involves modifications of donor and π -spacers. Aryl amines, carbazoles and indoles are the commonly used donors in high performing DSSCs.¹⁰⁻¹² There is a need to develop other alternative novel units with higher donor strength, more capability to reduce aggregation and to prevent recombination and which can be made with less complicated synthetic methodologies. Recently, we reported the synthesis of indole based heteroacenes *via* sequential multicomponent reaction-oxidation strategy.¹³ Soon after we utilized this methodology to synthesize three dyes following the D- π -A design, employing indolo[3,2-b]indole as the electron donor and cyanoacrylic acid as the acceptor group.¹⁴ The power conversion efficiency of these dyes were studied by varying the π -spacer between furan, thiophene and benzene. The dye with benzene as π -spacer was found to perform more efficiently than the other two dyes and this was attributed to the low recombination found in the benzene substituted dye due to its twisted conformation which prevented aggregation thus leading to better lifetime. In spite of having a broad absorption profile the furan substituted dye (**IID-3**) displayed much inferior performance due to higher recombination. In the present work, we report the synthesis, opto-electronic properties, theoretical analysis and photovoltaic properties of a new class of D- π -A dyes employing molecularly engineered benzothieno[3,2-b]indole as the donor unit. Benzothieno[3,2-b]indole, is an electron rich fused ring planar system which can serve as a good donor functionality in metal free organic sensitizers. Very recently, Lee and Hong reported the use of benzothieno[3,2-b]indole as a hole transport unit in the fabrication of OLEDs.¹⁵ Unlike indolo[3,2-b]indole, benzothieno[3,2-b]indole is an under explored tetracene and to the best of our knowledge,

FULL PAPER

this moiety has not been explored till date for photovoltaic applications. In the present work, we designed and synthesized three dyes with benzothieno[3,2-b]indole as the donor motif and by varying the π -spacer [benzene (**BID-1**), thiophene (**BID-2**) and furan (**BID-3**), Figure 1].

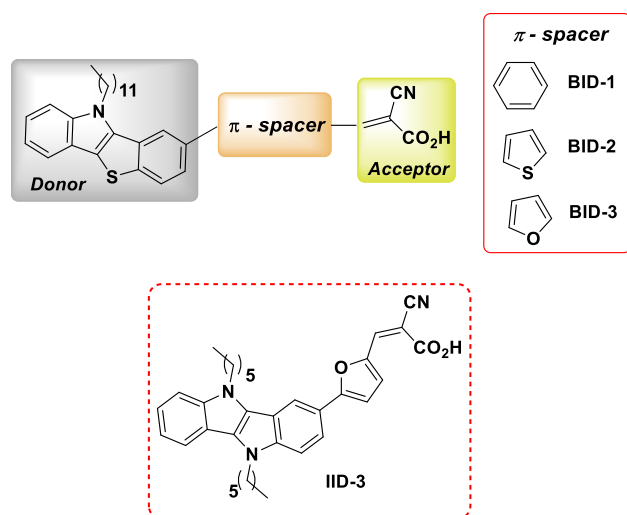


Figure 1. Benzothieno[3,2-b]indole based dyes **BID-1**, **BID-2** and **BID-3** and indolo[3,2-b]indole dye (**IID-3**).

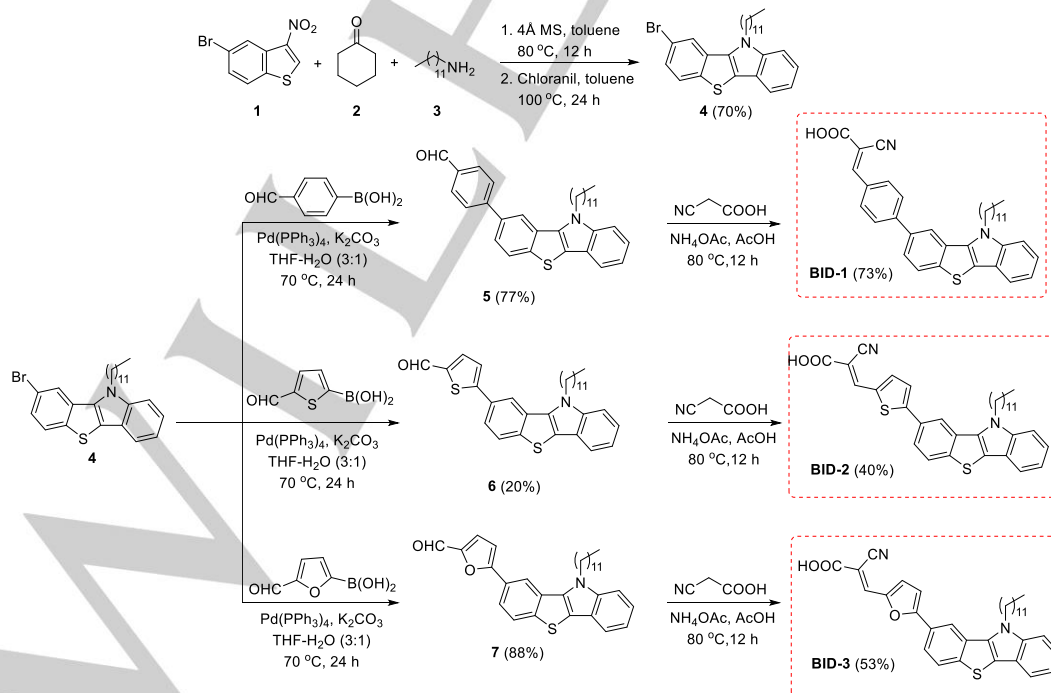
All the three dyes were used for the fabrication of dye-sensitized solar cells and benzothieno[3,2-b]indole dye with furan as π -spacer (**BID-3**) gave the best efficiency in the series delivering a PCE of 4.11%. There is an improvement of ~140% in PCE

compared to the analogous indolo[3,2-b]indole donor based organic dye with the same π -spacer. More importantly, we succeeded in arresting back electron transfer (recombination) efficiently by switching over to this tetracene donor which provided us the opportunity to use furan as π -spacer augmenting the light harvesting capabilities and thereby realizing improved photovoltaic performance. A detailed investigation of recombination pathways at various interfaces in these devices employing a range of electrical and optical perturbation techniques shines light in a way to probe the mechanism of electron transfer which helps to further fine tune the performance in future.

Results and Discussion

Synthesis and Characterization

The target molecules **BID-1**, **BID-2**, and **BID-3** were synthesized by following a five-step synthetic strategy. We commenced the synthesis with the nitration of 5-bromobenzothiophene by following reported protocols.¹⁶ Compound **1** was subjected to a one-pot MCR/oxidation process to afford benzothieno[3,2-b]indole (**4**) in 70 % yield. The π -spacer was then attached to the donor moiety by Suzuki reaction of 4-formyl phenyl boronic acid, (5-formylthiophen-2-yl)boronic acid and (5-formylfuran-2-yl)boronic acid with **4** to afford the molecules **5**, **6** and **7** respectively. Finally, the acceptor part was attached to **5**, **6** and **7** via Knoevenagel condensation with cyanoacetic acid furnishing the dyes **BID-1**, **BID-2**, and **BID-3** respectively. The entire synthetic route for **BID-1**, **BID-2**, and **BID-3** starting from **4** is given in Scheme 1. We have drawn the terminal double bonds of BID dyes in *E*-configuration by following the DFT results.



Scheme 1. Synthetic route adopted for benzothieno[3,2-b]indole based dyes **BID-1**, **BID-2** and **BID-3**.

FULL PAPER

Photophysical Properties

The absorption spectra of dyes **BID-1**, **BID-2** and **BID-3** in CHCl_3 are shown in Figure 2 and the corresponding data is listed in Table 1. All the three sensitizers exhibited absorption in the range of 300-520 nm. The absorption profile of **BID-2** and **BID-3** consists of three prominent bands. The bands at 300-360 nm wavelength is attributed to localized $\pi-\pi^*$ transitions and the bands positioned at lower energy wavelength regions can be attributed to the intramolecular charge transfer (ICT) transitions between donor and terminal acceptor units, respectively. In case of **BID-2** and **BID-3**, the ICT bands exhibited an extinction coefficient of $31060 \text{ M}^{-1}\text{cm}^{-1}$ and $28560 \text{ M}^{-1}\text{cm}^{-1}$ respectively. The absorption spectrum of **BID-1** is blue shifted compared to that of the other two dyes and is also not exhibiting significant intramolecular charge transfer band, which can be an indication of the interrupted delocalization between donor and acceptor moieties. The absorption spectra got red shifted on changing the π -spacer from benzene to furan *via* thiophene which is augmented by the dihedral angle between the donor and π -spacer unit which got decreased in the order 35.4° (benzene) $>$ 17.6° (thiophene) $>$ 7.0° (furan). With a more planar geometry in thiophene and furan substituted dyes, **BID-2** and **BID-3** showcased improved charge transfer properties leading to enhanced light harvesting. The ICT behavior of the dyes were investigated by solvatochromic studies. The absorption of dyes was taken in toluene, chloroform, tetrahydrofuran and acetonitrile (Figure S3, Figure S4 and Figure S5). It was found that upon increasing solvent polarity, significant shift in absorption was observed for the band at longer wavelength region for **BID 2** and **BID 3** and minimal changes were exhibited by **BID 1**. The negative solvatochromism displayed by the dyes indicates stabilization of the ground state of the dyes in polar solvents.

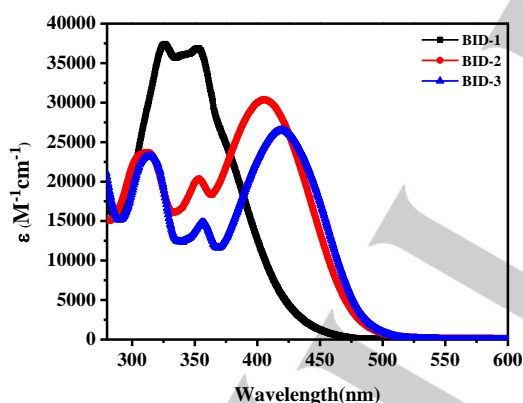


Figure 2. Absorption spectra of **BID-1**, **BID-2**, and **BID-3** measured in chloroform.

Electrochemical Properties

To investigate the molecular energy levels, cyclic voltammetry measurements were performed in CH_2Cl_2 , using tetrabutylammonium hexafluorophosphate (0.1 M) as the supporting electrolyte, Ag/AgCl as reference electrode, Pt as working and counter electrode and ferrocene as internal standard at 0.63 V vs. NHE (Figure 3). The oxidation potentials of **BID-1**, **BID-2**, and **BID-3** were calculated with respect to ferrocene and

were converted to NHE using the equation, $E_{\text{HOMO}} = [E_{\text{ox}}(\text{Fc}/\text{Fc}^+) + 0.63 \text{ V}]$.¹⁷ LUMO level (E_{LUMO}) was calculated as the difference $E_{\text{HOMO}} - E_{0-0}$. E_{0-0} (band gap) was determined from the tangent intercept of absorption edges. All photophysical and electrochemical values are tabulated in Table 1. The HOMO level of **BID-1**, **BID-2** and **BID-3** were observed to be 1.24 V, 1.28 V and 1.25 V vs. NHE. In all the three dyes, the donor unit being the same (benzothieno[3,2-b]indole) and HOMO being exclusively distributed on the donor site, very less change in the ground state oxidation potential was observed.

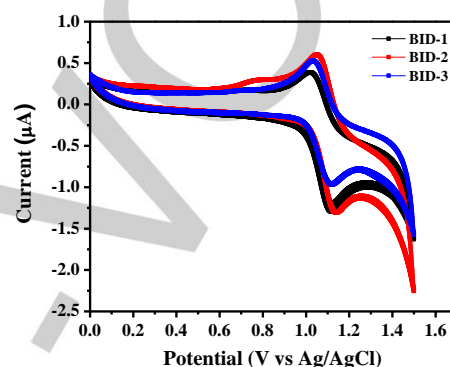


Figure 3. Cyclic voltammogram of **BID-1**, **BID-2**, and **BID-3** dyes in dichloromethane.

The schematic representation of dye energy levels along with TiO_2 conduction band and electrolyte redox potential are represented in Figure 4. The ground state redox potentials for all the BID dyes were substantially more positive than that of iodide/triiodide redox potential (0.4 V vs. NHE), indicating that regeneration is energetically favorable in all the three dyes. The optical transition energies (E_{0-0}) of **BID-1**, **BID-2** and **BID-3** were 2.9 eV, 2.58 eV and 2.54 eV respectively. The LUMO energy levels were determined by subtracting E_{0-0} from HOMO energy level which gave values of, -1.66, -1.30 and -1.29 V for **BID-1**, **BID-2** and **BID-3** respectively. The LUMO energy levels are relatively negative with respect to the position of the TiO_2 conduction band (-0.5 V vs. NHE) in a way to allow efficient electron injection.

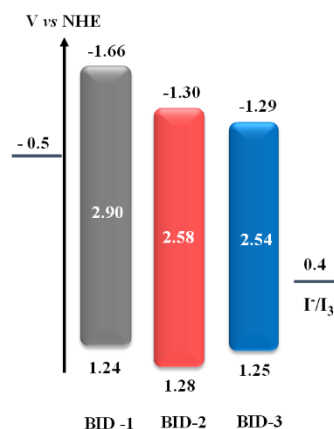


Figure 4. Energy level diagram of **BID** dyes.

FULL PAPER

Table 1. Photophysical and electrochemical data of **BID** dyes, V vs. NHE.

Sensitizer	λ_{\max} , nm (ϵ , M ⁻¹ cm ⁻¹)	$E_{\text{ox}}(\text{Fc}/\text{Fc}^+)$ (V)	E_{HOMO} (V)	E_{0-0} (eV)	E_{LUMO} (V)
BID-1	350 (37660)	0.61	1.24	2.90	-1.66
BID-2	406 (31060)	0.65	1.28	2.58	-1.30
BID-3	420 (28560)	0.62	1.25	2.54	-1.29

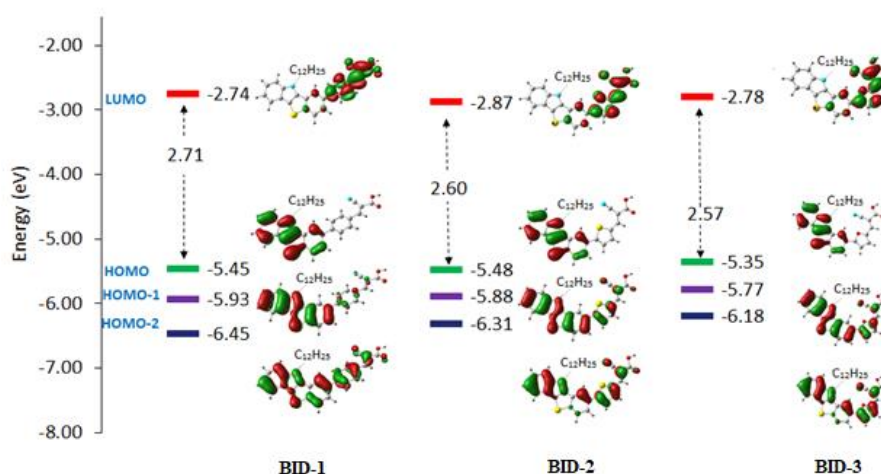
DFT Studies

A better knowledge on molecular geometry along with electron density distribution will pave the way towards deeper understanding of interfacial electron transfer dynamics in dye-sensitized solar cells. Additionally, the dihedral angle between the donor and π -spacer determines the dipole moment and is critical in determining the extend of donor-acceptor interactions in D- π -A organic dyes. The minimum energy structures of **BID-1**, **BID-2**, and **BID-3** are determined by density functional theory (DFT) calculations at B3LYP/cc-pVDZ level and are given in Figure S6. These structures show large variation in the twist angle (θ) between the aromatic moieties; **BID-3** with furan as π -spacer has the lowest θ (7.0°) followed by **BID-2** with thiophene (17.6°) and **BID-1** with phenyl (35.4°) moieties as π -spacers. The large variation in θ can significantly influence the π -electron distribution along the D- π -A framework. **BID-3** with a larger dipole moment of 3.8D clearly provides improved charge separation in comparison to **BID-2** (2.2D) and **BID-1** (1.9D). Further, a highly twisted structure such as **BID-1** is expected to show large difference in molecular packing compared to a nearly planar **BID-3**. Additionally, it also hampers efficient donor-acceptor interactions. The absorption spectra of **BID-1**, **BID-2**, and **BID-3** are calculated with the TD-DFT approach using the CAM-B3LYP/cc-pVDZ method in conjunction with the self-consistent reaction field method to include solvation effect of dichloromethane. The calculated λ_{\max} 345 and 397 for **BID-1** and **BID-2** respectively agrees well with their corresponding experimental values of 350 and 406 nm. In the case of **BID-3**, the calculated λ_{\max} 399 is in

reasonable agreement with the experimental value 420 nm. Good agreement between the trends in extinction coefficient and trends in the calculated oscillator strength is also observed (Table 2). Schematic representation of electronic distributions observed in frontier orbitals of benzothieno[3,2-b]indole based dyes at B3LYP/cc-pVDZ level along with MO energy and band gap values in eV are depicted in Figure 5. The molecular orbital (MO) composition corresponding to λ_{\max} indicates that the HOMO-1 to LUMO contribution is dominating π - π^* transition for **BID-2** and **BID-3** whereas in **BID-1** with phenyl as the π -spacer, the contributions from HOMO, HOMO-1 and HOMO-2 to LUMO are almost equal. In all cases, HOMO is distributed exclusively on the donor site while the LUMO is distributed largely on the π -spacer and acceptor unit which helps in efficient charge injection from dye excited state to semiconductor. The HOMO-1 of **BID-1** is more expressed at donor site than the π -A region compared to **BID-2** and **BID-3** dyes. The HOMO-2 of all the three molecules show a more delocalized distribution over the D- π -A region. The frontier MO analysis suggests that the electronic transition corresponding to the absorption peaks possess significant charge transfer character as the ground state electron mostly localized in the donor site is promoted to the π -A region in the excited state.

Table 2. Absorption maxima, oscillator strength, percentage contributions of orbital density, and dipole moments calculated at CAM-B3LYP/cc-pVDZ level.

Dyes	λ_{\max} (nm)	f	Composition	μ (Debye)
BID-1	345 (3.59 eV)	1.18	HOMO \rightarrow LUMO (23.62%) HOMO-1 \rightarrow LUMO (25.86%) HOMO-2 \rightarrow LUMO (29.44%)	1.9
BID-2	397 (3.12 eV)	0.99	HOMO \rightarrow LUMO (23.62%) HOMO-1 \rightarrow LUMO (51.13%) HOMO-2 \rightarrow LUMO (19.87%)	2.2
BID-3	399 (3.12 eV)	0.74	HOMO \rightarrow LUMO (24.89%) HOMO-1 \rightarrow LUMO (55.46%) HOMO-2 \rightarrow LUMO (15.23%)	3.8

**Figure 5.** Schematic representation of electronic distributions observed in frontier orbitals of benzothieno[3,2-b]indole based dyes at B3LYP/cc-pVDZ level. MO energy and band gap values in eV are also depicted.

FULL PAPER

Photovoltaic Performance

The photovoltaic performance of DSSCs fabricated with the newly synthesized benzothieno[3,2-b]indole donor unit attached dyes (**BID-1**, **BID-2** and **BID-3**) were evaluated under full sun AM 1.5G (100 mW cm⁻²) conditions. The current density-voltage (*J-V*) and incident-photon-to-current conversion efficiency (IPCE) curves are shown in Figure 6. The *J-V* parameters are summarized in Table 3.

Table 3. Solar Cell Characteristics of DSSCs Based on **BID-1**, **BID-2**, **BID-3** and **IID-3**.

Dye	V_{oc} (mV)	J_{sc} (mAcm ⁻²)	FF (%)	Efficiency (%)
BID-1	590 ± 2	2.86 ± 0.13	68.86 ± 1.2	1.16 ± 0.10
BID-2	652 ± 5	6.51 ± 0.16	73.27 ± 0.95	3.10 ± 0.25
BID-3	671 ± 8	8.38 ± 0.25	73.15 ± 0.56	4.11 ± 0.14
IID-3	540 ± 6	4.60 ± 0.32	69.00 ± 0.5	1.71 ± 0.12

The sensitizer **BID-3** with furan as π -spacer outperformed both **BID-1** and **BID-2** dyes having benzene and thiophene spacers displaying a power conversion efficiency of 4.11 ± 0.14% (J_{sc} = 8.38 ± 0.25 mA cm⁻², V_{oc} = 671 ± 8 mV, and FF = 73.15 ± 0.56) which is highest among the series, followed by **BID-2** with power conversion efficiency of 3.1 ± 0.25% (J_{sc} = 6.51 ± 0.16 mA cm⁻², V_{oc} = 652 ± 5 mV, and FF = 73.27 ± 0.95), and an efficiency of 1.16 ± 0.10 (J_{sc} = 2.86 ± 0.13 mA cm⁻², V_{oc} = 590 ± 2 mV, and FF = 68.86 ± 1.2) was realized for **BID-1**. The sensitizer with furan as π -spacer (**BID-3**) showcased an improvement in both short-circuit current density (J_{sc}) and open-circuit voltage (V_{oc}) than with benzene and thiophene spacers. The increase in J_{sc} is attributed to the increase in light harvesting ability of **BID-3** sensitizer which

is clearly seen from the extended absorption profile in the IPCE spectra. *J-V* results are in accordance with the IPCE data for all the three **BID** dyes. The results are also compared with the corresponding reported **IID-3** sensitizer having furan as π -spacer and indolo[3,2-b]indole as the donor unit.¹⁴ **IID-3** having N-hetero aromatic indolo[3,2-b]indole donor with furan as π -spacer displayed a power conversion efficiency of 1.71 ± 0.12% with the best optimized procedure.¹⁴ There is an increment of ~140% in PCE by changing the donor substituent from indolo[3,2-b]indole to benzothieno[3,2-b]indole which is attributed to the improvement associated with increase in both short-circuit current density and open-circuit potential. This point towards the role in nature of conjugated donor functionalities in determining the performance of D- π -A sensitizers. With addition of co-adsorbent (20 mM CDCA) the PV performance reduced in case of all **BID** dyes (Figure S1 and Table S1) to 1.01%, 2.52% and 3.58% for **BID-1**, **BID-2** and **BID-3**. In the present case having long alkyl chains attached to the donor functionality along with a slightly twisted conformation of the donor with respect to the π -spacer efficiently prevents aggregation eliminating the need for co-adsorbents for the benzothieno[3,2-b]indole donor based sensitizers.

Lower dihedral angle between the donor and π -spacer in **BID-3** (7°) compared with **BID-1** (35.4°) and **BID-2** (17.6°) along with a larger dipole moment of 3.8D for **BID-3** in comparison to 2.2D for **BID-2** and 1.9D for **BID-1** helped **BID-3** in achieving better donor: π -spacer interactions and enhanced charge separation leading to improved photovoltaic performance. Devices fabricated with **BID-3** sensitizer showed a broad absorption peak from 350 nm to 550 nm as evident from IPCE spectra with a maximum value of 88% at 460 nm, leading to a J_{sc} of 8.38 ± 0.25 mA cm⁻². **BID-2** showed highest EQE of 75% at 400 nm and **BID-1** showed 75% at 350nm respectively. The red shifted absorption spectra of both **BID-2** and **BID-3** compared to **BID-1** (Figure 2) contributed

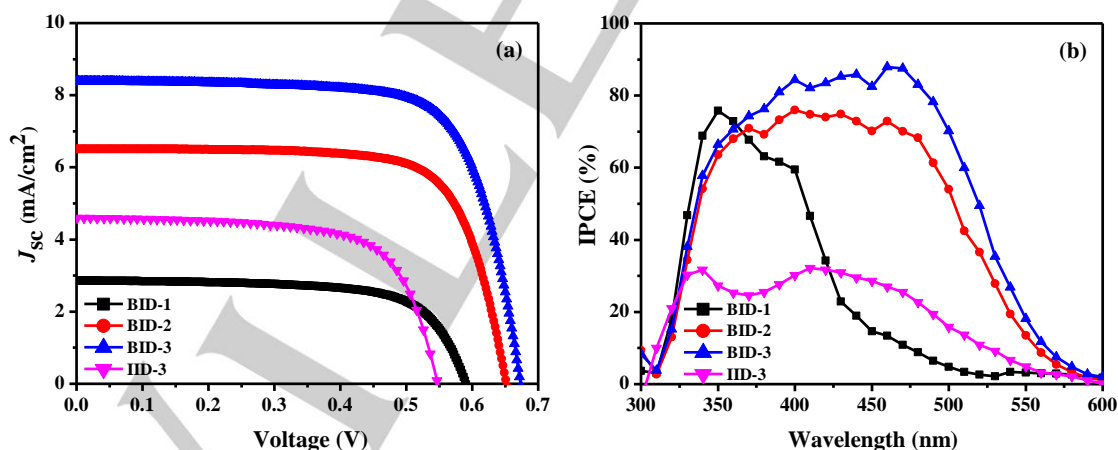


Figure 6. (a) Current-voltage (*J-V*) characteristics of DSSCs with sensitizers **BID-1**, **BID-2**, **BID-3** and **IID-3** under AM 1.5G illumination. (b) Spectra of incident photon-to-current conversion efficiency (IPCE) for DSSCs.

towards significant improvement in IPCE for both the dyes, leading to improvement in J_{sc} . Even though **BID-2** exhibited higher absorption coefficient in comparison to **BID-3**, it failed to achieve higher absorption in action spectra as IPCE involves contribution from other electron transfer process such as injection, regeneration and collection which again depends on transport

and lifetime of electrons in these devices. The IPCE spectra of **BID-3** also showed considerable increment in absorption around 350-550 nm wavelength range compared to **IID-3** (Figure S2) which contributed to enhanced PCE for the dye having benzothieno[3,2-b]indole donor in comparison with indolo[3,2-b]indole donor.

FULL PAPER

To get an in-depth understanding of the variation in photovoltaic performance, both electrical and light perturbation measurements were carried out involving Charge Extraction (CE), Intensity Modulated Photovoltage Spectroscopy (IMVS), and Electrochemical Impedance Spectroscopy (EIS). CE measurement provides the distribution of trap states and the position of conduction band.¹⁸ Figure 7(a) shows charge extraction as a function of applied voltage for devices fabricated with three newly synthesized BID sensitizers. There is a positive shift in the conduction band (CB) for **BID-3** compared to **BID-1** and **BID-2**. The positive shift in TiO₂ CB resulted in efficient electron injection, contributing to improved light harvesting efficiency for **BID-3**. Additionally, a positive shift in CB will lead to less recombination driving force, contributing towards lower electron lifetime. The average time injected electrons stays in the energy states of TiO₂ (lifetime, τ_n) was calculated using IMVS technique using the equation, $\tau_n = 1/(2\pi f_{max})$, where f_{max} is the frequency corresponding to the highest value in Bode curve obtained from IMVS plot. Lifetime as a function of light intensity is shown in Figure 7(b). The lifetime plot shows almost similar lifetime for **BID-3** and **BID-1** (furan and benzene π -spacers) sensitizers and both exhibits longer lifetime than **BID-2**. Improved lifetime is an indication of less recombination at TiO₂/dye/electrolyte interface. In our previous report, we observed slower rate of recombination for benzene π -spacer followed by thiophene and furan involving indolo[3,2-b]indole as donor whereas in the present case when we used benzothieno[3,2-b]indole as donor, furan substituted dye showcased almost same lifetime as that of the benzene analogue. This is quite interesting

which helped us to make use of the higher absorption profile exhibited by furan π -spacer and points to the fact that the trend we normally observe with respect to variation in π -spacers to the recombination lifetime will not hold good once we change the donor functionality.¹⁴ Even with a more negative shift in CB which contributes to higher recombination driving force, the added advantage of having a twisted conformation might have rendered **BID-1** the capability to prevent the approach of oxidized species in electrolyte coming closer to TiO₂ thereby achieving a lifetime similar to that of **BID-3**. **BID-3** with benzothieno[3,2-b]indole donor displayed a lifetime which is almost an order of magnitude higher than **IID-3** with indolo[3,2-b]indole as the donor functionality (Figure 7(b)). This is attributed to the longer alkyl chains grafted on the benzothieno[3,2-b]indole which is more effective in preventing back electron transfer in comparison to indolo[3,2-b]indole while used as electron donating functionality in D- π -A dyes. The less rate of recombination along with the broad visible absorption helped **BID-3** in achieving better open-circuit potential in comparison to other dyes. For all three sensitizers, LUMO levels are placed at potentials with more than 800 mV of driving force for electron injection (Figure 4). The injection of electrons from LUMO of the sensitizer to the conduction band of TiO₂ was qualitatively studied using Photo-Induced Absorption Spectroscopy (PIA) measurement.¹⁹ Figure S7 shows the PIA spectra of all the three sensitizers. The absorption peak observed at 500 nm - 850 nm range is indicative of efficient electron injection for all three dyes and the intensity of absorption being more or less the same indicate similar injection dynamics for all three sensitizers.

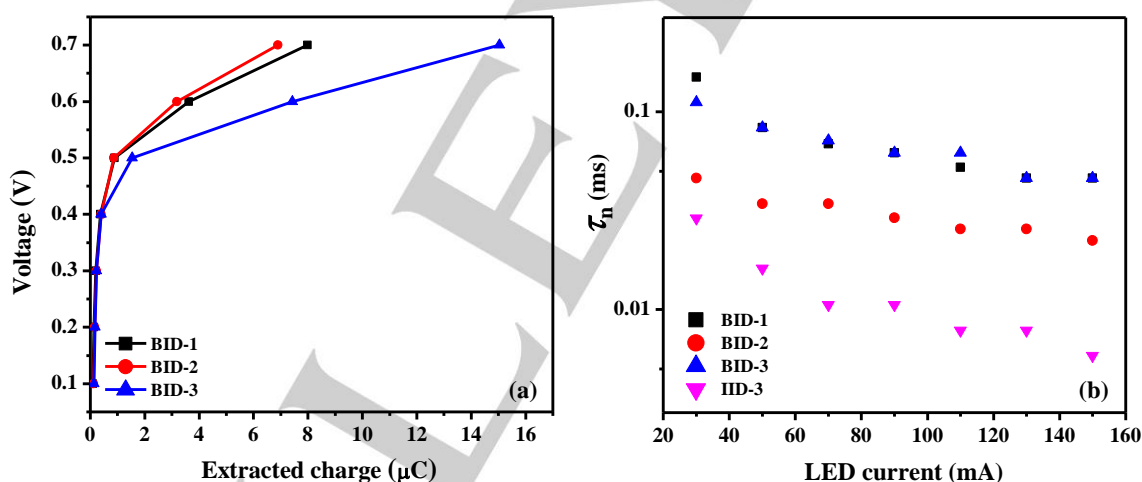


Figure 7. (a) Extracted charge versus voltage from charge extraction measurement and (b) Lifetime as a function of light intensity measured using IMVS technique.

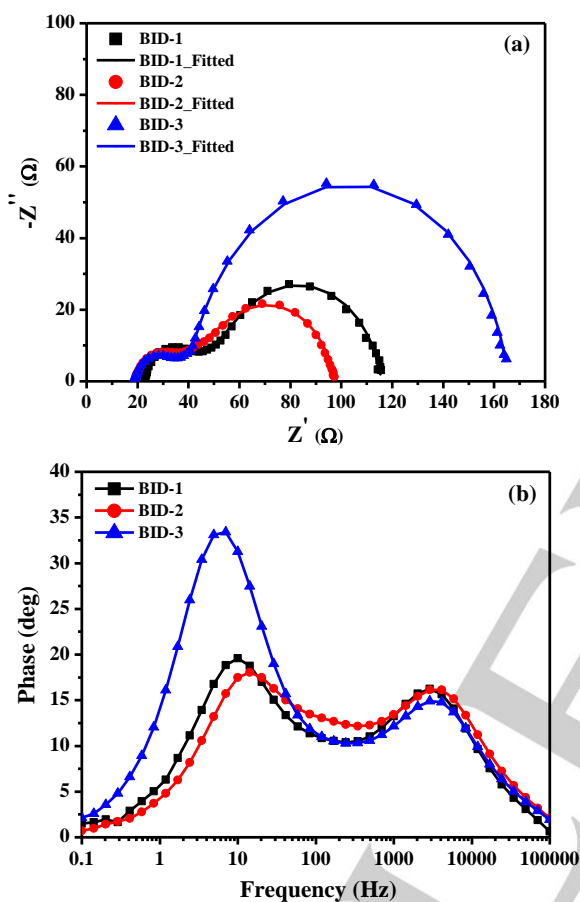
To probe the charge transfer processes under dark conditions bypassing the contribution of charge recombination from the injected electrons in TiO₂ to the overall lifetime, EIS was carried out at -0.66 V under forward bias in dark. Figure 8(a) shows the Nyquist plot of the devices measured using EIS technique at -0.66 V under forward bias. The frequency response of typical DSSC consists of three different semicircles in the complex plane plot due to the different time constants at various interfaces. The semicircles at high frequency, middle frequency and low frequency regions correspond to platinum/electrolyte interface, TiO₂/dye/electrolyte interface and the diffusion of ions in the electrolyte respectively. Generally, while employing

iodide/triiodide electrolyte, due to faster diffusion of ions in iodide electrolyte, the third semicircle is rarely seen. Here in, we observed two semicircles which corresponds to charge transfer at platinum/electrolyte interface and TiO₂/dye/electrolyte interface. Nyquist plot was fitted using equivalent circuit with transmission line model.^{6,14} The Transport Resistance (R_t), Charge-Transfer Resistance (Recombination Resistance, R_{ct}) and Chemical Capacitance (C_{μ}) were derived by fitting the Nyquist plots with equivalent circuit model and lifetime (τ_n) is calculated using the equation $\tau_n = C_{\mu} \times R_{ct}$. All the fitted, derived and calculated parameters are summarized in Table 4.

FULL PAPER

Table 4. Transport Resistance (R_t), Recombination Resistance (R_{ct}), Chemical Capacitance (C_{μ}) and Lifetime (τ_n) calculated from EIS at -0.66 V for **BID** dyes.

Dye	Transport Resistance (R_t), Ω	Recombination Resistance (R_{ct}), Ω	Chemical Capacitance (C_{μ}), mF	Lifetime (τ_n), ms
BID-1	48.77	63.25	666	42.12
BID-2	58.54	49.08	644	31.61
BID-3	27.93	131.3	687	90.20

**Figure 8.** (a) Nyquist plot and (b) Bode plot measured using EIS technique for DSSCs at -0.66 V under forward bias for **BID** dyes.

BID-3 sensitizer showcased a larger semicircle in the middle frequency region indicating a higher recombination resistance (131.3 Ω) followed by **BID-1** and **BID-2** with R_{ct} 63.25 Ω and 49.08 Ω respectively. For **BID** dyes the radii of second semicircle increases in the order **BID-2** < **BID-1** < **BID-3**, (Figure 8(a)) indicating that the electron recombination rate increased in the order of **BID-3** < **BID-1** < **BID-2** in dark. The Bode phase plot is given in (Figure 8(b)). The recombination process of injected electrons in TiO_2 is represented by the peak at higher frequency. A shift of higher frequency peak to lower frequency suggest the possibility of lower charge recombination rate which leads to a longer electron lifetime. The reciprocal of this frequency peak is regarded as electron lifetime, where $\tau_n = (1/2\pi f_n)$ where f_n is the frequency corresponding to the highest value in Bode plot. As

seen in Table 4, **BID-3** showed highest lifetime in **BID** series of dyes derived from EIS measurement which is in accordance with the lifetime data obtained from IMVS measurement. Apart from the red shifted absorption, lower transport resistance, higher recombination resistance and longer lifetime favored **BID-3** in achieving higher photovoltaic performance among **BID** dye series.

Conclusion

In summary, we successfully synthesized three new D- π -A organic dyes based on benzothieno[3,2-b]indole as donor and by varying the π -spacer unit with benzene (**BID-1**), thiophene (**BID-2**) and furan (**BID-3**). With judicious selection of π -spacer, the optical properties are controlled in a way to realize improved photovoltaic performance. Furan substituted dye, **BID-3** showcased the best performance with a PCE of 4.11%. The efficiency value increased in the order **BID-1** (1.16%) < **BID-2** (3.10%) < **BID-3** (4.11%). Better planarity of the molecular backbone helped **BID-3** in achieving improved donor-acceptor interactions and superior charge separation leading to larger dipole moment thereby realizing improved light harvesting and photovoltaic performance. Additionally, lower driving force for recombination attained with a positive CB shift also helped **BID-3** in achieving enhanced lifetime as evident from both IMVS and EIS measurements.

The newly introduced benzothieno[3,2-b]indole donor exhibits improved photovoltaic performance compared to its predecessor indolo[3,2-b]indole. This is mainly attributed to better light harvesting capacity, improved charge transport properties and the inherent capability of **BID** unit to prevent back electron transfer leading to increase in J_{sc} , V_{oc} and η for **BID** dyes in comparison to **IID** dyes. Presence of longer alkyl chains and a higher degree of planarity for **BID** unit also minimized the dye aggregation effects. We prepared these fused benzothieno[3,2-b]indole donor moieties by following our newly developed synthetic strategy involving a multicomponent reaction-oxidation sequence. Research is currently progressing in our laboratory in this direction to further engineer these molecular backbones by introducing new donor functionalities and to explore the possibilities of using these rigid units as π -spacers.

Experimental Section

General Methods

All chemicals were of the best grade commercially available and were used without further purification. All solvents were purified according to standard procedure; dry solvents were obtained according to the literature methods and stored over molecular sieves. Gravity column chromatography was performed using neutral alumina and mixtures of hexane-ethyl acetate were used for elution. Melting points were determined on a Buchi melting point apparatus and are uncorrected. Proton nuclear magnetic resonance spectra (^1H NMR) were recorded on a Bruker AMX 500 spectrophotometer (CDCl_3 and Acetone- d_6 as solvents). Chemical shifts for ^1H NMR spectra are reported as δ in units of parts per million (ppm) downfield from SiMe_4 (δ 0.0) and relative to the signal of chloroform- d (δ 7.25ppm) Acetone- d_6 (2.05 ppm). Multiplicities were given as: s (singlet); d (doublet); t (triplet); q (quartet); dd (double doublet); m (multiplet). Coupling constants are reported as J value in Hz. Carbon nuclear magnetic resonance spectra (^{13}C NMR) are reported as δ in units of parts per million (ppm) downfield

FULL PAPER

from SiMe₄ (δ 0.0) and relative to the signal of chloroform-d (δ 77.03 ppm) and Acetone-d₆ (29.84 and 206.26 ppm). Mass spectra were recorded under ESI/HRMS at 60,000 resolution using Thermo Scientific Exactive mass spectrometer. The UV-visible absorbance was studied using a SCHIMADZU UV-1800 UV-Visible spectrophotometer, using commercially available 1 cm quartz cuvette purchased from Sigma-Aldrich.

Synthesis of 8-Bromo-10-dodecyl-10H-benzo[4,5]thieno[3,2-b]indole (4)

The enolizable ketone, cyclohexanone (760 mg, 7.75 mmol) and primary amine, dodecylamine (1.43 g, 7.75 mmol) were weighed into a dry reaction tube. Dry toluene along with 4Å MS was added and allowed to stir at 80 °C for 1 hour, after which 5-bromo-3-nitrobenzothiophene (1 g, 3.87 mmol) was added into it and kept again for stirring at the same temperature for 11 hours. After the complete consumption of 5-bromo-3-nitrobenzothiophene, chloranil (2.8 g, 11.6 mmol) along with toluene was added and kept at 100 °C for 24 hours. The solvent was evaporated in vacuo and the residue on activated neutral alumina column chromatography yielded 8-bromo-10-dodecyl-10H-benzo[4,5]thieno[3,2-b]indole **4** as a colorless solid, Yield: 1.27 g, 70%; mp (65-67 °C); ¹H NMR (500 MHz, CDCl₃): δ 8.09 (d, J = 1.5 Hz, 1H) 7.78-7.76 (m, 2H) 7.49 (d, J = 8 Hz, 1H) 7.44 (dd, J_1 = 8.5 Hz, J_2 = 2 Hz, 1H) 7.39-7.35 (m, 1H) 7.24-7.21 (m, 1H) 4.54 (t, J = 7.5 Hz, 2H) 1.98-1.93 (m, 2H) 1.47-1.41 (m, 2H) 1.37-1.24 (m, 16 H) 0.87 (t, J = 7 Hz, 3H) ppm; ¹³C NMR (125 MHz, CDCl₃): δ 141.7, 141.7, 136.2, 128.5, 126.5, 125.7, 123.4, 122.6, 121.3, 119.6, 118.1, 116.8, 110.0, 45.0, 31.9, 30.4, 29.6, 29.6, 29.6, 29.5, 29.4, 29.3, 27.0, 22.7, 14.1 ppm; HRMS (ESI) m/z : (M+H)⁺ calcd for C₂₆H₃₃BrNS 470.1512, found 470.1583.

Synthesis of 4-(10-Dodecyl-10H-benzo[4,5]thieno[3,2-b]indol-7-yl)benzaldehyde (5)

A mixture of **4** (200 mg, 0.43 mmol), 4-formylphenylboronic acid (76 mg, 0.51 mmol), Pd(PPh₃)₄ (49 mg, 0.42 mmol), K₂CO₃ (294 mg, 2.1 mmol) were weighed into a Schlenk tube and degassed for 10 minutes. Degassed THF and water in a 3:1 ratio was then added and the reaction mixture was purged with argon and allowed to stir at 70 °C for 24 hours. The solvent was evaporated under vacuum and the residue on activated neutral alumina column chromatography (with mixtures of ethyl acetate in hexane as eluent) yielded the product **5** as a yellow colored solid. Yield 162 mg, 77%; mp (85-87 °C); ¹H NMR (500 MHz, CDCl₃): δ 10.10 (1H, s), 8.21-8.20 (m, 1H), 8.03-8.01 (m, 3H), 7.86 (d, J = 8.5 Hz, 2H), 7.80 (d, J = 8 Hz, 1H), 7.64-7.62 (m, 1H), 7.51 (d, J = 8.5 Hz, 1H) 7.40-7.36 (m, 1H), 7.26-7.22 (m, 1H), 4.63 (t, J = 7.5 Hz, 2H) 2.05-1.99 (m, 2H), 1.51-1.45 (m, 2H), 1.40-1.34 (m, 2H), 1.27-1.21 (m, 14 H), 0.86 (t, J = 7 Hz, 3H) ppm ¹³C NMR (125 MHz, CDCl₃): 191.9, 147.5, 143.4, 137.1, 136.2, 135.2, 130.4, 127.9, 127.6, 125.0, 123.2, 123.1, 121.5, 119.6, 119.5, 118.6, 110.0, 45.2, 31.9, 30.5, 29.7, 29.6, 29.6, 29.5, 29.4, 29.3, 27.1, 22.7, 14.1 ppm; HRMS (ESI) m/z : (M+Na)⁺ calcd for C₃₃H₃₇NNaOS 518.2488, found 518.2422.

Synthesis of 2-Cyano-3-(4-(10-dodecyl-10H-benzo[4,5]thieno[3,2-b]indol-7-yl)phenyl) acrylic acid (BID-1)

A mixture of aldehyde **5** (150 mg, 0.3 mmol), cyanoacetic acid (77 mg, 0.9 mmol), ammonium acetate (116 mg, 1.5 mmol) in acetic acid was heated at reflux overnight under argon atmosphere. After cooling to room temperature, it was precipitated by pouring into water. The precipitate was washed with water and dried in vacuum oven. The product **BID-1** was obtained as an orange color solid. Yield: 124 mg, 73%; mp: 160-165 °C; ¹H NMR (500 MHz, (CD₃)₂CO): δ 8.37 (d, J = 1.5 Hz, 1H), 8.26 (s, 1H), 8.12 (d, J = 8.5 Hz, 2H) 8.02 (d, J = 8.5 Hz, 1H) 7.94-7.92 (m, 2H), 7.70-7.68 (m, 2H), 7.58 (d, J = 8.5 Hz, 1H), 7.26-7.23 (m, 1H) 7.10-7.08 (m, 1H), 4.70 (t, J = 7 Hz, 2H) 1.90-1.87 (m, 2H) 1.37-1.32 (m, 2H) 1.26-1.22 (m, 2H) 1.14-1.04 (m, 14H) 0.71 (t, J = 7 Hz, 3H) ppm ¹³C NMR (125 MHz, (CD₃)₂CO): 162.9, 153.7, 145.5, 143.2, 141.8, 137.2, 136.0, 131.6, 130.8, 127.9, 127.8, 125.1, 123.2, 123.2, 121.4, 119.6, 119.1, 118.8, 115.8, 115.7, 110.6, 103.2, 44.6, 31.7, 30.3, 29.4, 29.3, 29.2, 29.2, 29.1, 26.6, 22.4, 13.4

ppm; HRMS (ESI) m/z : (M-CO₂)⁻ calcd for C₃₅H₃₇N₂S 517.2683, found 517.2686.

Synthesis of 5-(10-dodecyl-10H-benzo[4,5]thieno[3,2-b]indol-8-yl)thiophene-2-carbaldehyde (6)

A mixture of **4** (200 mg, 0.43 mmol), 5-Formyl-2-thiopheneboronic acid (80 mg, 0.51 mmol), Pd(PPh₃)₄ (49 mg, 0.042 mmol), K₂CO₃ (294 mg, 2.1 mmol) were weighed into a Schlenk tube and degassed for 10 minutes. Degassed THF and water in a 3:1 ratio was then added and the reaction mixture was purged with argon and allowed to stir at 70 °C for 24 hours. The solvent was evaporated under vacuum and the residue on activated neutral alumina column chromatography (with mixtures of ethyl acetate in hexane as eluent) yielded the product **6** as a yellow color solid. Yield: 43 mg, 20%; mp (80-83 °C); ¹H NMR (500 MHz, CDCl₃): δ 9.93 (1H, s), 8.25-8.20 (m, 1H), 7.96-7.94 (m, 1H), 7.79-7.78 (m, 2H) 7.70-7.64 (m, 1H), 7.51-7.48 (m, 2H), 7.38 (t, J = 7.5 Hz, 1H), 7.24-7.19 (m, 1H) 4.60-4.52 (m, 2H), 2.01-1.95 (m, 2H), 1.52-1.47 (m, 2H), 1.42-1.35 (m, 2H) 1.27-1.21 (m, 14H) 0.86 (t, J = 7 Hz, 3H) ppm; ¹³C NMR (125 MHz, CDCl₃): 182.7, 154.7, 144.2, 141.6, 137.6, 136.8, 125.1, 124.1, 124.0, 123.4, 122.0, 121.8, 121.4, 120.4, 119.6, 119.6, 117.7, 116.6, 109.9, 45.2, 31.9, 30.5, 30.1, 29.5, 29.3, 27.2, 27.1, 22.7, 14.1 ppm; HRMS (ESI) m/z : (M + H)⁺ calcd for C₃₁H₃₆NOS 502.2233, found 502.2233.

2-Cyano-3-(5-(10-dodecyl-10H-benzo[4,5]thieno[3,2-b]indol-8-yl)thiophen-2-yl)acrylic acid (BID-2)

A mixture of aldehyde **6** (151 mg, 0.30 mmol), cyanoacetic acid (77 mg, 0.90 mmol), ammonium acetate (116 mg, 1.5 mmol) in acetic acid was heated at reflux overnight under argon atmosphere. After cooling to room temperature, it was precipitated by pouring into water. The precipitate was washed with water and dried in vacuum oven. The product **BID-2** was obtained as red color solid. Yield: 68 mg, 40%; mp: 203-205 °C; ¹H NMR (500 MHz, (CD₃)₂CO): δ 8.40 (d, J = 1.5 Hz, 1H) 8.37 (s, 1H), 8.03 (d, J = 8.5 Hz, 1H), 7.93 (d, J = 4 Hz, 1H), 7.74-7.72 (m, 2H) 7.70 (d, J = 8 Hz, 1H) 7.60 (d, J = 8 Hz, 1H) 7.27-7.24 (m, 1H) 7.10 (t, J = 7.5 Hz, 1H), 4.69 (t, J = 7.5 Hz, 2H) 1.90-1.87 (m, 2H), 1.46-1.40 (m, 2H) 1.15-1.07 (m, 14 H) 0.72 (t, J = 7.5 Hz, 3H) ppm; ¹³C NMR (125 MHz, (CD₃)₂CO): 163.0, 154.3, 145.3, 146.4, 143.9, 141.8, 140.2, 136.8, 135.0, 129.4, 127.5, 125.3, 125.0, 123.4, 122.0, 121.2, 119.6, 119.1, 117.8, 116.1, 116.1, 110.6, 98.6, 44.8, 31.6, 30.1, 26.5, 22.4, 13.5 ppm; HRMS (ESI) m/z : (M-CO₂)⁻ calcd for C₃₃H₃₅N₂S₂ 523.2242, found 523.2232

Synthesis of 5-(10-Dodecyl-10H-benzo[4,5]thieno[3,2-b]indol-8-yl)furan-2-carbaldehyde (7)

A mixture of **4** (200 mg, 0.43 mmol), 5-Formyl-2-furanylboronic acid (71 mg, 0.51 mmol), Pd(PPh₃)₄ (49 mg, 0.42 mmol), K₂CO₃ (294 mg, 2.1 mmol) were weighed into a Schlenk tube and degassed for 10 minutes. Degassed THF and water in a 3:1 ratio was then added and the reaction mixture was purged with argon and allowed to stir at 70 °C for 24 hours. The solvent was evaporated under vacuum and the residue on activated neutral alumina column chromatography (with mixtures of ethyl acetate in hexane as eluent) yielded the product **7** as a yellow color solid. Yield: 182 mg, 88%; mp: 100-103 °C; ¹H NMR (500 MHz, CDCl₃): δ 9.71 (1H, s), 8.43 (1H, s), 7.98 (d, J = 8 Hz, 1H), 7.79 (t, J = 7 Hz, 2H) 7.52 (d, J = 8.5 Hz, 1H) 7.40-7.37 (m, 2H) 7.26-7.22 (m, 1H) 6.93 (d, J = 4 Hz, 1H) 4.65 (t, J = 7.5 Hz, 2H) 2.05-1.99 (m, 2H) 1.53-1.47 (m, 2H) 1.41-1.36 (m, 2H) 1.27-1.20 (m, 14H) 0.86 (t, J = 7 Hz, 3H) ppm ¹³C NMR (125 MHz, CDCl₃): 177.1, 159.7, 152.0, 144.3, 141.6, 136.9, 127.3, 125.4, 124.9, 123.3, 121.3, 120.6, 119.6, 119.6, 116.4, 110.1, 107.6, 45.2, 31.9, 30.4, 29.6, 29.6, 29.6, 29.5, 29.4, 29.3, 27.1, 22.7, 14.1 ppm. HRMS (ESI) m/z : (M + H)⁺ calcd for C₃₁H₃₆NO₂S 486.2461, found 486.2479.

Synthesis of 2-Cyano-3-(5-(10-dodecyl-10H-benzo[4,5]thieno[3,2-b]indol-8-yl)furan-2-yl)acrylic acid (BID-3)

A mixture of aldehyde **7** (146 mg, 0.30 mmol), cyanoacetic acid (77 mg, 0.90 mmol), ammonium acetate (116 mg, 1.5 mmol) in acetic acid was heated at reflux overnight under argon atmosphere. After cooling to room

FULL PAPER

temperature, it was precipitated by pouring into water. The precipitate was washed with water and dried in vacuum oven. The product **BID-3** was obtained as red color solid. Yield: 88 mg, 53 %; mp: 190-193 °C; ¹H NMR (500 MHz, (CD₃)₂CO): 8.69 (s, 1H), 8.03 (d, *J* = 8.5 Hz, 1H), 8.01 (s, 1H), 7.87 (dd, *J*₁ = 8.5 Hz, *J*₂ = 1.5 Hz, 1H), 7.70 (d, *J* = 7 Hz, 1H), 7.60 (d, *J* = 8.5 Hz, 1H), 7.46 (d, *J* = 4 Hz, 1H), 7.30 (d, *J* = 3.5 Hz, 1H), 7.27-7.24 (m, 1H), 7.11-7.08 (m, 1H), 4.72 (t, *J* = 7 Hz, 2H) 1.88-1.83 (m, 2H), 1.32-1.26 (m, 2H), 1.69-1.02 (m, 16H), 0.71 (t, *J* = 7.5 Hz, 3H)ppm; ¹³C NMR (125 MHz, (CD₃)₂CO) : 163.3, 159.8, 148.0, 144.2, 142.0, 137.9, 137.2, 127.5, 126.3, 125.5, 125.2, 123.4, 121.3, 120.9, 119.6, 119.1, 116.7, 116.4, 115.9, 110.9, 109.6, 97.2, 44.4, 31.7, 30.3, 26.3, 22.4, 13.4 ppm; HRMS (ESI) *m/z*: (M + H)⁺ calcd for C₃₄H₃₆N₂O₃S 553.2519, found 553.2526.

Device Fabrication

Working electrodes (FTO, TEC15, GreatCell Solar) were cleaned using ultrasonic bath in soap solution, deionized water and isopropyl alcohol followed by heating to 500 °C. The pre-blocking layer was coated on the UV-Ozone treated substrates by immersing in 40 mM TiCl₄ solution at 70 °C for 30 min. 16 μm titanium dioxide semiconductor layer (12 μm transparent layer and 4 μm scattering layer) was coated on the substrates and were heated to 500 °C through ramped heating. The TiO₂ coated electrodes were soaked in 0.2 mM of respective dye solutions with and without 20 mM chenodeoxycholic acid (CDCA) for 15 hours in acetonitrile at room temperature. Pre-drilled, platinum coated FTO was used as the counter electrodes and the cells were assembled using a 25 μm surlyn spacer. The space between working and counter electrodes were filled with electrolyte composed of 0.5 M BMII, 0.1 M Lil, 0.03 M I₂ and 0.5 M tpb in acetonitrile. The devices with standard sensitizer **IID-3** was fabricated using the best optimized procedure.¹⁴

The *J-V* curve was measured under AM 1.5G irradiation (Class AAA simulator form Newport, Sol3A-94023). The incident-photon-to-current conversion efficiency (IPCE) was measured using 350W Xenon lamp with Monochromator (Newport). The Charge Extraction (CE), Intensity Modulated Photovoltage Spectroscopy (IMVS) and Electrochemical Impedance Spectroscopy (EIS) were measured using electrochemical workstation (Autolab PGSTAT302N). PIA measurements were carried out on the completed devices with the three sensitizers without electrolyte to track injection.

Acknowledgements

J.V., S.C.P., C.H.S., J.J., S.S. and A.A. thank DST for DST-SERB Project [DST/SERB/F/481]. N.P.R thank CSIR, J.V. thank DST-SERB and S.C.P thank DST-SERI [DST/TMD/SERI/D46(G)] for research fellowships. N.P.R would also like to thank Mr. Yoosuf Muhammed for help in photophysics measurements

Keywords: Dye sensitized solar cell • Benzothieno(3,2-*b*)indole • Indolo(3,2-*b*)indole • π -spacer • Back electron transfer

References

- [1] a) N. Armaroli and V. Balzani, *Angew. Chemie - Int. Ed.*, **2007**, *46*, 52–66; b) X. Chen, C. Li, M. Grätzel, R. Kostecki and S. S. Mao, *Chem. Soc. Rev.*, **2012**, *41*, 7909–7937; c) R. Eisenberg and D. G. Nocera, *Inorg. Chem.*, **2005**, *44*, 6799–6801.
- [2] W. A. Badawy, *J. Adv. Res.*, **2015**, *6*, 123–132.
- [3] B. O'Regan & M. Grätzel, *Nature*, **1991**, *353*, 737–740.
- [4] a) Y. Cao, Y. Liu, S. M. Zakeeruddin, A. Hagfeldt and M. Grätzel, *Joule*, **2018**, *2*, 1108–1117; b) M. Freitag, J. Teuscher, Y. Saygili, X. Zhang, F. Giordano, P. Liska, J. Hua, S. M. Zakeeruddin, J. E. Moser, M. Grätzel and A. Hagfeldt, *Nat. Photonics*, **2017**, *11*, 372–378; c) A. Hagfeldt, G. Boschloo, L. Sun, L. Kloo, H. Pettersson, *Chem. Rev.* **2010**, *110*, 6595–6663; d) G. Gokul, S. C. Pradhan, S. Soman, *Adv. Solar Energy Res.*, **2019**, pp. 281–316.
- [5] A. Carella, F. Borbone and R. Centore, *Front. Chem.*, **2018**, *6*, 1–24.
- [6] a) T. Maeda, T. V. Nguyen, Y. Kuwano, X. Chen, K. Miyanaga, H. Nakazumi, S. Yagi, S. Soman and A. Ajayaghosh, *J. Phys. Chem. C*, **2018**, *122*, 21745–21754; b) M. K. Nazeeruddin, E. Baranoff and M. Grätzel, *Sol. Energy*, **2011**, *85*, 1172–1178; c) M. V. Vinayak, M. Yoosuf, S. C. Pradhan, T. M. Lakshmykanth, S. Soman and K. R. Gopidas, *Sustain. Energy Fuels*, **2018**, *2*, 303–314; d) M. Yoosuf, S. C. Pradhan, S. Soman and K. R. Gopidas, *Sol. Energy*, **2019**, *188*, 55–65; e) B. Hemavathi, V. Jayadev, P. C. Ramamurthy, R. K. Pai, K. N. Narayanan Unni, T. N. Ahipa, S. Soman and R. G. Balakrishna, *New J. Chem.*, **2019**, *43*, 15673–15680.
- [7] a) T. Bessho, S. M. Zakeeruddin, C. Y. Yeh, E. W. G. Diau and M. Grätzel, *Angew. Chemie - Int. Ed.*, **2010**, *49*, 6646–6649; b) C. Chen, M. Wang, J. Li, N. Pootrakulchote, L. Alibabaei, J. Decoppet, J. Tsai, C. Gra, C. Wu, S. M. Zakeeruddin and M. Gra, *ACS Nano*, **2009**, *3*, 3103–3109; c) F. Gao, Y. Wang, D. Shi, J. Zhang, M. Wang, X. Jing, R. Humphry-Baker, P. Wang, S. M. Zakeeruddin and M. Grätzel, *J. Am. Chem. Soc.*, **2008**, *130*, 10720–10728; d) T. Kinoshita, J. T. Dy, S. Uchida, T. Kubo and H. Segawa, *Nat. Photonics*, **2013**, *7*, 535–539; e) N. V. Krishna, J. V. S. Krishna, S. P. Singh, L. Giribabu, L. Han, I. Bedja, R. K. Gupta and A. Islam, *J. Phys. Chem. C*, **2017**, *121*, 6464–6477; f) J. V. S. Krishna, D. Koteswar, T. H. Chowdhury, S. P. Singh, I. Bedja, A. Islam and L. Giribabu, *J. Mater. Chem. C*, **2019**, *7*, 13594–13605; g) S. Mathew, A. Yella, P. Gao, R. Humphry-Baker, B. F. E. Curchod, N. Ashari-Astani, I. Tavernelli, U. Rothlisberger, M. K. Nazeeruddin and M. Grätzel, *Nat. Chem.*, **2014**, *6*, 242–247; h) V. Nikolaou, A. Charisiadis, S. Chalkiadaki, I. Alexandropoulos, S. C. Pradhan, S. Soman, M. K. Panda and A. G. Coutsolelos, *Polyhedron*, **2018**, *140*, 9–18; i) H. Ozawa, T. Sugiura, T. Kuroda, K. Nozawa and H. Arakawa, *J. Mater. Chem. A*, **2016**, *4*, 1762–177; j) S. Soman, Y. Xie and T. W. Hamann, *Polyhedron*, **2014**, *82*, 139–147; k) Y. Wang, B. Chen, W. Wu, X. Li, W. Zhu, H. Tian and Y. Xie, *Angew. Chemie - Int. Ed.*, **2014**, *53*, 10779–10783; l) Z. She, Y. Cheng, L. Zhang, X. Li, D. Wu, Q. Guo, J. Lan, R. Wang and J. You, *ACS Appl. Mater. Interfaces*, **2015**, *7*, 27831–27837.
- [8] a) A. Mishra, M. K. R. Fischer and P. Büuerle, *Angew. Chemie - Int. Ed.*, **2009**, *48*, 2474–2499; b) Y. Ooyama and Y. Harima, *European J. Org. Chem.*, **2009**, 2903–2934.
- [9] a) L. Alibabaei, J. H. Kim, M. Wang, N. Pootrakulchote, J. Teuscher, D. Di Censo, R. Humphry-Baker, J. E. Moser, Y. J. Yu, K. Y. Kay, S. M. Zakeeruddin and M. Grätzel, *Energy Environ. Sci.*, **2010**, *3*, 1757–1764; b) X. Qian, X. Wang, L. Shao, H. Li, R. Yan and L. Hou, *J. Power Sources*, **2016**, *326*, 129–136; c) L. Giribabu, R. K. Kanaparthi and V. Velkannan, *Chem. Rec.*, **2012**, *12*, 306–328; d) J. He, Y. Liu, J. Gao, L. Han, *Photochem. Photobiol. Sci.*, **2017**, *16*, 1049–1056; e) B. Hemavathi, V. Jayadev, S. C. Pradhan, G. Gokul, K. Jagadish, G. K. Chandrashekhara, P. C. Ramamurthy, R. K. Pai, K. N. Narayanan Unni, T. N. Ahipa, S. Soman and R. Geetha Balakrishna, *Sol. Energy*, **2018**, *174*, 1085–1096; f) W. Li, Y. Wu, Q. Zhang, H. Tian and W. Zhu, *ACS Appl. Mater. Interfaces*, **2012**, *4*, 1822–1830; g) P. Liu, B. Xu, K. M. Karlsson, J. Zhang, N. Vlachopoulos, G. Boschloo, L. Sun and L. Kloo, *J. Mater. Chem. A*, **2015**, *3*, 4420–4427; h) Y. Wu and W. Zhu, *Chem. Soc. Rev.*, **2013**, *42*, 2039–2058; i) Y. Wu, W. H. Zhu, S. M. Zakeeruddin and M. Grätzel, *ACS Appl. Mater. Interfaces*, **2015**, *7*, 9307–9318; j) Z. Yao, M. Zhang, H. Wu, L. Yang, R. Li and P. Wang, *J. Am. Chem. Soc.*, **2015**, *137*, 3799–3802; k) W. Zhu, Y. Wu, S. Wang, W. Li, X. Li, J. Chen, Z. S. Wang and H. Tian, *Adv. Funct. Mater.*, **2011**, *21*, 756–763; l) H. Zhu, W. Li, Y. Wu, B. Liu, S. Zhu, X. Li, H. Ågren, W. Zhu, *ACS Sustainable Chem. Eng.* **2014**, *2*, 1026–1034; m) H. Jiang, Y. Wu, A. Islam, M. Wu, W. Zhang, C. Shen, H. Zhang, E. Li, H. Tian and W. Zhu, *ACS Appl. Mater. Interfaces*, **2018**, *10*, 13635–13644.
- [10] a) L. Giribabu, V. K. Singh, C. V. Kumar, Y. Soujanya, P. Y. Reddy and M. L. Kantam, *Sol. Energy*, **2011**, *85*, 1204–1212; b) J. Tang, W. Wu, J. Hua, J. Li, X. Li and H. Tian, *Energy Environ. Sci.*, **2009**, *2*, 982–990; c) M. V. Vinayak, T. M. Lakshmykanth, M. Yoosuf, S. Soman and K. R. Gopidas, *Sol. Energy*, **2016**, *124*, 227–241; d) J. Wang, K. Liu, L. Ma and

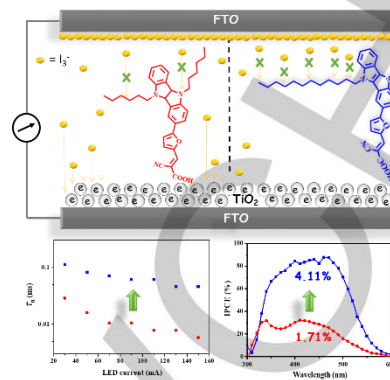
FULL PAPER

- X. Zhan, *Chem. Rev.*, **2016**, *116*, 14675–14725; e) M. Liang, J. Chen, *Chem. Soc. Rev.* **2013**, *42*, 3453.
- [11] a) K. Hara, Z. S. Wang, Y. Cui, A. Furube and N. Koumura, *Energy Environ. Sci.*, **2009**, *2*, 1109–1114; b) G. Marotta, M. A. Reddy, S. P. Singh, A. Islam, L. Han, F. De Angelis, M. Pastore and M. Chandrasekharam, *ACS Appl. Mater. Interfaces*, **2013**, *5*, 9635–9647; c) P. Naik, A. Planchat, Y. Pellegrin, F. Odobel and A. Vasudeva Adhikari, *Sol. Energy*, **2017**, *157*, 1064–1073.
- [12] a) D. D. Babu, S. R. Gachumale, S. Anandan and A. V. Adhikari, *Dye Pigment.*, **2015**, *112*, 183–191; b) D. D. Babu, R. Su, A. El-Shafei and A. V. Adhikari, *Electrochim. Acta*, **2016**, *198*, 10–21; c) Y. Hong, Z. Iqbal, X. Yin and D. Cao, *Tetrahedron*, **2014**, *70*, 6296–6302.
- [13] a) P. V. Santhini, S. A. Babu, A. Krishnan R, E. Suresh and J. John, *Org. Lett.*, **2017**, *19*, 2458–2461; b) P. V. Santhini, R. Akhil Krishnan, S. A. Babu, B. S. Simethy, G. Das, V. K. Praveen, S. Varughese and J. John, *J. Org. Chem.*, **2017**, *82*, 10537–10548.
- [14] P. V. Santhini, V. Jayadev, S. C. Pradhan, S. Lingamoorthy, P. R. Nitha, M. V. Chaithanya, R. K. Mishra, K. N. Narayanan Unni, J. John and S. Soman, *New J. Chem.*, **2019**, *43*, 862–873.
- [15] R. K. Konidena, K. hyung Lee, J. Y. Lee and W. P. Hong, *Org. Electron.*, **2019**, *70*, 211–218.
- [16] a) K. Tanemura, T. Suzuki, Y. Nishida, K. Satsumabayashi and T. Horaguchi, *J. Chem. Res. - Part S*, **2003**, 497–499; b) J. Q. Zhao, L. Yang, Y. You, Z. H. Wang, K. X. Xie, X. M. Zhang, X. Y. Xu and W. C. Yuan, *Org. Biomol. Chem.*, **2019**, *17*, 5294–5304.
- [17] S.-G. Li, K.-J. Jiang, J.-H. Huang, L.-M. Yang and Y.-L. Song, *Chem. Commun.*, **2014**, *50*, 4309–4311
- [18] a) M. Pazoki, U. B. Cappel, E. M. J. Johansson, A. Hagfeldt and G. Boschloo, *Energy Environ. Sci.*, **2017**, *10*, 672–709; b) L. Peter, *J. Electroanal. Chem.*, **2007**, *599*, 233–240.
- [19] a) G. Boschloo, A. Hagfeldt, *Chem. Phys. Lett.* **2003**, *370*, 381–386; b) G. Boschloo, A. Hagfeldt, *Inorganica Chim. Acta* **2008**, *361*, 729–734.; c) U. B. Cappel, S. M. Feldt, J. Schöneboom, A. Hagfeldt, G. Boschloo, *J. Am. Chem. Soc.* **2010**, *132*, 9096–9101

FULL PAPER

Entry for the Table of Contents

An enhancement in efficiency was achieved with benzothieno[3,2-b]indole donor based dyes in comparison to indolo[3,2-b]indole with the same spacer and acceptor groups. This could be attributed to the increased light harvesting ability of the former along with the longer alkyl chains, reducing back electron transfer reactions.



Cite this: *Mater. Adv.*, 2021,
2, 6136Received 8th June 2021,
Accepted 19th August 2021

DOI: 10.1039/d1ma00499a

rsc.li/materials-advances

Indole fused heterocycles as sensitizers in dye-sensitized solar cells: an overview

P. R. Nitha,^{ab} Suraj Soman *^{ab} and Jubi John *^{ab}

The past three decades have witnessed extensive research in developing a range of non-metallic organic dyes for dye sensitized solar cells (DSSCs). Dyes occupy a prominent position among components in DSSCs, and organic dyes have emerged as the most promising candidate for DSSCs due to their performance, ease of synthesis, stability, tunability, low cost and eco-friendly characteristics. In addition to this, so far, the best and highest performing DSSCs reported in the literature use metal-free organic dyes. Organic dyes also provide flexibility to be used along with alternate new generation cobalt and copper electrolytes. Among various organic dyes, heterocycles, mainly N- and S-containing, have found immense applications as sensitizers. Indole fused heterocycles were used by different research groups in their dye designs, mainly as a donor and π -spacer. The planarity of these electron-rich fused indole systems is advantageous as it helps to initiate a more prominent ICT transition in dye molecules. In addition, the possibility for selective functionalization of N-atoms with long or branched alkyl chains prevents the aggregation of the sensitizer, increasing the solubility and is effective in custom design dyes which are in turn capable of preventing back electron transfer (recombination). Fused indole moieties utilized in the design of sensitizers are stable and offer easy synthesis. In the present review, we examine different indole fused heterocycles as building blocks for sensitizers used in DSSCs.

Introduction

Fossil fuel-based resources have been primarily satisfying the energy demands of humankind for more than a century. The ever-increasing energy demands that are fuelled by the growing

^a Chemical Sciences and Technology Division, CSIR-National Institute for Interdisciplinary Science and Technology (CSIR-NIIST), Thiruvananthapuram 695019, India. E-mail: suraj@niist.res.in, jubijohn@niist.res.in

^b Academy of Scientific and Innovative Research (AcSIR), Ghaziabad-201002, India



P. R. Nitha

for Interdisciplinary Science and Technology (CSIR-NIIST), Thiruvananthapuram.

P. R. Nitha was born in 1992 in Thrissur, Kerala. She obtained her BSc Degree from K. K. T. M. College (University of Calicut), Kodungallur in 2012 and her MSc Degree from Cochin university of Science and Technology in 2014. She is currently pursuing her doctoral research on utilization of indole fused heterocycles for DSSC applications, under the combined supervision of Dr Jubi John and Dr Suraj Soman at the National Institute



Suraj Soman

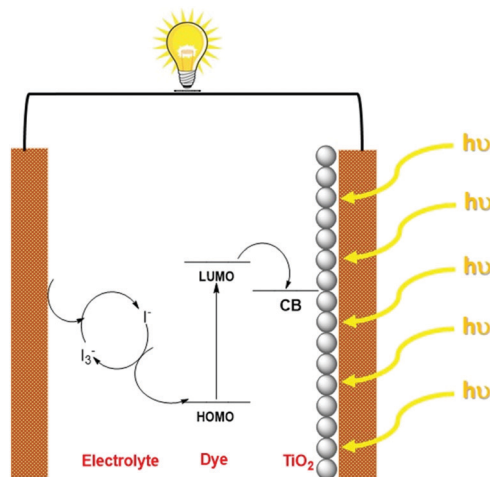
spanning from materials to devices to detailed dynamic measurements. His interdisciplinary research group also focus in module/prototype development through academia-industry collaborations in a way to exploit DSSC technology for indoor photovoltaics & BIPV applications.

Dr Suraj Soman obtained his PhD in molecular photocatalysis from Dublin City University (Ireland) under the supervision of Prof. Han Vos and Prof. Mary Pryce followed by postdoctoral tenure at Michigan State University (USA) with Prof. Thomas W. Hamann. Dr Suraj Soman joined CSIR-NIIST (India) in 2014 and is currently working as a Scientist at CSIR-NIIST. His prime research focus involves all aspects of Dye Sensitized Solar Cells (DSSCs)



human population have contributed to environmental issues with the depletion of conventional resources, necessitating the need for research into developing efficient methods to harness alternative energy sources.¹ Solar energy is considered one of the most promising alternatives that could sustainably provide inexhaustible energy.² The stepping stone for photovoltaic technology was laid with the demonstration of the first silicon-based solar cells by Bell laboratories, which exhibited an efficiency of ~6%. Since then, the technology has witnessed many advancements in introducing thin films in the late 1970's and finally reaching up to the third-generation solar cells.³ The third-generation photovoltaics consist of dye-sensitized solar cells, organic solar cells, quantum dot solar cells and perovskite solar cells.⁴ Though their efficiencies are still lagging behind the conventional silicon-based devices, the lower fabrication cost of these devices along with lesser environmental impact are promising factors that urge the scientific community to carry out research and technological advancements in third-generation photovoltaics.⁵

Dye sensitized solar cell research got momentum in 1991 with the pioneering work carried out by Brian O'Regan and Michael Gratzel, where they used Ru metal complex sensitized nanocrystalline TiO₂ film, generating a power conversion efficiency of 7%.⁶ DSSCs have many attractive features, including lower fabrication cost and short payback time with minimum environmental hazards.⁷ In addition, they can be designed for both outdoor as well as indoor light harvesting.⁸ DSSC consists of three major components, photoelectrode, electrolyte and a counter electrode. The dye sensitized mesoporous semiconductor layer coated on a conductive glass/plastic substrate collectively acts as the photoanode. The electrolyte is responsible for both regeneration of the dye as well as charge transport to the counter electrode. Liquid electrolytes which consist of redox mediators in organic solvents are typically used in DSSCs. To address the leakage and device lifetime issues originating



Scheme 1 Operating principle of DSSCs.

from the usage of liquid electrolytes, efforts are being made to explore quasi-solid electrolytes and solid conductors. The counter electrode is composed of transparent conductive oxides (ITO/FTO) coated with catalysts like platinum for fast electron transfer reactions. The mechanism of current generation with DSSCs starts with the absorption of light by the dye sensitizers that are adsorbed on the semiconductor surface. These photo-excited electrons are then injected into the conduction band of the semiconductor, which diffuses through the conductive substrate and finally reaches the counter electrode. The oxidized dye molecules are subsequently regenerated by the redox mediators present in the electrolyte, which are then reduced at the counter electrode. This cycle continues generating current without net chemical change in the system (Scheme 1).⁹

Unlike conventional PV devices, DSSCs excel with the advantage that different components are carrying out light absorption, charge generation, and charge transport. This opens up the broader possibility of achieving higher photovoltaic performance by selectively optimizing each component used in the device. The sensitizer represents the core unit in DSSCs, responsible for light absorption and electron injection into the semiconductor layer. An ideal sensitizer is supposed to display panchromatic absorption with a higher molar extinction coefficient. The optimum redox potential of the dye energy levels (HOMO–LUMO) is necessary to achieve efficient electron injection into the semiconductor conduction band and to realize effective regeneration of the dye ground state by the redox electrolyte. The sensitizer should also possess features such as suitable binding groups (–COOH, –PO₃H₂) to anchor onto the semiconductor surface and also needs to be engineered in such a way to minimize aggregation on the semiconductor. The prevention of dye aggregation is highly desirable to reduce recombination losses and increase the open circuit potential of the devices, which can also contribute to the stability of the device as a whole.¹⁰

Ruthenium-based sensitizers dominated the first two decades in DSSC research since their inception in the early nineties due to their broad absorption and higher power conversion efficiencies



Jubi John

Dr Jubi John obtained his PhD in synthetic organic chemistry from CSIR-NIIST under the supervision of Dr K. V. Radhakrishnan. Soon after he joined as a CEA-Euro-talents postdoctoral fellow with Dr Eric Doris at CEA Saclay, France. In 2011, he joined as an Alexander von Humboldt fellow with Prof. Henning Hopf at TU Braunschweig, Germany and from 2013, with Prof. Wim Dehaen at the KU Leuven, Belgium. He then joined CSIR-

NIIST in 2015 and is presently working as a senior scientist at the same institute. His research interests include development of novel synthetic methodologies, new antiviral drug candidates and dyes for material applications.



and reached up to a PCE of 11.5% using a conventional iodide/triiodide electrolyte.¹¹ Though these sensitizers appear to be feasible for practical applications, with progressing research, a lower molar extinction coefficient of metal complexes along with the scarcity of Ru have slowly paved the way for the advent of metal-free sensitizers. Additionally, the introduction of alternate cobalt and copper electrolyte further encouraged the scientific community to expand the research on organic dyes, which are most suitable with alternate electrolytes. The introduction of metal-free sensitizers has also opened up an arsenal of strategies to develop more efficient devices at a lower cost and in an eco-friendly manner.¹² Metal-free sensitizers generally display high molar extinction coefficients, but the narrow absorption of many sensitizers results in serious concern over light harvesting. The emergence of a co-sensitization strategy helped to alleviate this limitation by realizing panchromatic absorption through the sensitization of a combination of different dyes having complementary absorption.¹³ This also reduced the possibility for dye aggregation. The strongest side of organic sensitizers involves the flexibility in tuning the chemical structure with the help of the well-established synthetic strategies.¹⁴ According to the recent reports, the PCE of DSSCs based on single metal free organic sensitizers has reached 13.6% using a cobalt electrolyte, 11.7 for solid state DSSCs and 32% for indoor light harvesting. The co-sensitization strategy could realize 14.3% PCE using a cobalt based electrolyte.¹⁵

Molecular engineering of dyes deals with designing systems with potential light-harvesting ability over the entire visible region with proper energetics that realizes electron transfer from the excited state of the dye to the metal oxide upon light absorption. The most widely employed molecular architecture is the donor- π spacer-acceptor (D- π -A) strategy.¹⁶ Anchoring groups are supposed to be bifunctional, serving the purposes of adsorption as well as electron acceptance. Although many new anchoring groups have emerged, a cyanoacrylate group is generally found to outperform others because of its agreement with the two functions mentioned above. The strong electron withdrawing nature of the cyanoacrylate moiety facilitates the broadening of the absorption spectra of molecules and the strong adsorption capability to the semiconductor surface increases the injection ability and device lifetime. A wide variety of choices are present for both donor and π -spacer moieties. The derivatives of arylamine, carbazole, coumarins and phenothiazine are some of the popular donor groups of continued interest used in DSSCs.¹⁷ The π -linkers are also of paramount importance in tuning the communication between donor and acceptor units, thereby increasing the light-harvesting ability of the dyes. Though thiophene, furan, benzene and oligothiophenes have been used extensively as π -spacers in dyes, fused ring planar systems with strategies to prevent π - π aggregation have not been explored to the full extent.¹⁸ Apart from modulating each building block of a sensitizer, considerable effort was also laid in engineering new dye design strategies, which resulted in the introduction of architectures like D-A- π -A, D-D- π -A, A- π -D- π -A and D- π -A-A.¹⁹

The present review attempts to consolidate and analyse dye sensitizers which utilize fused indole units as components in

sensitizers used in DSSCs. These indole-fused heterocycles are found to exhibit more electron-donating ability than those with indole in conjugation with expanded π -systems.²⁰ Another advantage of the fused indole systems is the better planarity they possess, inducing better donor-acceptor interaction leading to improved PV performance. The possibility of functionalization of the N-atom with long or branched alkyl chains is another advantage of indole-based heterocyclic systems that increase the solubility and prevent aggregation of the sensitizer. The majority of fused indoles were used as a donor moiety in the sensitizers, and very few units were used as π -spacers. The indole fused systems explored as building blocks in DSSC sensitizers include indoloquinoline (IQ), indolocarbazole, indoloindole, benzothienoindole, indenoindole, triazatruxene, thienoindole, tetraindole, dithienopyrroloindole, fluorenylindolenine, and indole-imidazole. The exploration of these systems as donor and π -spacers are investigated fitting in different molecular architectures. This will help the scientific community further re-engineer these heterocycles with excellent optoelectronic properties in line with the requirements of the photovoltaic applications.

I. Indoloquinoline based sensitizers for DSSCs

Indolo[2,3-*b*]quinoline (IQ), a built-in donor-acceptor chromophore, consists of an electron-rich indole moiety fused with an electron-deficient quinoline unit. The condensation of isatin with *o*-phenylenediamine can efficiently synthesize these planar heteroarenes.²¹ By appropriately functionalizing the indole and quinoline motifs with electron-donating or electron-withdrawing groups, the electronic properties of this chromophore can be custom-tuned in line with the applications. It has been documented that the donating ability of the indole motif and the donor-acceptor interaction with the quinoline unit is enhanced by functionalizing the indole core with electron-donating groups.²²

The first utilization of this scaffold as a building block in DSSCs was carried out by Venkateswararao *et al.*²³ They constructed dyes 2-6, which are having IQ as an electron donor and cyanoacrylic acid as an anchoring unit (Fig. 1). The sensitizers differed in the π -spacer employed, which were either phenyl or thiophene fragments. Dye 1, which lacks any π -spacer, delivered the least efficiency of 0.86%. Among the remaining sensitizers, 6 showed a red shifted and distinct ICT band implying more effective conjugation. Two dye baths were used to fabricate devices, one with DCM and the other with a combination of CH₃CN/*tert*-butanol/DMSO (3.5/3.5/3, v/v). All the sensitizers exhibited better efficiencies in the latter case. The changes in PCE were mainly caused by significant changes in the photocurrent generated. Though ICT was more prominent in the case of 6, a relatively high degree of planarity might have caused aggregation of the dyes leading to decreased light harvesting. Dye 2 with simple thiophene as the π -spacer outperformed other dyes with PCE of 3.45% with J_{sc} of 9.29 mA cm⁻² and V_{oc} of 579 mV.



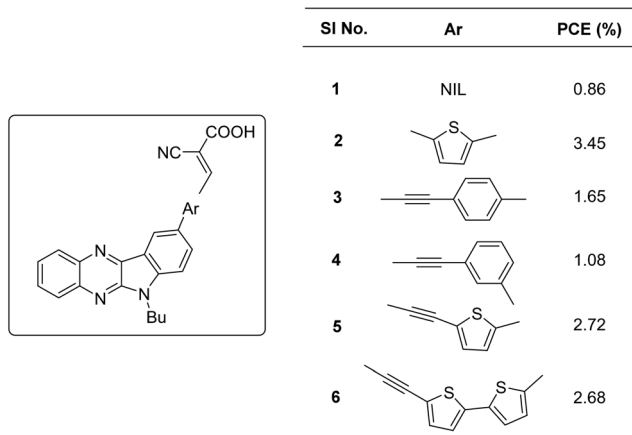


Fig. 1 Photosensitizers **1–6** based on an indolo[2,3-*b*]quinoxaline core.

Other dyes showcased PCE in the order **6** > **5** > **3** > **4** (Table 1). The introduction of acetylene was not found to be beneficial for transmitting charges in the current design.

Later, Qian *et al.* developed three D- π -A dyes having indolo[2,3-*b*]quinoxaline and cyanoacrylic acid as donor and acceptor groups, respectively.²⁴ Sensitizers **7**, **8**, and **9** differ in the selection of conjugated spacers, which were oligothiophene, thienylcarbazole, and furylcarbazole, respectively (Fig. 2). The dyes exhibited efficiencies in the order **7** > **9** > **8** (Table 1). The maximum efficiency of 7.62% was delivered by **7**, mainly contributed by the significantly larger short circuit current density ($J_{sc} = 16 \text{ mA cm}^{-2}$) of this dye. The electron-rich, oligothiophene

Table 1 Photovoltaic parameters of indoloquinoxaline based DSSCs

Sensitizer	J_{sc} (mA cm^{-2})	V_{oc} (mV)	FF	PCE (%)	Electrolyte	Coadsorbent (concentration)	Ref.
1	2.66	500	0.64	0.86	I^-/I_3^-	—	23
2	9.29	579	0.64	3.45	I^-/I_3^-	—	23
3	4.43	543	0.68	1.65	I^-/I_3^-	—	23
4	2.73	593	0.67	1.08	I^-/I_3^-	—	23
5	7.38	568	0.65	2.72	I^-/I_3^-	—	23
6	7.77	562	0.62	2.68	I^-/I_3^-	—	23
7	16.0	708	0.67	7.62	I^-/I_3^-	—	24
8	14.8	701	0.63	6.48	I^-/I_3^-	—	24
9	14.1	742	0.67	7.03	I^-/I_3^-	—	24
10	8.9	676	0.68	4.10	I^-/I_3^-	—	25
11	14.0	705	0.69	6.82	I^-/I_3^-	—	25
12	15.3	757	0.71	8.28	I^-/I_3^-	—	25
13	14.2	745	0.71	7.56	I^-/I_3^-	—	25
14	11.9	797	0.64	6.05	I^-/I_3^-	—	26
15	12.9	817	0.67	7.09	I^-/I_3^-	—	26
16	9.03	707	0.68	4.35	I^-/I_3^-	—	26
17	9.71	724	0.68	4.81	I^-/I_3^-	—	26
18	5.56	653	0.72	2.65	I^-/I_3^-	CDCA (10 mM)	27
19	5.68	622	0.73	2.72	I^-/I_3^-	CDCA (10 mM)	27
20	5.99	618	0.69	2.61	I^-/I_3^-	CDCA (10 mM)	27
21	19.0	649	0.61	7.46	I^-/I_3^-	CDCA (20 mM)	27
19/21	19.37	654	0.63	7.94	I^-/I_3^-	CDCA (20 mM)	27
22	4.73	637	0.73	2.21	I^-/I_3^-	CDCA (10 mM)	28
23	5.08	676	0.74	2.56	I^-/I_3^-	CDCA (10 mM)	28
22/21	17.79	683	0.67	8.16	I^-/I_3^-	CDCA (20 mM)	28
23/21	18.24	688	0.69	8.67	I^-/I_3^-	CDCA (20 mM)	28
24	11.10	676	0.70	5.27	I^-/I_3^-	CDCA (10 mM)	29
25	11.29	657	0.69	5.10	I^-/I_3^-	CDCA (10 mM)	29
26	11.84	638	0.65	4.92	I^-/I_3^-	CDCA (10 mM)	29

π -bridge makes the absorption spectra of **7** more red-shifted with an absorption maximum at 480 nm for the ICT band followed by **8** and **9**. The IPCE performance of the devices is following the absorption behaviour of the dyes. While **7** shows broad absorption from 400 to 770 nm, in the case of **8** and **9**, the absorption furnishes onset at 700 and 690 nm, respectively illustrating the trend in the dyes' J_{sc} and light-harvesting ability. Though lower current density was delivered by **9**, the higher open circuit potential ($V_{oc} = 742 \text{ mV}$) helped **9** outperform **8**.

Soon after, the authors used the same scaffold to realize D-D- π -A and D- π -A systems.²⁵ In D-D- π -A design, indoloquinoxaline was used as the primary donor and phenothiazine was used as an auxiliary donor, cyanoacrylic acid as an acceptor and thiophene/furan as a π -bridge to afford **12** and **13**, respectively (Fig. 3). These dyes were then compared with **10** and **11**, which were D- π -A dyes based on indoloquinoxaline and phenothiazine, respectively, as donors. Among the dyes, **12** having D-D- π -A design was found to outperform the rest. Sensitizer **12** excelled with an efficiency of 8.28% followed by **13** with 7.56%. Compared to furan, the electron richness of thiophene was aiding good ICT transitions reducing the HOMO-LUMO gap for **12**, which resulted in more red-shifted and enhanced absorption spectra for **12** compared to that of **13** with furan as a π -spacer. The IPCE spectra of the dyes show a similar trend, with **12** giving over 60% IPCE value from 359 to 600 nm with maximum absorption of 86% at 490 nm. This illustrates the reason for the highest light-harvesting ability and J_{sc} (15.3 mA cm^{-2}) for **12**. The V_{oc} values obtained are in the order **12** > **13** > **11** > **10** (Table 1).

Later in 2017, the authors utilized indoloquinoxaline as an acceptor in a (D)₂-A- π -A dye design in which two triphenylamine groups were used as two branches of the primary donor unit. The dyes **14–17** differed in the π -bridges (furan and thiophene) and acceptor groups (cyanoacrylic acid and 2-(1,1-dicyanomethylene)rhodanine or DCRD) (Fig. 4).²⁶ These dyes exhibited efficiencies in the range of 4.55% to 7.09%. Dyes **14** and **15**, which had cyanoacrylic acid as the acceptor group, outperformed the corresponding dyes having DCRD as the acceptor unit. Though the absorption spectra of **16** and **17** were much red-shifted compared to **14** and **15**, higher dye loading of the latter resulted in larger J_{sc} values. This is also apparent from the IPCE spectra. Though the spectra of **14** and **15** are blue-shifted with 30 and 20 nm differences respectively with respect to **17**, the increase in J_{sc} value contributed to a better PV performance. Dye **15** could deliver over 60% IPCE value from 400 to 600 nm with a maximum of 83% at 450 nm, resulting in a J_{sc} value of 12.9 mA cm^{-2} (Table 1). While comparing the π -spacers, furan substituted sensitizers **15** and **17** were found to deliver better efficiencies than their thiophene substituted counterparts. While **15** delivered a PCE of 7.09% with the highest J_{sc} and V_{oc} values, **14** slightly lagged with a power conversion efficiency of 6.05%. DCRD substituted dyes **16** and **17** showcased relatively poor performances with a PCE of 4.55% and 4.81%, respectively.

Later, Su and co-workers introduced sensitizers **18–20** based on new molecular architecture, D-D|A- π -A (Fig. 5).²⁷ Here, D|A



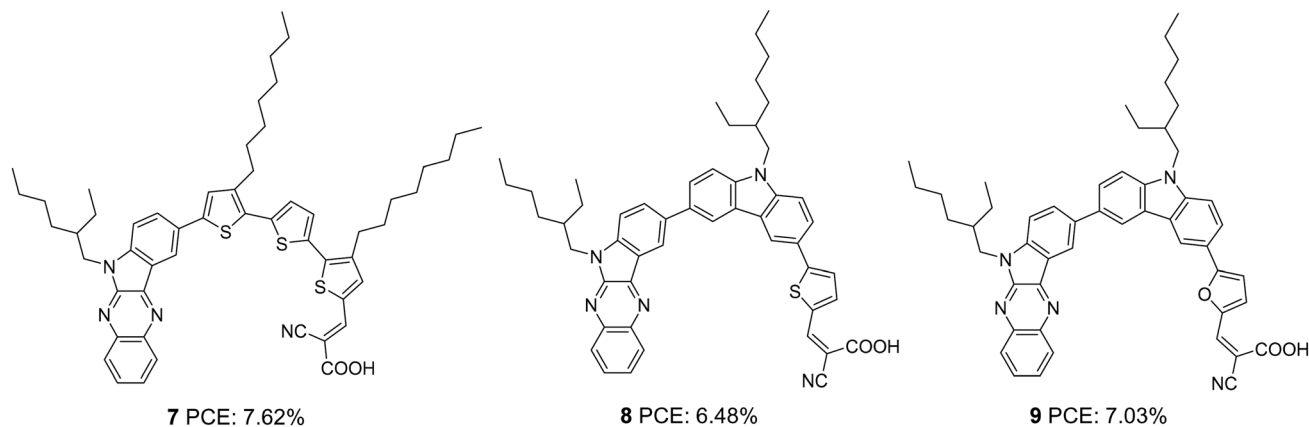


Fig. 2 Photosensitizers **7–9** based on an indolo[2,3-*b*]quinoxaline core.

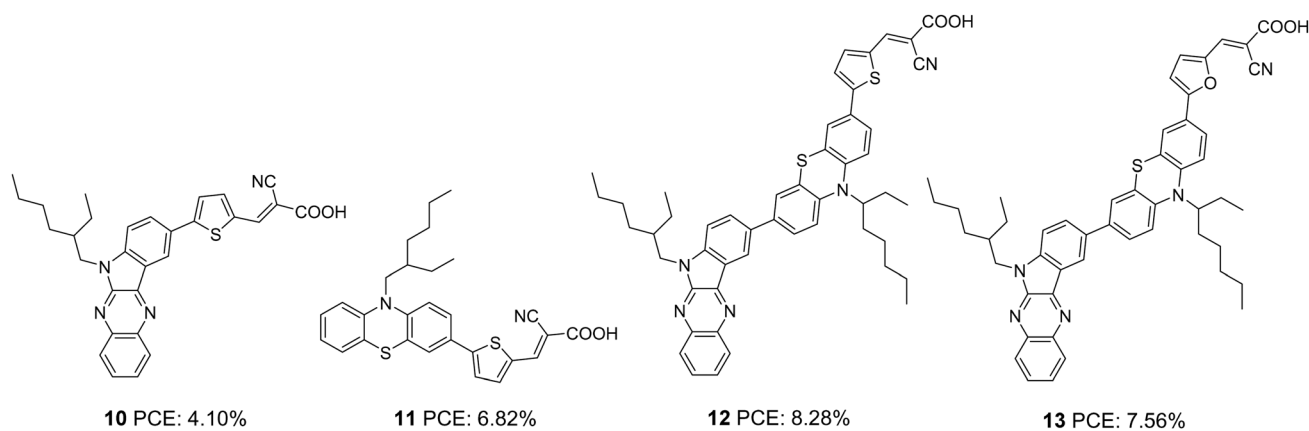


Fig. 3 Photosensitizers **10–13** based on indolo[2,3-*b*]quinoxaline and phenothiazine cores.

represents the fused donor–acceptor unit, indolo[2,3-*b*]quinoxaline. The effect of additional donors was investigated systematically by introducing triphenylamine, carbazole and phenothiazine donors to the indole unit. More significant dye loading in devices based on **18** resulted in effective monolayer formation on the TiO₂ surface, thereby preventing recombination effectively. This contributed to the highest open-circuit potential for devices fabricated using **18**. When it comes to photocurrent, the hexyl chains incorporated on the end donors of **19** and **20** helped decrease aggregations, contributing to improved J_{sc} . Maximum efficiency was delivered by **19** (2.72%), followed by **18** (2.65%) and **20** (2.61%). Later, these new generation D–D/A– π –A organic dyes were used successfully as co-sensitizers to improve the PCE of conventional Ru dye (**21**). The device fabricated with **21** alone showed an efficiency of 7.46%. Co-sensitization of **18–20** improved the efficiency in all three cases with a maximum of 7.94%, when **19** was employed as a co-sensitizer with **21** (Table 1). An increment in open-circuit potential was observed with the co-sensitization approach, which could be attributed to the improved surface coverage of TiO₂, resulting in retardation of aggregation and recombination. When it comes to photocurrent, only the device with **19** as a co-sensitizer

showed an increment in current density from 19.00 mA cm⁻² to 19.37 mA cm⁻². More significant dye loading in the remaining cases might have resulted in competitive absorption at the overlapping regions between the Ru dye and organic co-sensitizer.

Later, Su *et al.* introduced a di-branched di-anchoring approach to the previous molecular architecture to develop D–D[A–(π -A)₂] dyes **22** and **23**, which differed in additional donors between triphenylamine and carbazole, respectively (Fig. 6).²⁸ The performances were also compared with devices based on **19**. The dianchoring approach was found to help form adequate surface coverage, which is also evident from the higher dye loading present in these dyes. This could cause an increment in V_{oc} of dianchored dyes compared to **19** due to minimal recombination. Among the dianchored dyes, **23** with hexyl chain incorporated carbazole as the secondary donor exhibited the highest V_{oc} . Dye **19** excelled when photocurrent is taken into account, which even contributed to higher PCE compared to the rest. The downfall in light-harvesting efficiency of **22–23** was brought about by the increased dihedral angle and strain induced by the di-anchoring branches. A more prominent donating ability of carbazole caused a slightly higher increment in J_{sc} of **23** compared to **22**. Co-sensitization of these



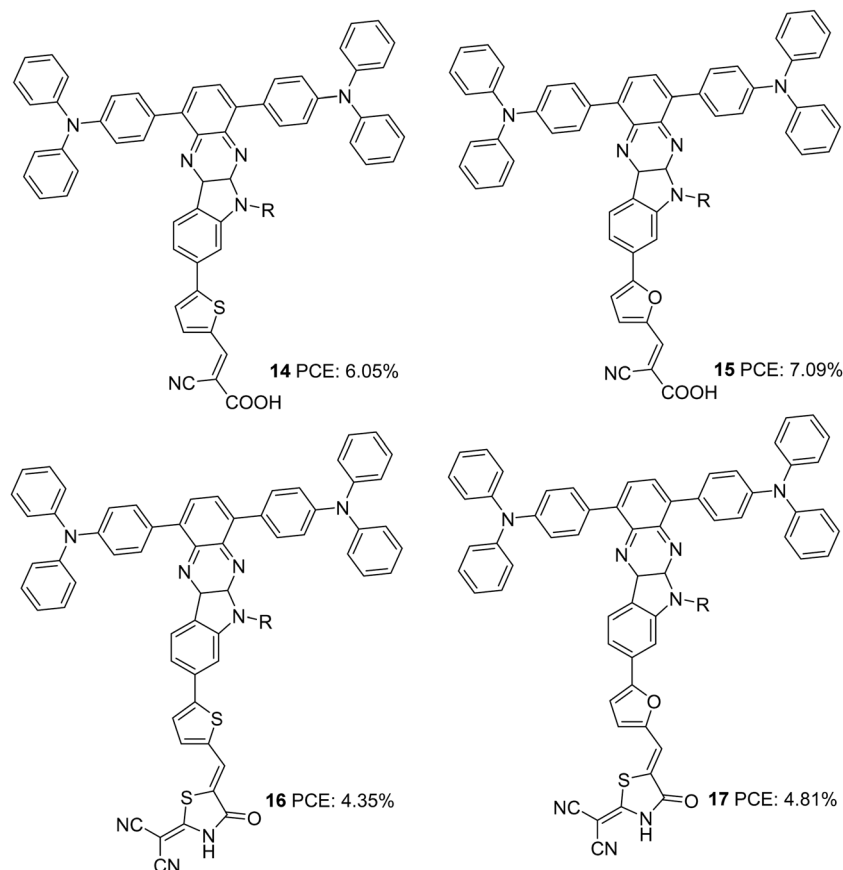


Fig. 4 Photosensitizers **14–17** with an indolo[2,3-*b*]quinoxaline core.

dyes with **21** could enhance the efficiency with the highest PCE of 8.67% for **23**, followed by **13** (8.16%) and **19** (7.50%). While the considerably improved V_{oc} contributed the increment in device performance of co-sensitized **22–23**, a slight increment in current density for **19** caused a corresponding increment in PCE.

In the subsequent work, the π -spacer in **18–20** was changed to thiophene from benzene, and the performance of the sensitizers (**24–26**) was evaluated under full sun illumination (Fig. 7).²⁹ The dyes exhibited efficiencies in the range 4.92–5.27%, which was higher than previously reported sensitizers having phenyl as a spacer. Dye **24**, having triphenylamine as a donor, displayed the maximum PCE of 5.27% with a V_{oc} of 0.67 V and FF of 70.1 with improved J_{sc} of 11.10 mA cm⁻² (Table 1). Higher dye loading seems to be responsible for improving FF and open-circuit potential for the triphenylamine donor dye **24**. Though the highest photocurrent was observed for **26** due to its increased light-harvesting ability, comparatively lower values obtained for the rest of the parameters contributed towards inferior PCE of 4.92% for **26**. Co-sensitization of **21** with these dyes also resulted in improved V_{oc} and FF. In addition, the competition for light absorption resulted in a considerable reduction of photocurrent, leading to net poor performance for the co-sensitized device compared to the individual dyes.

From Table 1, it is clear that indoloquinoxaline is a potential scaffold for dye sensitizers in DSSCs. The highest efficiency

achieved so far using IQ based sensitizer is 8.2%, where the IQ unit and π -spacer (thiophene) is attached to either end of the auxiliary donor (phenothiazine) with cyanoacrylic acid as the acceptor unit. In the same architecture itself, optimum tuning of auxiliary donors and π -spacers along with the alkyl groups could render sensitizers capable of delivering more than 10% PCE. From the reported sensitizers using IQ, it is impossible to generalize suitable π -spacers for the system that could change depending on the donor attached to it and the IQ position (indole/quinoxaline end) to which it is attached. Many studies were not carried out in this direction of anchoring units, opening up further possibilities towards efficient IQ-based devices.

II. Indolocarbazole based sensitizers for DSSCs

Indolocarbazole, especially indolo[3,2-*b*]carbazole isomer, is a linear pentacene with two N-atoms with the possibility of introducing alkyl chains of any length requirement either to improve solubility or to prevent back electron transfer. When compared to carbazole, indolocarbazole possesses better energetics, improved electron-donating capabilities and superior absorption profiles. These characteristics find indolocarbazoles



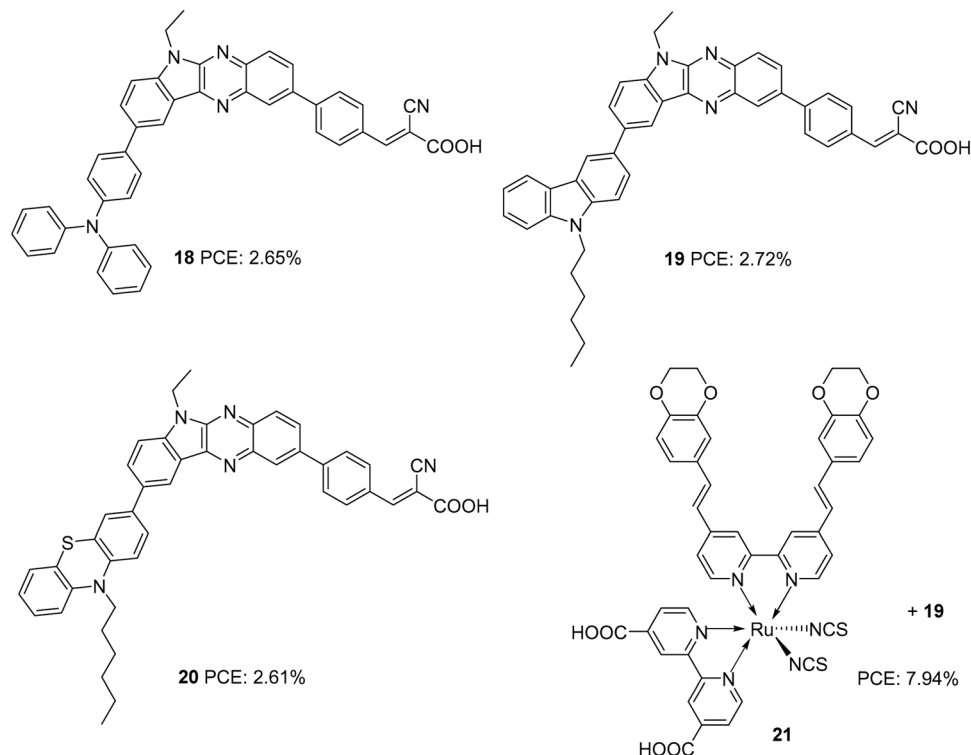


Fig. 5 Photosensitizers with an indolo[2,3-*b*]quinoxaline moiety and Ru-complex.

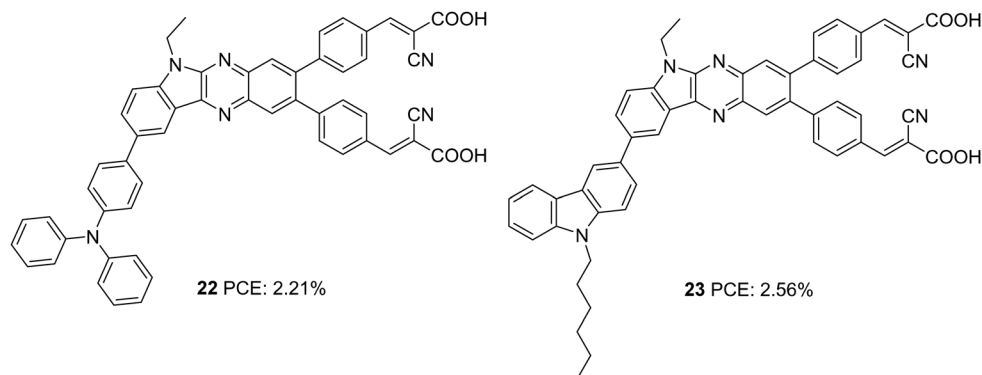


Fig. 6 Photosensitizers **22–23** with an indolo[2,3-*b*]quinoxaline moiety.

a unique position among various applications involving organic thin-film transistors, organic light-emitting diodes and photovoltaics.³⁰ Indolocarbazoles can be prepared either by Fischer indole synthesis of 1,4-bis(2-phenylhydrazono)cyclohexane or by a Cadogen reaction of appropriate nitroarenes.³¹

Indolocarbazole was first used as a donor in DSSCs by Zang *et al.* (Fig. 8).³² They synthesized dyes **27** and **28**, which differ in the number of thiophene groups incorporated as the π -linker. While a red shift in the absorption profile was observed for **28** when adsorbed on TiO₂, higher electron injection efficiency was obtained for **27** sensitized devices. The trade-off between the two factors renders **28** with slightly higher J_{sc} compared to that of **27**. The difference in efficiencies of the two dyes were also

brought about by the fill factor. While **27** possesses a FF of 0.67, the larger molecular size of **28** resulted in a FF of 0.62 (Table 2). This resulted in a higher PCE of 7.3% for **27** and 6.7% for **28**.

Cai *et al.* designed four dyes based on 5,7-dihexyl-6,12-diphenyl-5,7-dihydroindolo[2,3-*b*]carbazole (DDC) with benzothiadiazole (or thiophene) and thieno[3,2-*b*]thiophene (TT) (or thiophene) as the π -spacer and 2-cyanoacrylic acid as an acceptor (Fig. 9).³³ Along with the high electron-donating ability, the fused carbazole systems also contribute towards improved π -conjugation, which will be advantageous in promoting the ICT and the photostability of the system. The two phenyl rings integrated on the donor DDC unit, and the alkyl groups on the nitrogen atom effectively reduced the aggregation



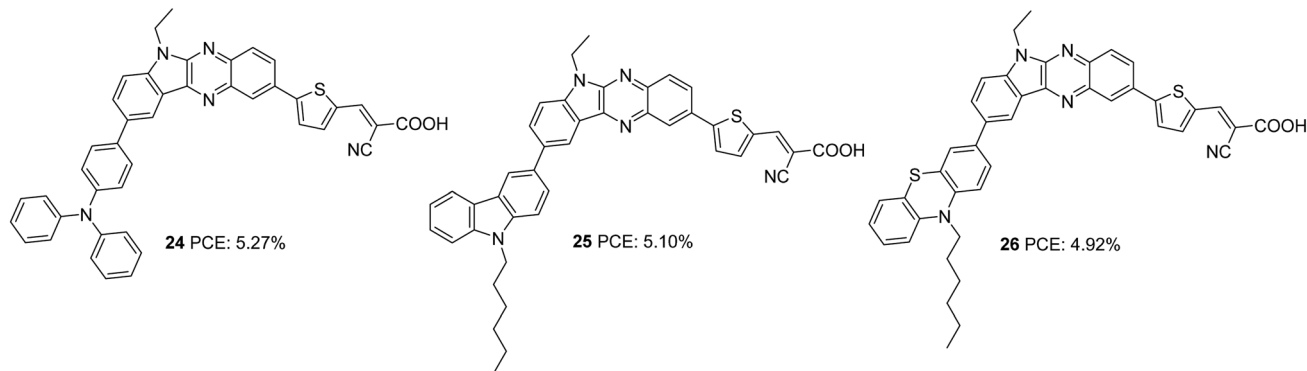


Fig. 7 Photosensitizers **24–26** with an indolo[2,3-*b*]quinoxaline moiety.

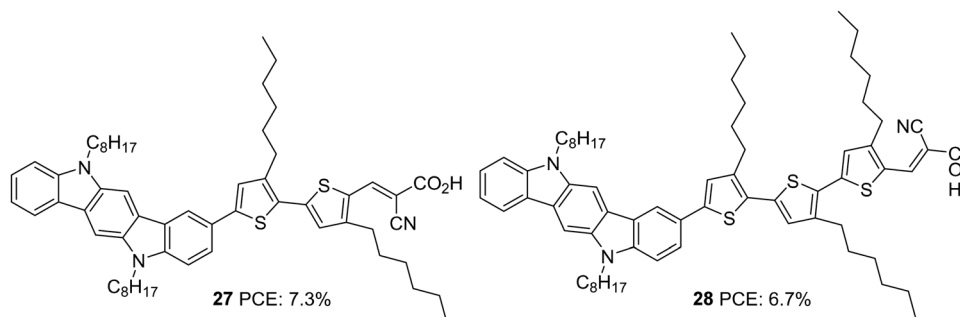


Fig. 8 Photosensitizers **27–28** with an indolocarbazole moiety.

and improved the lifetime for devices fabricated with these dyes. The devices were also subjected to comparison with carbazole based D- π -A sensitizer **33**. The molar extinction coefficients of both ICT and π - π transition bands display significant enhancement in **29–32** compared to **33** indicating the improved light-harvesting ability of the new fused conjugated donor. Except for **31**, the J_{sc} value for all other dyes was higher than **33**. This is apparent from the IPCE spectra, where the performance follows the order **32** > **29** > **30** > **33** > **31**, which is consistent with the dye loading present in the fabricated devices. Though the V_{oc} value of **32** (674 mV) was not very high compared to **31** (768 mV), **32** exhibited the highest efficiency of 6.4% among these sensitizers with a J_{sc} of 13.96 mA cm⁻² and FF of 0.68 (Table 2). The photostability evaluation of the dyes by adopting the methods of Katoh and co-workers revealed that the new donor is effective in stabilizing the cation formed after irradiation of light compared to the carbazole based dye. The benzothiadiazole containing dyes possess more stability which is consistent with the previous reports.³⁴ The results also paved the way to the observation that TT was also beneficial for contributing towards photostability. Compound **32**, having both BTD and TT as a π -spacer, exhibited maximum photostability, while **29** was least stable among the indolocarbazole based dyes. All the dyes were also found to be thermally stable.

The same group further attempted to introduce a bridge with extended conjugation to widen the absorption spectra of the indolocarbazole dyes (Fig. 10).³⁵ Among the dyes, **36**, which contains benzothiadiazole as an auxiliary acceptor along with

alkylated thiophenes flanked on both sides, showed maximum red-shifted spectra followed by **35** having alkyl-substituted benzothiadiazole as an auxiliary acceptor and **34** with simple D- π -A architecture having ter-thiophene as a spacer with a difference of 78 and 50 nm, respectively, compared to **36**. The device efficiency was tested under two conditions. In one case, the TiO₂ films were made of 3 μ m thickness with 13 nm sized nanoparticles (TSP) and scattering layer of 4 μ m thickness, and in the second case, the TiO₂ films were made of 3 μ m thickness with 13 nm sized nanoparticles (TSP) and scattering layer of 8 μ m thickness. Though higher dye loading is possible in the second case, a thick scattering layer can cause chances of recombination. This resulted in a trend of increase in current density and decrease in V_{oc} for all the dyes fabricated with an 8 μ m scattering layer when compared to those of 3 μ m thickness. A trade-off between these two factors leads to higher PCE with a thicker scattering layer for all the dyes. In the first condition, the highest IPCE value was obtained for **36** with an absorption maximum of 81.2% at 460 nm followed by **35** (77.2% at 500 nm) and **34** (69.9% at 520 nm). A more comprehensive absorption profile for **36** contributed towards the highest J_{sc} value of 14.91 mA cm⁻². The least J_{sc} value of 10.40 mA cm⁻² was obtained for **34** due to the narrow IPCE spectra resulting from a lower absorption profile (Table 2). When devices were fabricated using an 8 μ m scattering layer, dye **35** showed improved IPCE profile and J_{sc} value, while dye **36** resulted in lower molar extinction coefficients, low dye loading amount, and low electron injection yield. The trend in V_{oc} was the same in both the



Table 2 Photovoltaic parameters of indolocarbazole based DSSCs

Sensitizer	J_{sc} (mA cm ⁻²)	V_{oc} (mV)	FF	PCE (%)	Electrolyte	Coadsorbent (concentration)	Ref.
27	15.4	710	0.67	7.3	I ⁻ /I ₃ ⁻	—	32
28	15.5	700	0.62	6.7	I ⁻ /I ₃ ⁻	—	32
29	11.95	768	0.66	6.09	I ⁻ /I ₃ ⁻	—	33
30	11.57	707	0.68	5.55	I ⁻ /I ₃ ⁻	—	33
31	9.40	644	0.68	4.11	I ⁻ /I ₃ ⁻	—	33
32	13.96	674	0.68	6.40	I ⁻ /I ₃ ⁻	—	33
33	10.28	713	0.67	4.90	I ⁻ /I ₃ ⁻	—	33
34 ^a	10.40	747	0.70	5.43	I ⁻ /I ₃ ⁻	—	35
34 ^b	12.92	710	0.66	6.01	I ⁻ /I ₃ ⁻	—	35
35 ^a	13.44	752	0.65	6.53	I ⁻ /I ₃ ⁻	—	35
35 ^b	16.41	706	0.64	7.49	I ⁻ /I ₃ ⁻	—	35
36 ^a	14.91	651	0.67	6.48	I ⁻ /I ₃ ⁻	—	35
36 ^b	15.88	620	0.68	6.64	I ⁻ /I ₃ ⁻	—	35
37	12.6	729	0.68	6.25	I ⁻ /I ₃ ⁻	—	36
38	15.2	745	0.71	8.09	I ⁻ /I ₃ ⁻	—	36
39	13.9	738	0.68	6.98	I ⁻ /I ₃ ⁻	—	36
40	14.1	757	0.71	7.58	I ⁻ /I ₃ ⁻	—	36
41	5.69	750	0.72	3.11	I ⁻ /I ₃ ⁻	CDCA (1 mM)	37
42	5.09	750	0.74	2.83	I ⁻ /I ₃ ⁻	—	37
43	3.89	610	0.69	1.65	I ⁻ /I ₃ ⁻	—	37
44	10.16	710	0.71	5.12	I ⁻ /I ₃ ⁻	—	38
45	12.85	720	0.69	6.34	I ⁻ /I ₃ ⁻	—	38
44/45	13.38	740	0.71	7.03	I ⁻ /I ₃ ⁻	—	38
46	12.45	690	0.70	6.02	I ⁻ /I ₃ ⁻	—	39
47	10.73	731	0.74	5.78	I ⁻ /I ₃ ⁻	—	40
48	9.81	680	0.78	5.23	I ⁻ /I ₃ ⁻	—	40
49	10.95	754	0.72	5.97	I ⁻ /I ₃ ⁻	—	40
50	7.05	690	0.53	2.56	I ⁻ /I ₃ ⁻	—	41
51	9.78	660	0.57	3.68	I ⁻ /I ₃ ⁻	—	41
52	4.04	620	0.64	1.59	I ⁻ /I ₃ ⁻	—	41
53	7.57	640	0.53	2.5	I ⁻ /I ₃ ⁻	—	41
54	12.16	560	0.69	4.68	I ⁻ /I ₃ ⁻	CDCA (10 mM)	42
55	11.43	610	0.69	4.66	I ⁻ /I ₃ ⁻	CDCA (1 mM)	42

^a TiO₂ films were made with 4 μm thick scattering layer. ^b TiO₂ films were made with 8 μm thick scattering layer.

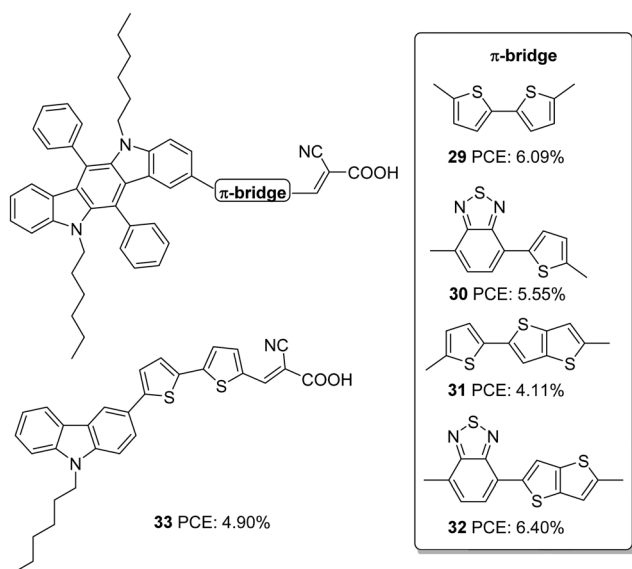


Fig. 9 Photosensitizers with indolo[2,3-*b*]carbazole (29–32) and carbazole (33) units.

conditions with the least value delivered by 36. While 35 excelled with the highest PCE of 7.49%, 34 delivered a lower

photovoltaic performance of 6.01%. The stability studies reinforced the observation that BTD units are capable of increasing the photo-stability of dyes.

Later in 2016, Qian *et al.* investigated the same donor groups in a new photosensitizer design. They synthesized four dyes utilizing modified donor units (Fig. 11) consisting of indolo[3,2-*b*]carbazole as the primary donor and groups such as ethylbenzene, *N,N*-diethylaniline, ethyloxybenzene, and octyloxybenzene grafted to indolo[3,2-*b*]carbazole as secondary donor groups, thiophene as the π -conjugated linker, and 2-cyanoacrylic acid unit as the electron acceptor/anchoring group.³⁶ The secondary donor groups assist in improving the donating strength of the system, but it was also highly beneficial for reducing the aggregation and recombination. Thus the nonplanar secondary groups could enhance the photovoltage of the device. The IPCE performance of the dyes parallels with the electron-donating ability of the secondary donor. The most robust donor, *N,N*-diethylaniline attached dye 38, displayed a broad IPCE response and highest J_{sc} of 15.2 mA cm⁻² followed by 40, 39 and 37 (Table 2). The efficiency of the devices also follows the same trend, with 30 having the highest PCE of 8.09%, and the most deficient performance was showcased by 37 with 6.25%.

Later, Xiao *et al.* also employed 6,12-diphenylindolo[3,2-*b*]carbazole as auxiliary donors in D–D– π –A dyes.³⁷ The sensitizers 41, 42 and 43 differ in the donor groups: triphenylamine, trimethoxyphenyl and trimethoxybromine, respectively (Fig. 12). Unlike the previous work, the additional donor and π -spacers were appended to the end of the phenylene groups attached to the indolo[3,2-*b*]carbazole moiety. The ICT absorption bands of these compounds did not show much difference compared to the π – π^* transition, which can be attributed to the interrupted charge transfer in the molecules resulting from the non-planar conformation of the attached phenyl groups. The absorption behaviour of the compounds was consistent with the electron-donating ability of the secondary donor. The triphenylamine donor in 41, which has a higher electron-donating ability, contributed to the broader absorption and higher molar extinction coefficient for 41, followed by 42 and 43. Though these dyes could deliver reasonably good V_{oc} (0.61–0.75 V) and FF (0.69–0.74) using I⁻/I₃⁻ electrolyte, a relatively low value of J_{sc} resulted in moderate PCE (1.65–3.11%). Dye 41 yielded the highest efficiency of 3.11% followed by 42 and 43 (Table 2).

Further investigations by the same group to increase the photoconversion efficiency of 41 resulted in the synthesis of 44 and 45 where a triphenylamine donor was attached to indolo[3,2-*b*]carbazole *via* the ninth and eighth positions, respectively (Fig. 13).³⁸ Co-planarity and π -electron delocalization were found to improve, which is apparent from the absorption profile of the new dyes 44 and 45. Dye 45, where the phenylene/thiophene rings were connected onto the para positions of the *N*-atom, showed more red-shifted absorption with an absorption maximum at 500 nm, whereas absorption of 44 was blue-shifted by 38 nm. While 44 showed improvement in PCE when it was used in conjunction with CDCA (10 mM), 45 responded in a reverse manner. This can be accounted for by



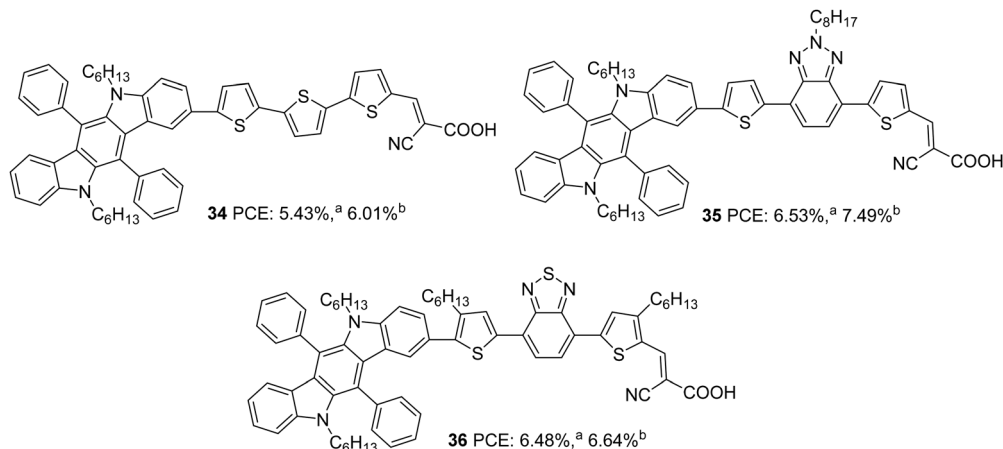


Fig. 10 Photosensitizers **34–36** with an indolo[2,3-*b*]carbazole moiety. ³⁹TiO₂ films were made with a 4 μm thick scattering layer. ³⁹TiO₂ films were made with an 8 μm thick scattering layer. In both cases, the active layer was made of 3 μm thick 13 nm particles.

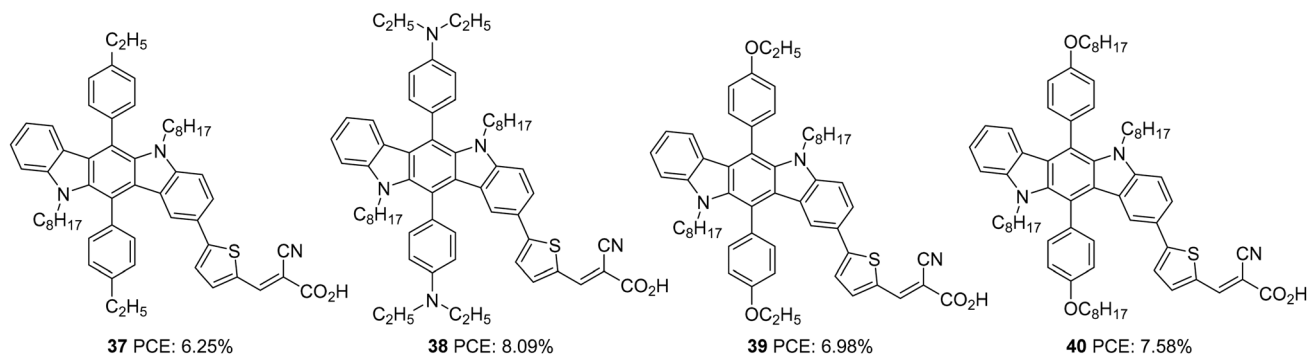


Fig. 11 Photosensitizers **37–40** with an indolo[2,3-*b*]carbazole moiety.

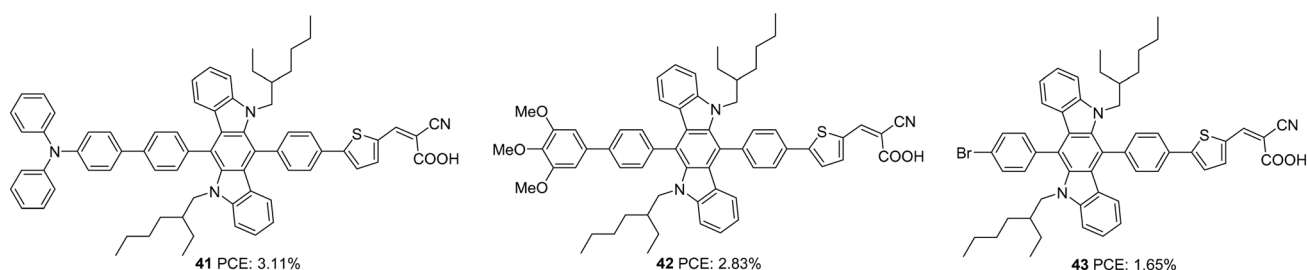


Fig. 12 Photosensitizers **41–43** with an indolo[2,3-*b*]carbazole moiety.

the molecular orientation of the dyes when adsorbed on TiO₂. Dye **44** adopted a perpendicular orientation to the substrate plane. Somewhat hindered conformation of **45** resulted in more inclination of the dye towards the TiO₂ surface. This resulted in fewer aggregations and recombinations, making **45** capable of delivering more photocurrent even with a lower dye loading of $3.64 \times 10^{-7} \text{ mol cm}^{-2}$ compared to $4.54 \times 10^{-7} \text{ mol cm}^{-2}$ for **44** and without co-adsorbent CDCA. Photosensitizer **45** outperformed **44** with a J_{sc} of 12.85 mA cm^{-2} , V_{oc} of 0.72 V, FF of 0.69 and PCE of 6.34% (Table 2). The co-sensitization of **44/45** further improved the performance to 7.03%.

Indolo[2,3-*b*]carbazoles were rarely explored for optoelectronic applications due to a lack of efficient synthetic strategies. Su *et al.* could establish new strategies for synthesising indolo[2,3-*b*]carbazoles and their utilization to construct DSSC sensitizers with a PCE of up to 6.02%.³⁹ The curved molecular conformation of indolo[2,3-*b*]carbazole dye synthesized by Su *et al.* (**46**), along with its rigid and planar nature, offer the possibility to be explored as a di-anchor dye. The sensitizer **46** adopts A- π -D- π -A architecture in which bithiophene is introduced as the π -bridge between the electron-rich indolo[2,3-*b*]carbazole core and cyanoacrylic acid acceptor unit (Fig. 14). FTIR analysis of the pristine **46**



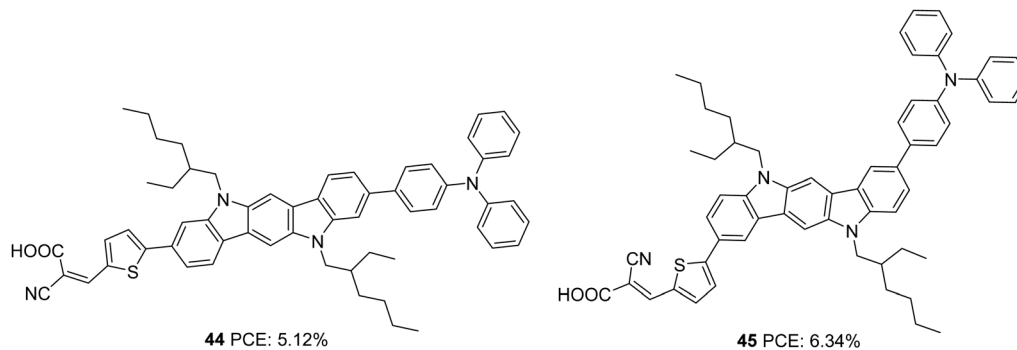


Fig. 13 Photosensitizers **44–45** with an indolo[2,3-*b*]carbazole moiety.

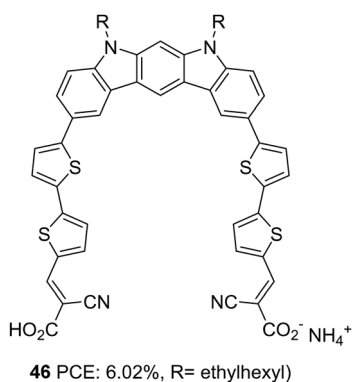


Fig. 14 Molecular structure of photosensitizer **46**.

and the compound loaded TiO₂ film reveals the involvement of both the carboxylic group in anchoring the dye on the TiO₂ surface. This is further confirmed by the Deacon Philips rule, where a frequency difference of 224 cm⁻¹ suggests a bidentate binding mode for **46**. An efficient electron transfer from the HOMO of **46**/(TiO₂)₇₀ (indolo[2,3-*b*]carbazole) to the LUMO of **46**/(TiO₂)₇₀ (TiO₂ nano cluster) was illustrated using computational analysis.

Indolo[2,3-*a*]carbazole was first introduced in DSSCs by Zhang *et al.*⁴⁰ Taking this new system as a donor and cyanoacrylic acid as an acceptor, they studied the effect of conjugate mode of π -spacers such as thienyl-thieno[2,3-*b*]thiophene and terthiophene in photovoltaic performance (Fig. 15). To control dye aggregation and prevent recombination, alkyl-substituted

terthiophene was employed as a π -spacer to construct **49**. Sensitizers **47** and **49** outperformed **48** in J_{sc} and V_{oc} . **48** gave an efficiency of 5.28%. The spatial effect of hexyl groups on the π -backbone of **49** resulted in the highest efficiency of 5.98% and the highest photocurrent and photovoltage, followed by **47** with 5.78% PCE (Table 2).

Indolo[3,2,1-*jk*]carbazole is another positional isomer of indolocarbazole where indole is fused with the carbazole moiety in a slightly strained manner. The system was found to be thermostable and showcase strong electron-donating ability, which resulted in its application as a charge transport material and conducting film material. Luo *et al.* utilized this core for developing a sensitizer for DSSCs by integrating it as a donor in a D- π -A architecture (Fig. 16).⁴¹ They developed four devices based on the dyes **50–53**, which exhibited PCE in the range 1.59–3.68%. Among the dyes, **51** outperformed others with a PCE of 3.68% (Table 2). With its lower stabilization energy, thiophene enabled the system to have more delocalization and efficient light-harvesting ability. This can be accounted for by the enhanced photocurrent in dyes **51** and **53** using thiophene as the π -linker. Low spectral coverage leads to decreased performance in **50** and **52**. Even an attempt to increase the π -bridge conjugation by introducing the phenyl group in **52** was not found to be an effective strategy to increase the PCE.

Further attempts were carried out to investigate the effect of π -linkers on the performance of indolo[3,2,1-*jk*]carbazole based dyes by Cao *et al.* (Fig. 17).⁴² Dyes **54** and **55** incorporate bithiophene and unsubstituted bithiophene, respectively as π -linkers. The slightly twisted conformation of **55** resulted in lower dye loading on TiO₂ than **54**, resulting in a slight increment in the J_{sc} value for **54**, the reverse trend of what was observed for V_{oc} . The significant improvement in J_{sc} of the **54** based device, when adsorbed with CDCA, illustrates the aggregation tendency of these sensitizers on TiO₂. While the **54** based devices delivered PCE of 4.68% in the presence of 10 mM CDCA, dye **55** could yield 4.66% with 1 mM CDCA (Table 2).

Among different isomers of indolocarbazole, indolo[3,2-*b*]carbazole is the most explored isomer for DSSC applications. The comparison of efficiency *versus* structure reveals that to improve the device's performance, systematic investigation of the position of attachment of the π -spacer and the additional

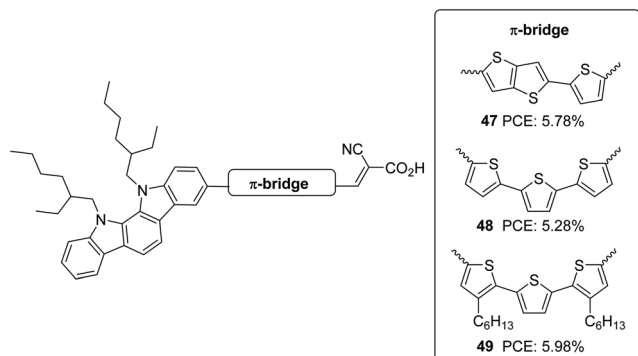


Fig. 15 Photosensitizers **47–49** with an indolo[2,3-*a*]carbazole moiety.



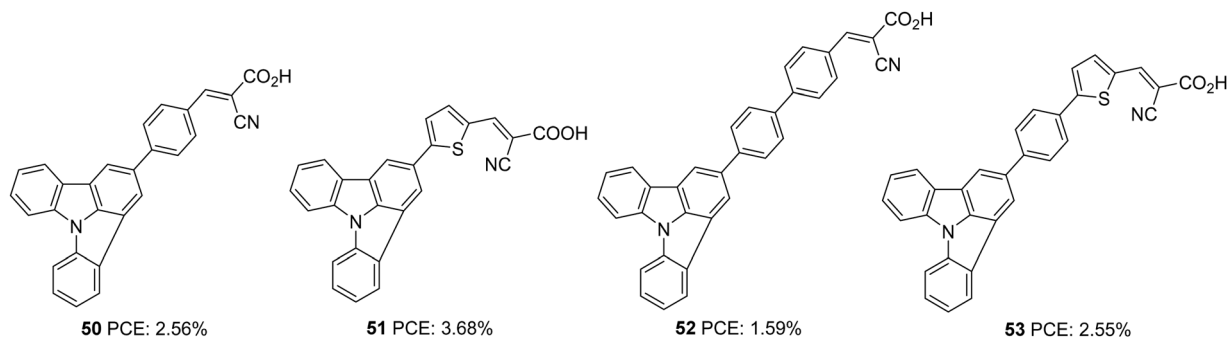


Fig. 16 Photosensitizers **50–53** with an indolo[3,2-*b*]carbazole moiety.

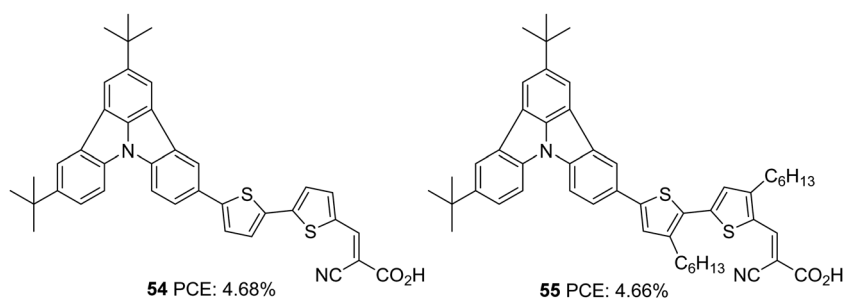


Fig. 17 Photosensitizers **54–55** with an indolo[3,2-*b*]carbazole moiety.

donor on indolo[3,2-*b*]carbazole is also needed, along with the integration of suitable donor and spacer groups. From the reported data so far, the substitution of donor and spacer units at the second and eighth positions of indolo[3,2-*b*]carbazole is more effective than substitution at the ninth and third positions. When the donor group was changed to DDC, the additional phenyl groups integrated at the sixth and twelfth positions were found to prevent recombination while preserving the donating ability and the backbone's planarity. However, attempts to increase the light-harvesting by allowing modifications at these phenyl groups could not lead to realize photovoltaic performance as expected due to the non-planar conformation of the phenyl groups as seen in the case of dyes **41** and **42**.

III. Triazatruxene based sensitizers for DSSCs

Triazatruxene (TAT) is an expanded π -conjugated system with good electron-donating capacity, consisting of three indole units combined using one benzene ring. Due to its favourable features such as electron richness and rigid π -extended structure, it has found application in various optoelectronic fields, like organic field-effect transistors (OFETs), organic light-emitting diodes (OLEDs), two-photon absorption (TPA) materials, non-linear optics and liquid crystal displays.⁴³ The most widely used method for the synthesis of TAT is by the reaction between indole and indolone in the presence of bromine and POCl_3 .⁴⁴

The first attempt to use TAT as a donor in DSSCs was reported by Qian *et al.*⁴⁵ They succeeded in developing three

D- π -A dyes (**56**, **57**, **58**) with variable π -spacers achieving more than 5% efficiency. These dyes were made using TAT as the donor and cyanoacrylic acid as the acceptor/anchoring group (Fig. 18). The system's efficiency was studied by changing the π -spacers (thiophene **56**, furan **57** and benzene **58**). Though high open-circuit voltage was found in dye **58**, with a reduced current density, devices fabricated with **58** only realized a low PCE of 5.11%. The highest efficiency of 6.1% was contributed by the device fabricated using dye **56**. The higher PCE resulted from higher current density showcased by **56**, which was also evident from the IPCE response (Table 3). Better electron delocalization and superior electron-donating capabilities render the TAT system improved light-harvesting behaviour to be used as an efficient sensitizer in DSSCs.

As an extension of the previous experiments, the effect of rhodanine-3-acetic acid as an electron-withdrawing/acceptor

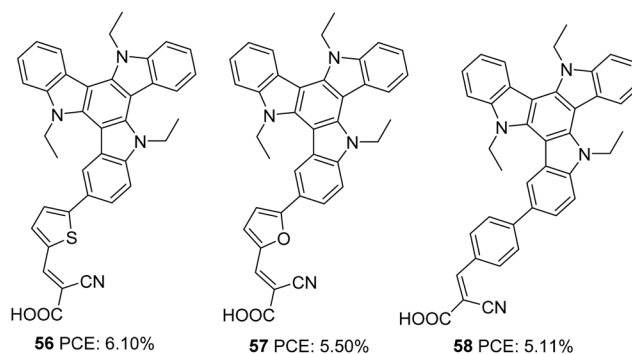
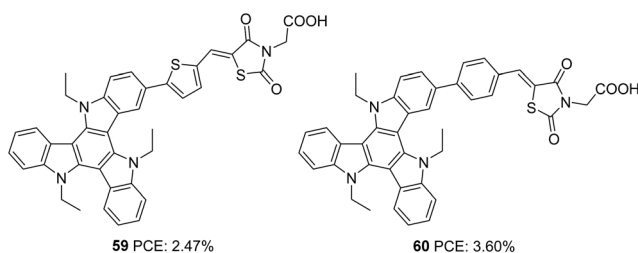


Fig. 18 Photosensitizers **56–58** with a triazatruxene moiety as a donor.



Table 3 Photovoltaic parameters of triazatruxene based DSSCs

Sensitizer	J_{sc} (mA cm ⁻²)	V_{oc} (mV)	FF	PCE (%)	Electrolyte	Coadsorbent (concentration)	Ref.
56	14.7	670	0.62	6.10	I ⁻ /I ₃ ⁻	—	45
57	13.6	654	0.62	5.50	I ⁻ /I ₃ ⁻	—	45
58	11.6	686	0.64	5.11	I ⁻ /I ₃ ⁻	—	45
59	5.89	582	0.72	2.47	I ⁻ /I ₃ ⁻	CDCA (10 mM)	46
60	8.33	617	0.70	3.60	I ⁻ /I ₃ ⁻	CDCA (10 mM)	46
61	14.97	793	0.63	7.5	I ⁻ /I ₃ ⁻	CDCA (5 mM)	47
62	16.45	707	0.62	7.15	I ⁻ /I ₃ ⁻	CDCA (5 mM)	47
63	13.46	775	0.62	6.50	I ⁻ /I ₃ ⁻	CDCA (5 mM)	47
64	15.89	743	0.62	7.26	I ⁻ /I ₃ ⁻	CDCA (5 mM)	47
65	11.4	722	0.68	5.55	I ⁻ /I ₃ ⁻	CDCA (0.4 mM)	48
66	13.2	741	0.68	6.65	I ⁻ /I ₃ ⁻	CDCA (0.4 mM)	48
67	11.0	849	0.53	5.2	I ⁻ /I ₃ ⁻	CDCA (0.5 mM)	49
68	20.73	956	0.69	13.6	[Co(bpy) ₃] ^{2+/3+}	CDCA (2 mM)	50
69	20.57	887	0.70	12.8	[Co(bpy) ₃] ^{2+/3+}	CDCA (2 mM)	50
68^a	9.9	952	0.70	6.6	[Co(bpy) ₃] ^{2+/3+}	CDCA (2 mM)	51
69^a	8.4	945	0.69	5.4	[Co(bpy) ₃] ^{2+/3+}	CDCA (2 mM)	51
70	11.94	808	0.74	7.20	[Co(bpy) ₃] ^{2+/3+}	CDCA (2 mM)	52
71	15.1	966	0.70	10.2	[Co(bpy) ₃] ^{2+/3+}	—	53
72	13.4	934	0.69	8.6	[Co(bpy) ₃] ^{2+/3+}	—	53
73	16.92	926	0.75	11.7	[Co(bpy) ₃] ^{2+/3+}	—	54
74	15.98	911	0.73	10.6	[Co(bpy) ₃] ^{2+/3+}	—	54

^a ssDSSC.Fig. 19 Photosensitizers **59–60** with a triazatruxene moiety as a donor.

group was studied by the same group (Fig. 19).⁴⁶ Though much broader absorption was obtained for dyes with rhodanine-3-acetic acid, the performance of these dyes was inferior to the dyes being synthesized using cyanoacrylic acid as the electron-withdrawing group. This is attributed to the interruption of electron transfer from the dyes to the semiconductor by the broken (NCH₂COOH) conjugation in rhodanine-3-acetic acid. Instead of displaying broader absorption spectra with higher ϵ , devices fabricated using **59** showed lower current density. The trend can be rationalized from the LUMO energy level of the dyes, which are in the order of **60** (−1.16 V) > **59** (−1.02 V), indicating more effective electron injection from **60** to the semiconductor. Thus **60** could yield a higher PCE of 3.60% with a short-circuit photocurrent density of 8.33 mA cm⁻², an open-circuit photovoltage of 617 mV, and a fill factor of 0.70 (Table 3).

Triazatruxene was incorporated as a donor in D–A– π –A based sensitizers by Pan and co-workers in 2018 (Fig. 20).⁴⁷ These sensitizers employed benzothiadiazole as an auxiliary acceptor, and they introduced variation in the acceptors (carboxylic acid and cyanoacrylic acid), and the connectivity between the donor and auxiliary acceptor was modified using single bond and ethynyl linkages. The introduction of the ethynyl linker and cyanoacrylic acid was found to increase the

conjugation of the dye molecules. Dyes **62** and **64** having cyanoacrylic acid as the acceptor group showed better light-harvesting capability with broader absorption and higher IPCE value. These observations were also reflected in the J_{sc} value of the corresponding sensitizers. Another critical parameter that determines the efficiency of the system is the V_{oc} . Dyes **61** and **63** with a single carboxylic acid acceptor exhibited higher photovoltage compared to the rest. Among the two sets of D–A– π –A sensitizers having a triazatruxene donor (single bonded and ethynyl bridged), dyes **61** and **64** showed maximum efficiencies of 7.51% and 7.26%, respectively, which indicates that a delicate balance between J_{sc} and V_{oc} is essential to obtain higher power conversion efficiencies (Table 3).

Qian and co-workers used triazatruxene as a secondary electron donor to construct porphyrin-based sensitizers (Fig. 21).⁴⁸ Triazatruxene was attached directly to the meso-position of the porphyrin ring, and two variants were synthesized by changing the acceptor groups (carboxylic acid and cyanoacrylic acid). When cyanoacrylic acid was employed as an acceptor group, improvement was found in the dye's light-harvesting ability, which is evident from the broader and enhanced IPCE spectra resulting in a higher J_{sc} value dye (Table 3). The V_{oc} value also follows the same trend, which resulted in a maximum PCE of 6.05% for **66**. The efficiencies of both dyes were found to improve when co-adsorbent chenodeoxycholic acid (CDCA) was used, which implies the possibility of intermolecular aggregation of the dyes on the TiO₂ surface.

Qin *et al.* also incorporated TAT into the meso-position of the porphyrin chromophore to obtain **67** (Fig. 22).⁴⁹ Dye **67**, which was used in ssDSSC, with spiro-MeOTAD being the HTM, showcased an efficiency of 5.2% in the presence of co-adsorbent CDCA.

The most efficient DSSC's based on TAT molecules were reported by Zhang and co-workers.⁵⁰ They systematically



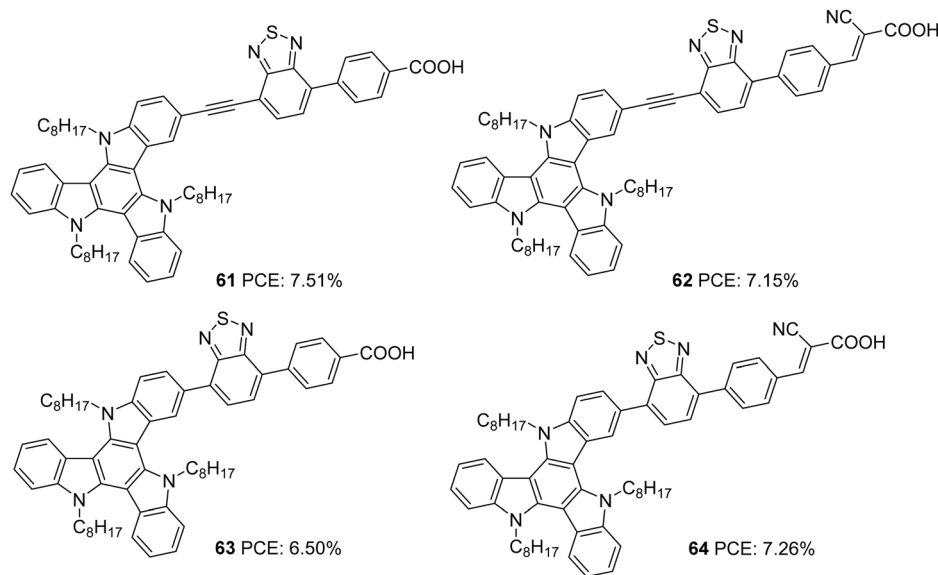


Fig. 20 Photosensitizers **61–64** with a triazatruxene moiety as a donor.

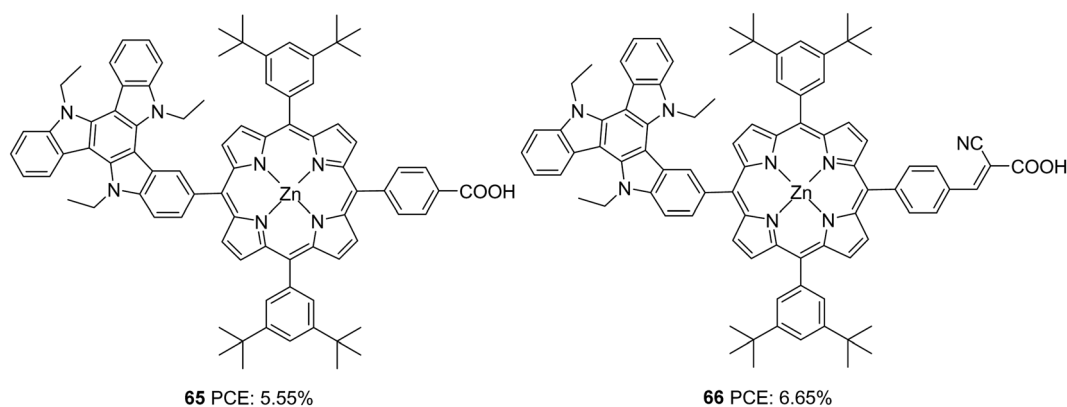


Fig. 21 Photosensitizers **65–66** with a triazatruxene moiety as a secondary donor and porphyrin ring as a primary chromophore.

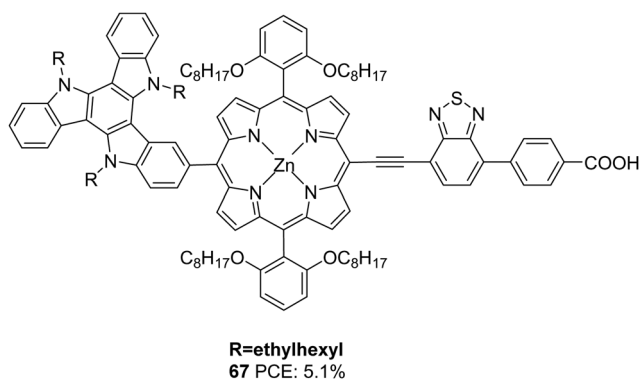


Fig. 22 Photosensitizer **67** with a triazatruxene moiety as a secondary donor and porphyrin ring as the primary chromophore.

modified the D- π -A backbone and developed two dyes employing TAT as a donor, 4,7-bis(4-hexylthiophen-2-yl)benzo[*c*][1,2,5]-thiadiazole (BTBT) as a π -bridge and 4-ethynyl benzoic acid

(EBA) as an acceptor, which differs in the linkage between the donor and π -bridge (Fig. 23). The study aimed to evaluate the effect of the rigid single bond and flexible z-type double bond on various parameters that determine the efficiency of the device. The optimized devices based on **68** and **69** achieved PCEs of 13.6% and 12.8%, respectively, using cobalt-based redox electrolyte ($[\text{Co}(\text{bpy})_3]^{2+/3+}$). Though the double bond was found to widen and enhance the absorption of the molecules, the J_{sc} value for **68** was found to be higher than **69**, which resulted from the more significant dye loading observed for the former. Devices fabricated using **68** also showcased better open-circuit potential (956 mV) than **69** (887 mV) (Table 3). The efficient electron injection in **68**, evident from the femtosecond transient absorption and up-conversion fluorescence studies, reinforces the observation mentioned earlier. Dye **68** and **69** were also applied to ssDSSCs using spiro-OmeTAD as the hole transporting material (HTM).⁵¹ Longer electron lifetime and high regeneration efficiency caused **68** to outperform **69** with a PCE of 6.6%. Dye **69** exhibited a PCE of 5.4% (Table 3).



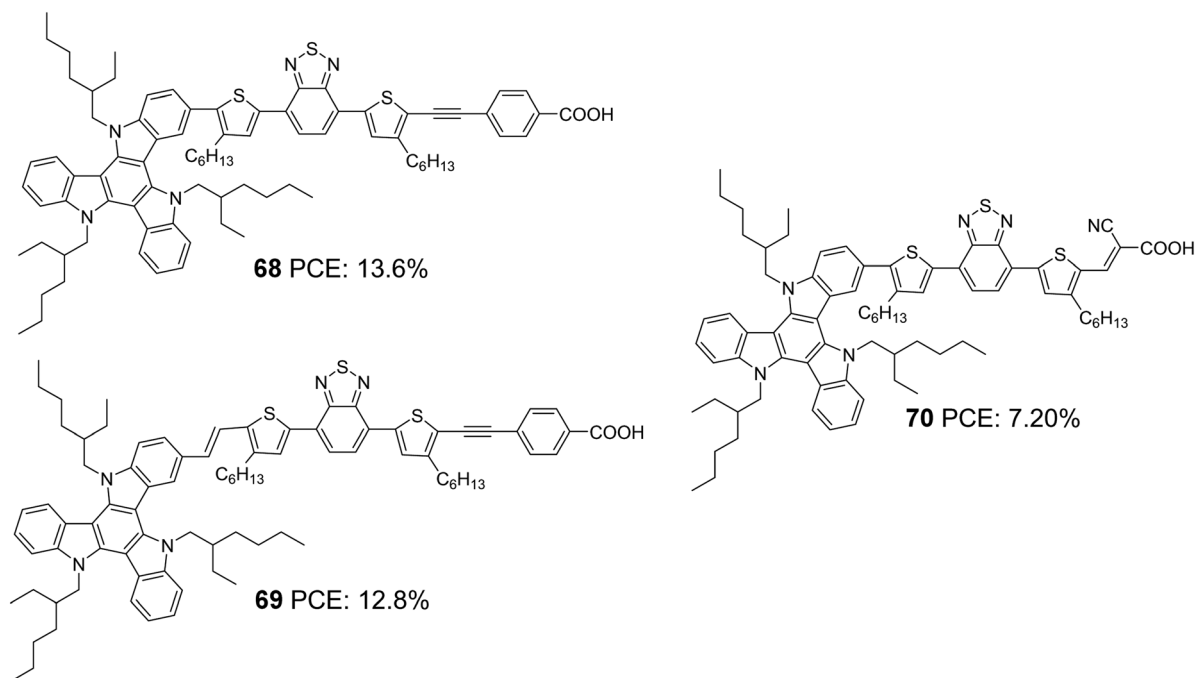


Fig. 23 Photosensitizers **68–70** with triazatruxene moiety as a donor.

In order to probe the effect of the rigid 4-ethynylbenzoic acid acceptor group in **68**, dye **70** was synthesized by the same group (Fig. 23) with Z-type cyanoacrylic acid and used to fabricate devices using a cobalt-based redox electrolyte $[\text{Co}(\text{bpy})_3]^{2+/3+}$.⁵² Higher dye loading, better light-harvesting ability and improved electron injection efficiency made **68** deliver the highest efficiency of 13.4%, while there was a drastic drop in PCE for **70**, which could only afford a PCE of 7.2% (Table 3). This again clearly illustrates that rigid structures are pertinent when it comes to designing sensitizers that will be beneficial for reducing energy loss during electron injection, leading to improved current density and photovoltage. Fine-tuning of the molecular backbone without compromising the energetics is highly required to realize higher PCE.

Later, Li *et al.* tried to improve the efficiency of **68** by developing two modified dyes **71** and **72** using a TAT donor (Fig. 24).⁵³ While benzothiadiazole (BT) functions as the auxiliary

acceptor in **71**, BT was replaced with difluorobenzo[*c*][1,2,5]-thiadiazole (DFBT) in **72**. The attempt to introduce fluorine on BT was justified by lowering the LUMO level of the molecule by the electron-withdrawing (inductive) effect of fluorine. The electron-donating mesomeric effect was found to dominate the former. This renders **72** with a large band gap and blue-shifted absorption spectrum compared to that of **71**. The higher dye loading in **71** (1.4 times) and wider absorption band compensated the reduction in molar extinction coefficient, resulting in a higher J_{sc} of 15.1 mA cm^{-2} . This ended up in maximum efficiency of 10.2% for **71** and a lower efficiency of 8.6% for **72** using cobalt-based redox electrolyte $[\text{Co}(\text{bpy})_3]^{2+/3+}$. (Table 3).

Yao *et al.* found that introducing bulky groups on TAT successfully hindered dye aggregation and recombination (Fig. 25).⁵⁴ They synthesized two modified TAT sensitizers (**73** and **74**) having a more conjugated TAT donor unit. Their attempt resulted in a larger V_{oc} for **73** (926 mV) and **74** (911 mV). Higher dye loading in **73** compared to **74** allowed adequate coverage of the semiconductor surface, abating the chances of dark current formation (recombination), leading to higher V_{oc} . DFT studies also revealed more planar conformation for **74** than **73**, which confirms the slightly red-shifted absorption profile of **74**. It was also observed that there was an upshift in HOMO level for **74**, which affected the regeneration rate of the dye adversely. Poor regeneration and lower dye loading resulted in lower current density and V_{oc} for **74** compared to **73**. Thus, PCEs of 11.7% and 10.6% were obtained for **73** and **74**, respectively (Table 3).

Triazatruxene was incorporated as a donor in D- π -A dyes and studies were carried out to evaluate the effect of different π -spacers and anchoring groups. When it comes to the anchoring group, cyanoacrylic acid has proved to outperform other

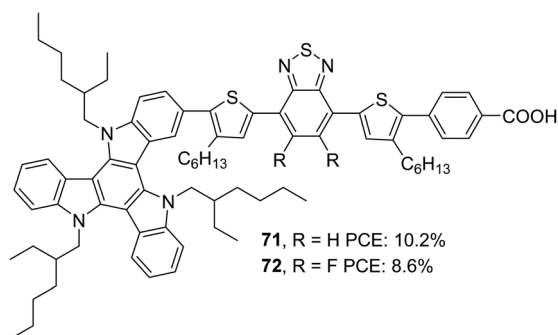


Fig. 24 Photosensitizers **71–72** with a triazatruxene moiety as a donor.



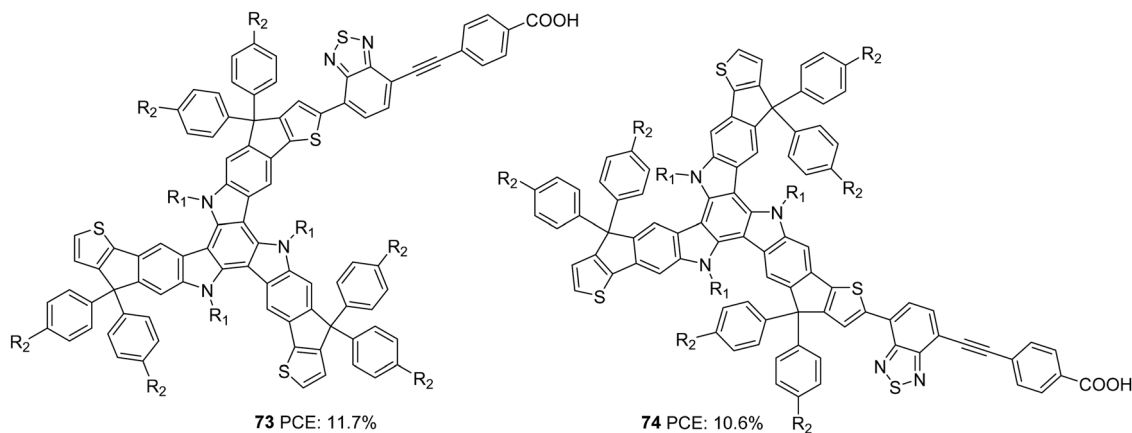


Fig. 25 Photosensitizers **73–74** with a triazatruxene moiety as a donor.

acceptor units (rhodanine-3-acetic acid, carboxylic acid) in terms of light-harvesting and electron injection capability, which is consistent with the many reports available. Though devices based on thiophene bridged dye **56** could showcase higher PCE than those of phenyl substituted dye **58**, this trend reverses when the anchoring group was changed to rhodanine-3-acetic acid. Devices fabricated with phenyl bridged dye **60** delivered higher PCE with higher J_{sc} and V_{oc} compared to those of **59** with a thiophene spacer. This implies that selecting a suitable π -spacer depends on the other components of the molecular architecture. The introduction of an auxiliary acceptor improved the photovoltaic parameters, and the highest efficiency achieved so far using metal-free dyes is from devices based on **68** (13.6%) where BTBT was used as the π -bridge (Table 3). The takeaway from the consecutive studies performed by Zang and co-workers is that molecular engineering has to be carried out in such a way as to reduce energy loss during electronic transitions, which could, in turn, lead to efficient PCE.

IV. Indeno[1,2-*b*]indole based sensitizers for DSSCs

Indeno[1,2-*b*]indole consists of an indole unit fused with an indene moiety, making it planar and electron-rich with efficient electron delocalization. In addition to the alkylation of the N-atom in the tetracene, the indene unit also offers the flexibility to be alkylated. This possibility has a positive effect on the photovoltaic performance as the presence of multiple alkyl groups increases the solubility of indeno[1,2-*b*]indole based dyes and prevents their aggregation. At the same time, the presence of alkyl groups is also effective in blocking the approach of the oxidized species coming close to the semiconductor and thereby improving lifetime. The well-established synthetic route towards preparing this tetracene is by the Fisher indole synthesis involving indanone and phenyl hydrazine.⁵⁵

The first report on the use of indeno[1,2-*b*]indole as a donor in a DSSC came in 2016 by Qian *et al.*⁵⁶ They designed four dyes (Fig. 26) based on D- π -A design, and the basic skeleton employs indeno[1,2-*b*]indole as a donor and cyanoacrylic acid

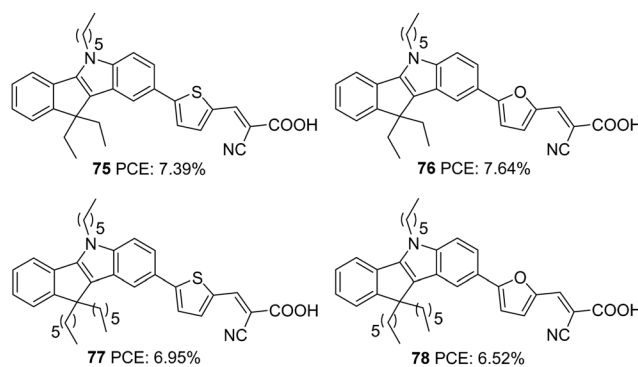


Fig. 26 Photosensitizers **75–78** with an indeno[1,2-*b*]indole moiety as a donor.

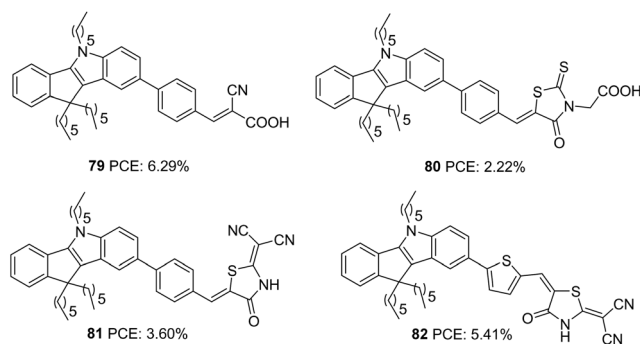
as the acceptor. Tuning of device performance was carried out by changing the π bridges (furan and thiophene) and introducing alkyl groups (ethyl and hexyl) on the indene ring. The attached alkyl groups were at a particular angle with the molecular plane, which was beneficial for reducing aggregation of dyes and thereby increasing the PCE. All four dyes exhibited good power conversion efficiency in the range 6.52–7.64%. Among these dyes, the sensitizer **76**, featuring furan as the π -spacer and ethyl groups as the alkyl chain, contributed the highest PCE of 7.64% with a J_{sc} of 15.8 mA cm⁻² and a V_{oc} of 763 mV (Table 4).

Qian and co-workers later designed three more dyes with indeno[1,2-*b*]indole as the donor to investigate the role of different acceptor groups on the photovoltaic performance of the devices.⁵⁷ The synthesized D- π -A dyes had indeno[1,2-*b*]indole as a donor and benzene as the π -bridge. The dyes differed in the acceptor groups incorporated, which were cyanoacrylic acid, rhodanine-3-acetic acid and 2-(1,1-dicyanomethylene)-rhodanine (DCRD), respectively (**79**, **80** and **81**) (Fig. 27). The results revealed better PCE for devices fabricated using dye having cyanoacrylic acid as the acceptor over the other two groups. Though dye **79** showed blue-shifted absorption, it contributed towards the highest efficiency of 6.29% with better J_{sc} and V_{oc} compared to other dyes. To assess the effect of different π -spacers on the DCRD acceptor, dye **82** was synthesized with thiophene as the π -bridge. The introduction of thiophene increased the



Table 4 Photovoltaic parameters of indenoindole based DSSCs

Sensitizer	J_{sc} (mA cm ⁻²)	V_{oc} (mV)	FF	PCE (%)	Electrolyte	Coadsorbent (concentration)	Ref.
75	15.6	710	0.67	7.39	Γ/I_3^-	—	56
76	15.8	763	0.63	7.64	Γ/I_3^-	—	56
77	14.6	742	0.64	6.95	Γ/I_3^-	—	56
78	13.7	733	0.65	6.52	Γ/I_3^-	—	56
79	11.0	813	0.70	6.29	Γ/I_3^-	—	57
80	4.23	700	0.75	2.22	Γ/I_3^-	—	57
81	7.10	695	0.73	3.60	Γ/I_3^-	—	57
82	11.9	707	0.64	5.41	Γ/I_3^-	—	57
83	10.4	843	0.66	5.74	Γ/I_3^-	CDCA (3 mM)	58
84	13.3	796	0.65	6.86	Γ/I_3^-	CDCA (3 mM)	58
85	14.1	829	0.68	7.99	Γ/I_3^-	CDCA (3 mM)	58
84/85	14.7	819	0.70	8.37	Γ/I_3^-	—	58
86	18.25	707	0.68	8.74	Γ/I_3^-	—	59
87	20.08	703	0.64	8.98	Γ/I_3^-	—	59
88	12.01	837	0.69	6.92	Γ/I_3^-	—	59
86/88	18.24	787	0.67	9.56	Γ/I_3^-	CDCA (4 mM)	59
89	11.59	840	0.66	6.43	$[\text{Co}(\text{phen})_3]^{2+/3+}$	—	60
90	6.84	770	0.63	3.31	$[\text{Co}(\text{phen})_3]^{2+/3+}$	—	60
91	12.43	829	0.65	6.69	$[\text{Co}(\text{phen})_3]^{2+/3+}$	—	60
92	13.52	855	0.64	7.40	$[\text{Co}(\text{phen})_3]^{2+/3+}$	—	60

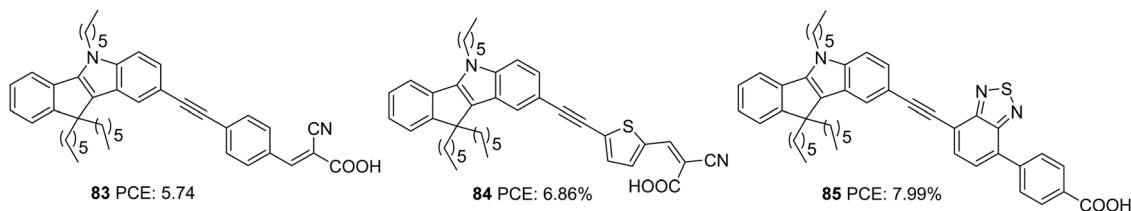
Fig. 27 Photosensitizers **79–82** with an indeno[1,2-*b*]indole moiety as a donor and variable acceptor groups.

efficiency of **81** from 3.60% to 5.41%, illustrating the importance of tuning the π -spacer of the sensitizer (Table 4) while changing the acceptor functionality in a way to achieve higher PCE.

Yan *et al.* later designed and synthesized indeno[1,2-*b*]indole based D- π -A dyes with extended conjugation of the π -spacer by introducing an ethynyl group and variation of the π -spacer and auxiliary acceptor. To this end, they constructed D- π -A dyes, which employ indeno[1,2-*b*]indole as the donor and cyanoacrylic acid as the acceptor group (Fig. 28).⁵⁸ The dyes **83** and **84** vary in the π -bridge between benzene and thiophene, respectively. They also incorporated the ethynyl group as the

linker between the donor and π -spacer to decrease the repulsion and increase the conjugation of the dye molecules. A third dye, **85** with benzothiadiazole as the auxiliary acceptor, was developed to compare with the previous set realizing D- π -A architecture. The dye with an auxiliary acceptor (**85**) was found to deliver the highest efficiency with the highest J_{sc} and V_{oc} . Among the D- π -A dyes, thiophene substituted dye **84** showed the highest efficiency with significantly improved current density, though V_{oc} was highest for the benzene substituted dye **83**. Co-sensitization of **84** and **85** outperformed all other dyes delivering an efficiency of 8.37% (Table 4). This is attributed to the increment in the J_{sc} value of the device.

Dai and co-workers first synthesized indeno[1,2-*b*]indole-spirofluorene (IISF) and used it as a donor unit in DSSC dyes. This molecular engineering was carried out to combine the electron-donating ability of the indenoindole with the steric effect of the spirofluorene.⁵⁹ They were successful in developing two dyes, **86** and **87**, with IISF as the donor, dithieno[3',2'-*b*:2',3'-*d*]pyrrole (DTP) as the π -bridge and cyanoacrylic acid as an acceptor (Fig. 29). The dye **87** also employs 2,1,3-benzothiadiazole (BTD) as an auxiliary acceptor. Both **86** and **87** delivered efficiencies above 8%, which was further enhanced with the combined effect of co-adsorption with CDCA and co-sensitization with **88**. The highest efficiency of 9.56% was obtained from the co-sensitization of **86** with **88** in the presence of co-adsorbent, CDCA (Table 4).

Fig. 28 Photosensitizers **83–85** with an indeno[1,2-*b*]indole moiety as a donor.

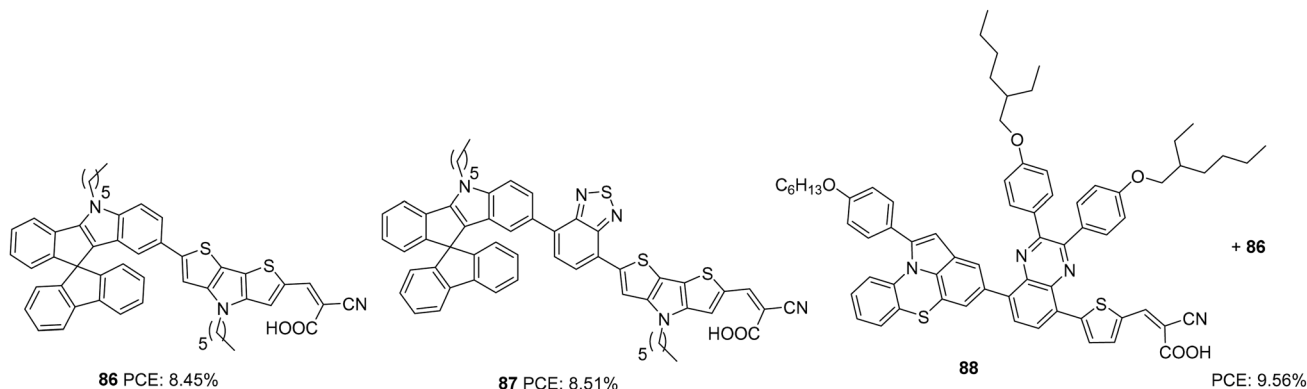


Fig. 29 Photosensitizers **86–87** with an indeno[1,2-*b*]indole-spirofluorene moiety as a donor.

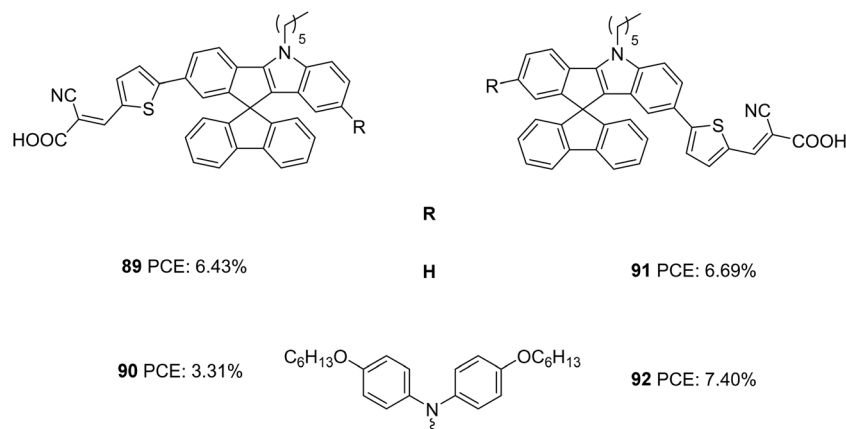


Fig. 30 Photosensitizers **89–92** with an indeno[1,2-*b*]indole-spirofluorene moiety as a donor.

Later the same group synthesized two sets of dyes based on IISF to study the effect of position of attachment of the π -spacer to IISF (indole/indene end) and the effect of the additional donors (Fig. 30).⁶⁰ The D- π -A dyes **89** and **91** consist of IISF as the donor, thiophene as the π -spacer and cyanoacrylic acid as the acceptor. While thiophene is attached to the indene ring in **89**, dye **91** has the π -spacer attached to the indole end. An additional donor group (hexyloxydiphenylamine) was attached to **89** to obtain **90**, and dye **92** is the latter's regioisomer. Dyes with additional donors exhibited bathochromic as well as intensified spectra compared to D- π -A dyes. Among the two regioisomers, the one with the π -spacer attached to the indole end of IISF is seen to facilitate more ICT transition. The IPCE spectra of **90** and **92** showed wider but downshifted absorption behaviour than **89** and **91**. A higher adsorption angle of **89** (41.83°) and **91** (42.33°) helped them to achieve higher dye loading of 115.83 and 118.14 nmol cm⁻², respectively. The bulkier donor group in **90** and **92** caused decreased dye loading compared to their D- π -A counterpart, but **92** managed to obtain 77% dye loading of **91** due to its larger adsorption angle (49.5°). Though dye loading was lower for **92** (90.97 nmol cm⁻²) than **89** and **91**, the broader absorption could compensate for it having the highest J_{sc} (13.52 mA cm⁻²). While **89** and **91** exhibited comparable J_{sc} of 11.59 and 12.43 mA cm⁻²,

respectively, **90** delivered the least J_{sc} value of 6.84 mA cm⁻². Apart from the lower dye loading, the weak driving force for degeneration also caused the downfall in current density for **90**. This was again illustrated by changing alternate electrolytes for device fabrication which are having lower oxidation potential than [Co(phen)₃]^{2+/3+} ([0.56 V for Co(bpy)₃]^{2+/3+}, and 0.43 V for [Co(dmbpy)₃]^{2+/3+}). The current density of **90** increased in the order [Co(dmbpy)₃]^{2+/3+} > [Co(bpy)₃]^{2+/3+} > [Co(phen)₃]^{2+/3+}. While the bulky hexyloxy diphenyl helped **92** alleviate recombination and achieve higher V_{oc} , the same group adversely affected the V_{oc} in **90** by breaking the compact layer formed by dye **89**. A trade-off between J_{sc} and V_{oc} in **89** and **91** lead to comparable efficiencies for them. While **92** showcased the highest PCE of 7.40%, dye **90** delivered the lowest PCE of 6.84%. Co-sensitization of **92** was carried out with **89/91**. In both cases, increment in current density was observed, **91/92** being the combination with the highest PCE (8.32%)

On comparing the sensitizers **77**, **78** and **79** having the same dye skeleton and differing only in their π -spacer, sensitizer **77** having thiophene as the π -spacer outperformed the rest of the dyes with higher current density. Though sensitizer **79** has higher V_{oc} , the least PCE was delivered due to lower current density. A triple bond was introduced between the indenoindole



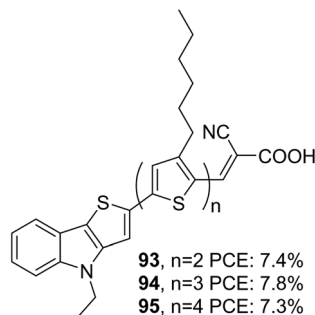


Fig. 31 Photosensitizers **93–95** with a thieno[3,2-*b*]indole moiety as a donor.

unit and π -spacer in **77** and **79** to furnish **84** and **83**. Though the motive was to increase the conjugation and PCE of the devices, it was found to showcase low PCE compared to its predecessor. Though the new structure could bring about an increment in V_{oc} , current density followed the reverse trend.

V. Thieno[3,2-*b*]indole (TI) and thieno[2,3-*b*]indole based sensitizers for DSSCs

In thieno[3,2-*b*]indole (TI), an electron-rich system like thiophene is fused to the five-membered ring of the indole moiety at the 2–3 positions. It has been proved that thieno[3,2-*b*]indole is a better donor than both indole and carbazole units. The introduction of thieno[3,2-*b*]indole as a component in the dye design would certainly improve photovoltaic performance due to the co-planarity and strong electron-donating ability of these heteroacenes. The thieno[3,2-*b*]indole moiety can be easily synthesized using a Cadogen reaction of suitable functionalized 2-(2-nitrophenyl)thiophene.⁶¹

The first report of a thieno[3,2-*b*]indole based DSSC was reported by Zang *et al.* in 2010.⁶² They synthesized three dyes

(**93**, **94** and **95**) employing 4-ethyl-4*H*-thieno[3,2-*b*]indole moiety as an electron donor, *n*-hexyl substituted oligothiophene units as a π -spacer and cyanoacrylic acid as an electron acceptor/anchoring group (Fig. 31). A comparison was also made with dyes having *N*-ethyl carbazole, which consists of the same dye skeleton.⁶³ The electron lifetime measurement values obtained for the TI based devices are lower than their parent D- π -A carbazole dyes, leading to lower V_{oc} for these devices, having the least value of 660 mV for the **95** based device. According to the DFT calculations, the dihedral angle between the thienyl group and the donor part is found to be less for TI based sensitizers in comparison to that of carbazole dyes. This increase in planarity and better electron-donating capability is reflected in the broader absorption spectra and higher ϵ values displayed by dyes employing thieno[3,2-*b*]indole as the donor unit. This resulted in an increment in current density, which was in line with the increment in the number of thiophene groups in the π -backbone. Among the TI dyes, **94** exhibited a higher PCE of 7.8%, and the minor performance was delivered by **95** (7.3%) (Table 5). An increase in the number of thiophene moieties resulted in higher HOMO levels for **95**. Though this tendency could produce low bandgap sensitizers with better light-harvesting, a decrease in driving force for dye regeneration and the chances of recombination of injected electrons with the oxidized dyes may be responsible for decelerating the performance of **95**.

The role of thieno[3,2-*b*]indole (TI) as a π -spacer was demonstrated successfully by Kim and co-workers.⁶⁴ In their initial work, they designed and synthesized D-A- π -A sensitizers using TI (**97**, **98**) as a π -spacer and a comparative investigation was made between dyes with thieno[3,2-*b*]benzothiophene (TAB) as a π -spacer (**96**) (Fig. 32). The more electron-donating nature of TI could induce effective charge transfer in **97** and **98** with resultant wider absorption behaviour and ϵ -values compared to those of **96**. These molecules also exhibited effective electron injection efficiency, with **98** being the best performer with improved light-harvesting ability. The IPCE performance of

Table 5 Photovoltaic parameters of thieno[3,2-*b*]indole and thieno[2,3-*b*]indole based DSSCs

Sensitizer	J_{sc} (mA cm ⁻²)	V_{oc} (mV)	FF	PCE (%)	Electrolyte	Coadsorbent (concentration)	Ref.
93	13.8	700	0.77	7.4	I ⁻ /I ₃ ⁻	—	62
94	14.6	700	0.76	7.8	I ⁻ /I ₃ ⁻	—	62
95	15.0	660	0.74	7.3	I ⁻ /I ₃ ⁻	—	62
96	16.84	810	0.72	9.83	[Co(bpy) ₃] ^{2+/3+}	CDCA (20 mM)	64
97	18.35	804	0.75	11.04	[Co(bpy) ₃] ^{2+/3+}	CDCA (20 mM)	64
98	19.39	825	0.74	11.84	[Co(bpy) ₃] ^{2+/3+}	CDCA (20 mM)	64
99	16.39	834	0.75	10.2	[Co(bpy) ₃] ^{2+/3+}	HC-A1 (0.6 mM)	65
100	17.15	839	0.74	10.5	[Co(bpy) ₃] ^{2+/3+}	HC-A1 (0.6 mM)	65
101	17.12	849	0.73	10.6	[Co(bpy) ₃] ^{2+/3+}	HC-A1 (0.6 mM)	65
102	17.49	898	0.72	11.4	[Co(bpy) ₃] ^{2+/3+}	HC-A1 (0.6 mM)	65
103	15.62	759	0.76	9.05	[Co(bpy) ₃] ^{2+/3+}	HC-A1 (6 mM)	66
104	16.42	846	0.77	10.69	[Co(bpy) ₃] ^{2+/3+}	HC-A1 (6 mM)	66
105	16.50	847	0.77	10.80	[Co(bpy) ₃] ^{2+/3+}	HC-A1 (6 mM)	66
106	1.06	490	0.73	0.37	[Co(bpy) ₃] ^{2+/3+}	—	68
107	3.2	360	0.69	0.79	[Co(bpy) ₃] ^{2+/3+}	—	68
108	19.0	590	0.56	6.3	[Co(bpy) ₃] ^{2+/3+}	—	69
109	19.9	390	0.44	3.4	[Co(bpy) ₃] ^{2+/3+}	—	69
110	4.7	470	0.61	1.3	[Co(bpy) ₃] ^{2+/3+}	—	69
111	6.6	370	0.56	1.4	[Co(bpy) ₃] ^{2+/3+}	—	69



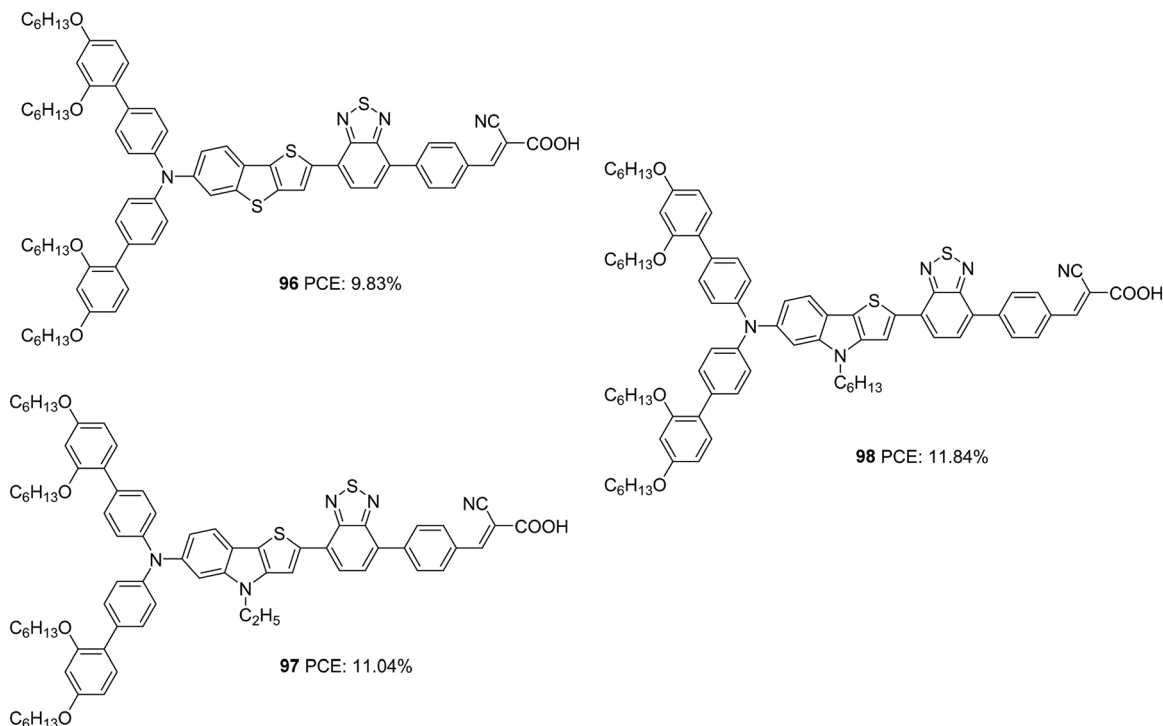


Fig. 32 Photosensitizers with a thieno[3,2-*b*]indole moiety (**97**, **98**) and thieno[3,2-*b*] benzothiophene (**96**) as a π -spacer.

the dyes parallels these observations leading to the highest J_{sc} for **98** (19.39 mA cm^{-2}) followed by **97** (18.35 mA cm^{-2}) and **96** (16.84 mA cm^{-2}). The hexyl chain was found to minimize the dye aggregations effectively in **98** with lesser recombination, which resulted in a higher V_{oc} (825 mV) for the same (Table 5). The trends described above in device parameters ended in highest PCE for **98** (11.84%) followed by **97** (11.04%) and **96** (9.83%) using CDCA co-adsorbent and cobalt electrolyte ($[\text{Co}(\text{bpy})_3]^{2+/3+}$).

Later the same group synthesized **99–102**. The objective was to reduce the aggregation-induced recombination occurring in devices fabricated with **98**. The donor group in **98** was substituted with fluorenyl derivatives with the other building blocks remaining unchanged using D-A- π -A architecture with BTD as an auxiliary acceptor and cyanoacrylic acid as an acceptor/anchoring group (Fig. 33).⁶⁵ The synthesized dyes **99–102** employ bis(9,9-dimethyl-9*H*-fluoren-2-yl)amino (FA), [20] bis(6,7-bis(hexyloxy)-9,9-dimethyl-9*H*-fluoren-2-yl)amino (HFA), bis(6,7-bis(decyloxy)-9,9-dimethyl-9*H*-fluoren-2-yl)amino (DFA), and bis(7-(2,4-bis(hexyloxy)phenyl)-9,9-dimethyl-9*H*-fluoren-2-yl)amine (BBFA) groups respectively as donors. To encounter solubility problems associated with the fluorene derivatives, all the devices were made with a change in dipping solvent resulting in lower PCE (10.5%, J_{sc} : 16.67 mA cm^{-2} , V_{oc} : 840 mV, FF: 0.75) for **98** than previously reported. All the devices were found to exhibit improved performance when the electrolyte was changed from iodide/triiodide to cobalt-based electrolyte ($[\text{Co}(\text{bpy})_3]^{2+/3+}$) and in the presence of HC-A1 as the co-adsorbent. The alkoxy, as well as phenyloxy substituted fluorene derivatives (**100–102**), were found to be more effective both in red shifting the

absorption spectrum as well as in preventing recombination, taking advantage of the electron-donating as well as the bulkiness of the donor groups, when compared to FA substituted dye **99**. This led to higher current density and photocurrent for **100–102** resulting in higher PCE. Though **99** does not have additional alkoxy substitutions integrated on it, the absorption profile shows a redshift when compared to those of **98** having

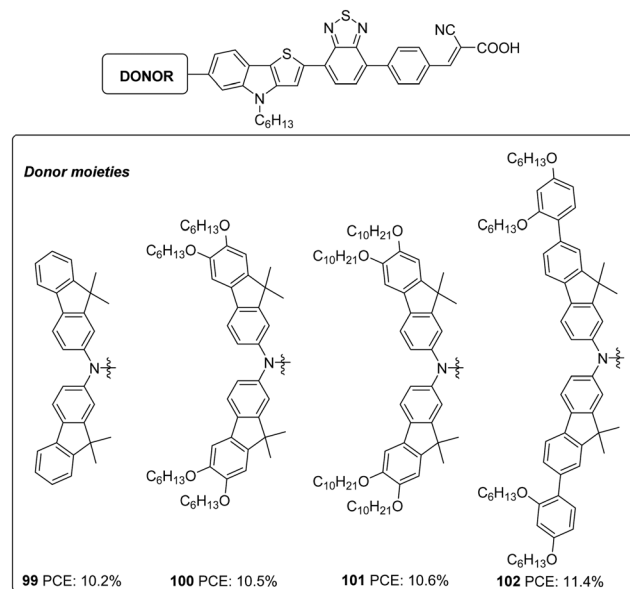


Fig. 33 Photosensitizers **99–102** with thieno[3,2-*b*]indole moiety as the π -spacer.



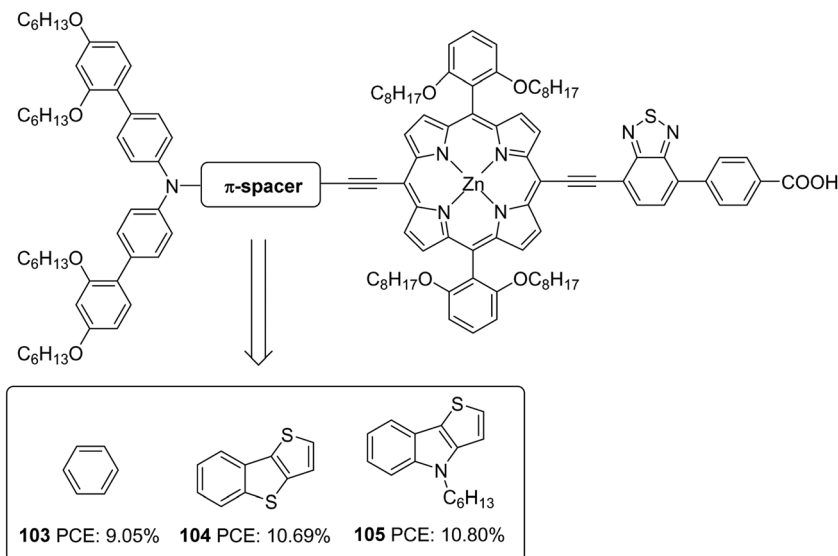


Fig. 34 Molecular structures of photosensitizers **103–105** with different π -spacers.

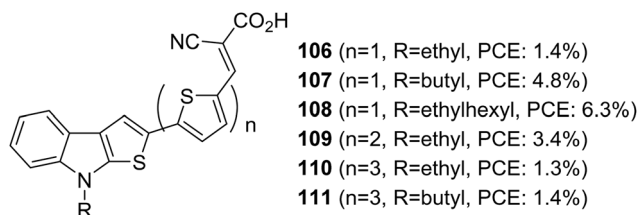


Fig. 35 Photosensitizers **106–111** with thieno[3,2-*b*]indole moiety as the donor.

BBPA (bis(2',4'-bis(hexyloxy)-[1,1'-biphenyl]-4-yl)amino) as the donor. This absorption behaviour can be accredited to a lack of electronic communication between the alkoxy groups and the tertiary amine in BBPA based dye **98**. A higher molar extinction coefficient of **98** contributed towards higher current density compared to **99**. The bulkier BBPA also rendered **98** to have higher V_{oc} and hence higher PCE when compared to those of **99**. The device fabricated based on **102** showcased the highest efficiencies of 11.4%, and **99** delivered the least efficiency of 10.2% (Table 5).

The superior performance of TI over TAB as a π -conjugator was again illustrated by Ji *et al.* (Fig. 34).⁶⁶ To this end, two porphyrin based D- π -A dyes (D-ethynyl-zinc porphyrinyl-ethynyl-benzothiadiazole-acceptor) with extended conjugation at the donor sites were constructed. The dyes **104** and **105** differ in the auxiliary spacer between thieno[3,2-*b*]benzothiophene (TBT) and 4-hexyl-4*H*-thieno[3,2-*b*]indole, and were also subjected to a comparison with phenylethylene based dye **103** from earlier work.⁶⁷ The dihedral angle between the donor part and π -spacer showed increment when the phenyl group in **103** was replaced with TI and TAB units with more conjugation. The trend observed in V_{oc} was following the increase in dihedral angle (**105** > **104** > **103**), which might have helped prevent the recombination effectively. The more electron-donating TI and TAB groups could also bring changes in the light-harvesting

ability of the dyes. In the Q-bands, significant changes were observed, having a more expansive and intensified absorption profile for **104–105**, leading to current densities in the order **105** > **104** > **103**. The more planar, electron-donating nature of the TI group along with the incorporated hexyl functionality contributed towards the best efficiency of 10.80% for **105** with higher J_{sc} (16.50 mA cm⁻²) and V_{oc} (0.847 V) (Table 5) in the presence of HC-A1 as the co-adsorbent, using [Co(bpy)₃]^{2+/3+} (bpy = 2,2'-bipyridine) redox electrolyte.

Thieno[2,3-*b*]indole was applied as a building block in DSSCs for the first time by Irgashev *et al.* (Fig. 35).^{68,69} They introduced a new synthetic route for constructing thieno[3,2-*b*]indole from 1-alkylisatin and 2-acetylthiophene. Among the dyes, **108** with thiophene as the π -bridge and ethyl hexyl as the alkyl group contributed towards the highest PCE of 6.3%. The bithiophene and terthiophene groups were entertaining aggregation of dyes which resulted in more recombination. Except for ethyl hexyl, other smaller alkyl groups like butyl and ethyl were not found to obstruct the dye aggregation, resulting in the downfall in efficiency using these spacers.

Thienoindoles have proved to have the potential to function both as donor as well as π -spacer units. Systematic engineering of different π -spacers and auxiliary donors to this moiety could bring impressive PCE in the future. In this line, dye designs that incorporate a TI unit with other indole fused systems open promising alternatives.

VI. Indolo[3,2-*b*]indole based sensitizers for DSSCs

Indolo[3,2-*b*]indoles⁷⁰ (IID) which consists of a central pyrrolo-pyrrole ring fused with two benzene rings on both sides, are considered as good electron donors with impressive hole-transporting properties. The planar nature of IID with a C_{2h}



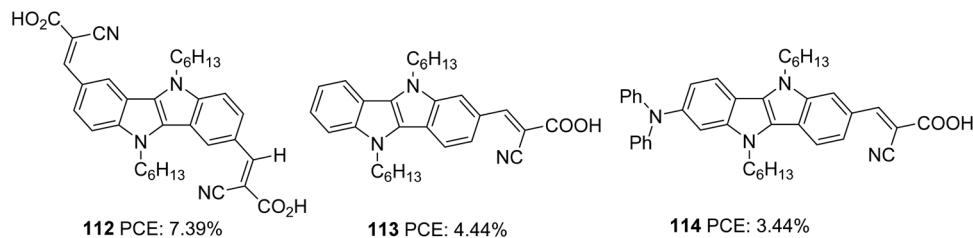


Fig. 36 Molecular structures of photosensitizers **112–114** with indolo[3,2-*b*]indole as a component.

symmetry facilitates better intermolecular interactions, which are beneficial for improving the hole transporting properties of these systems in the solid-state. In addition to these advantages, the two alkylation sites also make IID a potential candidate in various solution-processable optoelectronic applications such as organic thin film transistors, heterojunction solar cells, and organic light-emitting diodes.⁷¹

The first attempt to incorporate IID as a building block in a DSSC was carried out by Ruangsupapichat *et al.* (Fig. 36).⁷² They developed dyes that fall in three categories: double acceptor system (**112**), donor-acceptor system (**113**), and donor- π spacer-acceptor (**114**). While IID functions as a donor in **112** and **113**, it assumes the linker function in **114**. The additional acceptor group and donor moieties in **112** and **114** helped to redshift the absorption spectra of the compounds by 30 nm and 10 nm, respectively with respect to **113**. The PCE of the dyes was in the range 3–7%. The difference in PCE of the dyes resulted from the difference in J_{sc} values. The highest J_{sc} of 14.56 mA cm⁻² of **112** contributed towards achieving the highest efficiency of 7.39%. This resulted from the extra electron extraction pathways provided by the additional electron anchoring groups present in the molecule. The device fabricated with dye **114**, having an additional diphenylamine donor group, showcased the minor performance with only 3.44% PCE. According to the DFT studies, HOMO and LUMO energy levels of dye **114** are primarily localized on diphenylamine donors and cyanoacetic acid. Whereas in **112**, a good overlap of the HOMO and LUMO levels may favour effective electron injection to the semiconductor's conduction band. Less effective electron injection in **114** maybe lowering the J_{sc} (8.25 mA cm⁻²) and thus the efficiency of the device (Table 6).

The same group further attempted to improve the efficiency of A-D-A dye **99** by introducing extra donor methoxyphenyl (**115**) and hexyloxyphenyl (**116**) moieties at the *N,N'*-positions of the IID core (Fig. 37).⁷³ The dyes show involvement of both the carboxyl groups on anchoring but differ significantly in their performance. Dye **116** outperformed **112** and **115** in J_{sc} (17.04 mA cm⁻²) and V_{oc} (718 mV) values leading to a higher PCE of 7.86%. Dye **115** exhibited 5.20% PCE with J_{sc} of 11.59 mA cm⁻² and V_{oc} of 638 mV. While the introduction of a longer alkyl chain in **116** was found to minimise recombination effectively, it also helped to improve the homogeneity of dye adsorption on the semiconductor surface. Broader absorption and higher dye loading amount improved the current density for **116**.

Our group also tried to explore the potential of IID as a donor unit towards the development of D- π -A dyes by introducing an additional π -spacer between the IID donor and cyanoacrylic acid acceptor and also by varying π -linkers between benzene, thiophene and furan (Fig. 38, **117**, **118**, **119**).⁷⁴ The donor unit IID was synthesized utilizing the methodology we developed in our laboratory, which involves a sequential multi-component and oxidation approach.⁷⁵ The absorption spectra of **119** showed more red-shifted and intensified spectra followed by **118** and **117** in order. Nevertheless, the current density and V_{oc} produced by the compounds follow the reverse trend. To investigate the degree of conjugation, molecular geometry analysis of the dyes was also carried out. The acceptor group was found to be almost coplanar with the IID in all the dyes. But the dihedral angle between the donor and π -spacer increases in the order **119** (1.66°) < **118** (21.99°) < **117** (34.48°). Though the more planar geometry of **119** could help red shift the absorption spectra of the dye, it may also be entertaining

Table 6 Photovoltaic parameters of indolo[3,2-*b*]indole based DSSCs

Sensitizer	J_{sc} (mA cm ⁻²)	V_{oc} (mV)	FF	PCE (%)	Electrolyte	Coadsorbent (concentration)	Ref.
112	14.56	740	0.68	7.39	I ⁻ /I ₃ ⁻	—	72
113	10.09	660	0.66	4.44	I ⁻ /I ₃ ⁻	—	72
114	8.25	620	0.68	3.44	I ⁻ /I ₃ ⁻	—	72
115	11.59	638	0.70	5.20	I ⁻ /I ₃ ⁻	—	73
116	17.04	718	0.64	7.86	I ⁻ /I ₃ ⁻	—	73
117	5.51	620	0.69	2.38	I ⁻ /I ₃ ⁻	CDCA (20 mM)	74
118	5.22	570	0.67	2.00	I ⁻ /I ₃ ⁻	CDCA (20 mM)	74
119	4.60	540	0.69	1.71	I ⁻ /I ₃ ⁻	CDCA (20 mM)	74
120	14.55	671	0.69	6.73	I ⁻ /I ₃ ⁻	—	76
121	14.83	672	0.71	7.03	I ⁻ /I ₃ ⁻	—	76
122	16.65	691	0.69	8.00	I ⁻ /I ₃ ⁻	—	76
123	16.74	705	0.70	8.32	I ⁻ /I ₃ ⁻	—	76

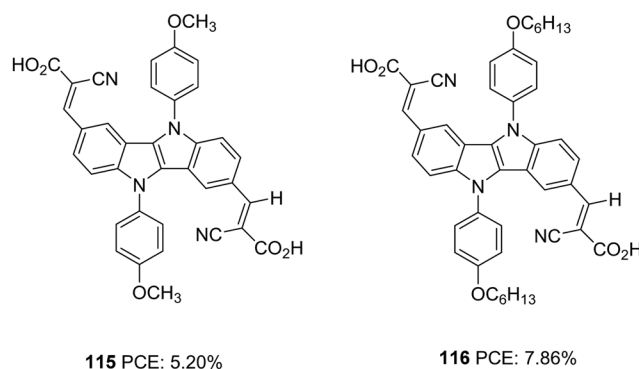


Fig. 37 Molecular structures of photosensitizers **115–116** with indolo[3,2-*b*]indole as the donor.



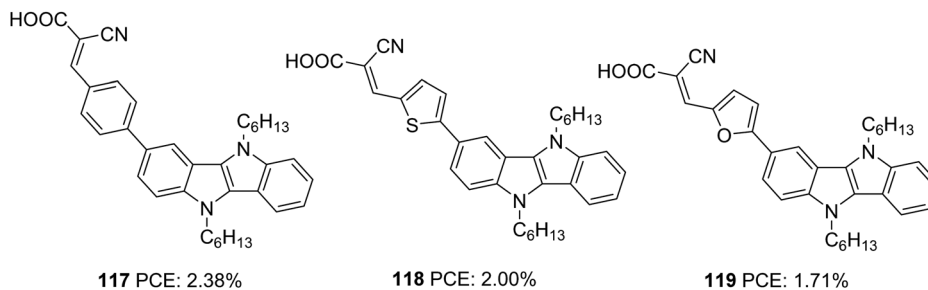


Fig. 38 Molecular structures of photosensitizers **117–119** with indolo[3,2-*b*]indole as the donor.

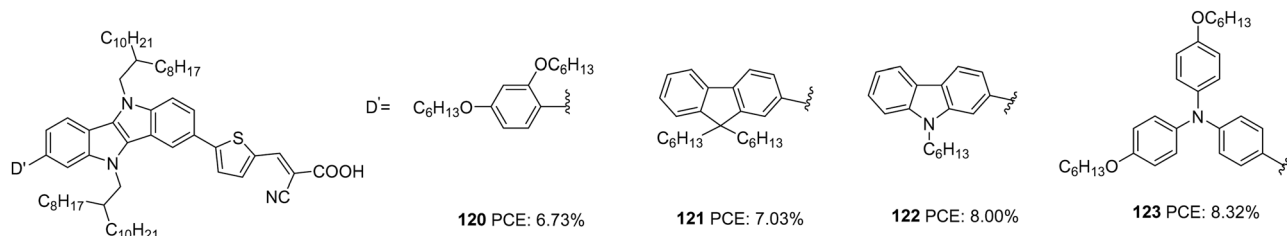


Fig. 39 Molecular structures of photosensitizers **120–123** with indolo[3,2-*b*]indole as the donor.

the aggregation between dye molecules, which could eventually lead to more recombination. A slightly twisted conformation of the benzene substituted dye could prevent the approach of oxidized species from the electrolyte to come close to the semiconductor and the formation of π -stacks, thereby decreasing the chance of recombination. The addition of CDCA enhanced the PCE in all the cases. To utilize the different absorption profile showcased by **119** where recombination destroyed the PCE, we custom designed BID dyes which will be discussed in detail in the next section.

Wang *et al.* synthesized four D–D– π –A dyes based on IID as the primary donor, thiophene as π -spacer and cyanoacrylic acid as an acceptor.⁷⁶ Dyes **120–123** contain hexyloxyphenyl, fluorene, carbazole and hexyloxytriphenylamine, respectively, as the auxiliary donor (Fig. 39). The current density and open-circuit potential followed the same trend, following the electron-donating ability and steric hindrance of the auxiliary donors. The bulkier and more electron-donating triphenylamine made **123** outperform other dyes with PCE of 8.32% with the highest J_{sc} of 16.74 mA cm⁻² and V_{oc} of 705 mV. Other dyes exhibited efficiency in the order **122** > **121** > **120** (Table 6).

VII. Benzothieno[3,2-*b*]indole based sensitizers for DSSCs

Benzothieno[3,2-*b*]indole (BID) is another unique tetracene with a benzothiophene moiety fused to indole. This heteroacene has found applications in medicinal chemistry but is seldom used in materials science and optoelectronic applications.^{77–79} Like what we discussed for indolo[3,2-*b*]indole; this fused indole moiety is also a planar conjugated system with the potential to be used both as a donor and a π -spacer. In

addition, the appropriate functionalization of the N-atom offers flexibility to engineer the BID core with features that render better solubility and will also prevent aggregation of the system, arresting recombination.

As a continuation to our previous studies with indolo[3,2-*b*]indole, the donor group was changed to dodecyl chain functionalized benzothieno[3,2-*b*]indole. Here also the newly developed methodology was employed for the synthesis of the BID core. The devices developed based on dyes **124** (phenyl spacer), **125** (thiophene spacer) and **126** (furan spacer) were found to showcase their best efficiency in the absence of any co-adsorbent. The addition of CDCA as a co-adsorbent decreased the photovoltaic performances of the devices. This illustrates the role of longer alkyl chains (dodecyl) in reducing aggregation of dyes and preventing back electron transfer. Unlike our observation with indolo[3,2-*b*]indole based dyes, furan substituted dye **126** outperformed the other two sensitizers with 4.11% efficiency with the highest J_{sc} and V_{oc} (Table 7 and Fig. 40).⁸⁰

VIII. Tetraindole based sensitizers for DSSCs

The synthesis of tetraindole was first reported in 2006, which involved a one-pot tetramerization of indolin-2-one mediated by phosphoryl chloride.⁸¹ This polyacene has four indole units fused to cyclooctatetraene, which acts as a promising donor motif for solar cell applications. In addition, the unique structural characteristics of this saddle-shaped scaffold will also prevent self-assembly of the dyes on the semiconductor surface.

Tetraindole found a place in DSSCs through the work of Qian and co-workers.⁸² The D– π –A dyes **127** and **128** use thiophene and bithiophene, respectively, as π -bridges (Fig. 41).



Table 7 Photovoltaic parameters of DSSCs **124–140**

Sensitizer	J_{sc} (mA cm ⁻²)	V_{oc} (mV)	FF	PCE (%)	Electrolyte	Coadsorbent (concentration)	Ref.
124	2.86	590	0.69	1.16	I ⁻ /I ₃ ⁻	—	79
125	6.51	652	0.73	3.10	I ⁻ /I ₃ ⁻	—	79
126	8.38	671	0.73	4.11	I ⁻ /I ₃ ⁻	—	79
127	12.1	750	0.64	5.79	I ⁻ /I ₃ ⁻	—	81
128	13.0	762	0.65	6.46	I ⁻ /I ₃ ⁻	—	81
129	14.0	725	0.68	6.90	I ⁻ /I ₃ ⁻	—	82
130	13.5	680	0.67	6.15	I ⁻ /I ₃ ⁻	—	82
131	10.5	650	0.65	4.43	I ⁻ /I ₃ ⁻	—	82
132	14.2	753	0.71	7.59	I ⁻ /I ₃ ⁻	—	82
133	13.0	640	0.72	5.99	I ⁻ /I ₃ ⁻	—	82
134	12.6	652	0.70	5.75	I ⁻ /I ₃ ⁻	CDCA (0.3 mM)	83
135	13.8	657	0.71	6.42	I ⁻ /I ₃ ⁻	CDCA (0.3 mM)	83
136	8.98	643	0.70	4.05	I ⁻ /I ₃ ⁻	CDCA (0.3 mM)	83
137	12.1	633	0.70	5.37	I ⁻ /I ₃ ⁻	CDCA (0.3 mM)	83
138	2.19	700	0.59	1.09	I ⁻ /I ₃ ⁻	—	84
139	12.56	780	0.62	6.04	I ⁻ /I ₃ ⁻	—	84
140	3.92	680	0.53	1.42	I ⁻ /I ₃ ⁻	—	84

The dyes exhibit improved open-circuit potential benefitting from the saddle like structure with flanked octyl alkyl chains of the new donor moiety. The sensitizer **128** exhibited a broader ICT band and better light-harvesting ability, which is evident from the broader and enhanced response of the IPCE spectra. **128** delivered a maximum efficiency of 6.21% with the highest J_{sc} (13.0 mA cm⁻²) and V_{oc} (762 mV), whereas dye **127** could only deliver a PCE of 5.79% with J_{sc} of 12.1 mA cm⁻² and V_{oc} of 750 mV. The reduced aggregation behaviour of these dye was further illustrated by the co-adsorption experiments using CDCA. Both dyes exhibited lower efficiencies in the presence of CDCA, the reduction mainly arose from lower J_{sc} values (Table 7). Decreased dye loading in the presence of CDCA can account for the decrease in photocurrent and hence the overall efficiency.

IX. Dithienopyrroloindole based sensitizers for DSSCs

Optimization of the π -bridge is also as important as other building blocks in a photosensitizer to realize improved PCE. Rigidified aromatics occupy a prominent space among various conjugated functionalities in this regard due to their better charge transfer ability, high molar extinction coefficient and reduced reorganization energies. The compound 4,5-dihexyl-4,5-dihydrothieno[2'',3'':4',5']pyrrolo[2',3':4,5]thieno[3,2-*b*]indole (DPTI) as a π -spacer was first employed by Zang *et al.* to construct photosensitizers **129**, **131–133** (Fig. 42).⁸³ To compare the efficiency of a dithienopyrroloindole (DTP) unit as a spacer, dye **130** was synthesized. Dye **129** outperformed **130** with improved light-harvesting ability and open-circuit potential, indicating the importance of DPTI over DTP. Dyes **131** and **132** were designed to investigate the effect of additional donor and alkylated spacer units on the performance of DPTI based dye. The introduction of an additional donor unit in **131** caused a negative shift in HOMO compared to **129**, whereas a positive shift in LUMO energy level was observed in **132** without much change in HOMO energy level. This low driving force for dye regeneration, enhanced recombination of electrons from the semiconductor with the oxidized dye and lowest dye loading may be responsible for the least efficiency of 4.4% for **131**. The broader spectra of **132** with its twisted conformation induced by the 3-hexylthiophene could deliver a maximum efficiency of 7.59%. In dye **133**, the DPTI unit assumes both the function of a donor and spacer, the indole ring acting as the donor and DTP as the spacer. The conjugated donor- π -spacer structure allows better delocalization of the HOMO and LUMO orbitals over the entire molecule and facilitates good charge transfer from donor to acceptor. Though it managed to perform better than **131**, the lack of additional donor decreased the charge

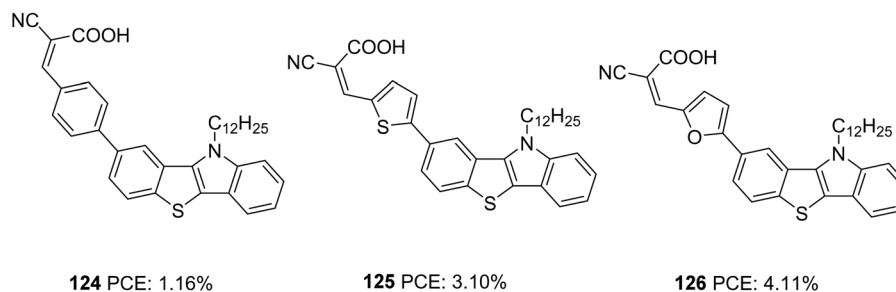


Fig. 40 Molecular structures of photosensitizers **124–126** with benzothieno[3,2-*b*]indole as the donor.

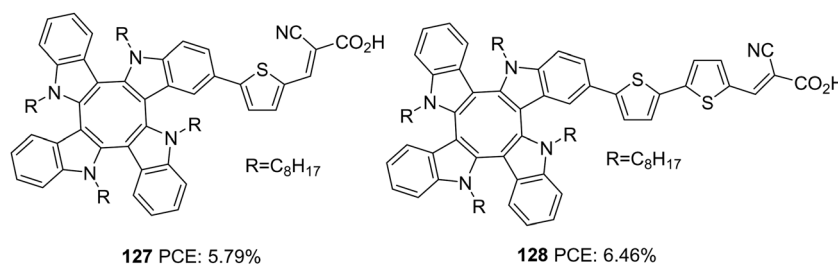


Fig. 41 Photosensitizers **127–128** with tetraindole as the donor.



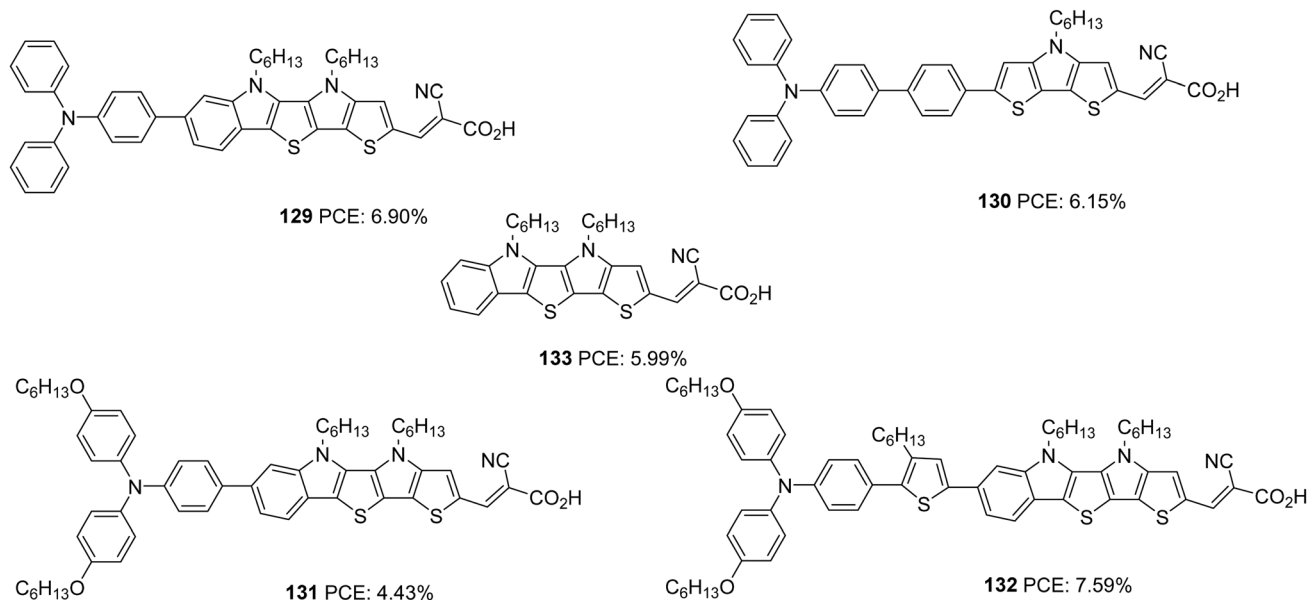


Fig. 42 Molecular structure of photosensitizers **129–133** with dithienopyrroloindole as a component.

separation and electron injection yield leading to lower photocurrent and an efficiency of 5.99%, lower than the rest of the dyes.

X. Fluorenylindolenine donor-based dyes for DSSCs

Jayaraj and co-workers synthesized four novel unsymmetrical squaraine dyes employing fluorenylindolenine as donor **134–137** (Fig. 43).⁸⁴ Apart from increasing the conjugation and NIR light-harvesting capability of the molecules, this skeleton also helps to modulate the charge recombination by incorporating an out of plane alkyl chain on sp^3 carbon and in-plane alkyl chain on the nitrogen. While **134** and **135** are composed of an indole unit toward the anchoring side with an *N*-methylated and *N*-hexylated fluorenylindolenine, **136** and **137** contained a benzo[*e*]indole unit toward the anchoring side with an *N*-methylated and *N*-hexylated donor, respectively. Though the latter set showcased more red-shifted spectra, they exhibited slightly lower efficiency. The difference in PCE of the devices might be due to the difference in dipole moment of the dyes.

The calculated dipole moments are in the order **135** (10.6) > **134** (10.0 D) > **136** (7.4 D) > **137** (7.3 D). The non-directionality induced by the benz[*e*]indole group in **136–137** may be responsible for lowering the dipole moment and electron injection efficiency. The larger dipole moment exerted by dyes **134–135** on TiO_2 may also be helping to upshift the conduction band of TiO_2 , which is evident from the higher V_{oc} observed for these dyes. In both sets of dyes, the hexyl substituted dyes were found to outperform the methylated dye. All the dyes exhibited an increment in PCE when dye and CDCA were used in 1:3 ratios, the effect majorly contributed by the increase in current density. It is already known that squaraines are prone to aggregation. Adding CDCA helps to reduce this aggregation leading to improved PCE.

XI. Indole–imidazole donor dyes for DSSC

An indole–imidazole fused system was incorporated as an auxiliary acceptor (AN) by Ramasami to construct three dyes with different molecular architectures: **138** (D–AN(π –A)–D), **139**

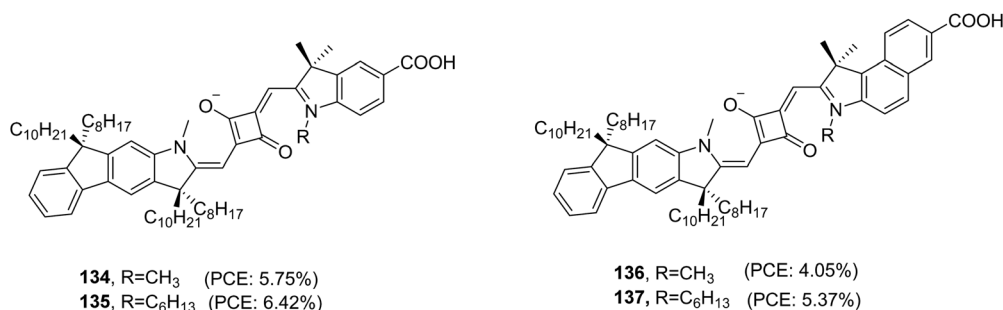


Fig. 43 Molecular structure of photosensitizers **134–137** with fluorenylindolenine as the donor.



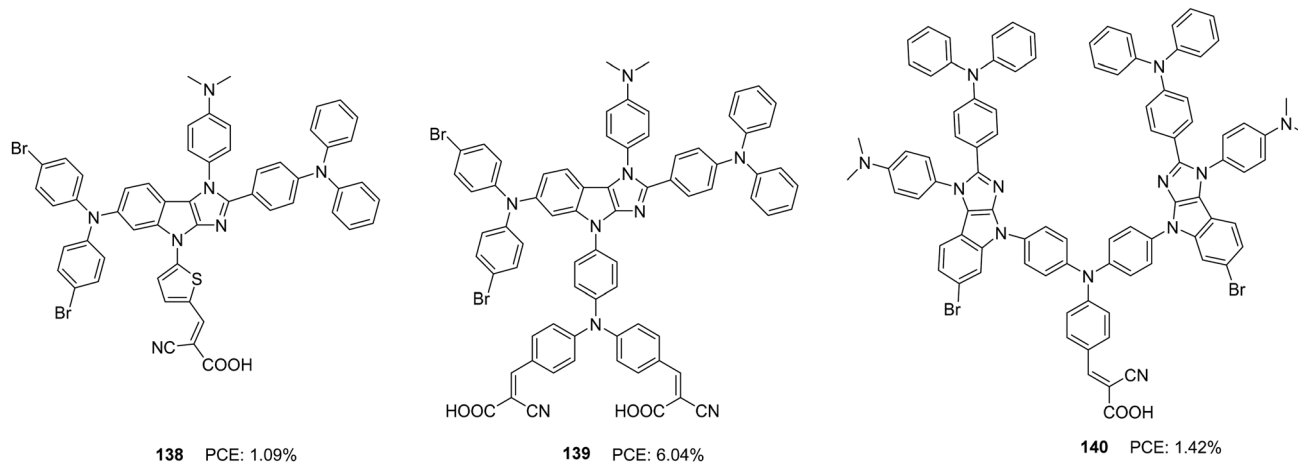


Fig. 44 Molecular structure of photosensitizers **138–140** imidazoloindole as the donor.

(D-AN-(DA₂)-D) and **140** (D-AN-D(A)-AN-D) (Fig. 44).⁸⁵ Dye **139** showed maximum efficiency with the highest current density and photovoltage. Along with the increment in molar extinction coefficient and red-shifted absorption, the anchoring approach also facilitated adequate surface coverage and helped to reduce back electron transfer between the semiconductor surface and electrolyte. The minimum reorganization energy calculated for the same also implies efficient charge injection to the semiconductor for these dyes. The photovoltaic parameters of DSSCs **124–140** are given in Table 7.

Conclusions and future perspectives

Engineering sensitizers have got their prime importance when efficiency enhancement of DSSCs is concerned. Electron rich fused heterocycles have proved their efficacy as donors as well as π -spacers in the sensitizer design. Indole fused aromatic systems have also been utilized to this end, effectively realizing efficient DSSCs. These systems were found to exhibit more electron-donating ability than indole in conjugation with expanded π -systems. Though the planarity could induce ICT in molecules, a trade-off between light harvesting and dye aggregations leads to a shortfall of the power conversion efficiency in many instances. The strategic introduction of bulky substituents on the donor side and the π -conjugator helped abate these situations to some extent. Another notable advantage is the ease of synthesising fused indole heterocyclic motifs with functionalities required for further transformations. In addition, the stability of these fused heterocycles has contributed to enhancing the device lifetime.

The most efficient DSSC (PCE: 13.6%) with a fused indole based sensitizer was reported with dye **68**, which had a triaza-truxene moiety as a donor unit. There are still a plethora of easily accessible fused indole heterocyclic moieties with the required structural features that can act as suitable donors and π -spacers in sensitizer designs. One of the simplest fused indole heteroacenes used as a sensitizer building block is

thieno[3,2-*b*]indole, which gave DSSCs up to 11% efficiency. Likewise, pyrrolo[3,2-*b*]indole can be utilized, resulting in high performing DSSCs. The class of indole fused tetraacenes such as indoloindoles, benzothienoindoles and benzofuroindoles, which are excellent donors, are seldom used building blocks in sensitizer designs. These tetraacenes can exist as different isomers based on the position of fusion, and these isomers differ in their structure and properties and these have all the structural and electronic characteristics to act as good π -spacers. Moreover, these heteroacenes can be used in alternate and new sensitizer designs such as D-A- π -A or (D)₂-A- π -A, resulting in highly efficient DSSCs. As part of our continued interest in this area, we focus on developing new and simpler methodologies to access indole fused heterocycles and extend our research detailed in Section VI and VII by incorporating additional donors and auxiliary acceptors to the D- π -A architecture being optimized.

The challenging task in realizing efficient DSSCs is to prevent back electron transfer/recombination. Along with the proper molecular design and keeping a delicate balance between electronic and steric factors, importance must also be given to the electrolyte used. Significant improvement in photovoltaic parameters and the devices' performance is reported for **98** to **102** when the electrolyte was changed from I^-/I_3^- to $[\text{Co}(\text{bpy})_3]^{2+/3+}$. Most of the sensitizers mentioned in the review use conventional iodide/triiodide electrolyte. This indicates that more promising results could be obtained in the future using appropriate alternate cobalt and copper electrolytes with these fused heterocyclic dyes. In addition, these fused heterocycles can serve as excellent co-sensitizers along with other dyes tapping the visible absorption for indoor photovoltaic applications. With continuing efforts to develop stable, easily accessible and efficient sensitizers for DSSCs, we hope significant advancements will be made with fused indole heterocyclic moieties in the near future.

Conflicts of interest

There are no conflicts of interest to declare.



Acknowledgements

The authors thank DST for DST-SERB Project [DST/SERB/F/481]. NPR thanks CSIR for the research fellowship. NPR and JJ also thanks CSIR (HCP-029) for financial assistance. SS would like to thank SERB CRG project (CRG/2020/001406) and CSIR-FIRST (MLP65) project. SS also acknowledges CSIR Mission (HCP30) and FTT (MLP38) Projects for financial support.

References

- 1 X. Chen, C. Li, M. Grätzel, R. Kostecki and S. S. Mao, Nanomaterials for renewable energy production and storage, *Chem. Soc. Rev.*, 2012, **41**, 7909–7937.
- 2 (a) N. Armaroli and V. Balzani, The future of energy supply: Challenges and opportunities, *Angew. Chem., Int. Ed.*, 2007, **46**, 52–66; (b) R. Eisenberg and D. G. Nocera, Preface: Overview of the forum on solar and renewable energy, *Inorg. Chem.*, 2005, **44**, 6799–6801.
- 3 (a) W. A. Badawy, A review on solar cells from Si-single crystals to porous materials and quantum dots, *J. Adv. Res.*, 2015, **6**, 123–132; (b) S. Sharma, K. K. Jain and A. Sharma, Solar cells: In research and applications—a review, *Mater. Sci. Appl.*, 2015, **06**, 1145–1155.
- 4 (a) M. Grätzel, Solar energy conversion by dye-sensitized photovoltaic cells, *Inorg. Chem.*, 2005, **44**, 6841–6851; (b) I. Chung, B. Lee, J. He, R. P. H. Chang and M. G. Kanatzidis, All-solid-state dye-sensitized solar cells with high efficiency, *Nature*, 2012, **485**, 486–489; (c) Y. Huang, E. J. Kramer, A. J. Heeger and G. C. Bazan, Bulk heterojunction solar cells: Morphology and performance relationships, *Chem. Rev.*, 2014, **114**, 7006–7043; (d) I. Mora-Seró, Current challenges in the development of quantum dot sensitized solar cells, *Adv. Energy Mater.*, 2020, **10**, 1–6; (e) O. E. Semonin, J. M. Luther and M. C. Beard, Quantum dots for next-generation photovoltaics, *Mater. Today*, 2012, **15**, 508–515; (f) M. A. Green, A. Ho-Baillie and H. J. Snaith, The emergence of perovskite solar cells, *Nat. Photonics*, 2014, **8**, 506–514; (g) R. Rajeswari, M. Mrinalini, S. Prasanthkumar and L. Giribabu, Emerging of inorganic hole transporting materials for perovskite solar cells, *Chem. Rec.*, 2017, **17**, 681–699.
- 5 G. Gokul, S. C. Pradhan and S. Soman, Dye sensitized solar cells as potential candidates for indoor/diffused light harvesting applications: From BIPV to self powered IoTs, *Adv. Sol. Energy Res.*, 2019, 281–316.
- 6 B. O'Regan and M. Grätzel, A low-cost, high-efficiency solar cell based on dye-sensitized colloidal TiO₂ films, *Nature*, 1991, **353**, 737–740.
- 7 (a) J. Gong, J. Liang and K. Sumathy, Review on dye-sensitized solar cells (DSSCs): Fundamental concepts and novel materials, *Renewable Sustainable Energy Rev.*, 2012, **16**, 5848–5860; (b) Z. Ning, Y. Fu and H. Tian, Improvement of dye-sensitized solar cells: What we know and what we need to know, *Energy Environ. Sci.*, 2010, **3**, 1170–1181; (c) T. Bessho, S. M. Zakeeruddin, C. Y. Yeh, E. W. G. Diau and M. Grätzel, Highly efficient mesoscopic dye-sensitized solar cells based on donor-acceptor-substituted porphyrins, *Angew. Chem., Int. Ed.*, 2010, **49**, 6646–6649; (d) A. Hagfeldt, G. Boschloo, L. Sun, L. Kloo and H. Pettersson, Dye-sensitized solar cells, *Chem. Rev.*, 2010, **110**, 6595–6663; (e) H. S. Jung and J. K. Lee, Dye sensitized solar cells for economically viable photovoltaic systems, *J. Phys. Chem. Lett.*, 2013, **4**, 1682–1693.
- 8 (a) H. Michaels, M. Rinderle, R. Freitag, I. Benesperi, T. Edvinsson, R. Socher, A. Gagliardi and M. Freitag, Dye-sensitized solar cells under ambient light powering machine learning: Towards autonomous smart sensors for the internet of things, *Chem. Sci.*, 2020, **11**, 2895–2906; (b) E. Tanaka, H. Michaels, M. Freitag and N. Robertson, Synergy of co-sensitizers in a copper bipyridyl redox system for efficient and cost-effective dye-sensitized solar cells in solar and ambient light, *J. Mater. Chem. A*, 2020, **8**, 1279–1287; (c) Y. Cao, Y. Liu, S. M. Zakeeruddin, A. Hagfeldt and M. Grätzel, *Joule*, 2018, **2**, 1108–1117; (d) S. Sasidharan, S. Soman, S. C. Pradhan, K. N. N. Unni, A. A. P. Mohamed, B. N. Nair and H. U. N. Saraswathy, *New J. Chem.*, 2017, **41**, 1007–1016; (e) M. Freitag, J. Teuscher, Y. Saygili, X. Zhang, F. Giordano, P. Liska, J. Hua, S. M. Zakeeruddin, J. E. Moser, M. Grätzel and A. Hagfeldt, Dye-sensitized solar cells for efficient power generation under ambient lighting, *Nat. Photonics*, 2017, **11**, 372–378; (f) S. Venkatesan, W. H. Lin, H. Teng and Y. L. Lee, High-efficiency bifacial dye-sensitized solar cells for application under indoor light conditions, *ACS Appl. Mater. Interfaces*, 2019, **11**, 42780–42789.
- 9 (a) J. M. Ji, H. Zhou and H. K. Kim, Rational design criteria for D- π -A structured organic and porphyrin sensitizers for highly efficient dye-sensitized solar cells, *J. Mater. Chem. A*, 2018, **6**(30), 14518–14545; (b) W. Wei, K. Sun and Y. H. Hu, An efficient counter electrode material for dye-sensitized solar cells – flower-structured 1T metallic phase MoS₂, *J. Mater. Chem. A*, 2016, **4**(32), 12398–12401; (c) W. Wei, K. Sun and Y. H. Hu, Direct conversion of CO₂ to 3D graphene and its excellent performance for dye-sensitized solar cells with 10% efficiency, *J. Mater. Chem. A*, 2016, **4**(31), 12054–12057; (d) D. Wang, W. Wei and Y. H. Hu, Highly efficient dye-sensitized solar cells with composited food dyes, *Ind. Eng. Chem. Res.*, 2020, **59**(22), 10457–10463.
- 10 (a) Q. Hualmé, V. M. Mwalukuku, D. Joly, J. Liotier, Y. Kervella, P. Maldivi, S. Narbey, F. Oswald, A. J. Riquelme, J. A. Anta and R. Demadrille, Photochromic dye-sensitized solar cells with light-driven adjustable optical transmission and power conversion efficiency, *Nat. Energy*, 2020, **5**, 468–477; (b) A. Gopi, S. Lingamoorthy, S. Soman, K. Yoosaf, R. Haridas and S. Das, Modulating FRET in organic-inorganic nano-hybrids for light harvesting applications, *J. Phys. Chem. C*, 2016, **120**, 26569–26578; (c) M. V. Vinayak, M. Yoosuf, S. C. Pradhan, T. M. Lakshmykanth, S. Soman and K. R. Gopidas, A detailed evaluation of charge recombination dynamics in dye solar cells based on starburst triphenylamine dyes, *Sustainable Energy Fuels*, 2018, **2**, 303–314; (d) H. Iftikhar, G. G. Sonai, S. G. Hashmi, A. F. Nogueira and P. D. Lund, Progress on electrolytes development in dye-sensitized solar



- cells, *Materials*, 2019, **12**, 1998–2065; (e) S. C. Pradhan, A. Hagfeldt and S. Soman, Resurgence of DSCs with copper electrolyte: a detailed investigation of interfacial charge dynamics with cobalt and iodine based electrolytes, *J. Mater. Chem. A*, 2018, **6**, 22204–22214; (f) S. Soman, Y. Xie and T. W. Hamann, Cyclometalated sensitizers for DSSCs employing cobalt redox shuttles, *Polyhedron*, 2014, **82**, 139–147; (g) S. Soman, M. A. Rahim, S. Lingamoorthy, C. H. Suresh and S. Das, Strategies for optimizing the performance of carbazole thiophene appended unsymmetrical squaraine dyes for dye-sensitized solar cells, *Phys. Chem. Chem. Phys.*, 2015, **17**, 23095–23103; (h) M. V. Vinayak, T. M. Lakshmykanth, M. Yoosuf, S. Soman and K. R. Gopidas, Effect of recombination and binding properties on the performance of dye sensitized solar cells based on propeller shaped triphenylamine dyes with multiple binding groups, *Sol. Energy*, 2016, **124**, 227–241; (i) Q. Wali, A. Fakhruddin and R. Jose, Tin oxide as a photoanode for dye-sensitized solar cells: Current progress and future challenges, *J. Power Sources*, 2015, **293**, 1039–1052.
- 11 (a) K. L. Wu, W. P. Ku, J. N. Clifford, E. Palomares, S. Te Ho, Y. Chi, S. H. Liu, P. T. Chou, M. K. Nazeeruddin and M. Grätzel, Harnessing the open-circuit voltage via a new series of Ru(II) sensitizers bearing (iso)-quinolinyl pyrazolate ancillaries, *Energy Environ. Sci.*, 2013, **6**, 859–870; (b) Z. She, Y. Cheng, L. Zhang, X. Li, D. Wu, Q. Guo, J. Lan, R. Wang and J. You, Novel ruthenium sensitizers with a phenothiazine conjugated bipyridyl ligand for high-efficiency dye-sensitized solar cells, *ACS Appl. Mater. Interfaces*, 2015, **7**, 27831–27837; (c) L. Han, A. Islam, H. Chen, C. Malapaka, B. Chiranjeevi, S. Zhang, X. Yang and M. Yanagida, High-efficiency dye-sensitized solar cell with a novel co-adsorbent, *Energy Environ. Sci.*, 2012, **5**, 6057–6060.
- 12 (a) Y. S. Yen, H. H. Chou, Y. C. Chen, C. Y. Hsu and J. T. Lin, Recent developments in molecule-based organic materials for dye-sensitized solar cells, *J. Mater. Chem.*, 2012, **22**, 8734–8747; (b) A. Mishra, M. K. R. Fischer and P. Büerle, Metal-free organic dyes for dye-sensitized solar cells: From structure: Property relationships to design rules, *Angew. Chem., Int. Ed.*, 2009, **48**, 2474–2499; (c) A. Carella, F. Borbone and R. Centore, Research progress on photosensitizers for DSSC, *Front. Chem.*, 2018, **6**, 1–24.
- 13 (a) J. J. Cid, J. H. Yum, S. R. Jang, M. K. Nazeeruddin, E. Martínez-Ferrero, E. Palomares, J. Ko, M. Grätzel and T. Torres, Molecular cosensitization for efficient panchromatic dye-sensitized solar cells, *Angew. Chem., Int. Ed.*, 2007, **46**, 8358–8362; (b) N. V. Krishna, J. V. S. Krishna, M. Mrinalini, S. Prasanthkumar and L. Giribabu, Role of co-sensitizers in dye-sensitized solar cells, *ChemSusChem*, 2017, **10**, 4668–4689.
- 14 (a) B. Hemavathi, V. Jayadev, P. C. Ramamurthy, R. K. Pai, K. N. Narayanan Unni, T. N. Ahipa, S. Soman and R. G. Balakrishna, Variation of the donor and acceptor in D–A– π –A based cyanopyridine dyes and its effect on dye sensitized solar cells, *New J. Chem.*, 2019, **43**, 15673–15680; (b) B. Hemavathi, V. Jayadev, S. C. Pradhan, G. Gokul, K. Jagadish, G. K. Chandrashekhara, P. C. Ramamurthy, R. K. Pai, K. N. Narayanan Unni, T. N. Ahipa, S. Soman and R. Geetha Balakrishna, Aggregation induced light harvesting of molecularly engineered D–A– π –A carbazole dyes for dye-sensitized solar cells, *Sol. Energy*, 2018, **174**, 1085–1096; (c) T. Maeda, T. V. Nguyen, Y. Kuwano, X. Chen, K. Miyana, H. Nakazumi, S. Yagi, S. Soman and A. Ajayaghosh, Intramolecular exciton-coupled squaraine dyes for dye-sensitized solar cells, *J. Phys. Chem. C*, 2018, **122**, 21745–21754; (d) V. Nikolaou, A. Charisiadis, S. Chalkiadaki, I. Alexandropoulos, S. C. Pradhan, S. Soman, M. K. Panda and A. G. Coutsolelos, Enhancement of the photovoltaic performance in D3A porphyrin-based DSCs by incorporating an electron withdrawing triazole spacer, *Polyhedron*, 2018, **140**, 9–18; (e) J. S. Panicker, B. Balan, S. Soman and V. C. Nair, Understanding structure–property correlation of metal free organic dyes using interfacial electron transfer measurements, *Sol. Energy*, 2016, **139**, 547–556; (f) S. Soman, S. C. Pradhan, M. Yoosuf, M. V. Vinayak, S. Lingamoorthy and K. R. Gopidas, Probing recombination mechanism and realization of marcus normal region behavior in DSSCs employing cobalt electrolytes and triphenylamine dyes, *J. Phys. Chem. C*, 2018, **122**, 14113–14127; (g) M. Yoosuf, S. C. Pradhan, S. Soman and K. R. Gopidas, Triple bond rigidified anthracene–triphenylamine sensitizers for dye-sensitized solar cells, *Sol. Energy*, 2019, **188**, 55–65.
- 15 (a) L. Zhang, X. Yang, W. Wang, G. G. Gurzadyan, J. Li, X. Li, J. An, Z. Yu, H. Wang, B. Cai, A. Hagfeldt and L. Sun, 13.6% Efficient organic dye-sensitized solar cells by minimizing energy losses of the excited state, *ACS Energy Lett.*, 2019, **4**, 943–951; (b) W. Zhang, Y. Wu, H. W. Bahng, Y. Cao, C. Yi, Y. Saygili, J. Luo, Y. Liu, L. Kavan, J. E. Moser, A. Hagfeldt, H. Tian, S. M. Zakeeruddin, W. H. Zhu and M. Grätzel, Comprehensive control of voltage loss enables 11.7% efficient solid-state dye-sensitized solar cells, *Energy Environ. Sci.*, 2018, **11**, 1779–1787; (c) Y. Cao, Y. Liu, S. M. Zakeeruddin, A. Hagfeldt and M. Grätzel, Direct contact of selective charge extraction layers enables high-efficiency molecular photovoltaics, *Joule*, 2018, **2**, 1108–1117; (d) K. Kakiage, Y. Aoyama, T. Yano, K. Oya, J. Fujisawa and M. Hanaya, Highly-efficient dye-sensitized solar cells with collaborative sensitization by silyl-anchor and carboxy-anchor dyes, *Chem. Commun.*, 2015, **51**, 15894–15897.
- 16 (a) L. Alibabaei, J. H. Kim, M. Wang, N. Pootrakulchote, J. Teuscher, D. Di Censo, R. Humphry-Baker, J. E. Moser, Y. J. Yu, K. Y. Kay, S. M. Zakeeruddin and M. Grätzel, Molecular design of metal-free D– π –A substituted sensitizers for dye-sensitized solar cells, *Energy Environ. Sci.*, 2010, **3**, 1757–1764; (b) A. Yella, R. Humphry-Baker, B. F. E. Curchod, N. Ashari Astani, J. Teuscher, L. E. Polander, S. Mathew, J. E. Moser, I. Tavernelli, U. Rothlisberger, M. Grätzel, M. K. Nazeeruddin and J. Frey, Molecular engineering of a fluorene donor for dye-sensitized solar cells, *Chem. Mater.*, 2013, **25**, 2733–2739.
- 17 (a) J. Wang, K. Liu, L. Ma and X. Zhan, Triarylamine: Versatile platform for organic, dye-sensitized, and perovskite solar cells,



- Chem. Rev.*, 2016, **116**, 14675–14725; (b) K. Hara, K. Sayama, Y. Ohga, A. Shinpo, S. Suga and H. Arakawa, A coumarin-derivative dye sensitized nanocrystalline TiO₂ solar cell having a high solar-energy conversion efficiency up to 5.6%, *Chem. Commun.*, 2001, 569–570; (c) Z. S. Wang, K. Hara, Y. Dan-oh, C. Kasada, A. Shinpo, S. Suga, H. Arakawa and H. Sugihara, Photophysical and (photo)electrochemical properties of a coumarin dye, *J. Phys. Chem. B*, 2005, **109**, 3907–3914; (d) B. Liu, R. Wang, W. Mi, X. Li and H. Yu, Novel branched coumarin dyes for dye-sensitized solar cells: Significant improvement in photovoltaic performance by simple structure modification, *J. Mater. Chem.*, 2012, **22**, 15379–15387; (e) M. Marszalek, S. Nagane, A. Ichake, R. Humphry-Baker, V. Paul, S. M. Zakeeruddin and M. Grätzel, Tuning spectral properties of phenothiazine based donor- π -acceptor dyes for efficient dye-sensitized solar cells, *J. Mater. Chem.*, 2012, **22**, 889–894; (f) S. H. Kim, H. W. Kim, C. Sakong, J. Namgoong, S. W. Park, M. J. Ko, C. H. Lee, W. I. Lee and J. P. Kim, Effect of five-membered heteroaromatic linkers to the performance of phenothiazine-based dye-sensitized solar cells, *Org. Lett.*, 2011, **13**, 5784–5787; (g) K. Srinivas, C. R. Kumar, M. A. Reddy, K. Bhanuprakash, V. J. Rao and L. Giribabu, D- π -A organic dyes with carbazole as donor for dye-sensitized solar cells, *Synth. Met.*, 2011, **161**, 96–105.
- 18 (a) Y. Liu, J. He, L. Han and J. Gao, Influence of the auxiliary acceptor and π -bridge in carbazole dyes on photovoltaic properties, *J. Photochem. Photobiol., A*, 2017, **332**, 283–292; (b) K. Hara, Z. S. Wang, T. Sato, A. Furube, R. Katoh, H. Sugihara, Y. Dan-Oh, C. Kasada, A. Shinpo and S. Suga, Oligothiophene-containing coumarin dyes for efficient dye-sensitized solar cells, *J. Phys. Chem. B*, 2005, **109**, 15476–15482; (c) J. Liu, X. Yang, A. Islam, Y. Numata, S. Zhang, N. T. Salim, H. Chen and L. Han, Efficient metal-free sensitizers bearing circle chain embracing π -spacers for dye-sensitized solar cells, *J. Mater. Chem. A*, 2013, **1**, 10889–10897; (d) L. Huang, P. Ma, G. Deng, K. Zhang, T. Ou, Y. Lin and M. S. Wong, Novel electron-deficient quinoxaline-dithienothiophene- and phenazinedithienothiophene-based photosensitizers: The effect of conjugation expansion on DSSC performance, *Dyes Pigment.*, 2018, **159**, 107–114.
- 19 (a) Y. Wu and W. Zhu, Organic sensitizers from D- π -A to D-A- π -A: Effect of the internal electron-withdrawing units on molecular absorption, energy levels and photovoltaic performances, *Chem. Soc. Rev.*, 2013, **42**, 2039–2058; (b) W. Zhu, Y. Wu, S. Wang, W. Li, X. Li, J. Chen, Z. S. Wang and H. Tian, Organic D-A- π -A solar cell sensitizers with improved stability and spectral response, *Adv. Funct. Mater.*, 2011, **21**, 756–763; (c) W. Li, Y. Wu, Q. Zhang, H. Tian and W. Zhu, D-A- π -A featured sensitizers bearing phthalimide and benzotriazole as auxiliary acceptor: Effect on absorption and charge recombination dynamics in dye-sensitized solar cells, *ACS Appl. Mater. Interfaces*, 2012, **4**, 1822–1830; (d) Y. Wu, W. H. Zhu, S. M. Zakeeruddin and M. Grätzel, Insight into D-A- π -A structured sensitizers: A promising route to highly efficient and stable dye-sensitized solar cells, *ACS Appl. Mater. Interfaces*, 2015, **7**, 9307–9318;
- (e) J. He, Y. Liu, J. Gao and L. Han, New D-D- π -A triphenylamine-coumarin sensitizers for dye-sensitized solar cells, *Photochem. Photobiol. Sci.*, 2017, **16**, 1049–1056; (f) W. Sharmoukh, J. Cong, J. Gao, P. Liu, Q. Daniel and L. Kloo, Molecular engineering of D-D- π -A-based organic sensitizers for enhanced dye-sensitized solar cell performance, *ACS Omega*, 2018, **3**, 3819–3829; (g) V. Cuesta, M. Vartanian, P. de la Cruz, R. Singhal, G. D. Sharma and F. Langa, Comparative study on the photovoltaic characteristics of A-D-A and D-A-D molecules based on Zn-porphyrin; a D-A-D molecule with over 8.0% efficiency, *J. Mater. Chem. A*, 2017, **5**, 1057–1065; (h) K. S. V. Gupta, T. Suresh, S. P. Singh, A. Islam, L. Han and M. Chandrasekharam, Carbazole based A- π -D- π -A dyes with double electron acceptor for dye-sensitized solar cell, *Org. Electron.*, 2014, **15**, 266–275.
- 20 (a) I. Cho, S. K. Park, B. Kang, J. W. Chung, J. H. Kim, K. Cho and S. Y. Park, Design, synthesis, and versatile processing of indolo[3,2-*b*]indole-based π -conjugated molecules for high-performance organic field-effect transistors, *Adv. Funct. Mater.*, 2016, **26**, 2966–2973; (b) Y. Y. Lai, J. M. Yeh, C. E. Tsai and Y. J. Cheng, Synthesis, molecular and photovoltaic properties of an indolo[3,2-*b*]indole-based acceptor-donor-acceptor small molecule, *Eur. J. Org. Chem.*, 2013, 5076–5084; (c) H. Jiang, H. Zhao, K. K. Zhang, X. Chen, C. Kloc and W. Hu, High-performance organic single-crystal field-effect transistors of indolo[3,2-*b*]carbazole and their potential applications in gas controlled organic memory devices, *Adv. Mater.*, 2011, **23**, 5075–5080.
- 21 For the synthesis of indolo[2,3-*b*]quinoxaline see: G. M. Badger and P. J. Nelson, Polynuclear heterocyclic systems. Part XIV. Indoloquinoxalines, *J. Chem. Soc.*, 1962, 3926–3931.
- 22 K. R. J. Thomas and P. Tyagi, Synthesis, Spectra, and Theoretical Investigations of the Triarylamines Based on 6H-Indolo[2,3-*b*]quinoxaline, *J. Org. Chem.*, 2010, **75**, 8100–8111.
- 23 A. Venkateswararao, P. Tyagi, K. R. J. Thomas and P. Chen, Organic dyes containing indolo [2, 3- b] quinoxaline as a donor: synthesis, optical and photovoltaic properties, *Tetrahedron*, 2014, **70**, 6318–6327.
- 24 X. Qian, H. H. Gao, Y. Z. Zhu, L. Lu and J. Y. Zheng, 6H-Indolo[2,3-*b*]quinoxaline-based organic dyes containing different electron-rich conjugated linkers for highly efficient dye-sensitized solar cells, *J. Power Sources*, 2015, **280**, 573–580.
- 25 X. Qian, X. Wang, L. Shao, H. Li, R. Yan and L. Hou, Molecular engineering of D-D- π -A type organic dyes incorporating indoloquinoxaline and phenothiazine for highly efficient dye-sensitized solar cells, *J. Power Sources*, 2016, **326**, 129–136.
- 26 X. Qian, X. Lan, R. Yan, Y. He, J. Huang and L. Hou, T-shaped (D)2-A- π -A type sensitizers incorporating indoloquinoxaline and triphenylamine for organic dye-sensitized solar cells, *Electrochim. Acta*, 2017, **232**, 377–386.
- 27 R. Su, L. Lyu, M. R. Elmorsy and A. El-Shafei, Novel metal-free organic dyes constructed with the D-D|A- π -A motif: Sensitization and co-sensitization study, *Sol. Energy*, 2019, **194**, 400–414.



- 28 R. Su, S. Ashraf, L. Lyu and A. El-shafei, Tailoring dual-channel anchorable organic sensitizers with indolo[2,3-*b*]quinoxaline moieties: Correlation between structure and DSSC performance, *Sol. Energy*, 2020, **206**, 443–454.
- 29 R. Su, L. Lyu, M. R. Elmorsy and A. El-Shafei, Structural studies and photovoltaic investigation of indolo[2,3-*B*]quinoxaline-based sensitizers/co-sensitizers achieving highly efficient DSSCs, *New J. Chem.*, 2020, **44**, 2797–2812.
- 30 (a) N. X. Hu, S. Xie, Z. Popovic, B. Ong, A. M. Hor and S. Wang, 5,11-Dihydro-5,11-di-1-naphthylindolo[3,2-*b*]carbazole: Atropisomerism in a novel hole-transport molecule for organic light-emitting diodes, *J. Am. Chem. Soc.*, 1999, **121**, 5097–5098; (b) S. Wakim, J. Bouchard, M. Simard, N. Drolet, Y. Tao and M. Leclerc, Organic microelectronics: Design, synthesis, and characterization of 6,12-dimethyl-indolo[3,2-*b*]carbazoles, *Chem. Mater.*, 2004, **16**, 4386–4388; (c) Y. Li, Y. Wu, S. Gardner and B. S. Ong, Novel peripherally substituted indolo[3,2-*b*]carbazoles for high-mobility organic thin-film transistors, *Adv. Mater.*, 2005, **17**, 849–853; (d) Y. Wu, Y. Li, S. Gardner and B. S. Ong, Indolo[3,2-*b*]carbazole-based thin-film transistors with high mobility and stability, *J. Am. Chem. Soc.*, 2005, **127**, 614–618; (e) P. T. Boudreault, S. Wakim, N. Blouin, M. Simard, C. Tessier, Y. Tao, M. Leclerc and V. La, Synthesis, characterization, and application of indolo[3,2-*b*]carbazole semiconductors, *J. Am. Chem. Soc.*, 2007, **129**, 9125–9136.
- 31 For the synthesis of indolocarbazole see: (a) B. Robinson, The Fischer indolisation of cyclohexane-1,4-dione bisphenylhydrazone, *J. Chem. Soc.*, 1963, 3097–3099; (b) J. I. G. Cadogan, M. Carmeron-Wood, R. K. Makie and R. I. J. Searle, The reactivity of organophosphorus compounds. Part XIX. Reduction of nitro-compounds by triethyl phosphite: A convenient new route to carbazoles, indoles, indazoles, triazoles, and related compounds, *J. Chem. Soc.*, 1965, 4831.
- 32 X. H. Zhang, Z. S. Wang, Y. Cui, N. Koumura, A. Furube and K. Hara, Organic sensitizers based on hexylthiophene-functionalized indolo[3, 2-*b*]carbazole for efficient dye-sensitized solar cells, *J. Phys. Chem. C*, 2009, **113**, 13409–13415.
- 33 S. Cai, G. Tian, X. Li, J. Su and H. Tian, Efficient and stable DSSC sensitizers based on substituted dihydroindolo[2,3-*b*]carbazole donors with high molar extinction coefficients, *J. Mater. Chem. A*, 2013, **1**, 11295–11305.
- 34 Y. Wu and W. Zhu, Organic sensitizers from D- π -A to D-A- π -A: Effect of the internal electron-withdrawing units on molecular absorption, energy levels and photovoltaic performances, *Chem. Soc. Rev.*, 2013, **42**, 2039–2058.
- 35 S. Cai, X. Hu, G. Tian, H. Zhou, W. Chen, J. Huang, X. Li and J. Su, Photo-stable substituted dihydroindolo[2,3-*b*]carbazole-based organic dyes: Tuning the photovoltaic properties by optimizing the π structure for panchromatic DSSCs, *Tetrahedron*, 2014, **70**, 8122–8128.
- 36 X. Qian, L. Shao, H. Li, R. Yan, X. Wang and L. Hou, Indolo[3,2-*b*]carbazole-based multi-donor- π -acceptor type organic dyes for highly efficient dye-sensitized solar cells, *J. Power Sources*, 2016, **319**, 39–47.
- 37 Z. Xiao, Y. Di, Z. Tan, X. Cheng, B. Chen and J. Feng, Efficient organic dyes based on perpendicular 6,12-diphenyl substituted indolo[3,2-*b*] carbazole donor, *Photochem. Photobiol. Sci.*, 2016, **15**, 1514–1523.
- 38 Z. Xiao, B. Chen, Y. Di, H. Wang, X. Cheng and J. Feng, Effect of substitution position on photoelectronic properties of indolo[3,2-*b*]carbazole-based metal-free organic dyes, *Sol. Energy*, 2018, **173**, 825–833.
- 39 J. Y. Su, C. Y. Lo, C. H. Tsai, C. H. Chen, S. H. Chou, S. H. Liu, P. T. Chou and K. T. Wong, Indolo[2,3-*b*]carbazole synthesized from a double-intramolecular Buchwald–Hartwig reaction: Its application for a dianchor DSSC organic dye, *Org. Lett.*, 2014, **16**, 3176–3179.
- 40 H. Zhang, Z. E. Chen, J. Hu and Y. Hong, Novel metal-free organic dyes containing linear planar 11,12-dihydroindolo[2,3-*a*]carbazole donor for dye-sensitized solar cells: Effects of π spacer and alkyl chain, *Dyes Pigm.*, 2019, **164**, 213–221.
- 41 C. Luo, W. Bi, S. Deng, J. Zhang, S. Chen, B. Li, Q. Liu, H. Peng and J. Chu, Indolo[3,2,1-*jk*] carbazole derivatives-sensitized solar cells: Effect of π -bridges on the performance of cells, *J. Phys. Chem. C*, 2014, **118**, 14211–14217.
- 42 W. Cao, M. Fang, Z. Chai, H. Xu, T. Duan, Z. Li, X. Chen, J. Qin and H. Han, New D- π -A organic dyes containing a *tert*-butyl-capped indolo[3,2,1-*jk*]carbazole donor with bithiophene unit as π -linker for dye-sensitized solar cells, *RSC Adv.*, 2015, **5**, 32967–32975.
- 43 X. C. Li, C. Y. Wang, W. Y. Lai and W. Huang, Triazatruxene-based materials for organic electronics and optoelectronics, *J. Mater. Chem. C*, 2016, **4**, 10574–10587 and references cited therein.
- 44 For the synthesis of triazatruxene see: (a) J. Bergman and N. Eklund, Synthesis of 2,2'-biindolyls by coupling reactions, *Tetrahedron*, 1980, **36**, 1439–1443; (b) J. Bergman and N. Eklund, Synthesis and studies of tris-indolobenzenes and related compounds, *Tetrahedron*, 1980, **36**, 1445–1450; (c) M. A. Eissenstat, M. R. Bell, T. E. D'Ambra, E. J. Alexander, S. J. Daum, J. H. Ackerman, M. D. Gruett, V. Kumar, K. G. Estep, E. M. Olefirowicz, J. R. Wetzler, M. D. Alexander, J. D. Weaver, D. A. Haycock, D. A. Luttinger, F. M. Casiano, S. M. Chippari, J. E. Kuster, J. I. Stevenson and S. J. Ward, Aminoalkylindoles: Structure–activity relationships of novel cannabinoid mimetics, *J. Med. Chem.*, 1995, **38**, 3094–3105.
- 45 X. Qian, Y. Z. Zhu, J. Song, X. P. Gao and J. Y. Zheng, New donor- π -acceptor type triazatruxene derivatives for highly efficient dye-sensitized solar cells, *Org. Lett.*, 2013, **15**, 6034–6037.
- 46 X. Qian, L. Lu, Y. Z. Zhu, H. H. Gao and J. Y. Zheng, Triazatruxene-based organic dyes containing a rhodanine-3-acetic acid acceptor for dye-sensitized solar cells, *Dyes Pigm.*, 2015, **113**, 737–742.
- 47 B. Pan, Y. Z. Zhu, D. Ye, F. Li, Y. F. Guo and J. Y. Zheng, Effects of ethynyl unit and electron acceptors on the performance of triazatruxene-based dye-sensitized solar cells, *New J. Chem.*, 2018, **42**, 4133–4141.
- 48 X. Qian, R. Yan, L. Shao, H. Li, X. Wang and L. Hou, Triindole-modified push-pull type porphyrin dyes for dye-sensitized solar cells, *Dyes Pigm.*, 2016, **134**, 434–441.



- 49 P. Qin, P. Sanghyun, M. I. Dar, K. Rakstys, H. ElBatal, S. A. Al-Muhtaseb, C. Ludwig and M. K. Nazeeruddin, Weakly conjugated hybrid zinc porphyrin sensitizers for solid-state dye-sensitized solar cells, *Adv. Funct. Mater.*, 2016, **26**, 5550–5559.
- 50 L. Zhang, X. Yang, W. Wang, G. G. Gurzadyan, J. Li, X. Li, J. An, Z. Yu, H. Wang, B. Cai, A. Hagfeldt and L. Sun, 13.6% Efficient organic dye-sensitized solar cells by minimizing energy losses of the excited state, *ACS Energy Lett.*, 2019, **4**, 943–951.
- 51 L. Zhang, X. Yang, B. Cai, H. Wang, Z. Yu and L. Sun, Triazatruxene-based sensitizers for highly efficient solid-state dye-sensitized solar cells, *Sol. Energy*, 2020, **212**, 1–5.
- 52 L. Zhang, X. Yang, S. Li, Z. Yu, A. Hagfeldt and L. Sun, Electron-withdrawing anchor group of sensitizer for dye-sensitized solar cells, cyanoacrylic acid, or benzoic acid?, *Sol. RRL*, 2020, **4**, 1900436.
- 53 S. Li, X. Yang, L. Zhang, J. An, B. Cai and X. Wang, Effect of fluorine substituents on benzothiadiazole-based D- π -A'- π -A photosensitizers for dye-sensitized solar cells, *RSC Adv.*, 2020, **10**, 9203–9209.
- 54 Z. Yao, X. Liao, Y. Guo, H. Zhao, Y. Guo, F. Zhang, L. Zhang, Z. Zhu, L. Kloo, W. Ma, Y. Chen and L. Sun, Exploring overall photoelectric applications by organic materials containing symmetric donor isomers, *Chem. Mater.*, 2019, **31**, 8810–8819.
- 55 For the synthesis of indeno[1,2-*b*]indole see: D. W. Brown, M. F. Mahon, A. Ninan, M. Sainsbury and H. G. Shertzer, The Fischer indolisation reaction and the synthesis of dihydroindenoindoles, *Tetrahedron*, 1993, **49**, 8919–8932.
- 56 X. Qian, R. Yan, C. Xu, L. Shao, H. Li and L. Hou, New efficient organic dyes employing indeno[1,2-*b*]indole as the donor moiety for dye-sensitized solar cells, *J. Power Sources*, 2016, **332**, 103–110.
- 57 X. Qian, R. Yan, Y. Hang, Y. Lv, L. Zheng, C. Xu and L. Hou, Indeno[1,2-*b*]indole-based organic dyes with different acceptor groups for dye-sensitized solar cells, *Dye. Pigment.*, 2017, **139**, 274–282.
- 58 R. Yan, X. Qian, Y. Jiang, Y. He, Y. Hang and L. Hou, Ethynylene-linked planar rigid organic dyes based on indeno[1,2-*b*]indole for efficient dye-sensitized solar cells, *Dyes Pigm.*, 2017, **141**, 93–102.
- 59 P. P. Dai, Y. Z. Zhu, Q. L. Liu, Y. Q. Yan and J. Y. Zheng, Novel indeno[1,2-*b*]indole-spirofluorene donor block for efficient sensitizers in dye-sensitized solar cells, *Dyes Pigm.*, 2020, **175**, 108099.
- 60 P. P. Dai, J. Han, Y. Z. Zhu, Y. Q. Yan and J. Y. Zheng, Orientation-dependent effects of indeno[1,2-*b*]indole-spirofluorene donor on photovoltaic performance of D- π -A and D-D- π -A sensitizers, *J. Power Sources*, 2021, **481**, 228901.
- 61 X. Zhou, J. Lu, H. Huang, Y. Yun, Z. Li and F. You, Dyes and pigments thieno[3,2-*b*]indole (TI) bridged A- π -D- π -A small molecules: Synthesis, characterizations and organic solar cell applications, *Dyes Pigm.*, 2019, **160**, 16–24.
- 62 X. Zhang, Y. Cui, R. Katoh, N. Koumura and K. Hara, Organic dyes containing thieno[3,2-*b*]indole donor for efficient dye-sensitized solar cells, *J. Phys. Chem. C*, 2010, **114**, 18283–18290.
- 63 N. Koumura, Z. S. Wang, S. Mori, M. Miyashita, E. Suzuki and K. Hara, Alkyl-functionalized organic dyes for efficient molecular photovoltaics, *J. Am. Chem. Soc.*, 2006, **128**, 14256–14257.
- 64 Y. K. Eom, S. H. Kang, I. T. Choi, Y. Yoo, J. Kim and H. K. Kim, Significant light absorption enhancement by a single heterocyclic unit change in the π -bridge moiety from thieno[3,2-*b*]benzothiophene to thieno[3,2-*b*]indole for high performance dye-sensitized and tandem solar cells, *J. Mater. Chem. A*, 2017, **5**, 2297–2308.
- 65 J. M. Ji, H. Zhou, Y. K. Eom, C. H. Kim and H. K. Kim, 14.2% efficiency dye-sensitized solar cells by co-sensitizing novel thieno[3,2-*b*]indole-based organic dyes with a promising porphyrin sensitizer, *Adv. Energy Mater.*, 2020, **10**, 2000124.
- 66 J. M. Ji, S. H. Kim, H. Zhou, C. H. Kim and H. K. Kim, D- π -A-structured porphyrins with extended auxiliary π -spacers for highly efficient dye-sensitized solar cells, *ACS Appl. Mater. Interfaces*, 2019, **11**, 24067–24077.
- 67 S. H. Kang, S. Y. Jung, Y. W. Kim, Y. K. Eom and H. K. Kim, Exploratory synthesis and photovoltaic performance comparison of D- π -A structured Zn-porphyrins for dye-sensitized solar cells, *Dye. Pigment.*, 2018, **149**, 341–347.
- 68 R. A. Irgashev, A. A. Karmatsky, S. A. Kozyukhin, V. K. Ivanov, A. Sadovnikov, V. V. Kozik, V. A. Grinberg, V. V. Emets, G. L. Rusinov and V. N. Charushin, A facile and convenient synthesis and photovoltaic characterization of novel thieno[2,3-*b*]indole dyes for dye-sensitized solar cells, *Synth. Met.*, 2015, **199**, 152–158.
- 69 R. A. Irgashev, A. A. Karmatsky, G. A. Kim, A. A. Sadovnikov, V. V. Emets, V. A. Grinberg, V. K. Ivanov, S. A. Kozyukhin, G. L. Rusinov and V. N. Charushin, Novel push-pull thieno[2,3-*b*]indole-based dyes for efficient dye-sensitized solar cells (DSSCs), *ARKIVOC*, 2017, 34–50.
- 70 For the synthesis of indolo[3,2-*b*]indole see: (a) S. A. Samsoniya and M. V. Trapaidze, The chemistry of indolindoles, *Russ. Chem. Rev.*, 2007, **76**, 313 and references cited therein; (b) A. N. Grinev and S. Y. Ryabova, New method for the synthesis of indolo [3,2-*b*] indole derivatives, *Chem. Heterocycl. Compd.*, 1982, **18**, 153; (c) P. Kaszynski and D. A. Dougherty, Synthesis and properties of diethyl 5,10-dihetera-5,10-dihydroindeno[2,1-*a*]indene-2,7-dicarboxylates, *J. Org. Chem.*, 1993, **58**, 5209; (d) L. Qiu, C. Yu, N. Zhao, W. Chen, Y. Guo, X. Wan, R. Yang and Y. Liu, An expedient synthesis of fused heteroacenes bearing a pyrrolo[3,2-*b*]pyrrole core, *Chem. Commun.*, 2012, **48**, 12225–12227; (e) L. Qiu, X. Wang, N. Zhao, S. Xu, Z. An, X. Zhuang, Z. Lan, L. Wen and X. Wan, Reductive ring closure methodology toward heteroacenes bearing a dihydropyrrolo[3,2-*B*]pyrrole core: Scope and limitation, *J. Org. Chem.*, 2014, **79**, 11339–11348; (f) M. A. Truong and K. Nakano, Synthesis of benzofuro- and indolo[3,2-*b*]indoles *via* palladium-catalyzed double *N*-arylation and their physical properties, *J. Org. Chem.*, 2015, **80**, 11566–11572; (g) H. E. Ho, K. Oniwa, Y. Yamamoto and T. Jin, N-Methyl transfer induced copper-mediated oxidative



- diamination of alkynes, *Org. Lett.*, 2016, **18**, 2487–2490; (h) L. H. Leijendekker, J. Weweler, T. M. Leuther and J. Streuff, Catalytic reductive synthesis and direct derivatization of unprotected aminoindoles, aminopyrroles, and iminoindolines, *Angew. Chem., Int. Ed.*, 2017, **56**, 6103–6106.
- 71 (a) M. M. Murray, D. A. Kaisaki, W. Chang, D. A. Dougherty and P. Kaszynski, Prototypes for the polaronic ferromagnet. Synthesis and characterization of high-spin organic polymers, *J. Am. Chem. Soc.*, 1994, **116**, 8152–8161; (b) J. Sim, K. Do, K. Song, A. Sharma, S. Biswas, G. D. Sharma and J. Ko, D–A–D–A–D push pull organic small molecules based on 5,10-dihydroindolo[3,2-*b*]indole (DINI) central core donor for solution processed bulk heterojunction solar cells, *Org. Electron.*, 2016, **30**, 122–130; (c) I. Cho, S. K. Park, B. Kang, J. W. Chung, J. H. Kim, K. Cho and S. Y. Park, Design, synthesis, and versatile processing of indolo[3,2-*b*]indole-based π -conjugated molecules for high-performance organic field-effect transistors, *Adv. Funct. Mater.*, 2016, **26**, 2966–2973; (d) Y. Y. Lai, J. M. Yeh, C. E. Tsai and Y. J. Cheng, Synthesis, molecular and photovoltaic properties of an indolo[3,2-*b*]indole-based acceptor-donor-acceptor small molecule, *Eur. J. Org. Chem.*, 2013, 5076–5084.
- 72 N. Ruangsupapichat, M. Ruamyart, P. Kanchanarugee, C. Boonthum, N. Prachumrak, T. Sudyoadsuk and V. Promarak, Toward rational design of metal-free organic dyes based on indolo[3,2-*b*]indole structure for dye-sensitized solar cells, *Dyes Pigment.*, 2018, **151**, 149–156.
- 73 C. Ruamyart, P. Chasing, T. Sudyoadsuk, V. Promarak and N. Ruangsupapichat, Double anchor indolo[3,2-*b*]indole-derived metal-free dyes with extra electron donors as efficient sensitizers for dye-sensitized solar cells, *New J. Chem.*, 2021, **45**, 7542–7554.
- 74 P. V. Santhini, V. Jayadev, S. C. Pradhan, S. Lingamoorthy, P. R. Nitha, M. V. Chaithanya, R. K. Mishra, K. N. Narayanan Unni, J. John and S. Soman, Indolo[3,2-*b*]indole donor-based D– π –A dyes for DSCs: Investigating the role of π -spacers towards recombination, *New J. Chem.*, 2019, **43**, 862–873.
- 75 (a) P. V. Santhini, S. A. Babu, A. Krishnan, R. E. Suresh and J. John, Heteroannulation of 3-nitroindoles and 3-nitrobenzo[*b*]thiophenes: A multicomponent approach toward pyrrole-fused heterocycles, *Org. Lett.*, 2017, **19**, 2458–2461; (b) P. V. Santhini, R. Akhil Krishnan, S. A. Babu, B. S. Simethy, G. Das, V. K. Praveen, S. Varughese and J. John, One-pot MCR-oxidation approach toward indole-fused heteroacenes, *J. Org. Chem.*, 2017, **82**, 10537–10548.
- 76 J. Wang, S. Liu, K. Chang, Q. Liao, S. Li, H. Han, Q. Li and Z. Li, Synergy effect of electronic characteristics and spatial configurations of electron donors on photovoltaic performance of organic dyes, *J. Mater. Chem. C*, 2020, **8**, 14453–14461.
- 77 For the synthesis of benzothieno[3,2-*b*]indole see: (a) T. Sugahara, K. Murakami, H. Yorimitsu and A. Osuka, Palladium-catalyzed amination of aryl sulfides with anilines, *Angew. Chem., Int. Ed.*, 2014, **53**, 9329–9333; (b) Y. Huang, D. Wu, J. Huang, Q. Guo, J. Li and J. You, Use of the Wilkinson catalyst for the *ortho*-C–H heteroarylation of aromatic amines: Facile access to highly extended π -conjugated heteroacenes for organic semiconductors, *Angew. Chem., Int. Ed.*, 2014, **53**, 12158–12162; (c) N. Kamimoto, D. Schollmeyer, K. Mitsudo, S. Suga and S. R. Waldvogel, Palladium-catalyzed domino C–H/N–H functionalization: An efficient approach to nitrogen-bridged heteroacenes, *Chem. – Eur. J.*, 2015, **21**, 8257–8261; (d) H. Huang, P. Dang, L. Wu, Y. Liang and J. Liu, Copper-catalyzed synthesis of benzo[*b*]thiophene-fused imidazopyridines *via* the cleavage of C–H bond and C–X bond, *Tetrahedron Lett.*, 2016, **57**, 574–577; (e) X. Zhao, Q. Li, J. Xu, D. Wang, D. Zhang-Negrerie and Y. Du, Cascade synthesis of benzothieno[3,2-*b*]indoles under oxidative conditions mediated by CuBr and *tert*-butyl hydroperoxide, *Org. Lett.*, 2018, **20**, 5933–5937; (f) X. H. Shan, B. Yang, J. P. Qu and Y. B. Kang, CuSO₄-Catalyzed dual annulation to synthesize O, S or N-containing tetracyclic heteroacenes, *Chem. Commun.*, 2020, **56**, 4063–4066.
- 78 (a) Q. Ji, J. Gao, J. Wang, C. Yang, X. Hui, X. Yan, X. Wu, Y. Xie and M. W. Wang, Benzothieno[3,2-*b*]indole derivatives as potent selective estrogen receptor modulators, *Bioorg. Med. Chem. Lett.*, 2005, **15**, 2891–2893; (b) S. A. Al-Trawneh, M. M. El-Abadelah, J. A. Zahra, S. A. Al-Taweel, F. Zani, M. Incerti, A. Cavazzoni and P. Vicini, Synthesis and biological evaluation of tetracyclic thienopyridones as antibacterial and antitumor agents, *Bioorg. Med. Chem.*, 2011, **19**, 2541–2548; (c) M. Ning, C. Zhou, J. Weng, S. Zhang, D. Chen, C. Yang, H. Wang, J. Ren, L. Zhou, C. Jin and M. W. Wang, Biological activities of a novel selective oestrogen receptor modulator derived from raloxifene (Y134), *Br. J. Pharmacol.*, 2007, **150**, 19–28.
- 79 R. K. Konidena, K. H. Lee, J. Y. Lee and W. P. Hong, A new benzothienindole-based bipolar host material for efficient green phosphorescent organic light-emitting diodes with extremely small efficiency roll-off, *Org. Electron. Phys., Mater. Appl.*, 2019, **70**, 211–218.
- 80 P. R. Nitha, V. Jayadev, S. C. Pradhan, V. Divya, C. H. Suresh, J. John, S. Soman and A. Ajayaghosh, Regulating back electron transfer through donor and π -spacer alterations in benzothieno[3,2-*b*]indole-based dye-sensitized solar cells, *Chem. – Asian J.*, 2020, **15**, 3503–3512.
- 81 For the synthesis of tetraindole see: (a) H. Hiyoshi, T. Sonoda and S. Mataka, Synthesis of cyclic novel symmetric cyclic indole-tetramers, *Heterocycles*, 2006, **68**, 763–769; (b) F. Wang, X. C. Li, W. Y. Lai, Y. Chen, W. Huang and F. Wudl, Synthesis and characterization of symmetric cyclooctatetraindoles: Exploring the potential as electron-rich skeletons with extended π -systems, *Org. Lett.*, 2014, **16**, 2942–2945.
- 82 X. Qian, H. H. Gao, Y. Z. Zhu, B. Pan and J. Y. Zheng, Tetraindole-based saddle-shaped organic dyes for efficient dye-sensitized solar cells, *Dye. Pigment.*, 2015, **121**, 152–158.
- 83 H. Cheng, Y. Wu, J. Su, Z. Wang, R. P. Ghimire, M. Liang, Z. Sun and S. Xue, Organic dyes containing indolodithienopyrrole unit for dye-sensitized solar cells, *Dyes Pigment.*, 2018, **149**, 16–24.



- 84 R. Bisht, V. Sudhakar, M. Fairros, M. Kavungathodi, N. Karjule and J. Nithyanandhan, Fused fluorenylindolenine donor based unsymmetrical squaraine dyes for dye-sensitized solar cells, *ACS Appl. Mater. Interfaces*, 2018, **10**, 26335–26347.
- 85 S. Ramasamy, ScienceDirect organic photosensitizers containing fused indole- imidazole ancillary acceptor with triphenylamine donor moieties for efficient dye-sensitized solar cells, *Int. J. Hydrogen Energy*, 2021, **46**, 3475–3483.

